Understanding the Transformation of Silica and Titania Particles in Food and their Interactions with Proteins of Relevance to Human Nutrition and Health

Wut Hmone Phue

Department of Food Science and Agricultural Chemistry

McGill University, Montreal

December 2021

A thesis submitted to McGill University in partial fulfillment of the requirements of the degree of Doctor in Philosophy

Abstract

Nanomaterials (NM) are added to food because of their unique properties for improving food quality, shelf life, and safety. NMs added to food (referred to as dietary nanomaterials (DNM) raise safety concerns prompted by studies showing their negative impacts on the structure and function of biosystems and biomolecules. While studies have been done to understand the acute toxicity of NMs (and DNMs), there are prominent knowledge gaps on the transformation of DNMs in response to food processing conditions and interaction with food and biological matrices. This thesis addressed the implications of DNMs transformation in their interactions with biological targets such as proteins and cells. The specific objectives of this thesis research were to understand the effects of the transformation of DNMs (silica and titania) on the structure and function of enzymes and proteins relevant to health and diseases. Chapter 2 detailed the state of knowledge on the applications and implications of NMs in food and identified prominent knowledge gaps. Chapter 3 described a comparative analysis of different grades of silica (food-grade nanoparticle (FG-NP), non-food grade nanoparticles (NFG-NP) and food-grade micron particles (FG-MP)) and temperature variants of FG-NP for their physicochemical properties and effect on trypsin. While the chemical composition and amorphous nature of FG-NPs were similar to NFG-NPs and FG-MPs, FG-NP had relatively fewer branched and ring siloxane groups. Changes in the agglomeration behaviour and relative abundance of different silica groups in FG-NPs were also observed when exposed to food handling temperatures. The 'mixed type inhibition' of trypsin by temperature variants of FG-NPs, and FG-MPs resulted in incomplete digestion of model protein-bovine serum albumin (BSA). Chapter 4 unveiled the consequences of surface modification of FG-NPs by a single protein (BSA) and complex food matrix (milk) on human salivary amylase (HSA) activity. Surface passivation of FG-NP with BSA decreased the partial inhibition of HSA.

Paradoxically, interactions of FG-NP with milk increased the HSA inhibition, which was ascribed to the presence of milk protease that digested HSA. In Chapter 5, factors influencing protein-DNMs (silica and titania) interactions were identified using individual proteins-DNM interaction and milk-DNM interaction (model food matrix). Individual Protein-DNM interaction studies revealed that both particle and protein characteristics influence proteins' adsorption onto the particles. In contrast, factors that determine the protein-biomolecule interactions dominated their surface adsorption to DNM in a complex food matrix. Outcomes from Chapters 3, 4 and 5 showed that interaction of DNMs with proteins changed their structure and function. Therefore, I hypothesized that DNM-protein interaction would alter the allergenicity of food proteins. Chapter 6 studies describe the alteration in allergenicity of bovine milk or major antigens of bovine milk (β-lactoglobulin and casein) after interacting with DNMs of silica and titania. It was found that the allergenicity of milk and milk proteins increased when interacted with DNMs, and this tendency persisted even after simulated gut digestion. The increase in allergenicity was found to be mediated by alterations in the secondary and tertiary structure of milk proteins, which could have exposed the epitopes. Thus, my studies demonstrated the transformation of DNMs in response to food processing conditions and their interaction with the food matrix and its effect on the structure and function of proteins of relevance to digestion and allergy. These studies also highlight the need to probe adverse health effects of DNMs using animal models to gain a deeper understanding on the consequence of DNMs entering the gastrointestinal system on human health.

Keywords: nanoparticles, silica, titania, food additives, food applications

Résumé

Les nanomatériaux (NM) sont ajoutés aux aliments pour leurs propriétés uniques pouvant améliorer la qualité, la durée de conservation et l'innocuité des aliments. Les nanomatériaux ajoutés aux aliments (désignés nanomatériaux alimentaires (DNM)) soulèvent des problèmes d'innocuité alimentaire tels que mis en évidence par des études démontrant leurs impacts nocifs sur la structure et la fonction de biosystèmes et de biomolécules. Bien que des études aient été menées pour comprendre la toxicité aiguë des nanomatériaux (et des DNM), il existe des lacunes importantes dans les connaissances liées à la transformation des DNM en réponse aux conditions de traitement des aliments et à leur interaction avec des matrices alimentaires et biologiques. Ma thèse porte sur les implications de la transformation des DNM lors de leurs interactions avec des cibles biologiques telles que les protéines et les cellules. Plus spécifiquement, les objectifs de cette thèse de recherche visent à comprendre les effets de la transformation des DNM (silice et oxyde de titane) sur la structure et la fonction des enzymes et des protéines liées à la santé et aux maladies. Le chapitre 2 présente l'état des connaissances sur les applications des nanomatériaux et leurs implications au niveau de l'alimentation et identifie les principaux écarts des connaissances sur le sujet. Le chapitre 3 comprend une analyse comparative des propriétés physico-chimiques et effets de différents types de particules de silice sur l'enzyme trypsine : nanoparticules de qualité alimentaire (FG-NP) et non-alimentaire (NFG-NP), microparticules de qualité alimentaire (FG-MP) ainsi que les variantes de FG-NP liées à la température. Malgré que les résultats ont démontré des similarités entre les FG-NP et les NFG-NP et FG-MP quant à leur composition chimique et leur nature amorphe, les FG-NP se sont avérés contenir relativement moins de groupes siloxane ramifiés et cycliques. Des changements dans le comportement d'agglomération et dans l'abondance relative des différents groupes de silice dans les FG-NP ont également été observés lors de leur exposition à des températures auxquels les aliments peuvent être traités. De plus, l'inhibition de type mixte de la trypsine par des variantes liés à la température des FG-NP et des FG-MP a entrainé une digestion incomplète de la protéine d'albumine de sérum bovin (BSA). Le chapitre 4 dévoile

les conséquences résultant de la modification des surfaces des FG-NP par une protéine isolée (BSA) et une matrice alimentaire complexe (lait) sur l'activité de l'amylase salivaire humaine (HSA). La passivation des surfaces des FG-NP avec la protéine BSA a entrainé la diminution de l'inhibition partielle de HSA. Paradoxalement, les interactions des FG-NP avec le lait ont augmenté l'inhibition de la HSA, ce qui a été attribué à la présence de protéases présentes dans le lait qui digèrent la HSA. Dans le chapitre 5, les facteurs influençant les interactions protéines-DNM (silice et oxyde de titane) ont été identifiés en se basant sur les interactions de protéines individuelles avec les DNM et les interactions du lait avec les DNM (matrice alimentaire modèle). Les études individuelles d'interactions protéine-DNM ont révélé que l'adsorption des protéines sur les particules est influencée à la fois par les caractéristiques des particules et des protéines. En revanche, les facteurs qui déterminent les interactions protéine-biomolécule dominent leur adsorption de surface aux DNM dans une matrice alimentaire complexe. Les résultats des chapitres 3, 4 et 5 démontrent que l'interaction des protéines avec les DNM modifie la structure et la fonction de ces derniers. Par conséquent, j'ai formulé l'hypothèse que l'interaction DNM-protéine pourrait modifier l'allergénicité des protéines alimentaires. Les études détaillées au chapitre 6 décrivent l'altération de l'allergénicité du lait bovin ou des principaux antigènes du lait bovin (β-lactoglobuline et caséine) suite à leur interaction avec les DNM de silice et d'oxyde de titane. Il fut constaté que l'allergénicité du lait et des protéines du lait augmentent lors de leur interaction avec les DNM, et que cette tendance persiste même après une digestion intestinale simulée. L'augmentation de l'allergénicité s'avère être médiée par des altérations de la structure secondaire et tertiaire des protéines du lait, ce qui pourrait avoir exposé les épitopes. Par conséquent, mes études établissent que les DNM sont transformés à la fois par les conditions de traitement des aliments et par leur interaction avec la matrice alimentaire, et démontrent les effets de cette transformation sur la structure et la fonction des protéines qui jouent un rôle dans la digestion et les allergies. Ces études soulignent la nécessité de sonder les effets subléthaux des DNM à l'aide de modèles animaux pour mieux comprendre les conséquences de l'entrée des DNM dans le système gastro-intestinal sur la santé humaine.

Mots clés : nanoparticules, nanoparticules de silice, dioxyde de titane, additifs alimentaires, applications alimentaires

Table of Contents

Lists of Figures

Chapter 2. Introduction & Literature Review

Chapter 3. A comparative analysis of different grades of silica particles and temperature variants of food grade silica nanoparticles for their physicochemical properties and effect on trypsin

Chapter 3. Supporting Information

Chapter 6. Supporting Information

Lists of Tables

Acknowledgement

I want to express my heartfelt gratitude to my PhD supervisor, Professor Saji George, for all the intellectual discussions, patience and guidance. It was a real honour and pleasure to have the opportunity to work with him. My sincere thanks go to my committee members, Dr. Jannifer Ronholm and Dr. Stan Kubow, for encouraging words, thoughtful advice and feedback.

I would also like to thank all Professors and the staff in the Department of Food Science and Chemistry for their support, especially Dr. Varoujan Yaylayan and Dr. Ashraf Ismail, for guiding my experiments and allowing me to use their lab freely. My sincere thanks go to Dr. Joanne Turnbull, Concordia University and Dr. Chithra Karunakaran, Canadian Light Source, for helping and guiding me to complete the enzyme kinetic studies and STXM study.

My colleagues' emotional, technical, and strategic support was essential to completing my dissertation. Especially, I am thankful to Ke Xu for her patience to discuss and find solutions to my problems, Divya Srinivasan, Beatrice Vuilleumier-Kaufmann, and Mengxi Liu for their contribution in some work in chapter 3, and chapter 4. Amarpreet Brar, Ruby Liu, Estee Ngew Shwen Qii, Trisha Sackey, Elisa Ferrante, Joby Bernard, Satwik Majumder, Dr. Aneela Hameed, Amal Sahyoun and Park Soyoung for the encouragement and friendship we have had throughout these years.

I would like to express my gratitude to my friends, Tin Zar Lin, Ei Ei Chan, Khine Haymar Thaung, Hnin Pann Phyu, Khaing Khaing Oo and Khin Mi Mi, who comforted me during difficult times and cared like my close family throughout these years. Also, a big thank you to Uncle Myo Nyunt Swe and Aunty Saw Yee Mya, for their support and care me like their own daughter.

Last but not least, I am infinitely grateful to my parents and my brothers, Kyaw Htay Lynn, Htet Aung and Pyae Phyo Aung, for their endless support and love. Without their support, I would not have come this far and could not have completed my Ph.D. studies overseas. Thank you!

Contribution of Authors

This thesis is presented in manuscript form and consists of seven chapters. In Chapter 1, a general introduction of nanomaterials (NM) in food, the hypothesis and research objectives of the thesis are presented. Chapter 2 is a detailed review of the literature on the properties of dietary nanomaterials (DNMs) and their application, risk assessment of DNMs and the knowledge gaps. Chapters 3 to 6 are presented in the form of manuscripts, which are published in peer-reviewed scientific journals. The connecting statements provide the rational link between the different chapters. Out of these four chapters, Chapter 3 has been published in the 'Journal of Agricultural and Food Chemistry', Chapter 4 has been published in the journal 'Nano Select', and Chapter 5 has been published in the journal 'Nanoscale'. Chapter 6 was submitted for publication in 'Food and Chemical Toxicity'. Finally, Chapter 7 presents an overall conclusion of the thesis as well as scientific contributions and recommendations for future research.

Wut Hmone Phue, the candidate, was responsible for designing and performing the experiments, interpreting the results, and preparing the manuscripts and the thesis. Professor Saji George, the candidate's supervisor, guided experiments of this work, provided direction and research facilities for the experiments, and reviewed the manuscripts and thesis before submission.

The presenting Abstract in French language, Beatrice Vuilleumier-Kaufmann, Elisa Ferrante and Joby Bernard are credited for editing the language issues. In Chapter 3 'A comparative analysis of different grades of silica particles and temperature variants of food grade silica nanoparticles for their physicochemical properties and effect on trypsin', Mengxi Liu contributed in preliminary research work, Ke Xu and Divya Srinivasan contributed in conducting part of experiments and helped with editing the manuscript before submission and Dr. Ashraf Ismail provided research facilities and helped with interpreting the FTIR results, are co-author for chapter 3.

In Chapter 4 'Food Grade Silica Nanoparticles Cause Non-competitive Type Inhibition of Human Salivary α-amylase because of Surface Interaction', Divya Srinivasan contributed in designing this work, Dr. Aneela Hameed edited the manuscript and Dr. Varoujan Yaylayan provided research facilities for the experiments, are co-author for chapter 4.

In Chapter 5 'Protein-biomolecule interactions play a major role in shaping corona proteome: Studies on milk interacted dietary particles', Dr. Mazen Bahadi guided for partial least squares (PLS) analysis, and Dr. James J Dynes, Dr. Jian Wang, and Dr. Venkata S. C. Kuppili conducted a portion of the biocorona imaging and are listed as co-authors for chapter 5. Dr. Ashraf Ismail and Dr. Aneela Hameed provided advice for this work and edited the manuscript before submission, are also listed as co-authors for chapter 5.

In Chapter 6 'Inorganic food additives nanomaterials alter the allergenicity of milk proteins', Ke Xu conducted a part of the degranulation assay experiment and edited the manuscript, is hence a co-author for chapter 6.

Publications

1. A comparative analysis of different grades of silica particles and temperature variants of food grade silica nanoparticles for their physicochemical properties and effect on trypsin. **Phue, W. H.**, Liu, M., Xu, K., Srinivasna, D., Ismail, A. A., George, S., *J. Agric Food Chem*. **2019**, 67(44): 12264-12272.
2. Food grade silica nanoparticles cause non-competitive type inhibition of human salivary α-amylase because of surface interaction. **Phue, W. H.**, Srinivasan, D., Hameed, A., Yaylayan, V., George, S. *Nano Select.* **2020**; 1-10.
3. Protein-biomolecule interactions play a major role in shaping corona proteome: studies on milk interacted dietary particles. **Phue, W. H.,** Bahadi, M., Dynes, J. J., Wang, J., Kuppili, V. S. C., Ismail, A., Hameed, A., George, S. *Nanoscale*. **2021**, *13*, 13353-13367.
4. Inorganic food additives nanomaterials alter the allergenicity of milk proteins. **Phue, W. H.,** Xu, K., George, S. *Food Chem Toxicol.* 2022; 162:112874.
5. The type of dietary nanoparticles influences salivary protein corona composition. Srinivasna, D., **Phue, W. H.**, Xu, K., George, S., *Nanoimpact.* **2020,** 100238.
6. Enhancing the bioavailability of silver through nanotechnology approaches could overcome efflux pump mediated silver resistance in methicillin resistant staphylococcus aureus. George, S., Ignacius, T., **Phue, W. H.**, Gardner, H., Sukumaran, B., *J. Biomed. Nanotechnol.* **2019**, *15*, 2216-2228.

Conference Presentations

1. "Transformation of silica nanoparticles in response to food processing conditions and its effect on trypsin-nanoparticles interaction", **Wut Hmone Phue**; Mengxi Liu; Ashraf Ismail; Saji George*, **2018**, 256th ACS National Meeting, Boston, MA, United States. *(Poster presentation)*
2. "Nanomaterials in food: understanding the fate of protein-nanoparticle interactions", **Wut Hmone Phue**, Saji George*, **2019**, 63rd ICASS conference, Montreal, QC, Canada. *(Oral presentation)*
3. "Interaction of dietary nanoparticles with proteins could negatively impact their nutritional and functional properties", **Wut Hmone Phue**, Mazen Bahadi, Ashraf Ismail, Saji George*, **2020**, SETAC North America 41st Annual Meeting, Toronto, ON, Canada. *(Poster presentation)*

List of Abbreviation

ADI	Acceptable daily intake
ATR	Attenuated Total Reflectance
BApNA	Nα-benzoyl-DL-arginine 4-nitroanilide hydrochloride
BSA	Bovine serum albumin
CAS	Chemical abstracts service
CD	Circular Dichroism
DLS	Dynamic light scattering
DNA	Deoxyribonucleic acid
DNM	dietary nanomaterial
DNS	Dinitro salicylic acid method
DTNB	5,5'-dithio-bis-2-nitrobenzoic acid
ELISA	Enzyme-linked immunosorbent assay
EU	European Union
FCM	Food Contact Materials
FDA	US Food and Drug Administration
EFSA	European Food Safety Agency
FTIR	Fourier Transform Infrared
GI	Gastrointestinal
HPLC	High performance liquid chromatography
HSA	Human salivary α-amylase
IARC	International Agency for Research on Cancer
IDCR	Ionic detergent compatible reagent

Ip	Isoelectric point
IUIS	International Union of Immunological Societies
JECFA	Joint FAO/WHO Expert Committee on Food Assiitves
LAD2	Human Laboratory of Allergic Diseases 2
LC-MS	Liquid chromatography mass spectrometry
LD	Lethal dose
LOAEL	Lowest observed adverse effect level
MNM	manufactured nanomaterial
MW	Molecular weight
NM	nanomaterial
NP	Nanoparticle
PAGE	Polyacrylamide gel electrophoresis
PBS	Phosphate buffered saline
PLS	Partial least squares
PMT	Photon multiplier tube
PQ	partitioning quotient
RB	Rose Bengal
RT	Room temperature
SAS	Synthetic amorphous silica
SD	Standard deviation
SDS	Sodium dodecyl sulphate
SEM	Scanning electron microscopy
SGF	Simulated gastric fluid

SIF	Simulated intestinal fluid
SML	Specific Migration Limit
SPION	Superparamagnetic iron oxide nanoparticles
SSF	Simulated salivary fluid
STXM	Scanning transmission X-ray microscopy
SVD	Singular value decomposition
TEM	Transmission electron microscopy
TMB	Tetramethylbenzidine
US	United States
VIP	Variable importance in projection
WHO	World Health Organization
XRD	X-ray diffractometry
XPS	X-ray photoelectron spectroscopy

Chapter 1. General introduction

1.1 Introduction

'*Nanotechnology is the creation of functional materials, devices and systems through control of matter on the nanometer length scale (1-100 nm), and exploitation of novel phenomena and properties (physical, chemical, biological, mechanical, electrical) at that length scale*' [1]. The term 'manufactured nanomaterials (MNM)' is used to describe a material purposefully manipulated at the nanoscale that exhibits novel properties and behaviors as a result [2]. Due to their unique properties, they have a wide range of applications including applications in food, medicine, cosmetics, consumer products and agriculture apart from electronic, and other industrial sectors. Applications of nanotechnology are rising in agriculture, food and feed sectors with new and enhanced properties.

In September 2003, the US Department of Agriculture projected the potential of nanotechnology to address current and emerging challenges for the Agri-food sector [3]. Currently, nanotechnology is applied in every step of the food supply chain from cultivation, production, processing to consumption. According to European Nanotechnology Gateway definition, NMs, or nanotechnology used in the food supply chain is referred as 'nanofood' [4].

There are two types of nanofood applications in the food industry viz- food packaging (outside application) and food additives (inside application) to improve quality, shelf life, safety, and healthiness of foods. The innovation of NMs has resulted in a steady increase in number of NM-containing food and agriculture products. While there are obvious benefits from the use of NMs in the food sector, there are also some concerns about public safety and environmental, ethical, policy, and regulatory issues [5].

NMs are significantly different from their bulk counterpart due to their high surface area, surface exposed atoms/molecules, and dominance of quantum effects. Unprecedented chances for

exposure of MNM to human health and/or environment are increasing and the interactions of MNM at the molecular or physiological levels are cause of concern for human health [6]. The applications of NMs in food products (Dietary nanomaterials -DNMs) present direct human exposure scenario through oral route. Although, results from studies on the acute toxicity of DNMs suggest these materials to be benign, there are several knowledge gaps on the transformation of these materials in the food supply chain and how these changes influence the health risk aspects of DNMs. For instance, there are evidence to suggest that DNM becomes surface coated with biomolecules (biomolecular corona), especially with proteins (called protein corona) that can alter their bioavailability in the body [7]. Protein corona formation is influenced by particles size and size distribution, surface charge, particle composition and solubility [8]. On the other hand, the surface chemistry of DNMs tends to change during the food processing stages including heating and that transformation could affect the adsorption of protein onto the particles [9].

1.2 Hypothesis

The physicochemical properties of DNMs such as surface chemistry, surface charge, size, and morphology are the key players that shape outcomes of DNMs interactions with biological systems. Previous studies have shown that the physicochemical properties of NMs are likely to change in response to physical and chemical factors of the microenvironments in which they are embedded [10]. With this background knowledge, there were hypothesize that,

(1) the physicochemical properties of DNMs could be altered by food processing and storage temperature and this change would alter DNM-protein interactions

(2) the surface passivation of DNMs would ameliorate adverse outcomes from DNM-protein interactions

(3) factors identified through studies involving individual protein-DNM interaction could be used for predicting the type of protein present in the surface corona of DNMs interacted with varied food matrices

(4) allergenicity of food proteins could be altered when interacted with DNMs because of alterations in protein structure

1.3 Research objectives

The overall objective of this research is to understand the transformations of DNMs in food and its influence on hazard potential. The specific objectives are:

I. to understand the physicochemical transformation of DNMs when subjected to simulated food handling temperatures and their effect on functional properties of a digestive enzyme (trypsin)

II. to understand the effect of DNMs surface modification with single protein and food matrix on the functional properties of a digestive enzyme (human salivary α-amylase- HSA)

III. to understand factors influencing the adsorption and persistence of proteins in the surface corona of DNMs interacted with milk

IV. to understand the adverse effect of DNMs on food allergy.

Chapter 2: Introduction & Literature Review

2.1 Introduction

Nanotechnology is an emerging technology platform that is widely exploited in many industrial sectors including electronic, engineering, medical, consumer products and Agri-food. NMs have unique properties relative to their macroscale counterparts as their high surface area to mass ratio amplifies availability of surface exposed atoms/molecules for interactions with external entities [11]. Currently, NM application in food industry stretches from food production, manufacturing, and processing to packaging. Silica, titania, silver, and zinc are the manufactured NMs (MNMs) commonly used for various applications in food. MNMs of silica and titania are high-volume production NMs that are used as food additives. This chapter reviews the current and emerging application of MNMs in food and highlights the knowledge gaps in understanding the material transformation during food processing and its possible health implications.

2.2 Nanoscience and Nanotechnology

Nanoscience is the science of studying structures at the scale of nanometers [12]. The European Union (EU) defines nanotechnology as the "*term given to those areas of science and engineering where phenomena that take place at dimensions in the nanometer scale are utilized in the design, characterization, production, and application of materials, structures, devices and systems*" [13]. In biochemistry and biology, the study of nanoscale objects such as deoxyribonucleic acid (DNA), viruses, cells components, subcellular organelles and gap junctions is the main focus; while in the food industry, the interest is more directed towards the applications and the safety implications of nanostructured food additives [12, 14].

2.2.1 Nanomaterials

Broadly, materials with any external dimension in the nanoscale or having internal or surface structure in the nanoscale can be regarded as nanomaterials (NMs) [15]. The European Commission defines a NM as a "*natural, incidental or manufactured material containing particles, in an unbound state or as an aggregate or as an agglomerate and where, for 50% or more of the particles in the number size distribution, one or more external dimensions is in the size range 1nm-100 nm*" [16]. The ability to synthesize and stabilize MNM has been revamping materials applications in diverse sectors such as pharmaceuticals, drug delivery systems, diagnostics, medical technology, electronics, food, and agricultural technology [17-19].

MNMs can be designed to be of different shapes, sizes, structures, and properties depending on manufacturing and environmental conditions. MNMs can either be classified as nano-objects, which are at the nanoscale in any external dimension, or as nanostructured materials if they exhibit nanoscale dimensions in an internal or surface structure [20]. Nano-objects can be sub-categorized into three groups: nanoparticles, nanofibers, and nanoplates. These MNMs can be organic, inorganic, and combined organic and inorganic. The classification of MNMs is shown in Figure 2.1.

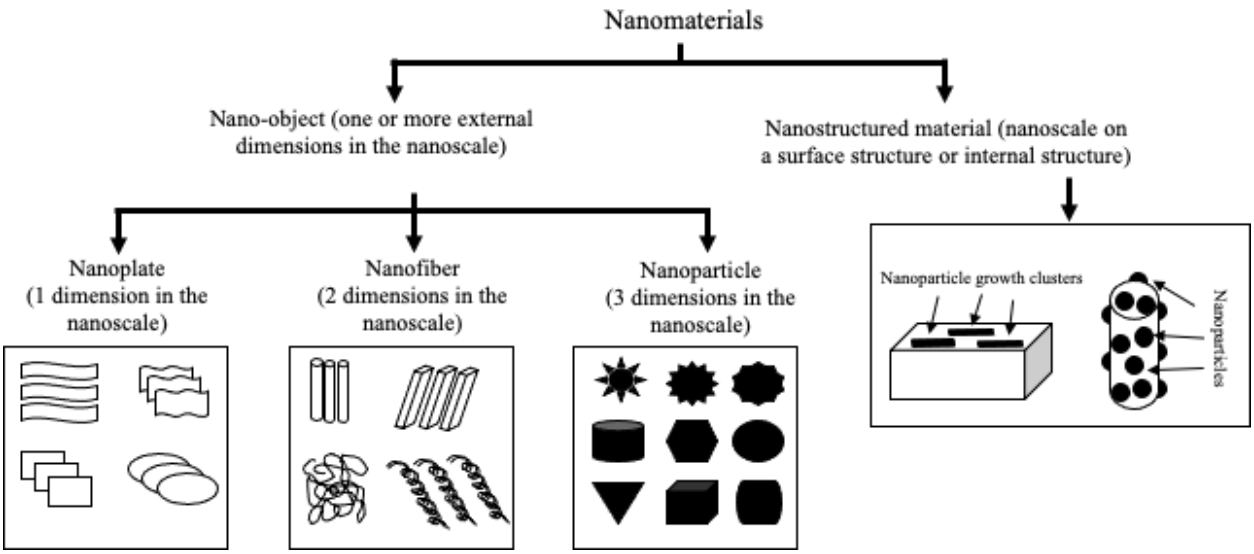

Figure 2. 1 Classification of MNMs [20]

MNMs can be produced by two different approaches: bottom-up and top-down. The bottom-up approach creates MNMs by the self-assembly of atoms or molecules in the nanoscale [19]. Sol-gel methods, crystallization/precipitation, chemical vapour deposition, and self-assembly routes are commonly used for bottom-up synthesis [21]. The top-down approach breaks down a larger scale material into fine nanoscale particles by various size-reducing techniques such as sputtering, milling, grinding, chemical reactions, and thermal or laser ablation [19]. Bottom-up synthesis of MNMs gives better control, homogeneity, and fewer defects than the top-down approach [22].

2.2.2 Properties of MNMs

MNMs are in the transition region between atomic/molecular structures and bulk materials. The properties of MNMs change largely depending on size, structure, surface chemistry, and quantum confinement [23]. When the dimensions of materials are reduced to nano range, the surface area and interface of particles increase, and the gap between energy levels decrease. As a result, novel optical, magnetic, electronic, physical, chemical, and mechanical properties appear [21, 24]. MNMs generated with same chemistry but with variations physical dimension would exhibit

different properties [21, 25]. When the dimensions of MNMs are in the visible range (400-700 nm), colour and luminescent properties can be observed [23]. Depending on the size, shape, and type of materials, their light emissions are significantly different. For example, the color of silver nanoparticles solutions vary from yellow to reddish based on size and shape [26]. The properties of MNM will be different depending on size, size distribution, shape, concentration, agglomeration, surface charge, surface area, composition, and structure. For example, the catalytic properties of gold nanoparticles were significantly enhanced when their size was reduced to 2-10 nm [27]. As the size of the particles get smaller, the hardness of particles gets stronger. Gerberich and colleagues proved that 20-50 nm radii range silicon nanospheres are four times harder than bulk silicon [28, 29].

2.2.3 MNMs in Food

The novel properties of MNMs opens unprecedented opportunities to address various challenges faced by the food industry [30]. MNMs can be utilized at every stage of the food supply chain: in farming, processing, storage, and quality control [31, 32]. At the farming stage, MNMs are used to deliver pesticides, drugs, feed additives, and antibiotics to prevent pathogens growth and to increase the growth rate of plants and animals [31]. The application of MNMs in food processing is mainly to achieve higher efficiency. One advantage of bringing water-insoluble additives to the nanoscale is that they can disperse well in food formulations without the use of additional fats or surfactants [33].

To develop and improve color, flavor, texture, and shelf-life of food products, MNMs are used as food at the food processing stage [34]. For example, silica nanoparticles are added to dried powdered foods to prevent caking and clumping. MNMs are also used in nanoencapsulation and nanoemulsion systems to deliver nutrients, flavour compounds, and bioactive molecules more

effectively at the consumption stage. Nanoencapsulation and nanoemulsion are methods meant to protect bioactive food components during food processing and digestion in the gastrointestinal (GI) tract [35]. At the food storage stage, MNMs are incorporated as sensors and as nano polymer matrices to improve food packaging. This advanced form of packaging can detect spoilage and contamination of food, extend shelf-life and freshness to food the products, improve the gas barrier, and prevent microbial growth [31]. For example, silver nanoparticles have been given a lot of attention due to their antimicrobial properties, which are higher compared to organic compounds such as essential oils, organic acids, enzymes [36], and as a result, they are utilized in food packaging to protect microbial proliferation on food. MNMs are also used in food supplements for targeted delivery of nutraceutical compounds. The application of MNMs in the food industry is summarized in Figure 2.2.

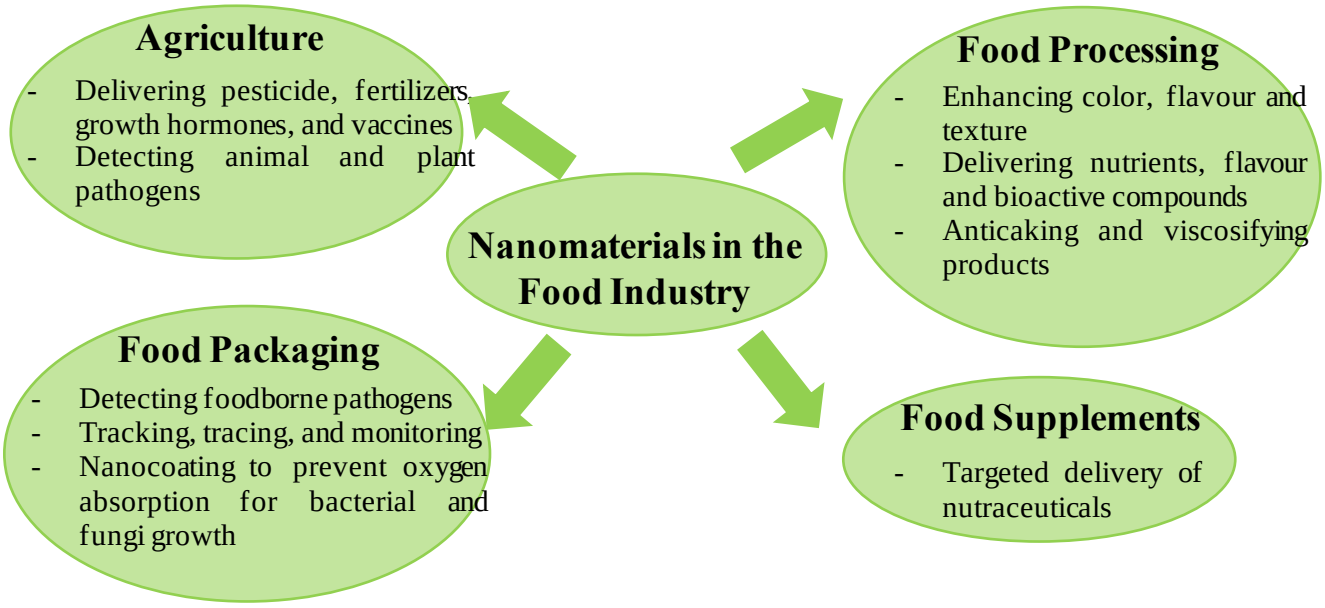

Figure 2. 2 Application of MNMs in the food industry

As of 2014, according to a report by the EFSA (European Food Safety Agency), 276 NMs were commercially available and 55 types of NMs were already used in food products, food contact materials, feed, and for agricultural purposes [37]. Most of the MNMs belong to the inorganic category and can be commonly found in food products themselves or in the packaging. The second-generation MNMs, surface-functionalized MNMs, are created to impart specific functions in the food matrix, allowing to improve shelf-life and antimicrobial activity [33]. Most of the organic NMs are naturally occurring substances and/or are developed and used in food and feed applications such as food additives, supplements, and antibiotics [33].

The four most popular MNMs in food applications are silica, titania, zinc oxide, and silver [38]. The Acceptable Daily Intake (ADI) of food additives reported to contain NMs, as determined by the Joint FAO/WHO Expert Committee on Food Additives (JECFA) and the EFSA reports, are presented in Table 2.1. Aluminum-based silicates is not specified; instead, the accepted value is that of aluminum itself, which is an ADI of 2 $mg.kg^{-1}$ body weight [39]. The summary of the purposes, functions, and ADI/SML of NMs in food applications are shown in Table 2.1.

Table 2. 1 Application of nanoparticles in food products

Type of NMs	EU Code	Area of application	Purpose	Function	ADI/SML	References
Silica	E 551	Food processing, food packaging	Additive, packaging	Flowability, anti-caking properties, anti-clumping properties	Not specific or not limited ADI	[40-43]
Sodium aluminum silicate	E 554	Food packaging, dietary food supplements	Packaging, supplement	Thermal stability, mechanical strength, gas barrier properties	Not specified	[39, 44]
Potassium aluminum silicate	E 555	Food packaging, dietary food supplements	Packaging, Supplement	Thermal stability, mechanical strength, gas barrier properties	Not specified	[39, 44]
Calcium aluminum silicate	E 556	Food packaging, dietary food supplements	Packaging, Supplement	Food packaging, dietary food supplements	Not specified	[39, 45]

Aluminum silicate	E 559	Food packaging, dietary food supplements	Packaging, supplement	Thermal stability, mechanical strength, gas barrier properties	Not specified	[39, 46]
Titania	E 171	Food processing	Coloring agent	Enhancing food colour/brightness	Not available	[47-49]
Zinc oxide	FCM 1050	Food processing, food packaging	Packaging, supplement	Antimicrobial properties	SML- 25mg/kg	[36, 50, 51]
Metallic silver	E 174	Food packaging	Packaging	Antimicrobial properties	SML- $\leq$0.05 mg/kg	[36, 52, 53]
Iron oxide	E 172	Food processing	Coloring agent	Food colour enhancer	ADI of 0-0.5 mg/kg	[54, 55]
Metallic gold	E 175	Food processing	External colour coating	Decoration of chocolates and liqueurs	Not available	[53, 56]

FCM- Food Contact Materials, **E**- Europe, **ADI**- Acceptable Daily Intake, **SML**- Specific Migration Limit

2.3 Silica (SiO_2) Nanoparticles and their Surface Chemistry

Silica, also known as silicon dioxide, is composed of silicon and oxygen molecules. It has been existing since the Earth was formed and is commonly found as the major constituent of sand, as quartz, and in various living organisms [57]. The world did not notice the existence of the silicon element until Swedish chemist Jons Jacob Berzelius made the discovery in 1824 [58]. The element name, "silicon", was proposed by Thomas Thomson in 1831; it comes from the Latin word "silex" or "silicis", which means "flint" [59]. Before silicon was defined as an element, a "semisolution of silica" was created as early as 1747 by Pott, who published a paper about the preparation of sol of "hydrated silica" in 1820 [60, 61]. Silica gels were firstly investigated by Graham in 1861 [60]. Starting from 1887, silica has been used in the production of electrical components and since 1907, it has been used on an industrial scale by the B.F. Goodrich Company [60]. The production of high silica volumes started only in 1946 because the previous production methods resulted in an unstable silica with both low yield and low reproducibility [59, 60]. The first pure precipitated silica was introduced to the European market in 1951 [60]. After Muller and colleagues stated that mesoporous silica might have pharmacological activity in 1998, it was developed into a drug delivery device by Balkus and colleagues in 2001 [62].

Initially, silica particles have been used as catalysts, coating materials and in electronic components, and in 1933, silica sols were used in tobacco to keep its freshness [60]. Fumed silica was firstly introduced in 1942 for food applications by using the original flame hydrolysis process with SiF_4, which was replaced by $SiCl_4$ in 1955 due to its high toxicity through inhalation [60]. Silica nanoparticles were approved as food additives by the WHO in 1987 [63] and since 1999, silica has been used in the production of plastic materials for food packaging [64].

Silica particles can be classified based on their crystallinity, dispersity, surface composition, and porosity [65]. According to crystallinity, silica particles can be divided further into two types: crystalline and non-crystalline. Quartz, tridymite, cristobalite, stishovite, and coesite fall under the crystalline group, whereas opal, lechatellierite, and kieselguhr fall under the non-crystalline group (amorphous silica group) [65]. The physical phase of silica can change depending on temperature, pressure, and degree of hydration [66]. The crystalline state of silica at room temperature changes to the tridymite phase at 870˚C, then to the cristobalite phase at 1470˚C, and finally becomes amorphous silica at 1670˚C [66]. The tridymite phase can be found in volcanic siliceous rocks and the cristobalite phase, on the other hand, is present in metamorphosed sandstones and some volcanic siliceous rocks [67]. Soluble silica, silica sols, hydrogel silica, xerogel silica, aerogel silica, and precipitated silica are separated based on dispersity and are mostly found in the amorphous form [65]. The classification of silica particles depends on the composition of their surface functional groups such as Si-OH/ Si-O-Si, Si-O-C, Si-C, and Si-N. The porosity of silica particles also plays an important role in classifying silica particles. Shape, width, and pore distribution within the solid particles are used to characterize the pore system [65]. Porous silica can be either amorphous or crystalline. Porous silica is one of the amorphous products that is thermodynamically and kinetically unstable [65].

Understanding the surface chemistry of silica particle is helpful to better tune the adsorption behaviour and chemical reactivity of silica for different purposes. The surface of silica particles is mainly composed of a siloxane group (Si-O-Si/ Si-O) and silanol groups (Si-OH) [68]. The bond length of Si-O is the shortest and strongest bond in silica, and it is responsible for the stability of the siloxane group [65]. The silicon atom forms a tetrahedral unit with four oxygen atoms $[SiO_4]^{4-}$. Hydroxyl groups are attached to oxygen at room temperature and form silanol groups. The silanol

groups on the surface of silica are important for surface modification and reactions between silica particles and other components [68]. There are three types of silanol groups on the amorphous silica surface depending on the number of hydroxyls attached on the surface: isolated, germinal, and vicinal [65, 69]. Amorphous silica is highly disordered because it is influenced by hydroxyl groups [70]. According to the previous research report, 20 percent of isolated silanols and 9-30 percent of germinal silanols are present on amorphous silica particles [68]. The possible structures of silanol groups are shown in Figure 2.3.

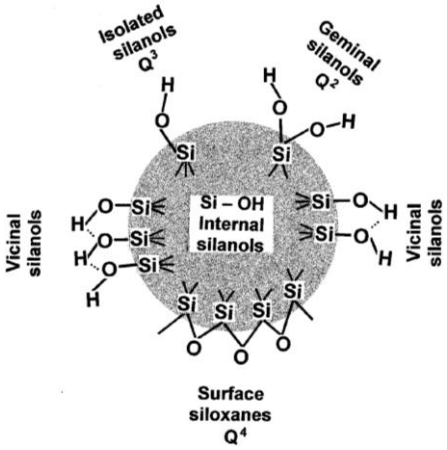

Figure 2. 3 Different functional groups encountered on the amorphous silica surface [71]

Two main type of silica particles are commercially available: hydrophilic and hydrophobic silica. Silica particles that have a freely accessible silanol group (Si-OH) on their surface are hydrophilic silica, and those that have organic groups attached to silanol groups via covalent bonds or siloxane groups on their surface are hydrophobic silica. The surface structure of silica particles changes depending on thermal treatment and pH. The dehydration process, which happens at different temperature as presented in Figure 2.4, affects the surface chemistry of silica particles. The physically bound water on silica surface is removed at 343 K (~ 70˚C) and the silanol groups (chemisorption water) on the silica surface (external silanol groups) are removed at 873-1073 K

(436-800 ˚C). Finally, the silanol groups under the silica surface (internal silanol groups) are removed at 1273 K (~1000 ˚C) or above [68]. At about 773 K, hydroxylation and dihydroxylation processes are reversible, which means that silanol can be converted into siloxane when the dehydration process is done up to about 773 K [65].

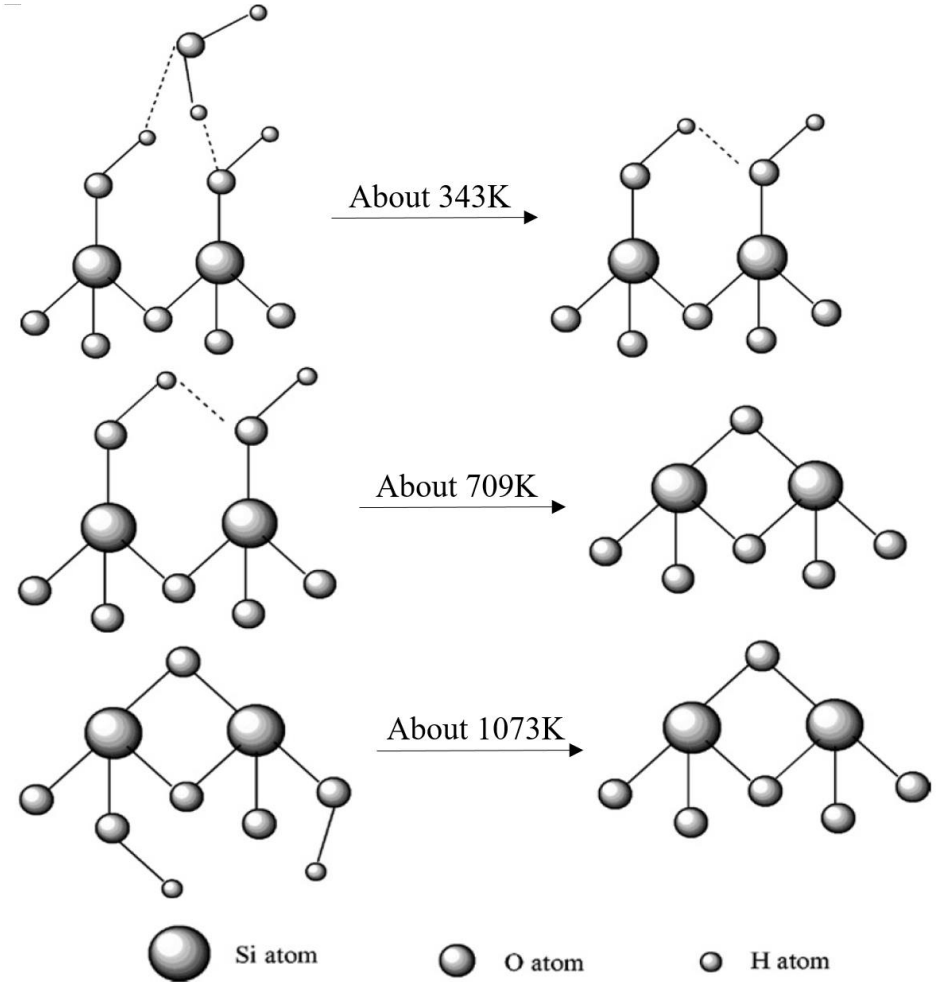

Figure 2. 4 Dehydration process of silanol groups at different temperatures [68]

The pH level is one of the important factors regarding the modification of the silica surface because protonation and deprotonation processes occur. Barisik and colleagues reported that a high pH level and a high salt concentration decreased the concentration of H^+ ions on the silica surface and

as a result, SiOH groups dissociated to SiO^- [10]. Hence, increasing pH and salt concentration leads to higher negative surface charge density on the silica surface.

The density of silanol groups and ring structures on the silica surface also depends on the synthesis process. Colloidal silica has a high total hydroxyl content with vicinal silanol but isolated silanol groups are not present. As for fumed silica, it has a lower total hydroxyl content and a higher level of isolated silanol groups relative to colloidal silica [69]. The surface area and smoothness of particles might change depending on the concentration of hydrogen-bonded silanol groups [69]. When the temperature increases, surface dihydroxylation occurs on colloidal silica and the concentration of hydrogen-bonded silanol groups decreases. While the surface area and smoothness of colloidal silica might change after thermal treatment, it does not affect the integrity of fumed silica, making the latter more thermally stable than the former [69].

Three-membered siloxane rings are present in the fumed silica structure, while they are not encountered in colloidal silica [69]. It is due to thermal quenching freezes in a high-temperature environment. The hydroxyl radicals are formed in exothermic reactions when fumed silica is hydrated with water and oxyradicals [69]. The large-membered rings on the surface are formed by cleaving bonds of three-membered ring and four-membered ring [72, 73].

2.4 Titania (TiO_2) Nanoparticles and their Surface Chemistry

Titania, also known as titanium dioxide, was first discovered in the late eighteenth century, and since the early twentieth century, it has been used in many different applications such as paints, cosmetics, energy storage, photocatalysis and food. Titania has a high refractive index, brightness color, and resistance to discoloration, and it is commonly used as a pigment due to its physical properties [74-76]. Three crystalline forms exist: anatase, rutile, and brookite. Synthesized anatase

and rutile are commonly used as pigments in many different areas due to their high oxidative power, photostability, low cost, and less toxic effect [77]. Anatase and rutile have a tetragonal structure and brookite has a rhombohedral structure, as shown in Figure 2.5 [78].

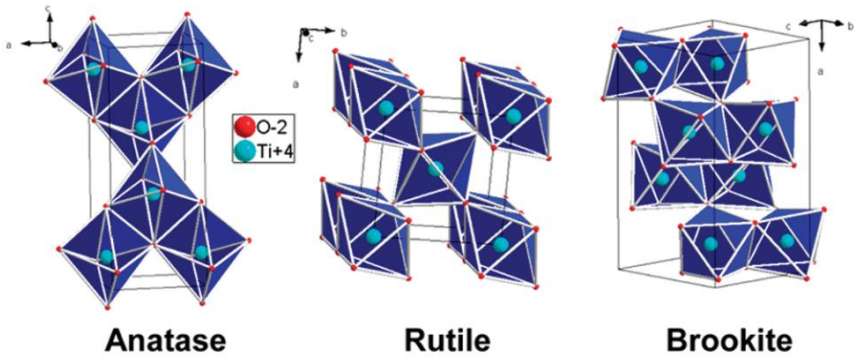

Figure 2. 5 Structure of titania in the anatase, rutile, and brookite forms [78]

In the late 1800s, titania was used as an opacifier, and it was upgraded to be used in glazes and vitreous enamels as an additive to increase acid resistance. From 1908 onward, Norway and the United States (US) researchers started to develop a range of colors from reddish to off-white by using titania. The commercial manufacturing of anatase-based pigments was ramping up from 1916 in the US and from 1918 in Norway. In the beginning, the titania pigment was composited with barium sulfate and calcium phosphate, and the pure pigment started to be manufactured in 1923 in France and 1926 in the US. The anatase form was converted to rutile at high temperatures, and the rutile pigment was found to have a better masking power and weathering properties than anatase. From 1948 onward, rutile pigment has been commercially manufactured. Titania was mixed with other compounds: calcium, silicon, magnesium, zinc, and antimony, to improve properties or reduce cost. Titania can be made into color pigments by adsorbing an organic colorant onto titania. Titania pigments started being printed on damask and cotton from 1923 and was found in artists' palettes since 1925 [79, 80]. Since 1969, the EU approved anatase form titania to use as coloring food additive (E171) [81].

Among the three crystalline forms of titania, rutile and anatase are commonly found in consumable products. Anatase and rutile are composed of titanium and oxygen atoms, and one titanium atom is coordinated octahedrally by oxygen [78, 82]. In the anatase phase, the structure is constructed by four titania units (12 atoms) in the conventional unit cell. In the rutile phase, the structure is assembled by two titania units (6 atoms) in the conventional unit cell. Each O atom is linked with three Ti atoms through one long bond (apical) and two short bonds (equatorial) [83]. Thus, the main difference between rutile and anatase is the assembly pattern of the octahedra and the distortion of each octahedron. Each octahedron is in contact with ten neighbour octahedra in the rutile structure, while eight in the anatase structure [84]. Due to this reason, the rutile structure is more thermodynamically stable than its anatase counterpart. When the temperature is higher than 373K, anatase is transformed to rutile [84, 85].

2.5 Use of Silica and Titania Particles in Food

Silica particles have been widely used as food additives in powdered food products and go under the designation E551 (European Union code-551) on the label of food products [40]. They have useful applications not only in the food industry, but also in the areas of medicine, electronics, construction, and space technology. Silica is approved as a food additive by the World Health Organization (WHO) since 1987 and the use of silica nanoparticles in the food industry has expanded over the past decade [63]. The European Union (EU) also permits synthetic amorphous silica (SAS) nanoparticles as E551, with a CAS registry number of 231-545-4 to be used in food [40].

Silica comes in a white, fluffy powder or granules with hygroscopic properties [86]. SAS nanoparticles are mainly used as an anticaking agent in powdered foods such as sweeteners, milk powder, salt, instant powder, and so on. Food supplements, soups, seasonings, processed cheese,

sausages, and certain confectioneries also contain silica nanoparticles [86]. SAS particles are also used in the food packaging process [87]. Dekkers et. al. examined the proportion of nanosized silica compared to bulk silica in 12 commercial edible products that contained E551, such as vitamins, instant noodles, powdered products, creamers, and cake mixes. The size of the particles analyzed ranged from 10 to 200 nm, and in worst-case estimations, there was 50% of the total silica present in the nano form [88]. Natural inorganic silicon compounds are present in foodstuffs as hydrated silica $SiO_2.nH_2O$ and as derivatives of orthosiliceous acid $Si(OH)_4$ such as calcium, sodium, and magnesium silicates [89]. This inorganic silicon may also increase the concentration of silica nanoparticles in food products.

The estimated daily intake (EDI) of E551 is 9.4 mg SAS.kg^{-1} body weight per day, and the primary particles size is 30-200 nm including aggregated and agglomerated particles [90]. However, the properties of SAS nanoparticles do not stay constant throughout the gastrointestinal tract because silica nanoparticles aggregate at high electrolyte and low pH conditions [91]. For example, studies have found that silica nanoparticles maintain their nanosize in low-fat coffee creamer while aggregating in gastric fluid and saliva [92].

Titania nanoparticles are widely used in food products as a coloring agent to enhance food color [76] and are commonly known as “titanium white”. It is authorized for use in the EU as E171 [48]. US FDA also approved it as a color additive not only in food but also in drugs, cosmetics, and contact lenses [93]. Both the anatase and rutile forms of titania particles are used as food additives [48]. Titania is mainly used in dairy products and candy including chewing gums, chocolate, and powdered sugar toppings, as well as in beverages [76]. Titania particles are highly stable as they are resistant to heat, light, oxygen, and pH; therefore, almost any food processing conditions do not affect their properties [94]. In the US, exposure of titania nanoparticles is approximately 1.1-

2.2 mg/kg body weight/day. Young children are the most exposed to titania consumption, due to its high presence in candies [76, 84]. The EU stated that E171 is under Group II: food colors authorized at *quantum satis* which means that "no maximum level is specified and that should be used at levels not higher than deemed necessary for the product". In the US, the FDA allows the presence of E171 below 1% of the total weight of the product [81]. Titania nanoparticles are also used not only in food but also in medical products, toothpaste, and UV protection cosmetic[76], with potential to enter human body through oral route.

2.6 Interaction of Silica and Titania Nanoparticles with Proteins

Proteins strongly interact with hydrophobic particles, while the interactions with hydrophilic particles dependent on the conformational stability of the proteins themselves [95]. The interaction between nanoparticles and proteins are based on entrapment, adsorption, and covalent binding, as influenced by pH. In a study by Bharti and colleagues, adsorption of lysozyme on silica particles occurred only at a pH value above 4, because the isoelectric point of silica nanoparticles is around 3 (SiO_2- pI ~3) [96]. When the pH level reached 10, the charge of protein-adsorbed silica nanoparticles was stabilized, thus causing less aggregation than around pH 4-6 [96]. The adsorption of lysozyme on silica nanoparticles lead to the protein-mediated aggregation of silica nanoparticles, which increased the primary size of the particles [97]. At pH 7-9, the lysozyme and the silica nanoparticles were completely bound and loosely aggregated because of the repulsion between the negatively charged complexes [96].

The interaction of silica nanoparticles and proteins was found to be a function of the size of silica nanoparticles [98]. The stability of the protein corona is inversely correlated with the size of the nanoparticles on which proteins are adsorbed, since larger particles have a greater degree of interactions, which causes perturbation in the protein structure [98].

Stazer and colleagues examined the conformational changes of proteins after adsorbing onto silica nanoparticles. Lysozyme, β-casein, and ribonuclease A did not undergo any conformational modification upon interacting with any size of silica nanoparticles, whereas the conformation of myoglobin and BSA (bovine serum albumin) did change after adsorption on larger silica nanoparticles (above 150 nm) [99]. For cytochrome C and ovalbumin, the results were unclear. Authors claimed that the higher α-helical content of myoglobin and BSA is what made them more vulnerable to conformational changes upon contact with the nanoparticles. These changes were either reversible or irreversible [99]. One study showed that irreversible

conformational changes occurred in proteins when they were exposed to superparamagnetic iron oxide nanoparticles (SPIONs) [100]. In short, the conformational changes are dependent on both the types of nanoparticles and types of proteins.

In 2016, Momeni and colleagues found that titania nanoparticles affect the stability and structure of bovine pancreas trypsin. They claimed that the interaction between trypsin and titania nanoparticles are electrostatic interaction, and titania nanoparticles inhibit trypsin enzymatic activity non-competitively. The secondary structure of trypsin also changed by decreasing the % of α-helix structure content and increasing β-sheet content [101]. The α-helical structure of human serum albumin was lost, and the random coil content was increased after interacting with the titania nanoparticles [102].

Based on outcomes from the above-mentioned studies, it can be concluded that the health risks associated with the consumption of nanoparticles vary based on size, concentration, physicochemical properties, and form of nanoparticles in food products. Environmental conditions also affect the properties of nanoparticles. Without a deep understanding of the transformation of MNMs in food during processing and digestion, it is difficult to comprehend health risks associated with consumption of MNMs.

2.7 Fate of ingested MNMs and cellular processing

MNMs are used in many different applications, which all involve direct contact with the human body. When MNMs enter biological environment or interact with food matrix, they encounter larger biomolecules (proteins, lipids, carbohydrates), sugars, salts, and metabolites. These molecules promptly adsorb onto MNM's surface and create a coating around the materials, referred to as the surface corona. Protein is one of the major components of surface corona and the protein layer formed on the surface of materials is termed as protein corona. Protein corona comprises hard protein corona and soft protein corona [103]. The hard corona

is defined as '*the corona composed by tightly bound proteins that do not readily desorb from the MNMs*', whereas soft corona is specified as '*the corona featured by loosely bound proteins*' [104]. Hard corona has larger net binding energy adsorption (ΔG_{ads}), indicating higher stability of the protein-MNMs complex. Proteins in soft corona characterized by low ΔG_{ads} are those that get adsorbed easily onto material surface and return to the solution [103].

The adsorbed biomolecules influence the biodistribution and toxic potential of MNMs. Consequently, the surface corona defines the biological identity of MNMs. For instances, studies conducted on gold nanoparticles suggested that preformed protein corona could lower nanoparticle adhesion onto the cell membrane [105]. Further, the surface free energy of the particles was decreased due to corona formation, and it reduced the contact of nanoparticles with the cell membrane. Subsequently, the cellular uptake of nanoparticles was lowered in the presence of serum proteins that effect will be varies according to the type of corona, cell and nanoparticles [105].

2.8 Risk Assessment of Silica and Titania Nanoparticles

The risks assessment of silica nanoparticles is based on the ADME (adsorption, distribution, metabolism, and excretion) parameters. According to the World Health Organization (WHO 2000), "Environmental exposure to ambient quartz dust can occur during natural, industrial, and agricultural activities" [67]. The estimated daily intake (EDI) of the food additive amorphous silica (E551) is 9.4 $mg.kg^{-1}$ body weight per day [90]. In comparison, the LD50 of silica nanoparticles is higher than 3,000 $mg.kg^{-1}$ body weight as determined from exposure studies conducted rodent models [88]. Different lowest-observed-adverse-effect level (LOAEL) were calculated based on experimental conditions and type of SAS nanoparticles. Zande and colleagues proposed the LOAEL of 1000 $mg.kg^{-1}$ body weight per day for NM 202 (fumed silica), based on 84 days of exposure by oral gavage [106]. Another experiment by

Nishimori and colleagues showed that the LOAEL of SP 70 (colloidal silica) was 10 $mg.kg^{-1}$ body weight per day following 30 days of exposure by intravenous injection [107]. According to these results, SAS nanoparticles injected intravenously have a higher toxic effect compared those administered orally.

In 2010, Fent and colleagues identified the uptake of silica nanoparticles in the early stage of zebrafish development, as monitored by fluorescence labelling of silica nanoparticles. The fluorescence signal was not observed in zebrafish, which suggests that the uptake of silica nanoparticles might be lower than the limit of detection of confocal microscopy. No toxic effect on the embryos at concentrations between 0.0025 and 200 $mg.L^{-1}$ of fluorescent-labelled silica nanoparticles was observed [108].

In 2013, Dekkers and colleagues investigated the health risks linked to the ingestion of silica nanoparticles in food as they progressed through the gastrointestinal tract. They reported two possible scenarios: when the particles were dissolved in the gastrointestinal tract, no adverse effect were observed; but when they remained undissolved, they posed some risk. They demonstrated that 10 to 40 percent of the total silica weight found in soup and pancake products were not dissolved in the gastrointestinal tract, and that number rose to 80 percent in the case of coffee creamer. They confirmed that the undissolved silica nanoparticles from the food products were still remaining as nanoparticles after the intestinal phase by using an *in vitro* digestion model mimicking gastrointestinal tract conditions. Dekkers and colleagues also summarized the available data on the distribution of silica nanoparticles in body tissues from in vivo studies, and they concluded that silica nanoparticles accumulated mainly in the liver and spleen [90].

Kesteren and colleagues found that the gastrointestinal absorption, tissue distribution, and accumulation of SAS nanoparticles in tissues varied depending on administration time, types

and sizes of SAS nanoparticles, concentration, pH level, and different routes of exposure [109]. The level of accumulation of SAS nanoparticles was different from one tissue to another, and consistently decreased with a longer recovery time. The authors concluded that dose and bioavailability may not correlate, and this phenomenon may happen because of pH dependent gelation properties of silica [106].

During food processing, the primary SAS agglomerate, causing changes in size, shape, as well as physical and chemical properties [88]. The surface charge of silica nanoparticles is important for the delivery of food components into the human body, and the surface charge density depends on the size of the particle, pH, and ionic concentration [10]. One study by Zhang and colleagues showed that under temperature variation, the size and properties of colloidal silica nanoparticles changed, while they remained the same in fumed silica nanoparticles [69]. Fumed silica nanoparticles have a higher thermal stability than colloidal silica nanoparticles because of their lower hydroxyl content. Physicochemical properties of silica nanoparticles may also change after interacting with macro or micro biomolecules such as nucleic acids, carbohydrates, lipids, proteins, minerals, ions, and water in food. Bantz and colleagues investigated the agglomeration state and size of silica nanoparticles changing under physiological conditions. In their study, two types of silica nanoparticles were used: negatively charged silica nanoparticles and positively charged polymer-coated silica nanoparticles. They found that negatively charged silica nanoparticles were stable under physiological salinity and unstable in the presence of proteins, while positively charged polymer-coated silica nanoparticles were unstable in both conditions [110]. These findings are of relevance when silica nanoparticles are used for the delivery of bioactive components in the human body.

Titania is commonly used in the food and pharmaceutical industries. The acute oral toxicity of titania is very low: the oral LD_{50} value for mice is > 10g.kg^{-1} body weight per day and for rats is > 25 g.kg^{-1} body weight per day [48]. However, the toxic effect of nano-size particles is

different than the bulk material. In a porcine buccal model, smaller particles penetrate the mucosa layer than the bigger particles in the range of 140, 36 and 28 nm size [111]. In the Caco-2 cell monolayer model, exposure to TiO2 nanoparticles disrupted the cytoskeletal integrity, increased tight-junction (TJ) permeability and downregulation of genes encoding for tight junction proteins [112, 113].

Roberta and colleagues studied the short-term oral exposure to titania nanoparticles in Sprague-Dawley rats and they found that five-day exposure to 1 or 2 $mg.kg^{-1}$ body weight per day of anatase titania nanoparticles caused increased titanium levels in their ovaries and spleen and affected hormone secretion. The primary size of titania nanoparticles (< 25 nm) reached a size up to 1.6 µm due to agglomeration in the internal organs [114]. Suxin and colleagues also examined intragastric exposure to titania nanoparticles induced nephrotoxicity in mice. Several negative effects on the kidneys such as renal inflammation, tissue necrosis, and renal apoptosis were observed after 90 days of intragastric exposure to 2.5, 5 and 10 $mg.kg^{-1}$ anatase titania nanoparticles (primary size 5.5 nm and hydrodynamic size ~ 300 nm) [115].

In 2010, the International Agency for Research on Cancer (IARC) classified nano-sized titania as a potential carcinogen based on the rate of incidence of respiratory tract cancer in rats after prolonged inhalation of titania dust particles [82]. In June 2016, EFSA re-evaluated titania (E171) food additives and the ADI value was not established yet because of its insufficient database. But the absorption and the bioavailability of orally administered titania was found to be extremely low [48].

Although silica and titania has been authorized as a food additive, the risk assessment of these particles are still under-discovered and the oral exposure to nanoparticles is difficult to identify because of their presence in a number of food matrixes [116]. Another consequence of these interactions is the change in functional and nutritional properties of the primary proteins.

Understanding the interactions between proteins and nanoparticles is crucial not only regarding their potential beneficial applications in food products, but also in the light of their potential risks to human health and to the environment.

2.9 Alteration of immune response by MNMs

When MNMs are ingested, the interaction of MNMs with the body's immune systems was expected to cause allergic responses because the immune system is sensible for foreign substances and consequently trigger various immune response, causing immune hypersensitivity reactions [117]. According to Gell Coombs classification, there are four types of immune hypersensitivity reactions: type I (immediate, IgE-mediated), type II (cytotoxic, IgG- and IgM- mediated), type III (antigen-antibody complexes), and type IV (delayed, T cell-mediated) [118]. According to current knowledge, MNMs can mainly cause type I and type IV allergenic reactions [119, 120]. Immediate-type allergies are also known as IgE-mediated allergies or type I allergies. Accordingly, the foreign substances induce T_H2 and T_H9 cell subsets and produce IL-4 and IL-13. These cytokines induce B cells and secrete IgE-type antibodies. The IgE antibodies bound to high-affinity receptors on the surface of basophils, mast cells, and eosinophils result in release of allergy mediators [119]. Immediate-type allergies are the most common types of allergies, and 30-40% of the world population has one or more allergic conditions [121]. Hay fever, house dust allergy, food allergies, and allergic asthma are type I allergies' conditions. Delayed-type allergies are also known as type IV allergies depending on T cells, including T-helper cells, cytotoxic T cells and macrophages [119]. Type IV allergies were mainly caused in the workplace where unusual chemicals or substances were exposed over a long time, repeatedly, and at high doses [122].

Evidence suggests that MNMs could influence allergy responses. The mechanism of MNMs allergy responses was most likely due to the adjuvant effect and induced specific cytokines,

antibodies, and cells rather than inducing specific IgE production. Repeated oral administration of silver nanoparticles induces allergic responses by secreting cytokines including IL-1, IL-6, IL-4, IL-10, IL-12 and TGF-b [123]. Titania nanoparticles have an adjuvant effect when administered in combination with ovalbumin in mice. The adjuvant effect was evidenced from the increased IgE and IgG1 levels and a Th2-dominant immune response [124]. Both silica and titania nanoparticles stimulate pulmonary inflammation activities via IL-1R signalling through the activation of IL-1a and IL-1b [125].

2.10 Knowledge gaps

With the increasing use of MNMs in food products, their incidental, accidental, or intentional exposure to human are inevitable. To date, most studies in the literature have been carried out using pristine MNMs, which are unlikely to be found in the real-life environment, and these studies may not reflect realistic exposure scenarios. Considering the abovementioned knowledge of DNMs, studying the transformation of nanoparticles under physiological conditions is necessary to assess the hazards of transformed particles on human health and the environment. Although acute toxicity, cytotoxicity and genotoxicity of pristine silica and titania nanoparticles have been studied under *in vitro* and *in vivo* conditions, the hazard assessment of food grade silica and titania DNMs under exposure conditions relevant to food remains largely elusive. Specifically, studies aimed that understanding the transformation of DNMs under the influence of food handling temperatures, and interaction with food matrix components, and the relevance of material transformation on potential adverse outcomes of relevance to gastrointestinal system have been overlooked. Lack of knowledge on the hazard potential of DNMs in the 'as exposed' state is a major limitation in the current risk assessment of DNMs.

2.11 Conclusion

In this chapter, the current and emerging applications, as well as the risk assessment of MNM in food products were discussed. The physicochemical properties of MNMs are dependent on their size, shape, structure, and concentration. The hazards associated with MNMs exposure through food depend on their bioavailability and bioaccessibility, which can be broken down into their absorption, distribution, metabolism, and excretion. While, *in vivo*, *in vitro*, and *in silico* assessment tests have been performed to study the transformation of MNMs in response to physical and chemical factors of the microenvironments in which they are embedded, as well as the molecular mechanisms involved in MNMs and proteins interactions studies relevant to human exposure to MNMs through oral route is acutely insufficient to comprehend their health risk assessment. In-depth understanding of their physicochemical properties, kinetics, and interactions with biological systems, along with toxicity studies involving different forms of MNMs are all crucial for safe use of MNMs in food.

Connecting Text

Chapter 2 provided the literature summary of DNMs' application, characterization, and physicochemical transformation of food additives in the food value chain. Considering the knowledge mentioned above of DNMs, studying the transformation of DNMs under physiological effects is vital to understanding the hazard identification of DNMs used in food products. Chapter 3 presents the transformation of food additive silica nanoparticles at the different food handling temperatures and their effects on the functional properties of the trypsin enzyme. Chapter 3 is published in the Journal of Agricultural and Food Chemistry, Phue, W. H., Liu, M., Xu, K., Srinivasan, D., Ismail, A., and George, S. (2019).

Chapter 3. A comparative analysis of different grades of silica particles and temperature variants of food grade silica nanoparticles for their physicochemical properties and effect on trypsin

3.1 Abstract

While silica particles are used extensively in food products, different grades and temperature variants of silica particles have not been compared for their physicochemical and biological properties. Different grades of silica (food-grade nanoparticle (FG-NP), non-food grade nanoparticles (NFG-NP) and food-grade micron particles (FG-MP)) and the temperature variants generated by exposing FG-NPs to wet heating, dry heating and refrigeration were compared for their physicochemical properties and interaction with trypsin. While the chemical composition and amorphous nature of FG-NPs were similar to NFG-NPs and FG-MPs, they had relatively less branched and ring siloxane groups. There were subtle but noticeable changes in the agglomeration behaviour and relative abundance of different silica groups in FG-NPs exposed to food handling temperatures. Secondary structure and function of trypsin were negatively impacted by FG-NPs and their temperature variants. Silica particles showed a 'mixed type inhibition' of trypsin resulting in partial digestion of bovine serum albumin. In conclusion, our studies showed differences in the surface chemistry of different grades of silica particles and temperature variants of FG-NPs and their negative impact on the structure and function of trypsin.

Keywords: Food grade silica nanoparticles, physicochemical transformation, surface chemistry, trypsin, protein, secondary structure

3.2 Introduction

Nanocale materials that offer unique functional advantages over their bulk counterparts are copiously incorporated in food and food contacting materials for novel functionalities. According to European Food Safety Agency (EFSA), fifty five different types of nanomaterials are used in food products, food contacting materials, feed and other agricultural purposes [1] with growing number of novel nanoparticles under development. While some of these materials have been in use for a considerable amount of time, the potential adverse health effect of these relatively new class of materials remains largely unknown.

Silica particles have been used as food additives, primarily because of their abilities to absorb moisture and to keep dry powders dispersed (anticaking agents) [2, 3]. A study analysing commercially available food products incorporating silica particles (E551) showed that a subtantial portion of silica exists in nano-scale size range [4, 5]. The estimated daily intake (EDI) of E551 is 9.4 mg SAS (synthetic amorphous silica).kg^{-1} body weight per day and the primary particles size ranges from 30-200 nm [6, 7]. Despite the relatively long history of silica particles application in food, there are knowledge gaps on their transformation during their transitions through the food value chain and their interaction with biomolecules.

Processing dependent changes in the surface chemistry of silica particles were reported in a study published by Zhang *et al.* [8]. They noticed that subjecting fumed silica to high calcination temperature followed by hydration increased their toxicity due to an increase in dangling Si-O groups. This difference in the toxic potentials of two silica particles with same core chemistry was shown to be attributed to the difference in surface chemistry. Studies have also noted the formation of siloxane groups (Si-O-Si/Si-O) by the condensation of silanol groups (Si-OH) when subjected to increasing temperatures [9, 10]. Thus, while there are ample evidence to suspect transformation of silica particles in response to temperatures and that silica

particles with same core chemistry may respond differently to processing temperatures, such studies using food grade silica particles are grossly missing in literature. In addition, the influence of different grades of silica and material transformation on the nature of their interactions with proteins of significance to human physiology is another aspect that warrants deeper understanding.

High surface-to-volume ratio of nanoparticles offers great opportunities for binding with proteins and other biomolecules along the gastrointestinal tract. Trypsin is one of the serine protease enzymes which is involved in controlling pancreatic exocrine function as well as digestion of proteins in digestive systems [11, 12]. The functional properties of the trypsin have been reported to be altered by nanomaterials used in food products [13, 14]. For example, titania nanoparticles interfere with enzyme activity of trypsin by altering the secondary structure of trypsin [14].

In view of the existing knowledge gaps, we assessed differences between different grades of silica particles and the temperature variants generated by subjecting FG-NPs to food handling temperatures, for their physicochemical properties and interactions with trypsin. In this article, we demonstrate that FG-NP, differed in morphology and surface chemistry in comparison to NFG-NPs and FG-MPs. Exposing FG-NPs to food handling temperatures had noticeable effect on their agglomeration behaviours and surface chemistry. FG-NPs and their temperature variants affected the secondary structure of trypsin resulting in incomplete digestion of bovine serum albumin (model protein substrate). These studies highlight the relevance of using food grade particles when investigating their potential adverse effects and that silica nanoparticles could have negative impact on nutrient assimilation.

3.3 Materials and methods

Food grade silica nano (AEROSIL® 200F) and micron size particles (SIPERNAT® 22) were obtained from Evonik Industry, (Essen, Germany) and non-food grade silica nanoparticles (cat# 637238, 10-20 nm particle size (BET), 99.5% trace metals basis) were purchased from Sigma-Aldrich (Missouri, USA). Trypsin from porcine pancreas and Nα-benzoyl-DL-arginine 4-nitroanilide hydrochloride (BApNA) were purchased from Sigma-Aldrich. Stock buffers of 0.1 M of Tris-HCl (pH 8.5) were prepared using deionized water and were stored at 4°C before making the working concentration prior to each experiment. All reagents and samples were prepared using deionized water obtained from a Milli-Q water system (Millipore Sigma, Massachusetts, USA).

3.3.1 Sample preparation

Silica particles originally obtained in powder form were dispersed in distilled Milli-Q water (deionized water) at 10 $mg.mL^{-1}$ concentration (stock solution). Food grade silica nanoparticles (FG-NPs) were subjected to different food handling temperatures. For this, 5 mL each of stock solution was taken in five set (n=3) of clean glass bottles. One set was kept at room temperature (23 ^{0}C) which served as the reference (FG-NP-RT). One set each of the particle suspension were either boiled for one hour using a Corning hotplate (FG-NP-BL), or subjected to microwave (Sharp, Osaka, Japan) for 3 min using a kitchen microwave (100% power, 1100W) (FG-NP-MW). Refrigerated storage temperatures (refrigeration and frozen) were simulated by storing one set each of the particle suspension at 4°C (FG-NP-RF) and -20 ^{o}C (FG-NP-FR) in laboratory refrigerator. Dry heating was conducted by subjecting dry powders of SiO_2 to baking temperature at 160°C for an hour in an oven (Isotemp, Model 281A, Fisher Scientific, USA) (FG-NP-BK). Particles were also subjected to calcination temperature at 600°C for 6 hours (FG-NP-CA) using a Thermolyne Furnatrol II furnace (A1740 muffle furnace, USA) to compare the transformation of FG-NPs at extreme high temperature. Food grade micron

particles (FG-MP) and non-food grade nanoparticles NFG-NPs (NFG-NP) of silica in their pristine states, suspended in water (without any heat treatment) were used for comparison with FG-NP kept at room temperature (FG-NP-RT).

3.3.2 Physicochemical characterization of silica particles

All particles in their pristine state and FG-NPs exposed to simulate food handling temperatures were characterized for their agglomeration size, shape, surface charge, hydrophobicity, crystallinity and surface chemistry. The morphology of air-dried particles was assessed by scanning electron microscopy. Briefly, 5 µL of nanoparticle suspensions (50 µg.mL-1) were dropped onto SEM stubs and were air dried at room temperature. SEM images were acquired at 50 kV accelerating voltage using Hitachi SU-8000 SEM (Hitachi high-technologies corporation, Japan).

The hydrodynamic diameter and zeta potential of the particles dispersed in Milli-Q water at a concentration of 50 µg.mL^{-1} were determined by dynamic light scattering (DLS) (NanoBrook OMNI instrument, USA). Particles suspended in water were filled into pre-rinsed cuvettes and were placed in a DLS instrument and the measurements were made at an applied voltage of 100 V.

We used Attenuated Total Reflectance- Fourier Transform Infrared (ATR-FTIR) Spectroscopy for the identification of silica groups (ALPHA-P, Bruker, Billerica, Massachusetts, United States). For this, 5 µL-aliquots of silica particles (stock concentration 10 mg.mL^{-1}) were dropped on the ATR probe and left to dry for 15 min. Wavelength range of 400 to 4000 cm^{-1}, with a resolution of 4 cm^{-1} and 24 scans were used for obtaining the FTIR spectrum. Qualitative analysis of Si-O-Si groups (cyclic and linear) was performed by deconvolution of the FTIR spectra region between 1200 and 900 cm^{-1} using the OMNIC 8.2.0.387 software (Thermo Scientific, MA, USA).

X-ray diffractometry (XRD) was conducted with pristine particles and FG-NPs subjected to food handling temperatures to assess the original atomic structure and to evaluate potential changes in the amorphous nature of FG-NPs under different food handling temperatures. For this, silica particles (in powder form) were placed on the XRD specimen holder and pressed with glass plate to fit in the holder. Subsequently, samples were analyzed using XRD (Bruker D8 Discover diffractometer with VANTEC-2000 detector system and Cu source), with a diffraction angle range of 4°-104°. Diffraction pattern was measured in 4 frames and the exposure time for each frame was 300 s. The results were analyzed using the software Diffrac Eva 4.0.

X-ray photoelectron spectroscopy (XPS) was performed for assessing the chemical composition of particle surface using VG ESCALAB 3 MKII spectrometer with Mg Kα as a radiation source where the limit of detection was ~0.1 atomic % and analyzis depth was < 10 nm. Survey scans were run at a step size of 1.0 eV energy with a pass energy of 100 eV used for elemental profiling of the surface of silica particles.

Relative hydrophobicity of silica particles was assessed using a dye staining method as reported earlier [15]. Particles suspended in water (5 $mg.mL^{-1}$) were mixed with 2 $\mu g.mL^{-1}$ Rose Bengal in 0.1 M phosphate buffer (pH = 7.4) for 3 hours under dark conditions. Subsequently, particles were separated from the supernatant by centrifugation at 11,000 rpm for 30 min. Rose Bengal (RB) added to Milli-Q water in the same proportion was used as the baseline control. The absorbance of the supernatant at 542 nm was measured using a UV-Vis spectrophotometer (Spectra Max M2, Molecular Devices, USA). The partitioning quotient (PQ) was calculated with equation 3.1 (Eq 3.1).

$$PQ = \frac{Mass\ of\ RB\ adsorbed\ on\ particle\ surface}{Mass\ of\ RB\ in\ water} \quad \textbf{(Eq 3.1)}$$

3.3.3 Trypsin activity and inhibition assays

Standard curve for trypsin activity was generated by incubating increasing units of trypsin (0-1 $mg.mL^{-1}$) with 0.3 $mg.mL^{-1}$ of the substrate- Nα-Benzoyl-L-arginine 4-nitroanilide hydrochloride (BApNA) in 50 mM Tris HCl buffer, pH 8.0, containing 20 mM $CaCl_2$. The total volume was kept at 200 µL and the solution was kept at 37°C for 10 min. The reaction was stopped by adding 20 µL of 5.3 M acetic acid and absorbance at 410 nm was measured using a UV-Vis spectrophotometer (Spectra Max M2, Molecular Devices, USA).

In order to assess the inhibition of trypsin due to its interaction with silica particles, 40 $µg.mL^{-1}$ of trypsin was mixed with silica particles at working concentrations ranging from 0 to 160 $µg.mL^{-1}$ and incubated for 30 min at 37°C. BApNA (substrate) at a concentration of 0.3 $mg.mL^{-1}$ was added to trypsin-particle mix and incubated for 10 min at 37°C and the trypsin activity was measured as detailed above.

3.3.4 Adsorption of trypsin on silica particles

Silica particles were mixed with trypsin (working concentrations of 160 $µg.mL^{-1}$ and 50 $µg.mL^{-1}$, respectively) in 500 µL at pH 8.5 and were incubated at 37°C for 1 h. Controls were prepared by adding the same proportions of water (without nanoparticles) to the enzyme solution. These suspensions were centrifuged at 14,000 rpm for 30 min to separate the supernatant (unbound proteins) from the pellets (particles and bound proteins). The concentration of unbound protein was measured using Bradford assay and the value was deducted from the initial protein concentration to estimate amount of proteins bound onto different silica particles.

3.3.5 Fluorescence measurement

The intrinsic fluorescence of tryptophan residues in trypsin (40 $µg.mL^{-1}$ in 20 mM tris-HCl buffer at pH 8.5) was measured in the absence and presence of 6, 4, 2, 1, 0.5 $mg.mL^{-1}$ concentrations of silica particles. All quenching experiments were carried out at 37°C. The

fluorescence spectra were obtained from 310 to 600 nm with the excitation wavelength at 280 nm by using a plate reader (Spectra Max M2, Molecular Devices, USA). Fluoresence intensity measured was analysed against silica particle concentration using Stern-Volmer equation in order to obtain the binding parameters (Stern-Volmer constant (K_{sv})), as shown below equation 3.2 (Eq 3.2),

$$\frac{F0}{F} = 1 + Ksv\ .[Q] = 1 + Kq\tau 0\ [Q] \qquad \textbf{Eq (3.2)}$$

where F_0 and F represent the steady-state fluorescence intensities in the absence and presence of silica particles, respectively, K_q is the bimolecular quenching constant and τ_0 is the lifetime of the fluorescence in absence of particles. The value of τ_0 is a constant- 10^{-8} s for trypsin [16]. K_{sv} is the Stern-Volmer quenching constant and [Q] is the concentation of the silica particles.

3.3.6 Kinetic study of trypsin activity

Silica particles (800 µg.mL^{-1}) were incubated with trypsin (final concentration 40 µg.mL^{-1}, ~740 BAEE Units) for 30 min at 37°C. Increasing concentrations of BApNA from 0.08-1.28 mg.mL^{-1} were added and the reaction rates were monitored by measuring changes in absorbance values (λ=410 nm) at intervals of 10 s for a total of 5 min. The initial straight-line portion was used to determine reaction velocity. Michaelis-Menten constant (K_m) and V_{max} were calculated from Lineweaver-Burk plot, which were developed by plotting inverse of reaction velocity against inverse of substrate concentration.

3.3.7 Effect of silica particles on tryptic digestion of bovine serum albumin (BSA)

BSA was used as a model protein to assess if the interactions of trypsin with silica particles could alter its proteolytic activity. For this, 50 µL silica particles (stock concentration of 10 mg.mL^{-1}) was mixed with 50 µL of trypsin (20 mg.mL^{-1}, 13,000 BAEE Units) for 1 hour at 37°C. Subsequently, 100 µL of BSA (stock concentration of 11 mg.mL^{-1}) was added to the

suspension and incubated for 10 min at 37°C. A 5 µL aliquot of protein digest was loaded onto a sodium dodecyl sulfate-polyacrylamide gradient gel electrophoresis (SDS-PAGE) (gradient gel 4%, 8%, 10%, 11% and 12%) and the proteins were separated in the gel using 50 V for 3 h using Bio-Rad, model 3000Xi, CA, USA. The gel was stained with Coomassie brilliant blue and was imaged using a gel-doc station (Alpha Innotech Corp., California, USA).

3.3.8 HPLC analysis of the digested peptides

HPLC analysis was performed using Varian ProSTar HPLC system (Varian, California, USA). Digested samples (20 µL) were applied to a Gemini-NX 5u C18 110A column (100x4.60 mm 5 micron, Phenomenex, California, USA). Two buffers were prepared as the mobile phase: 10% acetonitrile/90% water containing 0.05% trifluoroacetic acid (TFA) (buffer A) and 60% acetonitrile/40% water containing 0.05% TFA (buffer B). Elution was performed using a linear gradient of 100:0 to 40:60 A:B delivered at 1mL/min over 40 min. Absorbance at 215 nm was used for the detection of eluting peptide fractions.

3.3.9 CD and FTIR spectroscopy-based analysis of particle induced secondary structure changes in trypsin

Silica particles were interacted with trypsin (final concentrations of 2 and 0.2 $mg.mL^{-1}$, respectively) in 20 mM phosphate buffer (pH 8) for 1 h at 37°C. Four hundred µL of the trypsin-particle complex solution was added to a quartz cell with 0.1 cm-path length and the CD spectra were recorded on a Jasco J-810 spectro-polarimeter (Jasco Corp., Oklahoma, USA) from 190 to 260 nm at 37°C. Each spectrum was an average of three scans and the percentage of helices, strand, turns, and unordered were calculated using the DICHROWEB online software (DWA03771307) at http://www.cryst.bbk.ac.uk/ cdweb (access date- 16/05/2018).

We conducted FTIR analysis of trypsin before and after interacting with silica particles in order to assess changes in secondary structure of trypsin upon binding with silica particles. FTIR

spectra were recorded using Cary 630 FTIR with DialPath accessory in 50 µm pathlength. Trypsin solution was prepared in Tris-HCl buffer (pH 8.5) with D_2O. Trypsin and D_2O (to avoid signals of amide and H_2O groups from overlapping at 1750-1500 cm^{-1}) suspended silica particles were mixed and incubated for one hour, the final concentration for each solution was 5 $mg.mL^{-1}$. Twenty µL-aliquots of trypsin-silica particles were dropped on the probe and the FTIR spectra were taken in the range of 650 to 4000 cm^{-1}, with a resolution of 4 cm^{-1} and 120 scans. The spectra were deconvoluted and were used for assessing the secondary structure of trypsin.

3.3.10 Statistical analysis

Experiments were performed in triplicates and replicated at least three times. The data collected in this study are expressed as the mean value ± standard deviation (SD). Statistical comparisons were made by paired t test and p value ≤ 0.05 was considered significant.

3.4 Results

3.4.1 The agglomerate size of FG-NPs changed in response to food handling temperatures

SEM images of pristine silica particles and those subjected to simulated food handling temperatures are presented in Figure 3.1. All the tested silica particles showed agglomerates of spherically shaped particles and the average diameter of primary particle was about 30 nm (Figure 3.1). Food grade SiO_2 sold as micro particles (FG-MP) had primary particles of size ~30 nm which were aggregated (fused primary particles) to form particle aggregates of size 1-5 µm (Figure 3.1 b). FG-NPs exposed to wet heating (FG-NP-MW and FG-NP-BL) showed a slight decrease in average agglomerate size (Figure 3.1 d and 3.1 e and Figure 3.2 a). The agglomerates of particles stored at -20°C (FG-NP-FR) and those exposed to extreme heat treatment (FG-NP-CA) (Figure 3.1 g & i and Figure 3.2 a) were comparatively bigger than those exposed to other temperature conditions. Notably, the agglomerates of NFG-NPs were bigger than the FG-NPs.

XRD analysis showed that all the tested particles have amorphous structure (Figure SI 3.3). Notably there was no change in the amorphous nature of FG-NPs after being exposed to different temperature conditions. Similarly, there was no noticeable difference among the tested silica particles on the type of surface atoms as shown by XPS results (Figure SI 3.2).

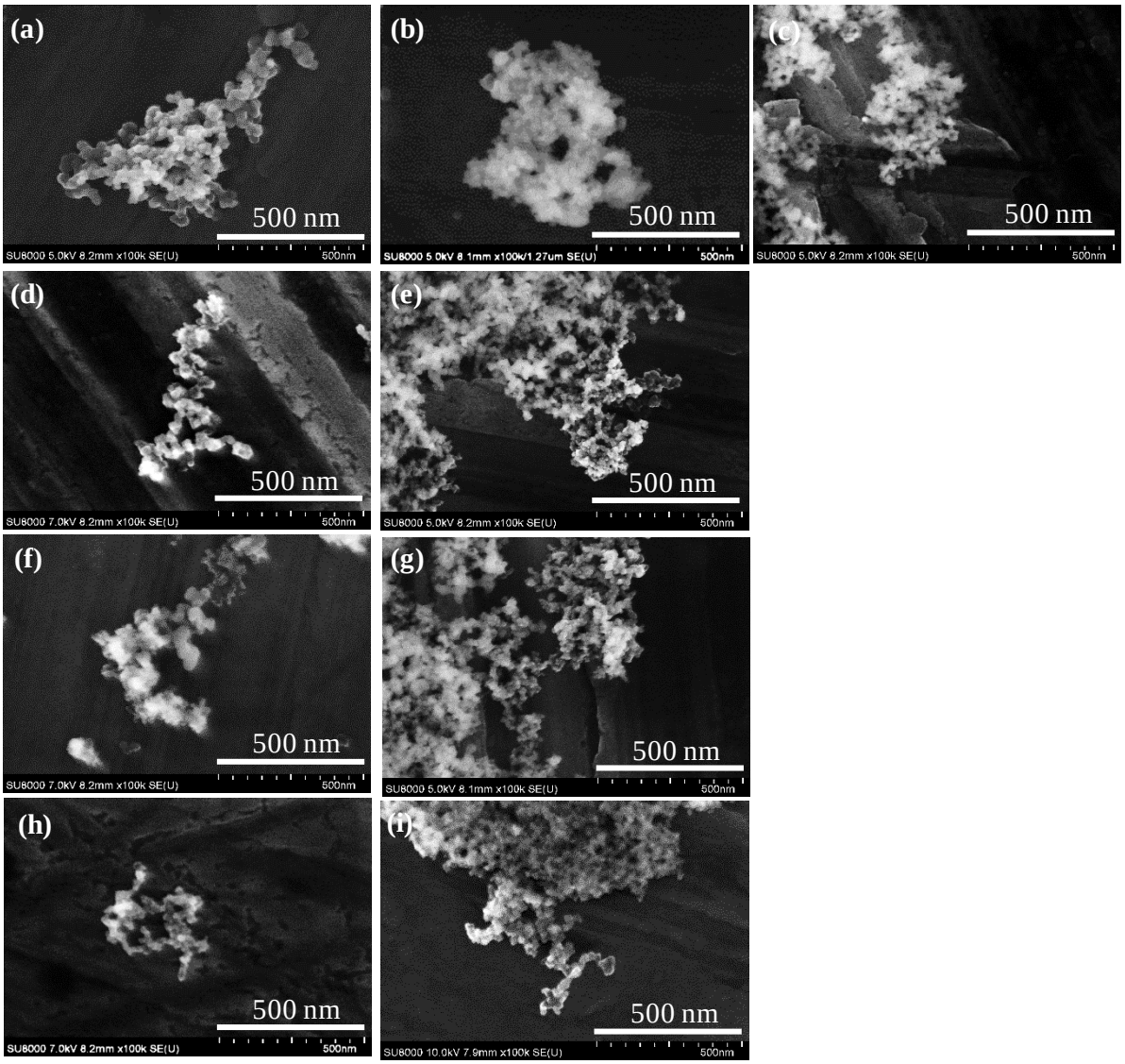

Figure 3. 1 Scanning electron microscope (SEM) images of silica particles subjected to different food handling temperatures. (a) FG-NP-RT, **(b)** FG-MP, **(c)** NFG-NP, **(d)** FG-NP-MW, **(e)** FG-NP-BL, **(f)** FG-NP-BK, **(g)** FG-NP-CA, **(h)** FG-NP-RF and **(i)** FG-NP-FR. A drop of silica suspension (50 µg.mL^{-1}) was placed on to SEM stubs, dried overnight and the images were acquired at 50 kV accelerating voltage using Hitachi SU-8000 SEM.

3.4.2 The surface charge and chemistry of FG-NPs in different food handling temperatures

The zeta potential measured using DLS for silica nanoparticles exposed to different food handling temperature is given in Figure 3.2 b. Generally, all silica particles showed a net negative surface charge. The net negative charge increased when FG-NPs were exposed to refrigerated and frozen conditions. While no statistically significant differences were found in the hydrophobicity among silica particles, there was a notable increase in the hydrophobicity of FG-NPs subjected to calcination temperature. Figure 3.3 compares the FTIR spectra of pristine silica particles and those subjected to different food handling temperatures. These spectra were captured in full scan from 4000 to 420 cm^{-1}, and the region between 1300-420 cm^{-1} range is magnified in order to highlight the siloxane and silanol groups. The surface of the silica particles is composed of siloxane (Si-O-Si) and silanol (Si-OH) groups and the relative abundance of siloxane groups was highest in FG-MP, followed by NFG-NP. The absorbance at 800 cm^{-1} corresponds to symmetric stretching vibration v_s (Si-O-Si), 1098 cm^{-1} for asymmetric stretching vibration v_{as} (Si-O-Si), 464 cm^{-1} for Si-O-Si bending mode and 953 cm^{-1} to Si-OH stretching vibration [17]. Fourier self-deconvolution method was used in a more detailed study of overlapping spectra. Figure SI 3.1 a compares the FTIR spectra of pristine silica particles (NFG-NP, FG-MP, FG-NP-RT) and those FG-NPs subjected to different food handling temperatures. The relative abundance of siloxane groups was highest in FG-MP, followed by NFG-NP based on peak intensity. The peak height for branched siloxane group (at 1050cm^{-1}) [18] was lower in FG-NPs in comparison to NFG-NPs and FG-MPs. Similarly, NFG-NPs had the least linear Si-O-Si (1030 cm^{-1}) [18] on their surface and they also showed a prominent peak for four membered cyclic siloxane (1096 cm^{-1}) [19]. The peak areas corresponding to silanol groups (960 cm^{-1}) [20] were high in FG-MP and NFG-NP particles in comparison to FG-NPs.

Notably, the relative abundance of siloxane and silanol was also observed to change in accordance with the type of food handling temperatures received by FG-NPs. Accordingly, those exposed to calcination temperature had the highest level of siloxane ring followed by those exposed to boiling (Figure SI 3.1 b). FG-NP-FR showed the lowest abundance of siloxane groups. Based on a deconvoluted spectra region between 1200 and 900 cm^{-1}, the relative abundance of cyclic siloxane ring (1000-1020 cm^{-1} and 1096 cm^{-1}) [19, 20] was highest in FG-NP-CA among the FG-NPs exposed to different food handling temperatures. Branched or linear siloxane group (1050 cm^{-1}) was higher in FG-NP-BL and FG-NP-CA followed by FG-NP-RT and FG-NP-BK. Calcination of FG-NPs (FG-NP-CA) showed a notable reduction in the peak corresponding to silanol group (960 cm^{-1}) [20]. Thus, while we observed that the material properties of FG-NPs change in response to food handling temperatures, we were interested in exploring the consequences of material transformation on its interaction with proteins. Trypsin was taken as a model protein to study this effect because of its relevance in protein digestion and its well-established structural and functional properties.

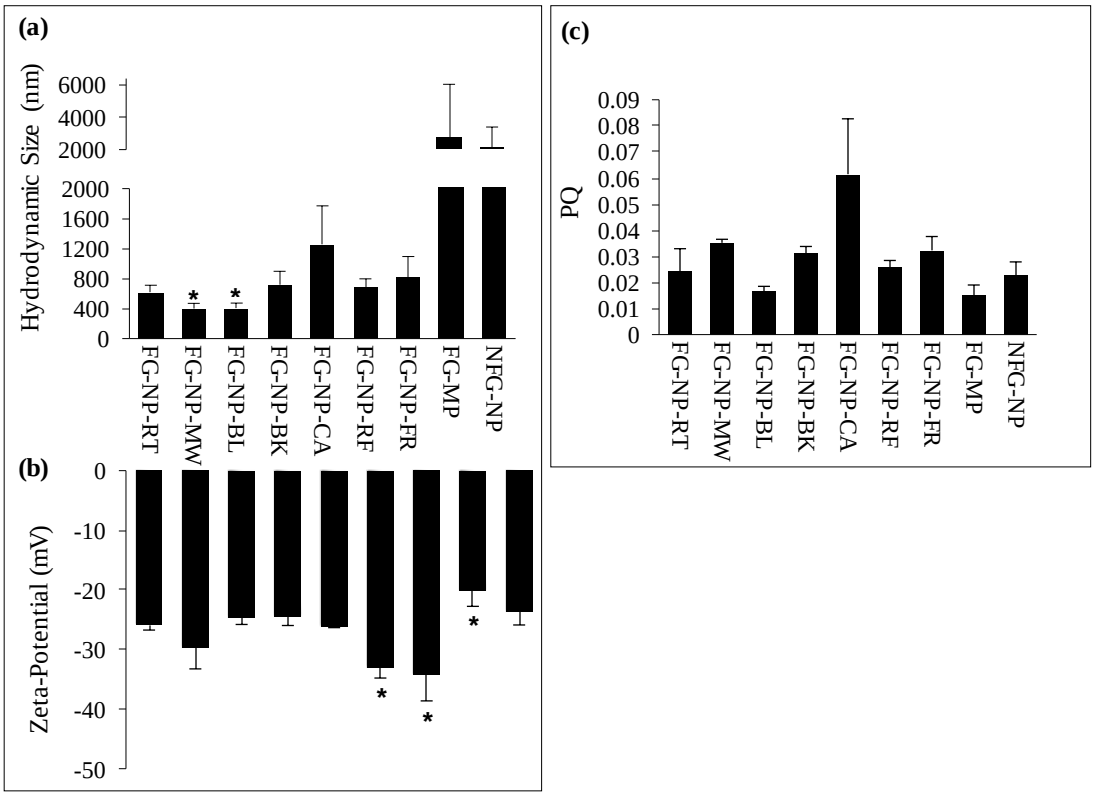

Figure 3. 2 Characterization of silica particles subjected to different food handling temperatures. (a) hydrodynamic size of the silica particles at 50 µg.mL^{-1} concentration was measured using dynamic light scattering techniques (NanoBrook OMNI). **(b)** Zetapotential of the silica particles in water at 50 µg.mL^{-1} was measured using NanoBrook OMNI. **(c)** Surface hydrophobicity of the silica particles was assessed by quantifying the amount of hydrophobic dye (Rose Bengal) bound on particles using UV-Vis absorbance spectroscopy. * Indicates statistical significance in comparison to FG-NP-RT, $p \leq 0.05$, N=3.

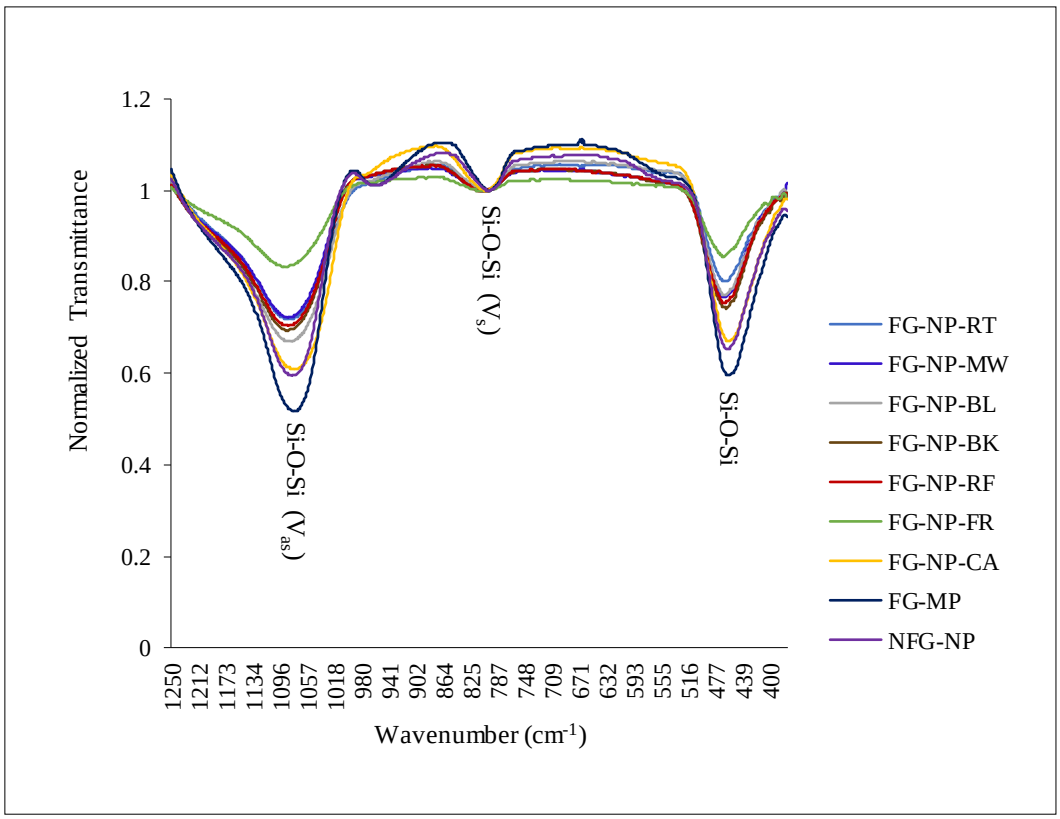

Figure 3. 3 FTIR analysis of silica particles subjected to food handling temperatures. The spectra were taken for a wavenumber range of 375-1250 cm^{-1} using ATR-FTIR.

3.4.3 Silica nanoparticles interfered with trypsin activity

We quantified the amount of trypsin bound onto silica particles. On an equal mass basis, protein bound onto FG-NPs was higher than those bound onto FG-MPs or NFG-NPs (Figure 3.4 a). Except for nanoparticles subjected to baking temperature (160°C), there was no significant difference in the amount of trypsin bound onto FG-NPs that were subjected to different temperatures (Figure 3.4 a).

Generally, inhibition of trypsin was higher when it was interacted with FG-NPs in comparison to NFG-NPs and FG-MPs (Figure 3.4 b). Among all the temperature variants of FG-NPs, those exposed to calcination temperature showed the highest inhibition activity followed by particles that were kept frozen. Unlike a concentration depended inhibition of trypsin by silica nanoparticles (both food grade and non-food grade), the inhibition of trypsin was not responding to the increasing concentration of FG-MPs.

3.4.4 Effect of silica particles on enzyme kinetics of trypsin

Enzyme kinetics was monitored as a function of increasing substrate concentration in the presence and absence of silica particles in order to understand the type of trypsin inhibition. Lineweaver-Burk plots were developed, and the V_{max} and K_m values were calculated for enzyme reactions. Food grade silica particles (both nano and micron sized) showed difference in the V_{max} and K_m values when compared with those of trypsin control. This type of inhibition is suggestive of a 'mixed inhibition'. However, NFG-NP showed a decrease in V_{max} without affecting K_m value indicative of a 'non-competitive' type of enzyme inhibition (Table 3.1, Figure SI 3.4 and Figure SI 3.5 a).

The enzymatic activity of trypsin after interacting with the silica particles was investigated using BSA as a model protein substrate. BSA was digested by trypsin in the presence and absence of silica particles and the polypeptide patterns were compared using one dimension-sodium dodecyl surface-polyacrylamide gel electrophoresis (SDS-PAGE) and HPLC (Figure 3.5 a & b). While the digestion patterns of reaction mixes with and without FG-MPs was similar, the interference of FG-NPs was evidenced by the appearance of two additional bands at 45 kDa and 24 kDa as compared to the control in lane 7 (Figure 3.5 a). The difference in digestion pattern between silica nanoparticles (both FG-NPs and NFG-NPs) and FG-MPs was further reaffirmed in the polypeptide patterns of trypsin digest obtained from HPLC analysis (Figure 3.5 b). Evidently, trypsin digest showed similar peptide patterns in the absence or presence of FG-MPs. However, BSA digestion was incomplete when the reaction mixture contained FG-NPs (Figure 3.5 b). Bigger peptide fractions suggestive of incomplete digestion was evident from the HPLC profile of FG-NPs and their temperature variants (Figure 3.5 b).

3.4.5 Fluorescence quenching

Quenching of protein's intrinsic (tryptophan) fluorescence was employed for more detailed understanding of protein-particles interactions. The type of fluorescence quenching of trypsin-silica complexes was distinguished using the Stern-Volmer diagrams in the range of silica concentrations of 0.5-6 $mg.mL^{-1}$ (0.008-0.1 M). The dynamic quenching constant (K_{sv}) values are presented in the Table 3.2. Generally, the bimolecular quenching rate (Kq) of trypsin was higher when it was interacted with FG-NPs in comparison to FG-MPs or NFG-NPs. For instance, the Kq value for FG-NP-RT was ~6 fold higher in comparison with that of FG-MP. There was also a noticeable difference between non-food grade ($Kq=5.44 \times 10^7$) and food-grade silica nanoparticles ($Kq=6.04\ 10^7$) on their binding affinities to trypsin (Table 3.2).

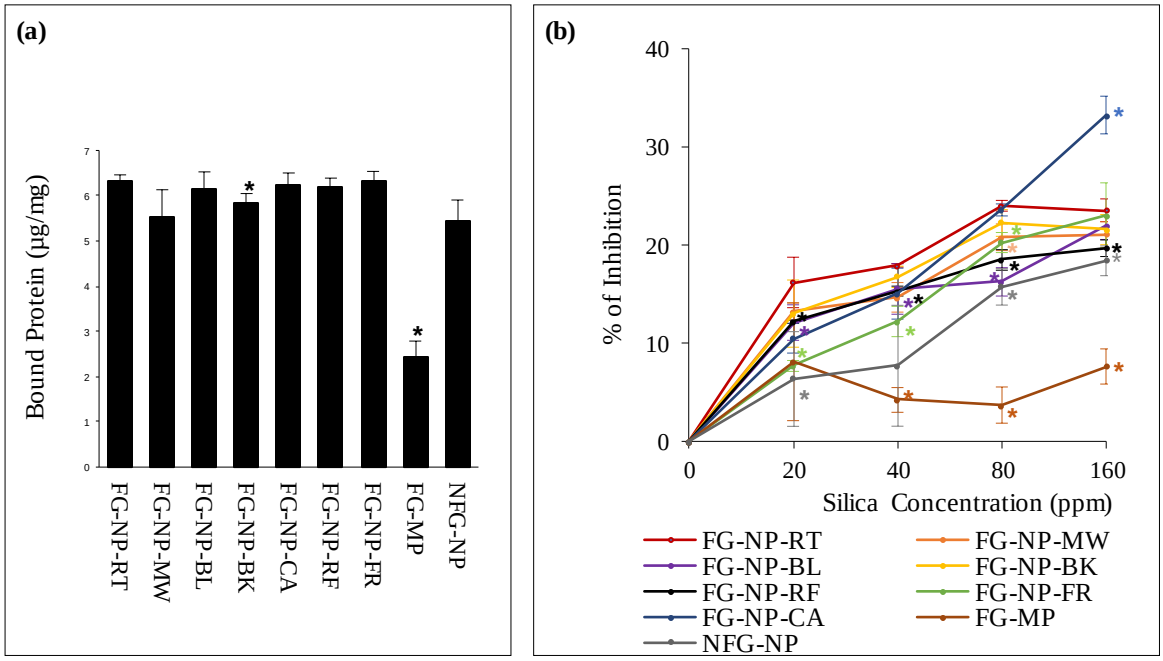

Figure 3. 4 Interaction of silica particles with trypsin. (a) Adsorption of trypsin on silica particles were measured by quantifying the proteins left in the solution after removing particles from the protein suspension. The concentration of unbound protein was measured using Bradford assay and the value was deducted from the initial protein concentration to estimate amount of proteins bound to different nanoparticles. **(b)** Silica particles-mediated inhibition of trypsin. The trypsin activity was determined using substrate, BApNA and the absorbance was measured by spectraMax i3x Microplate Reader at λ=410 nm. * Indicate statistical significance in comparison to FG-NP-RT, $p \leq 0.05$, N=3.

Table 3. 1 Types of inhibition of silica particles subjected to different food handling temperatures

	Vmax	Km	Types of Inhibition
Trypsin	0.008	0.819	
Tryp-FG-NP-RT	0.003	0.129	Mixed
Tryp-FG-NP-MW	0.004	0.233	Mixed
Tryp-FG-NP-BL	0.004	0.277	Mixed
Tryp-FG-NP-BK	0.004	0.216	Mixed
Tryp-FG-NP-CA	0.005	0.397	Mixed
Tryp-FG-NP-RF	0.003	0.232	Mixed
Tryp-FG-NP-FR	0.003	0.249	Mixed
Tryp-FG-MP	0.005	0.479	Mixed
Tryp-NFG-NP	0.007	0.822	Non-competitive

Table 3. 2 Stern-Volmer constants (K_{sv}), biomolecular quenching rate parameter (K_q) of trypsin in the presence of silica particles

	K_{sv} (M^{-1})	K_q ($M^{-1}s^{-1}$)
FG-NP-RT	6.037	6.04×10^7
NFG-NP	5.4395	5.44×10^7
FG-MP	1.1485	1.15×10^7
FG-NP-MW	6.5941	6.59×10^7
FG-NP-BL	7.8266	7.83×10^7
FG-NP-BK	7.0615	7.06×10^7
FG-NP-RF	9.1452	9.15×10^7
FG-NP-FR	4.0177	4.02×10^7
FG-NP-CA	6.7554	6.76×10^7

$\tau_o = 10^{-8}$ s for trypsin in the absence of quencher.[16]

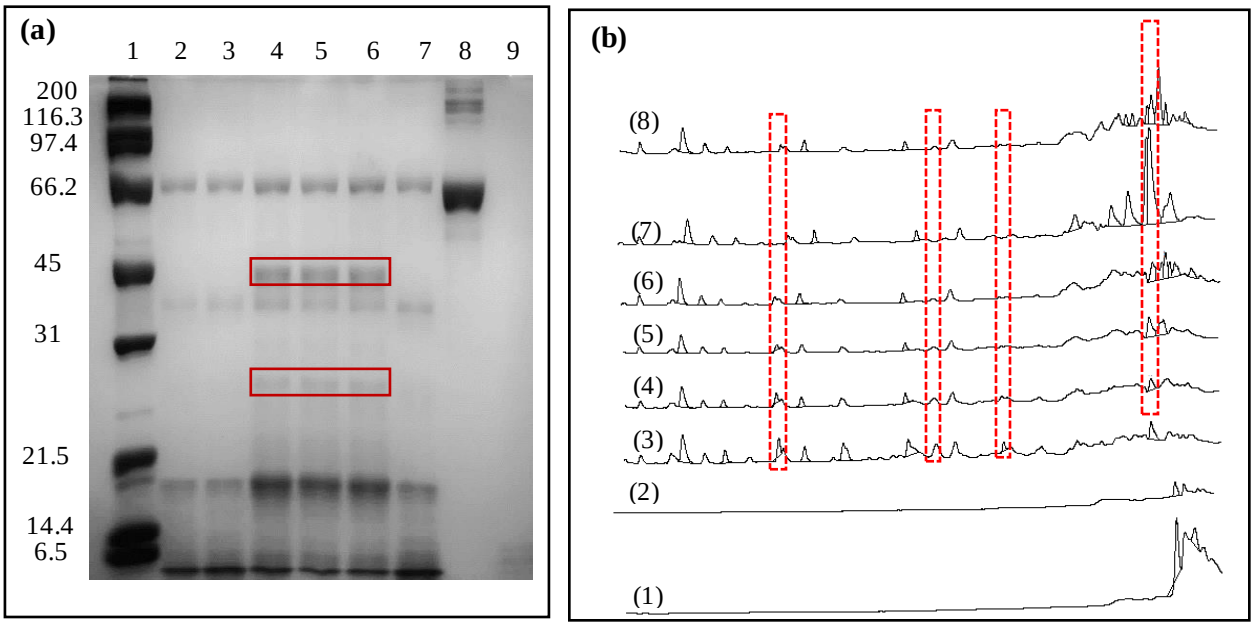

Figure 3. 5 Trypsin-digested bovine serum albumin (BSA) in the presence and absence of silica particles at tris buffer pH 8.5. (a) SDS-PAGE gel. Lane (1) marker, (2) NFG-NP+Tryp+BSA, (3) FG-MP+Tryp+BSA, (4) FG-NP-CA+Tryp+BSA, (5) FG-NP-BL+Tryp+BSA, (6) FG-NP-RT+Tryp+BSA, (7) Tryp+BSA, (8) BSA, and (9) Tryp. The rectangles show most prominent bands that were present when BSA digestion with trypsin was carried out in the presence of food grade silica nanoparticles.

(b) HPLC profile of BSA digested with trypsin in the absence and presence of silica particles. (1) BSA, (2) Tryp, (3) BSA+Tryp, (4) FG-MP, (5) NFG-NP, (6) FG-NP-RT+BSA+Tryp, (7) FG-NP-BL+BSA+Tryp, (8) FG-NP-CA+BSA+Tryp. Boxed peaks show prominent difference in the digestion products of BSA when trypsin was interacted with different silica particles.

3.4.6 CD spectroscopy of trypsin

Representative CD spectra of trypsin with and without interacting with silica particles are shown in Figure 3.6 and the secondary structure is presented in Table 3.3. Based on the spectra, the secondary structure of silica particles interacted trypsin was different from free trypsin. Generally, interactions of trypsin with silica particles reduced the percentage of helix and turns and increased the % of 'strand' and 'unordered' structure. The loss of secondary structure as evidenced by reduction in helix and increase in unordered levels was comparatively higher when trypsin was interacted with frozen FG-NPs.

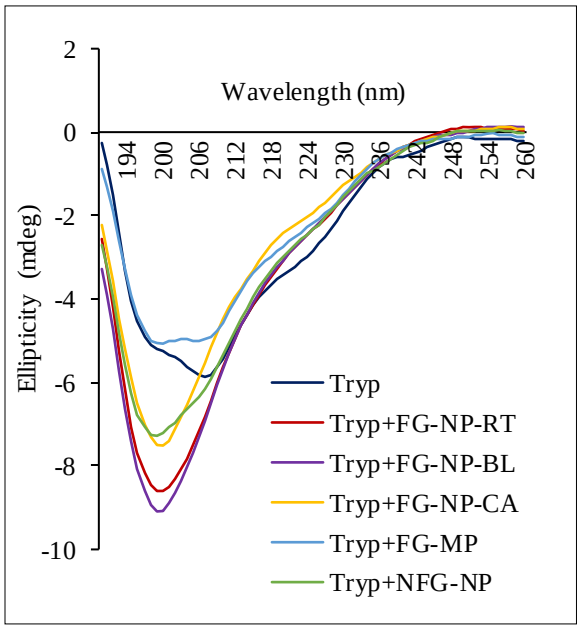

Figure 3. 6 The representative CD spectra of trypsin in the presence and absence of silica particles

Table 3. 3 Summary of the secondary structure assessed using CD after interacting trypsin with silica particles.

	Helix (%)	Strand (%)	Turns (%)	Unordered (%)
Tryp	11.1	33.3	13.6	42.2
Tryp-FG-NP-RT	6.8	37.5	12.1	43.8
Tryp-FG-NP-MW	8.1	35.9	12.4	43.7
Tryp-FG-NP-BL	6.7	37.1	12.5	43.8
Tryp-FG-NP-BK	6.5	37.1	12.7	43.8
Tryp-FG-NP-CA	6.3	37.0	13.2	43.6
Tryp-FG-NP-RF	5.9	38.4	12.9	42.9
Tryp-FG-NP-FR	5.3	38.7	12.6	43.4
Tryp-FG-MP	6.0	37.7	13.0	43.4
Tryp-NFG-NP	6.6	37.5	12.8	43.2

3.5 Discussion

Silica particles are copiously incorporated in food and drug formulations as additives, binder and filling materials that lead to human exposure through oral route. While these particles are generally perceived as harmless, the difference between food grade and non-food grade silica particles and the effect of food handling conditions on the physicochemical properties of these materials- especially for food grade silica particles- are seldom reported in literature. Here we show that silica nanoparticles undergo subtle but definite changes in surface chemistry that affect the interactions with trypsin. Notably, FG-NP differed in their ability to cause structural and functional changes to trypsin in comparison with NFG-NPs and FG-MPs. These observations suggest that FG-NPs are not benign in their interactions with biological entities and highlight the importance of selecting FG-NPs when studying the adverse effects of ingested silica nanoparticles.

Silica particles are composed of Si and O, and these elements can combine as siloxane (Si-O-Si/Si-O) or silanol (Si-OH) groups [8, 21]. These surface functional groups play an important role in aggregation and agglomeration of the particles. We observed that NFG-NP exhibited more Si-OH groups on their surfaces in comparison to FG-NPs (Figure 3.3). The morphology of NFG-NPs was also different from that of the FG-NPs (Figure 3.1 c), although there was no evident difference in the type of surface atoms as noted from XPS analysis (Figure SI 3.2). While the FG-NPs seemed agglomerated, NFG-NPs exhibited higher level of aggregation than agglomeration (fused primary particles). Thus, while NFG-NPs had more silanol groups, their hydrodynamic size was comparatively larger because of the difference in primary structure. In addition, the higher content of branched and four membered cyclic siloxane groups on the surface of NFG-NPs differentiated them from FG-NPs in terms of surface chemistry.

The silanol peaks (950-960 cm-1) were relatively shorter for calcinated and baked FG-NPs. Together with an increase in cyclic siloxane signature (for FG-NP-CA) the data suggest the dehydration mediated condensation of silanol groups during high temperature heating in dry condition [22]. The influence of heat treatment on the silanol group was studied by several groups and it was noted that external silanol group could condense to form siloxane groups in a temperature range of 436˚C-800˚C [8, 10, 21], while temperature above 1000 ˚C is required for condensation of internal silanol groups [10]. Inferring from our own data and results from the reported studies, the silanol groups present on the particle surface condense to form cyclic siloxane rings when subjected to calcination temperature. The relative increase in cyclic siloxane on the surface of calcinated particles could also explain an increase in the hydrophobicity of this material (Figure 3.2 c). These results on the relative increase in hydrophobicity of silica particles upon heating are in agreement with similar observation reported earlier [8, 21]. Tahiri et al. had showed a correlation between heat treatment of particles and increase in hydrophobicity where, the increase in temperature caused a decrease in silanol content, making the material more hydrophobic [10]. The elemental composition of the surfaces of FG-NP-RT, FG-MP, and NFG-NP were determined by XPS analysis and the results are given in supporting information (Figure SI 3.2.). Only Si and O were detected during the surface scan of these particles. The atomic structures of FG-NPs subjected to simulated food handling temperatures were analysed by X-Ray Diffractometer. Despite different heat treatments, there was no apparent change in the amorphous nature of the FG-NPs (Figure SI 3.3). Overall, the above results showed that while the core chemistry and the amorphous nature of tested silica particles are the same, there are differences in the relative abundance of surface groups (silanol and siloxane groups) and morphology of the particles. Further, the surface chemistry and morphology of FG-NPs changed in response to simulated food handling temperatures.

Nanoparticles are known to interact with proteins present in biological media which forms an absorbed layer of proteins known as protein corona. The formation of protein corona not only affect the biological identify of particle but also influences the structure and function of proteins [23]. As revealed by protein quantification (Figure 3.4 a) and binding affinity studies (Table 3.2), FG-NPs exhibited higher interactions with trypsin in comparison to FG-MPs. The relative abundance of silanol and siloxane groups on particle surface together with the unique features of proteins defined by charge, hydrophobicity, and divalent cation binding sites are proposed as major factors dictating protein-particle binding. Negative charge and hydrophilic nature of silanol groups (at neutral pH) and hydrophobic nature of siloxane ring structure provide anchoring points for proteins on silica particles. Since the core chemistry of micro- and nano- sized particles are the same, the higher amount of trypsin associated with nanoparticle could be explained by the higher surface area of nanoparticles that provide more binding sites per unit mass of silica. Notably, the changes in surface functional groups on FG-NPs subjected to different food handling temperatures had no major net influence on the total amount of bound proteins but affected their relative binding affinities (Table 3.2). This may be attributed to the fact that effect due to decreasing silanol group is compensated by an increase in siloxane group, as exemplified by FTIR spectra of calcinated FG-NPs.

The enzyme activity assays showed that particles interactions with trypsin could lead to partial loss of enzyme activity. Trypsin is an allosterically regulated monomeric enzyme with a single catalytic unit and a subsite loop that binds calcium. Binding of calcium to the subsite loop stabilizes the trypsin structure and thus regulates the catalytic activity of the enzyme [24]. While in general allosteric enzymes do not follow Michalis Menten kinetics, saturating the buffer with co-factor could render them to behave as non-allosteric enzyme. This is evidenced by the perfectly fitting hyperbola curve of Michalis-Menten chart, characteristics of non-allosteric enzyme, when the initial enzyme velocity was plotted over increasing substrate

concentration (Figure SI 3.5). Further, studies have shown the utility of Michalis-Menten chart and Lineweaver-Burk plot for discerning differences in trypsin activity when subjected to potential inhibitors [25, 26].

The percentage inhibition of trypsin was higher and dose dependent for FG-NPs in comparison to FG-MPs (Figure 3.4 b). Lineweaver-Burk plots for trypsin kinetics in the presence of different silica particles revealed the difference in type of trypsin inhibition. As the data presented in Table 3.1, the Km and Vmax values of trypsin were changed in the presence of food grade silica particles indicating a 'mixed inhibition'. Although there were differences among the temperature variants of FG-NP in the percentage of trypsin inhibition, all these particles showed a mixed type inhibition when interacted with trypsin. In the case of NFG-NP, however, V_{max} value decreased while K_m was unchanged which was suggestive of a non-competitive inhibition [27]. Non-competitive inhibition is also regarded as a type of mixed inhibition involving enzyme-substrate-inhibitor complex [14]. As such, these data suggest that binding of trypsin to silica particles may not preclude their binding to substrate. Together with data from CD studies of particle bound trypsin, it is imperative that the alteration in the secondary structure of trypsin during its complexation with silica could negatively impact the enzyme kinetics. The partial loss of digestive function when trypsin was interacted with silica nanoparticles could be resulting from the change in secondary structure of trypsin as demonstrated by the CD and FTIR spectra (Figure 3.6 and Figure SI 3.6). Binding of trypsin on to FG-NPs showed a change in the net percentage of α-helices and β-sheets. Among different grades of silica particles tested, FG-NPs showed the highest level of enzyme inhibition, which concurred with this materials higher binding affinity for trypsin molecules and alteration in secondary structure. Observations from enzyme kinetic studies were in agreement with results obtained from SDS-PAGE and peptide profile analysis using HPLC (Figure 3.5 a & b). Larger mass fractions seen in SDS PAGE and HPLC profile suggested

altered and incomplete digestion of BSA when trypsin was bound onto FG-NPs. Interestingly, these results suggest that FG-NP behaved differently from micro and NFG-NPs and emphasizes the need to use food grade particles when trying to understand the adverse effects of ingested particles. Further studies are warranted for understanding the exact mechanism involved in the reduction of enzyme activity when trypsin is bound to FG-NPs and its consequence on nutrient assimilation in the body.

In conclusion, this studies delineated the differences in morphology and surface chemistry of different grades of silica particles (food-grade nano-size, food-grade micron size, and non-food grade nano-size). This research also demonstrated subtle but definite change in the relative abundance of different silica groups when FG-NPs were subjected to simulated food handling temperatures. Further, we showed that different grades of silica and the temperature variants of FG-NPs differ in their ability and affinity to bind with trypsin with concurring effect on its structure and function. Among different grades of silica tested, FG-NPs showed higher, affinity, loss of secondary structure and loss of enzyme function suggesting potential negative consequence of ingested silica nanoparticles on nutrient assimilation.

3.6 References

1. Peters, R., et al., *Inventory of Nanotechnology applications in the agricultural, feed and food sector.* EFSA supporting publications, 2014. **11**(7).
2. Winkler, H.C., M. Suter, and H. Naegeli, *Critical review of the safety assessment of nano-structured silica additives in food.* Journal of nanobiotechnology, 2016. **14**(1): p. 44.
3. Frewer, L., et al., *Consumer attitudes towards nanotechnologies applied to food production.* Trends in food science & technology, 2014. **40**(2): p. 211-225.
4. Dekkers, S., et al., *Presence and risks of nanosilica in food products.* Nanotoxicology, 2011. **5**(3): p. 393-405.
5. Heroult, J., et al., *The potential of asymmetric flow field-flow fractionation hyphenated to multiple detectors for the quantification and size estimation of silica nanoparticles in a food matrix.* Analytical and bioanalytical chemistry, 2014. **406**(16): p. 3919-3927.
6. Dekkers, S., et al., *Knowledge gaps in risk assessment of nanosilica in food: evaluation of the dissolution and toxicity of different forms of silica.* Nanotoxicology, 2013. **7**(4): p. 367-377.
7. van Kesteren, P.C., et al., *Novel insights into the risk assessment of the nanomaterial synthetic amorphous silica, additive E551, in food.* Nanotoxicology, 2015. **9**(4): p. 442-452.
8. Zhang, H., et al., *Processing pathway dependence of amorphous silica nanoparticle toxicity: colloidal vs pyrolytic.* Journal of the american chemical society, 2012. **134**(38): p. 15790-15804.
9. Peng, L., et al., *Investigation of the states of water and OH groups on the surface of silica.* Colloids and Surfaces A: Physicochemical and engineering aspects, 2009. **334**(1-3): p. 112-115.

10. Tahiri, N., et al. *Study of the thermal treatment of SiO2 aggregate*. IOP conference series: materials science and engineering. IOP Publishing, 2014.

11. Yamashita, K., et al., *A tumor-suppressive role for trypsin in human cancer progression.* Cancer research, 2003. **63**(20): p. 6575-6578.

12. Hirota, M., M. Ohmuraya, and H. Baba, *The role of trypsin, trypsin inhibitor, and trypsin receptor in the onset and aggravation of pancreatitis.* Journal of gastroenterology, 2006. **41**(9): p. 832-836.

13. Zhang, H., et al., *Mechanism of gold nanoparticles-induced trypsin inhibition: a multi-technique approach.* Molecular biology reports, 2014. **41**(8): p. 4911-4918.

14. Momeni, L., et al., *Interaction of TiO 2 nanoparticle with trypsin analyzed by kinetic and spectroscopic methods.* Monatshefte für chemie-chemical monthly, 2017. **148**(2): p. 199-207.

15. Xiao, Y. and M.R. Wiesner, *Characterization of surface hydrophobicity of engineered nanoparticles.* Journal of hazardous materials, 2012. **215**: p. 146-151.

16. Li, X. and T. Ni, *Probing the binding mechanisms of α-tocopherol to trypsin and pepsin using isothermal titration calorimetry, spectroscopic, and molecular modeling methods.* Journal of biological physics, 2016. **42**(3): p. 415-434.

17. Kim, J.M., et al., *Control of hydroxyl group content in silica particle synthesized by the sol-precipitation process.* Ceramics international, 2009. **35**(3): p. 1015-1019.

18. Darmawan, A., et al., *Structural evolution of nickel oxide silica sol-gel for the preparation of interlayer-free membranes.* Journal of non-crystalline solids, 2016. **447**: p. 9-15.

19. Fidalgo, A., et al., *The sol-gel entrapment of noble metals in hybrid silicas: a molecular insight.* Chemistry central journal, 2013. **7**(1): p. 161.

20. Saputra, R.E., Y. Astuti, and A. Darmawan, *Hydrophobicity of silica thin films: The deconvolution and interpretation by Fourier-transform infrared spectroscopy*. Spectrochimica acta part A: molecular and biomolecular spectroscopy, 2018. **199**: p. 12-20.

21. Zhuravlev, L., *The surface chemistry of amorphous silica. Zhuravlev model.* Colloids and surfaces A: physicochemical and engineering aspects, 2000. **173**(1): p. 1-38.

22. Warring, S.L., D.A. Beattie, and A.J. McQuillan, *Surficial siloxane-to-silanol interconversion during room-temperature hydration/dehydration of amorphous silica films observed by ATR-IR and TIR-raman spectroscopy.* Langmuir, 2016. **32**(6): p. 1568-1576.

23. Casals, E., et al., *Time evolution of the nanoparticle protein corona.* ACS nano, 2010. **4**(7): p. 3623-3632.

24. Shamaladevi, N. and V. Pattabhi, *Secondary binding site of trypsin: revealed by crystal structure of trypsin-peptide complex.* Journal of biomolecular structure and dynamics, 2005. **22**(6): p. 635-642.

25. Jiang, H., et al., *On-line characterization of the activity and reaction kinetics of immobilized enzyme by high-performance frontal analysis.* Journal of chromatography A, 2000. **903**(1): p. 77-84.

26. Erlanger, B.F., N. Kokowsky, and W. Cohen, *The preparation and properties of two new chromogenic substrates of trypsin.* Archives of biochemistry and biophysics, 1961. **95**(2): p. 271-278.

27. Saboury, A., *Enzyme inhibition and activation: a general theory.* Journal of the iranian chemical society, 2009. **6**(2): p. 219-229.

3.7 Supporting information

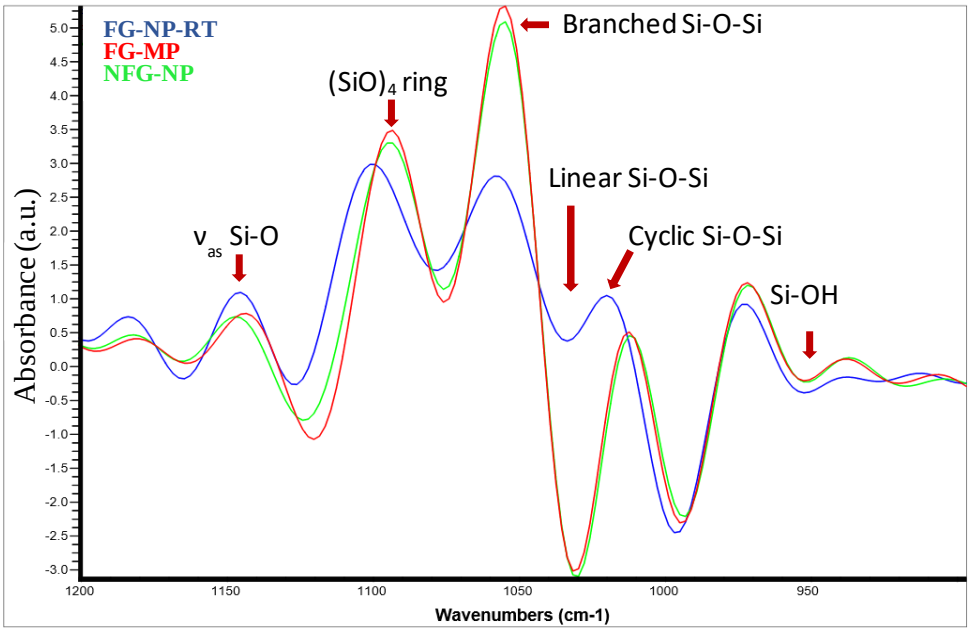

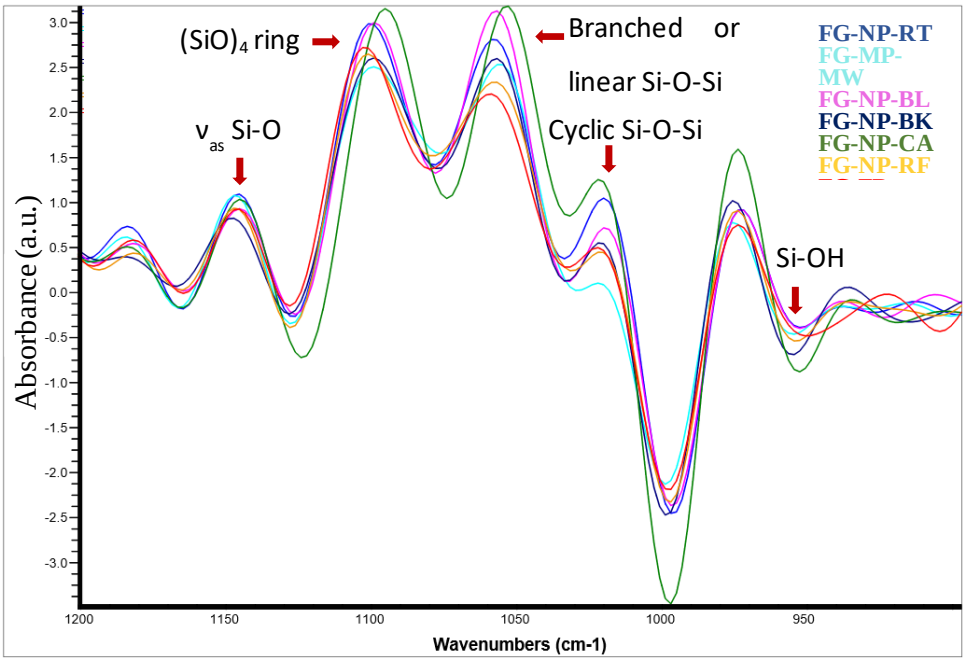

Figure SI 3. 1 FTIR analysis of silica particles subjected to food processing temperatures. The spectra were generated by Fourier self-deconvolution for a wavenumber range of 1200-900 cm^{-1}. (a) FG-NP-RT, FG-MP and NFG-NP. **(b)** FG-NP-RT, FG-NP-MW, FG-NP-BL, FG-NP-BK, FG-NP-CA, FG-NP-RF and FG-NP-FR.

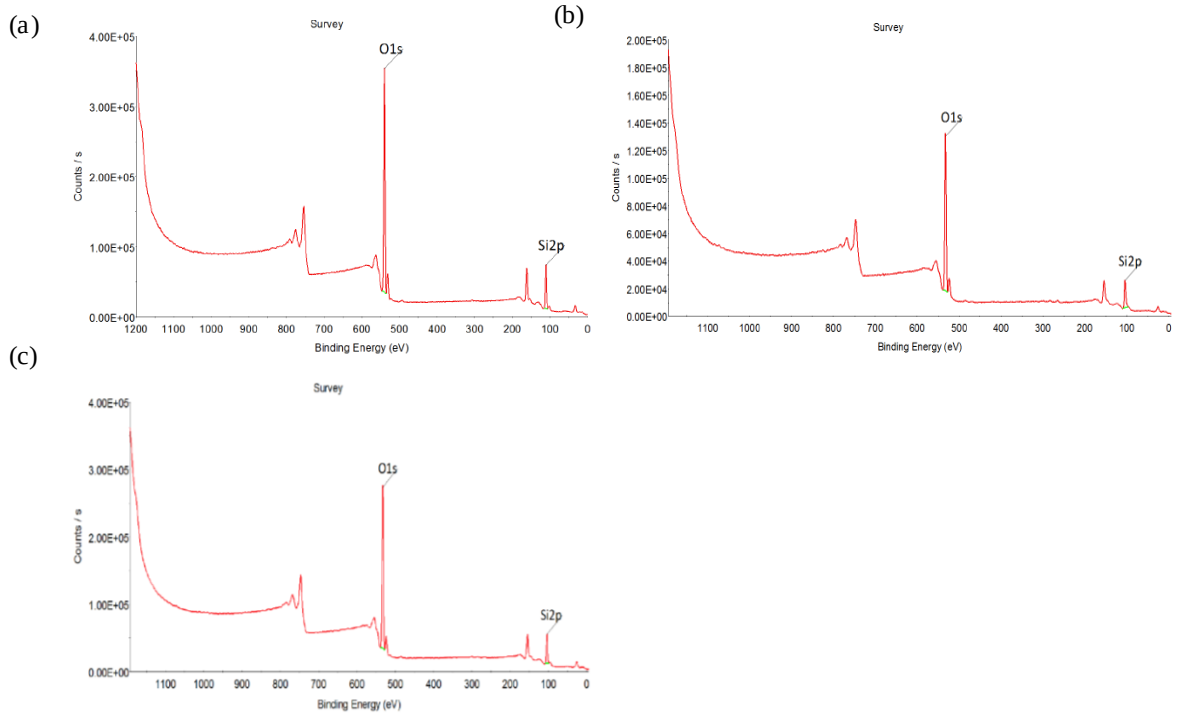

Figure SI 3. 2 Wide scan XPS spectrum of silica particles. (a) FG-NP-RT, **(b)** FG-MP, and **(c)** NFG-NP. The spectra were taken using VG ESCALAB 3 MKII spectrometer with Mg Kα as radiation source. The limit of detection for that instrument is ~0.1% atomic and analyzed depth is < 10 nm. Survey scans were run with 1.0 eV energy step size and 100 eV pass energy.

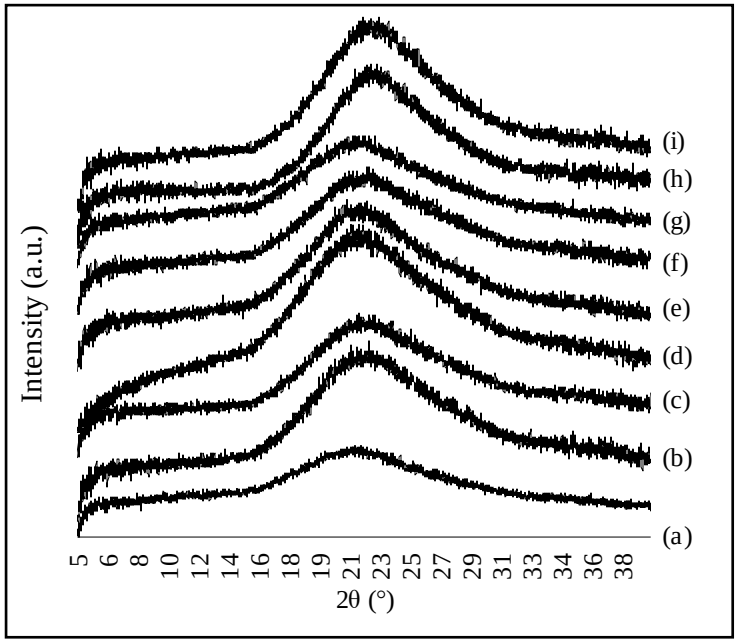

Figure SI 3. 3 XRD spectra of silica particles subjected to different food processing temperatures. (a) FG-NP-RT, **(b)** FG-NP-MW, **(c)** FG-NP-BL, **(d)** FG-NP-BK, **(e)** FG-NP-CA, **(f)** FG-NP-RF, **(g)** FG-NP-FR, **(h)** FG-MP, and **(i)** NFG-NP. The spectra were taken using Bruker D8 Discovery X-Ray Diffractometer (VANTEC Detector Cu-Source).

(a)

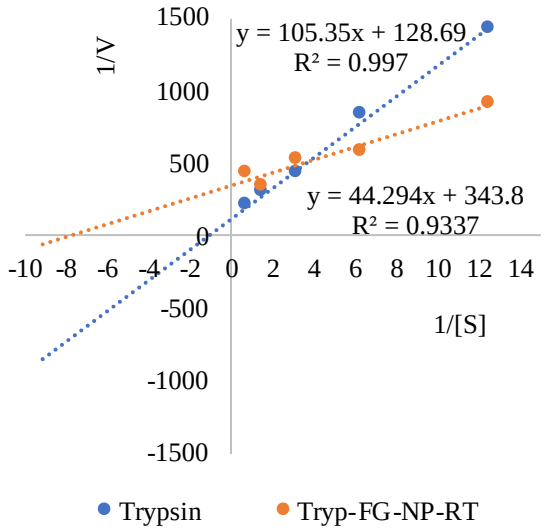
y = 105.35x + 128.69
R² = 0.997
y = 44.294x + 343.8
R² = 0.9337
1/V
1/[S]
Trypsin
Tryp-FG-NP-RT

(b)

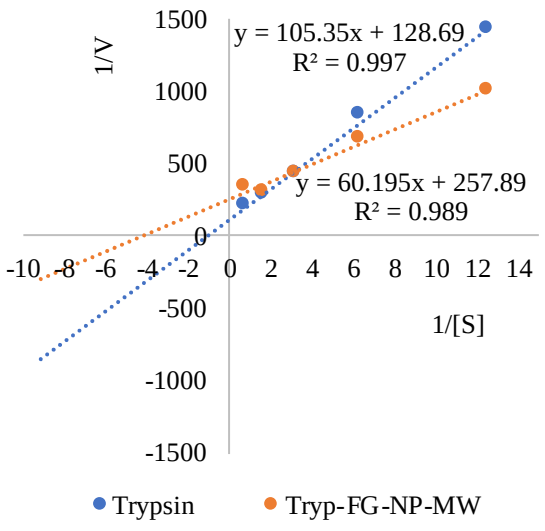
y = 105.35x + 128.69
R² = 0.997
y = 60.195x + 257.89
R² = 0.989
1/V
1/[S]
Trypsin
Tryp-FG-NP-MW

(c)

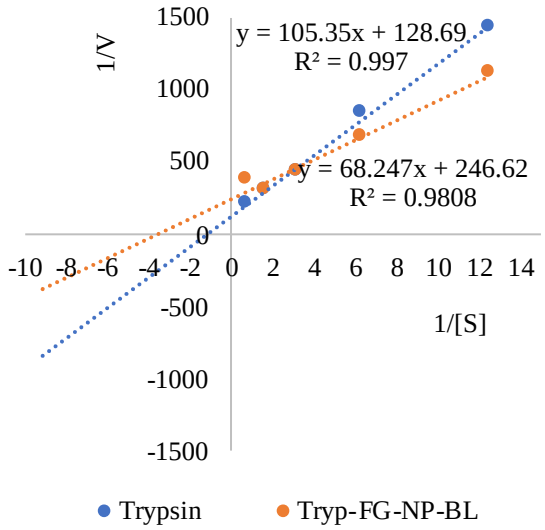
y = 105.35x + 128.69
R² = 0.997
y = 68.247x + 246.62
R² = 0.9808
1/V
1/[S]
Trypsin
Tryp-FG-NP-BL

(d)

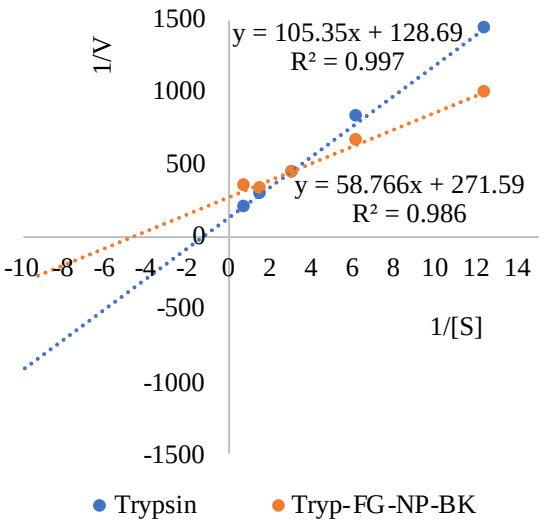
y = 105.35x + 128.69
R² = 0.997
y = 58.766x + 271.59
R² = 0.986
1/V
1/[S]
Trypsin
Tryp-FG-NP-BK

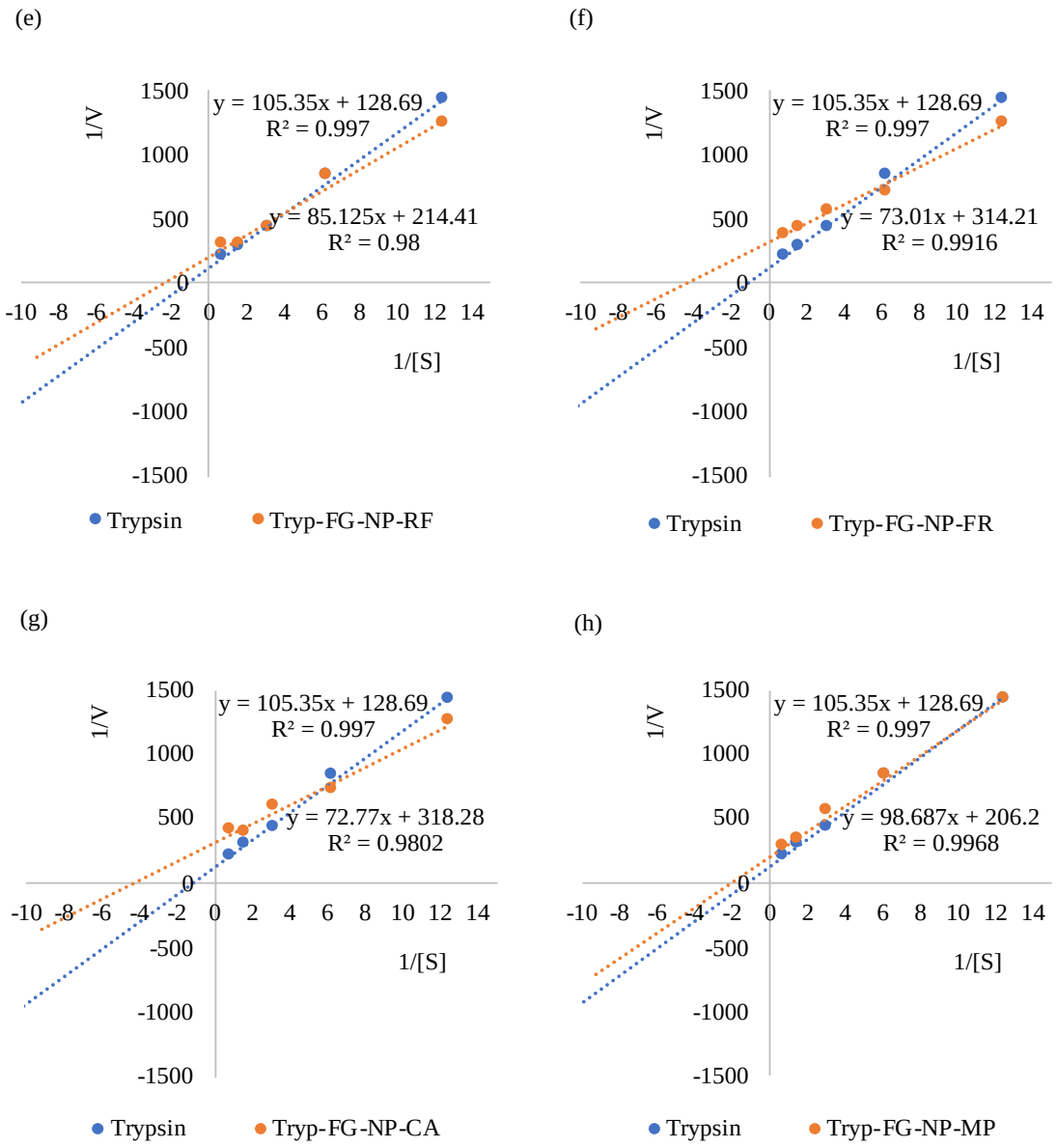

Figure SI 3. 4 Lineweaver-Burk plots of trypsin in the presence and absence of silica particles subjected to different food processing temperatures at various substrate concentrations (0-1.28 mg.mL^{-1}) at 37°C and pH 8.5. (a) FG-NP-RT, **(b)** FG-NP-MW, **(c)** FG-NP-BL, **(d)** FG-NP-BK, **(e)** FG-NP-CA, **(f)** FG-NP-RF, **(g)** FG-NP-FR, **(h)** FG-MP, and **(i)** NFG-NP.

Effect of particle binding on trypsin kinetics

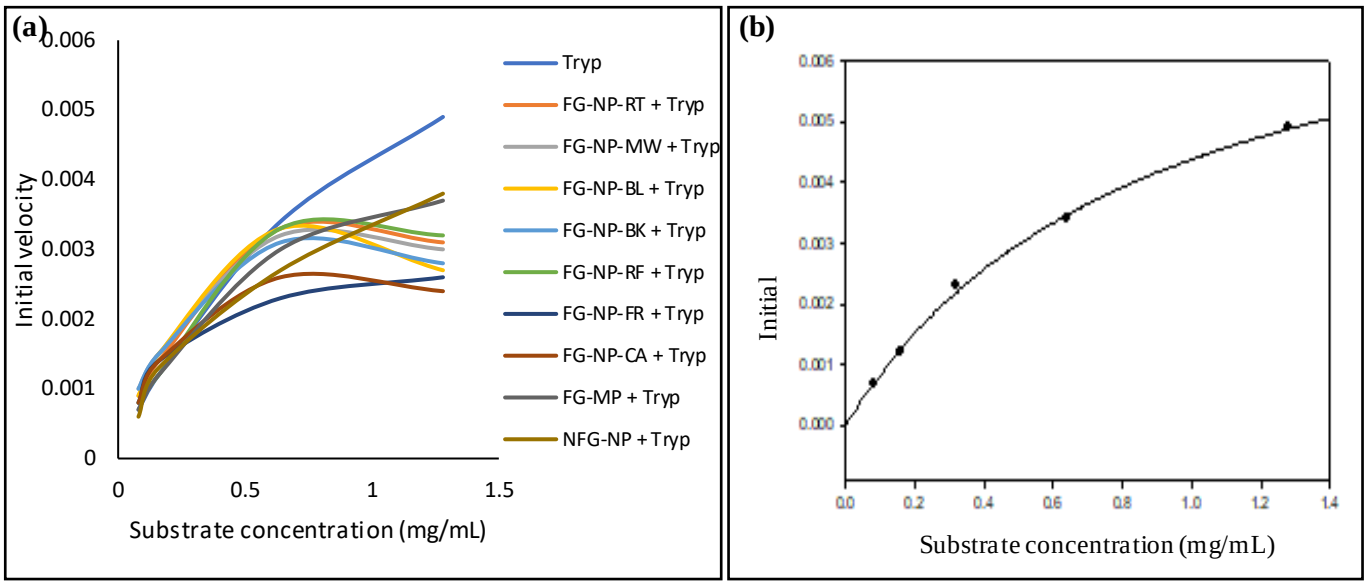

Figure SI 3. 5 Effect of particle binding on trypsin kinetics. (a) Michaelis-Menten plot of trypsin activity in the present and absence of silica particles subjected to different food processing temperatures at various substrate concentrations (0.8-1.28 $mg.mL^{-1}$) at 37°C and pH 8.5. **(b)** Hyperbola curve of trypsin activity was performed using the Sigma Plot software (12.3, Systat software Inc., California, USA) with hyperbola equation during curve fitting.

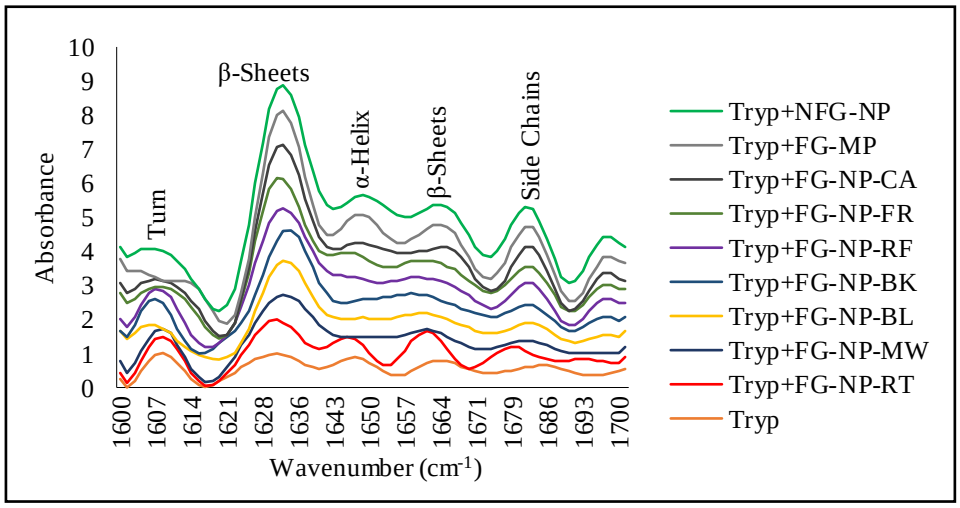

Figure SI 3. 6 The FTIR spectra of trypsin in the presence and absence of silica particles subjected to different food processing temperatures. The spectra were taken for a wavenumber range of 1600-1700 cm^{-1} using Cary 630 FTIR at pH 8.0.

Connecting Text

Chapter 3 reported the physicochemical transformation of silica nanoparticles in different food handling temperatures and the negative impact on trypsin enzyme activity. While this study helped us to understand the changes in physicochemical properties of pristine DNMs, it overlooked the effect of DNM interaction with food matrix. DNMs applied in food interact with organic and inorganic components present in food and biological fluids (when entering human body) and, as a result, acquire a surface layer of adsorbed molecules (surface corona). The surface corona formation changes the surface chemistry of pristine DNMs, and it is a critical determinant of the hazard potential of DNMs. Therefore, chapter 4 addressed the impact of transformed DNM (silica) by a single protein and food matrix on enzyme activity. Chapter 4 is published in Nano Select, Phue, W. H., Srinivasan, D., Aneela, H., Yaylayan, V., and George, S. (2020).

Chapter 4. Food grade silica nanoparticles cause non-competitive type inhibition of human salivary α-amylase because of surface interaction

4.1 Abstract

Given the potential of ingested particles to interact with enzymes in oral cavity, we compared different grades of SiO_2 particles (food-grade and non-food grade nanoparticles (FG-SiO_2-NP, NFG-SiO_2-NP), and food grade microparticles (FG-SiO_2-MP)) for their interaction with human salivary α-amylase (HSA). There were differences in the agglomeration behavior and relative abundance of silanol and siloxane groups among different grades of SiO_2 particles where FG-SiO_2-NPs contained less cyclic siloxane groups but more silanol groups. Secondary structure and function of HSA were negatively impacted by FG-SiO_2-NPs. In order to verify if this inhibition is mediated through surface interactions, pristine particles were compared with those interacted with pure protein (bovine serum albumin-BSA) and with food matrix (milk) for HSA inhibition. BSA coating of SiO_2 particles ameliorated HSA inhibition, but milk interacted ones showed an enhanced the HSA inhibition because of the presence of milk protease suggesting the relevance of surface interactions in manifesting potential negative impacts of silica particles used in food.

Keywords: enzyme inhibition, food grade SiO_2 particles, food matrix, human salivary α-amylase, nanoparticle-protein interactions, SiO_2 nanoparticle

4.2 Introduction

Applications of nano-sized particles in food, pharmaceuticals and nutraceutical industries for enhancing the stability, quality, and the bioavailability of active ingredients and overall functions of the final product are increasing exponentially [1]. The growing trend in the application of manufactured nanoparticles in food and consumer products undeniably leads to human exposure through oral route. While the consequences of nanoparticles entering human body through oral route remains largely elusive [1, 2], there are ample reasons for concern as emerging studies point towards potential negative health effect of nanoparticles applied in food [3, 4]. For instance, oral administration of titanium dioxide (TiO_2) nanoparticles was observed to induce preneoplastic lesions and promote aberrant crypt development in the rat colon [5]. Similarly, nanoparticles of amorphous silica (SiO_2) had shown the potential to activate inflammasome [6] and enhance intestinal permeability due to negative surface charge of the particles [7]. Thus, while these studies indicate the potential health risks of nanoparticles, studies addressing the interaction of dietary nanoparticles with proteins of relevance to the gastro-intestinal system are grossly lacking [1, 8].

Upon entry into the human body, particles encounter various biological fluids and ultimately their surface gets coated with a wide range of biomolecules- generally referred to as "corona". Surface corona plays an important role in the biological identity of particles and influences their fate and transport into the body [9, 10]. Proteins form a major portion of the biocorona on the particle surface. The presence of corona on the particles can modify the size, shape, surface charge of the pristine particles. These modifications can influence the biocompatibility of the particles [11]. While ingested nanoparticles are likely to interact with salivary proteins, there are prominent knowledge gaps on implications to the structure and function of salivary enzymes.

Human salivary α-amylase (HSA), the most abundant enzyme in human saliva is characterized by single polypolypeptide chain of ~475 amino acid residues, 2 sulfahydryl groups and 4 di-sulfide bridges. HSA initiates the digestion of complex carbohydrates in the oral cavity, where starch molecules get partially digested into oligosaccharides, maltose and glucose [12]. Previous studies have shown the potential of amorphous SiO_2 nanoparticles to negatively impact the structure and function of lysozyme [13]. Although there are reports about the use of SiO_2 nanoparticles for the immobilization of amylase [14], detailed investigation on the differential effect of food grade SiO_2 nano and micro sized particles on the structure and function of HSA is lacking. Further, there are knowledge gaps on the differences among pristine and food matrix interacted nanoparticles on their interaction with digestive enzymes.

We investigated the effects of different grades of SiO_2 particles- food grade SiO_2 nanoparticles (FG-SiO_2-NPs), food grade SiO_2 microparticles (FG-SiO_2-MPs) and non-food grade SiO_2 nanoparticles (NFG-SiO_2-NPs)- on the structure and enzyme kinetics of HSA. In addition, pristine particles were compared with those surfaces interacted with pure proteins (BSA) and with a food matrix (milk) to evaluate their consequences on HSA function. We report the differential effects of different grades of SiO_2 particles on the structure and function of HSA and effect of surface passivation with BSA and milk.

4.3 Materials and Methods

4.3.1 Chemicals and reagents

All the chemicals and reagents used were of analytical grade. Human Salivary α-Amylase (HSA, 1000 U/mg) was purchased from Lee BioSolutions (Maryland Heights, USA). Soluble potato starch, 3,5-Dinitrosalicylic acid and N-α-benzoyl-DL-arginine 4-nitroanilide hydrochloride (BApNA) were purchased from Sigma Aldrich (St. Louis, Missouri, USA). Food grade silica particles (SiO_2) in nano size (AEROSIL 200F) and micro size (SIPERNAT 22) also known as E551 were obtained from Evonik Corporation (NJ, United States). Similar primary size of non-food grade SiO_2 nanoparticle was selected to compare the effect of the different grade of the particles and it was purchased from Sigma-Aldrich (cat# 637238, 10−20 nm particle size (BET), 99.5% trace metals basis) (Missouri, USA). Deionized (DI) water obtained from Milli-Q system (Millipore Sigma, MA, USA) was used to prepare all reagents and samples.

4.3.2 Physical Characterization

All the particles in their pristine state were characterized for their agglomeration/aggregation size, shape, surface charge, and surface chemistry. The shape and size of the silicon dioxide particles (FG-SiO_2-NP, FG-SiO_2-MP and NFG-SiO_2-NP) were observed by scanning electron microscopy (SEM). For SEM analysis, samples (5 µL of 50 ppm particles dispersed in DI water) were dropped on the SEM stub, dried at room temperature overnight and were examined at 50 KV accelerating voltage without coating using SEM-SU8230 (Hitachi, Japan) [15]. The hydrodynamic size, polydispersity index and surface charges of particles (pristine and those interacted with proteins) were measured by dynamic light scattering (DLS) using NanoBrook Omni instrument (Brookhaven's, New York, USA) at 25˚C at a concentration of 50 ppm in

PBS. Samples prepared for the DLS were loaded into a pre-rinsed folded capillary cell and for the zeta potential measurement, voltage of 100 V was applied [16].

Attenuated total reflectance-Fourier transform infrared (ATR-FTIR) was used for the identifications of the surface chemistry of SiO_2 particles (ALPHA-P, Bruker, Billerica, MA, USA). For this, 5 μL aliquots of SiO_2 particles (stock concentration 10 $mg.mL^{-1}$ in DI water) were dropped on the ATR probe and left to dry for 15 min. Wavelength range of 400−4000 cm^{-1}, with a resolution of 4 cm^{-1}, and 24 scans were used for obtaining the FTIR spectra. Qualitative analysis of Si−O−Si groups (cyclic and linear) was performed by deconvolution of the FTIR spectra region between 1200 and 900 cm^{-1} using the OMNIC 8.2.0.387 software (Thermo Scientific, MA, USA).

4.3.3 Interaction of SiO_2 particles with HSA

A stock solution of HSA (1000 U) was prepared in 20 mM PBS buffer at pH 6.5 and diluted with the same buffer for the working stock (2 U). Depending on the experiment protocol the concentration of the enzyme was either kept constant and/or varied. The reaction mixture was equilibrated for the optimal incubation time at 37 ˚C for 1 h to ensure the dynamic equilibrium in the protein corona formation [17].

4.3.4 Effect of SiO_2 particles on HSA activity and enzyme kinetics

HSA activity was assessed by measuring the amount of reducing sugars generated by the action of HSA on starch (substrate) by dinitrosalicylic acid method (DNS). For this purpose, 10% (w/v) soluble potato starch solution was prepared by dissolving 5 g of potato starch in 50 mL of 20 mM sodium phosphate buffer (pH 6.9 with 0.006 M of sodium chloride). The resulting solution was heated directly on a hot plate under constant stirring, till boiling and the solution was maintained at that temperature for 15 minutes to enhance the solubility of the starch solution. DNS reagent was prepared by dissolving 1 g of 3,5-dinitrosalicylic acid in 50 mL

dH_2O. It was then mixed with sodium potassium tartrate tetrahydrate solution prepared in 2N sodium hydroxide, heated on a hot plate at 70˚C and made up to 100 mL with dH_2O. The working solution of standard enzyme HSA (2 U mL^{-1}) was prepared from stock solution (1000 U mL^{-1}) in PBS buffer and used to hydrolyze the starch. The HSA inhibitory activity of silica particles and tannic acid (as the positive control) were determined according to the procedure described earlier with modifications [18]. The inhibitors (SiO_2 particles and tannic acid) (40 µL of 2 $mg.mL^{-1}$)) and HSA (40 µl) were added in the 96 well microplate and incubated at 37 ˚C for 1 h. Subsequently, 20 µL of starch solution was added to the wells, incubated for 10 mins at 37 ˚C and the reaction was terminated by adding 100 µL of DNS reagent and keeping the plate in boiling water bath maintained at 100 ˚C for 15 min.

The plate was cooled to room temperature and the absorbance was measured at 540 nm for each well using a plate reader (Spectra max i3x, Molecular Devices, USA). The % of amylase inhibition was calculated using following equation 4.1 (Eq. 4.1):

$$\% \text{ of Amylase Inhibition} = [(A_{Control} - A_{Sample})/A_{Control}] \times 100\% \quad \textbf{(Eq. 4.1)}$$

where reaction mixer without the presence of any particles or inhibitor was taken as negative control.

The effect of particles on enzyme kinetics was elucidated by measuring enzyme activity in particles interacted HSA at increasing concentrations of soluble starch. Kinetic parameters were obtained by incubating 2 $U.mL^{-1}$ HSA with incremental concentrations of inhibitors (SiO_2 particle from 2-16 $mg.mL^{-1}$) and the substrate (starch) concentration (from 1-10 $mg.mL^{-1}$). Types of enzyme inhibition when interacted with particles were determined by fitting the kinetic data in to Dixon plot and Cornish-Bowden plot graphs.

4.3.5 HSA-SiO_2 particles interaction: Determining enzyme binding constant

The binding constants for HSA interactions with different SiO_2 particles were determined by measuring fluorescence intensity of protein. Samples for fluorescence spectroscopy were

prepared by mixing 100 µL of HSA (10 $U.mL^{-1}$) with 30 µL of increasing concentration of the SiO_2 particles from 0.5-10 $mg.mL^{-1}$. The resulting mixture was then incubated at 37 ˚C for 1 h. Fluorescence measurements were obtained using a plate reader (Spectra max i3x, Molecular Devices, USA). The emission spectra were recorded in the range of 320-600 nm upon excitation with 280 nm, using 10 nm/10 nm slit widths, and each spectrum was the average of three scans.

The binding constant and number of binding sites were obtained by Stern -Volmer equation (Eq. 4.2):

$$\frac{I_0}{I} = 1 + K_q \tau_0 [Q] = 1 + K_{sv}[Q] \qquad \textbf{(Eq. 4.2)}$$

where I_0 and I represent the fluorescence intensities in the absence and the presence of the quencher (SiO_2 Particles), respectively, K_{sv} is the dynamic quenching constant and Q is the concentration of the quencher. The slope of the fitted data to the equation gives the value of K_{sv}. K_q is the bimolecular quenching rate constant, and τ_0 is the biomolecular fluorescence lifetime in the absence of quencher, which is considered to be 2.97 ns for α-amylase [19].

4.3.6 Circular dichroism spectroscopy

SiO_2 particles were interacted with HSA (final concentrations of 1 $mg.mL^{-1}$ and 0.15 $mg.mL^{-1}$, respectively) in 20 m_M phosphate buffer (pH 6.5) for 1 h at 37 °C. Four hundred microliters of the HSA-particle complex solution was added to a quartz cell with 0.1 cm path length, and the CD spectra were recorded from 190 to 260 nm at 37 °C using a Jasco J-810 Spectro-polarimeter (Jasco Corp., OK, USA). Each spectrum was an average of three scans, and the percentages of helices, strand, turns, and unordered were calculated using the DICHROWEB online software (DWA03771307) at http://www.cryst.bbk.ac.uk/cdweb (access date 16/05/2018).

4.3.7 Effect of BSA and milk interacted SiO_2 particles on HSA activity

SiO_2 nanoparticles exposed to the pure protein/food matrix were hypothesized to lower their inhibitory action on HSA. In order to verify this effect, SiO_2 particles were prior exposed to BSA and skimmed milk obtained from a local grocery store (Quebon, Agropur Dairy Cooperative, QC, Canada). Milk stored at 4˚C was subjected to centrifugation (14,000 rpm for 15 mins) and the supernatant was collected for further studies. Two hundred µL of 10 $mg.mL^{-1}$ of particles were mixed with 800 µL processed milk or 800 µL of 1 $mg.mL^{-1}$ BSA (control) and incubated for 1 hr at 37°C. Higher concentration of particles were chosen to enhance the protein corona formation. Particles were then pelleted out by centrifugation (14,000 rpm), excess of milk or BSA in the supernatant was discarded. The washing step was repeated 3 times by suspending particles in phosphate-buffered saline (PBS) and pelleting by centrifugation. The milk/protein interacted particles were used to test HSA enzyme activity using DNS method as described in the preceding section.

4.3.8 Protease activity of milk interacted SiO_2 particles

The milk interacted particles were prepared the same way as described above. After the last wash, the pellet was added with 500 µL of substrate- N-α-benzoyl-DL-arginine 4-notroanilide hydrochloride (BApNA)- prepared in 50 m_M Tris HCl buffer, pH 8.0, and containing 20 m_M $CaCl_2$. After addition of BApNA (0.6 $mg.mL^{-1}$) the pellet containing milk interacted SiO_2 particles were suspended by vortexing. The solution was kept at 37°C overnight. Subsequently, the absorbance of the supernatant was measured at 420 nm using a UV-vis spectrophotometer (Spectra Max M2, Molecular Devices, USA) after removing particles from the suspension by centrifugation at 14,000 rpm for 15 min. The absorbance value was used for measuring the level of protease activity in milk interacted particles.

4.3.9 Statistical analysis

Experiments were performed in triplicates and replicated at least three times. The data collected in this study are expressed as the mean value ± standard deviation (SD). Statistical comparisons were made by Duncan and p value ≤ 0.05 was considered significantly difference.

4.4 Results

In this study, FG-SiO_2-NPs, FG-SiO_2-MPs and NFG-SiO_2-NPs were characterized prior to their interaction with the HSA enzyme to assess their size and shape using SEM as shown in the Figure 4.1A-C. According to the suppliers, the primary particle sizes of FG-SiO_2-NP, FG-SiO_2-MP and NFG-SiO_2-NP were 12 nm, 110 µm and 20 nm respectively. However, results of FG-SiO_2-NP from SEM analysis showed agglomerates of spherically shaped particles, and the average diameter of primary particle was around 30 nm (Figure 4.1A). FG-SiO_2-MP and NFG-SiO_2-NP had primary particles of size ~30 nm which were aggregated to form particle aggregates of size 0.5-5 µm (Figure 4.1B and C). The difference in hydrodynamic size when suspended in buffer was evident among these particles as 274 nm, 602 nm and 1046 nm for FG-SiO_2-NP, FG-SiO_2-MP and NFG-SiO_2-NP, respectively (tabular data, Figure 4.1D). The increase in hydrodynamic size of protein interacted particles suggested protein corona formation on the particles. All tested particles exhibited negative surface charge.

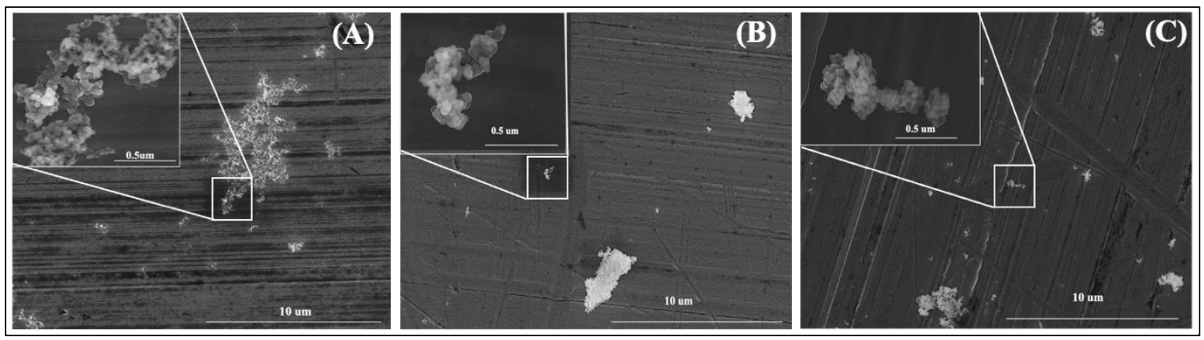

(D)

	Hydrodynamic size [nm ± Std dev]		**Polydispersity index [PdI ± Std dev]**		**Zetapotential [mV ± Std dev]**	
	M	SD	M	SD	M	SD
FG-SiO_2-NP	274.42 [a]	4.2	0.277[a]	0.008	-21.9[b,c]	6.3
FG-SiO_2-MP	602.16 [a]	17.8	0.356[a]	0.02	-25.02[a,b]	3.3
NFG-SiO_2-NP	1046.16 [a,b]	38.0	0.494[a,b]	0.06	-24.09[a,b]	0.5
BSA-FG-SiO_2-NP	3218.26 [c]	119.3	0.46 [b]	0.02	-18.13[b,c]	4.8
BSA-FG-SiO_2-MP	4460.69 [d]	1437.5	0.507[b]	0.02	-30.18[a,b]	6.2
BSA-NFG-SiO_2-NP	2632.78 [b,c]	231.2	0.361[a]	0.02	-21.43[b,c]	0.9
Milk-FG-SiO_2-NP	827.49 [a]	80.9	0.293[a]	0.03	-16.21[c]	2.4
Milk-FG-SiO_2-MP	269.31[a]	15.8	0.312[a]	0.04	-16.53[c]	0.8
Milk-NFG-SiO_2-NP	1066.62 [c,b]	76.9	0.387[a,b]	0.02	-18.38[b,c]	1.5

Figure 4. 1 SEM images of SiO_2 particles obtained after atmospheric drying of particle suspensions (50 ppm) on SEM stub. Images were obtained using SEM (Hitachi, SEM-SU8230) without coating. **(A)** FG-SiO_2-NP **(B)** FG-SiO_2-MP and **(C)** NFG-SiO_2-NP. **(D)** Agglomeration size, polydispersity index and surface charge of SiO_2 particles in the presence

and absence of proteins suspended in PBS were determined using dynamic light scattering method. Means with different small letters in the same column are significantly different (Duncan, $p<0.05$).

4.4.1 The surface chemistry of different grades of SiO_2 particles

The surface chemistry of different grades of pristine SiO_2 particles were compared using FTIR spectra (Figure 4.2). These spectra were measured in full scan from 4000 to 400 cm^{-1}, and the region between 1200-900 cm^{-1} was Fourier self-deconvoluted in order to identify the ring, branched and linear structure of siloxane and silanol groups. Core of the SiO_2 particles contain siloxane (Si-O-Si) rings and silanol (Si-OH) groups are found on the surface of the particles. As presented in Figure 4.2, more Si-OH groups (963 cm^{-1}) [15,20] were detected in FG-SiO_2-NP while higher Si-O groups (940 cm^{-1}) were identified in the FG-SiO_2-MP and NFG-SiO_2-NP. The branched siloxane group (at 1050cm^{-1}) was present in FG-SiO_2-MPs and NFG-SiO_2-NPs with similar intensity. Most of the siloxane groups in FG-SiO_2-NP existed as linear structure (1030 cm^{-1}) [15,21] while cyclic structures (1000-1020 cm^{-1}) [15,22] were noted in FG-SiO_2-MPs and NFG-SiO_2-NPs.

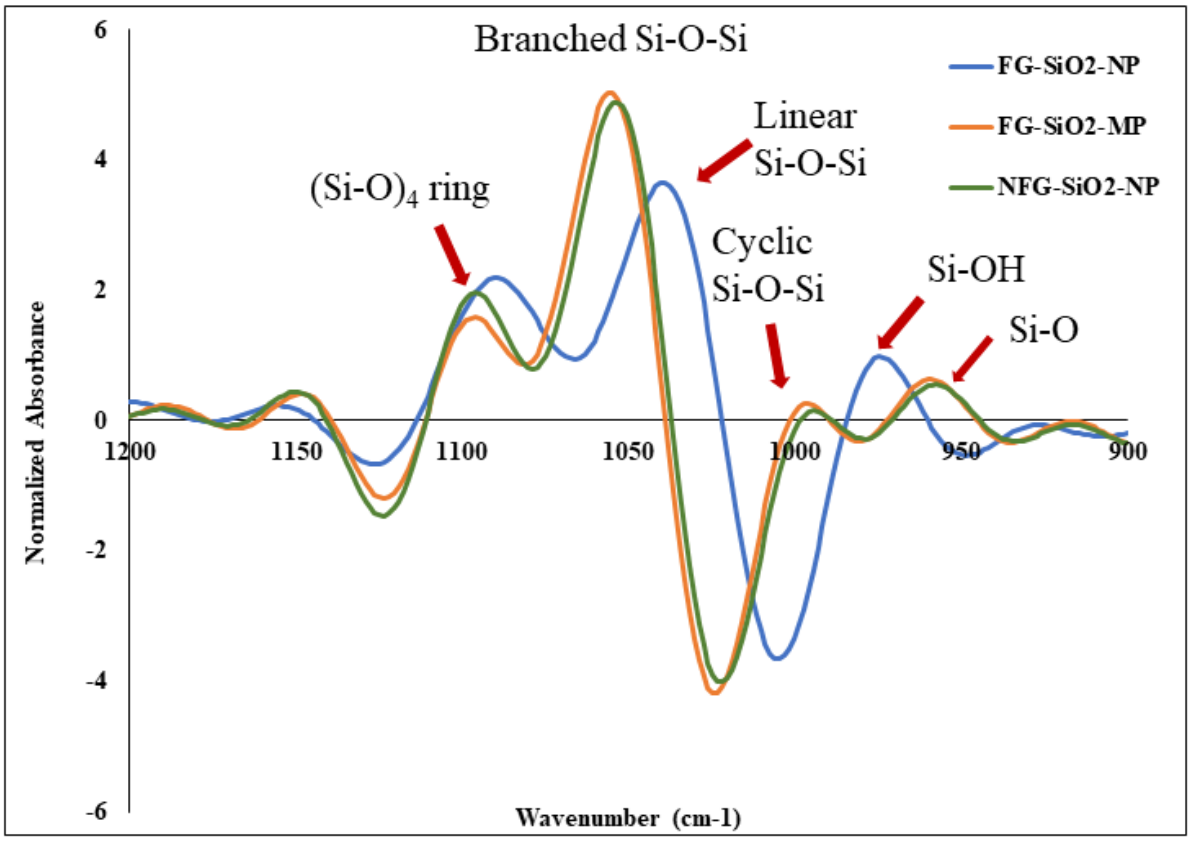

Figure 4. 2 FTIR analysis of SiO_2 particles. Particles suspended in water were dropped and dried on the ATR probe before taking the spectra for a wavenumber range of 400-4000 cm^{-1} using ATR-FTIR. The spectra were generated by Fourier self-deconvolution of wavenumber between 1200-900 cm^{-1}.

4.4.2 Enzyme kinetics studies

The inhibition of HSA activity was determined by DNS method and the inhibition percentage of silica particles were compared with positive control (tannic acid) (Figure 4.3A). It was found that the inhibition was higher when the enzyme interacted with FG-SiO_2-NP followed by NFG-SiO_2-NP and FG-SiO_2-MP. We observed 20% reduction in HSA activity when it was interacted with FG-SiO_2-NP while the inhibition was only ~ 10% for the enzyme interacted with FG-SiO_2-MP and NFG-SiO_2-NP at comparable concentrations of particles. The inhibition percentage of silica nanoparticle was one-fourth lower than the positive control. The dissociation constant (K_i) for enzyme-inhibitor complex was obtained using Dixon plot. The effect on the enzyme rate of HSA was determined at increasing substrate concentration from 1 to 10 $mg.mL^{-1}$ and over a range of inhibitor (FG-SiO_2-NP, FG-SiO_2-MP and NFG-SiO_2-NP particles) concentrations from 2 to 16 $mg.mL^{-1}$. The type of enzyme inhibition was deducted from Dixon plot given in Figure 4.3 B, C & D wherein the inhibition constant K_i is the concentration required to produce half maximum inhibition that suggest the potency of an inhibitor.

The FG-SiO_2-NP interacted HSA (Figure 4.3B) showed non-competitive inhibition as the inhibition curves obtained with different substrate concentrations converged below the x axis. The value of [I] where they intersect is typical of non-competitive type inhibition with the Ki value of 0.4 M. The types of inhibition were also confirmed by Cornish-Bowden plot (Figure SI 4.1 A) which intercepted below the x axis [23]. HSA interacted with FG-SiO_2-MP and NFG-SiO_2-NP showed a mixed type inhibition as the lines converged above the x axis and the value of [I] where they intersect was at K_i value of 0.45 $_M$ (Figure 4.3 C and D) [24].

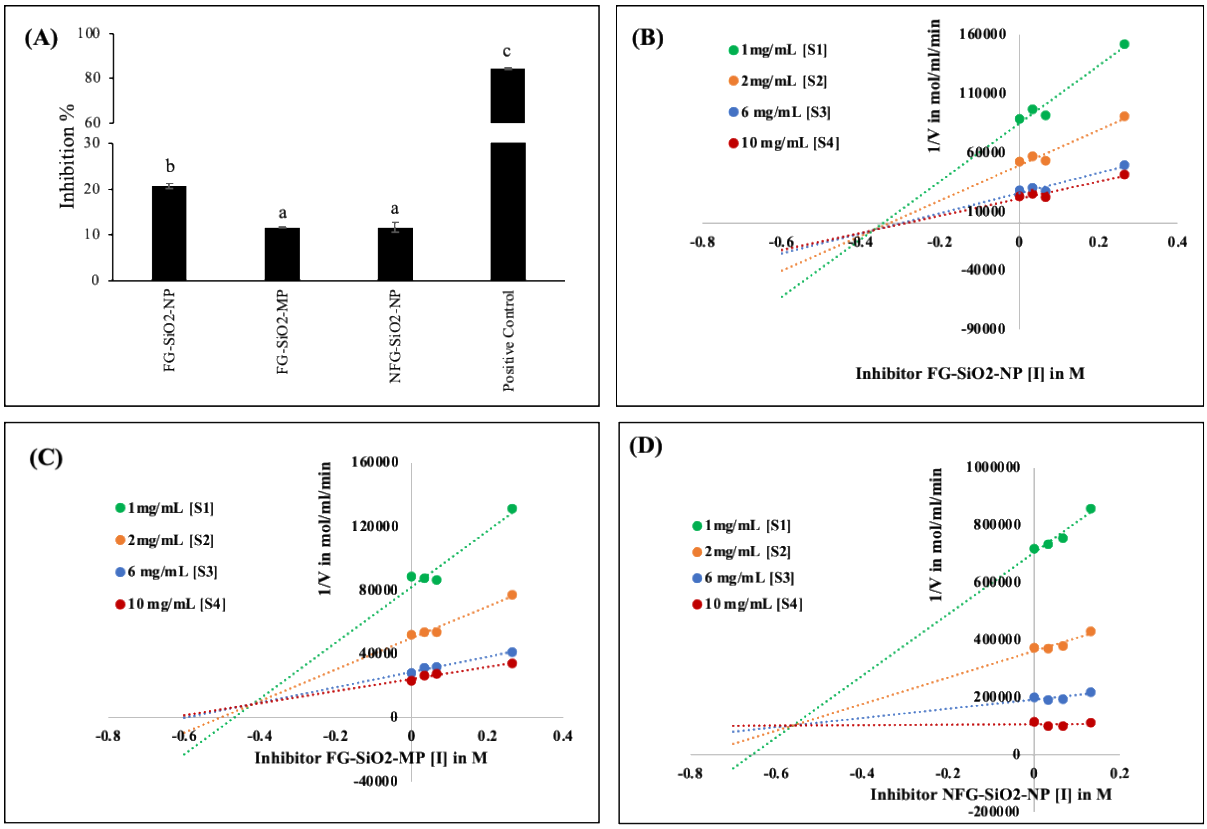

Figure 4. 3 (A) HSA inhibition (%) of pristine SiO_2 particles compared with positive control (tannic acid). Average values plotted in the graph with different small letters indicate significant difference (Duncan, $p<0.05$). Dixon plot was developed by following enzyme activity with increasing concentration of silica particles at incremental concentrations of substrate (starch) **(B)** FG-SiO_2-NP, **(C)** FG-SiO_2-MP, **(D)** NFG-SiO_2-NP.

4.4.3 Fluorescence quenching studies of HSA in the presence of SiO_2 particles

Quenching of protein's intrinsic (tryptophan) fluorescence was employed for more detailed understanding of protein-particle interactions. HSA showed strong fluorescence emission at 360 nm when excited with 280 nm. The fluorescence value gradually decreased along with increasing concentrations of SiO_2 particles. As expected, fluorescence quenching was relatively higher for HSA interacted with FG-SiO_2-NP compared to that of FG-SiO_2-MP and NFG-SiO_2-NP (Figure SI 4.3). Stern–Volmer (SV) equation was applied to determine the nature of fluorescence quenching after interaction of HSA with SiO_2 particles. K_{sv} was calculated for FG-SiO_2-NP, FG-SiO_2-MP and NFG-SiO_2-NP interacted HSA from SV plot and values were 1.5454 $_M{}^{-1}$, 0.3177 $_M{}^{-1}$ and 0.359 $_M{}^{-1}$, respectively (Table 4.1). Similarly, the biomolecular quenching rate constant K_q for HSA interacted with FG-SiO_2-NP, FG-SiO_2-MP and NFG-SiO_2-NP were $5.2x10^8$ ($_M{}^{-1}$ s^{-1}), $1.07x10^8$ ($_M{}^{-1}$ s^{-1}) and $1.21x10^8$ ($_M{}^{-1}$ s^{-1}) respectively (Table 4.1).

Table 4. 1 Table summarizing binding affinity of HSA.

	K_{sv} (M^{-1})	K_q ($M^{-1}s^{-1}$)
FG-SiO_2-NP	1.5454	5.2×10^8
FG-SiO_2-MP	0.3177	1.07×10^8
NFG-SiO_2-NP	0.359	1.21×10^8

$\tau_o = 2.97 \times 10^{-9}$ s for trypsin in the absence of quencher.

*Stern-Volmer constant (K_{sv}) and bimolecular quenching rate parameter (K_q) of HSA in the presence of SiO_2 particles calculated from Stern-Volmer plot given in Figure SI 4.3.

4.4.4 Circular dichroism spectroscopy to understand the changes in the secondary structure of HSA during interaction with SiO_2 particles

The Circular dichroism (CD) spectroscopy was used to determine changes in the secondary structure of HSA upon interaction with SiO_2 particles. The typical pattern of α- helical protein with negative band at 222 nm and 208 nm and a positive band at 190 nm secondary structure pattern [25] was observed (Figure 4.4A). Tabular data (Figure 4.4B) summarises percentage of prominent secondary structure features of HSA with and without SiO_2 particles interaction. Based on the spectra, the secondary structure of SiO_2 particles interacted HSA was only slightly different from free HSA. Generally, the percentage of helix and unordered structures were reduced by the interactions of HSA with SiO_2 particles while the percentage of strand and turns increased. The alteration in secondary structure as evidenced by the reduction in helix and increase in turns was comparatively higher when HSA was interacted with SiO_2 nanoparticles (Figure 4.4B).

We hypothesized that the inhibitory effect of pristine SiO_2 particles on HSA could be ameliorated by pre-treatment of particles with albumin and food matrix. Bovine serum albumin was used as the pure protein to coat pristine SiO_2 particles while skimmed milk (0% fat) obtained from a local grocery store was used as a model food matrix.

(A)

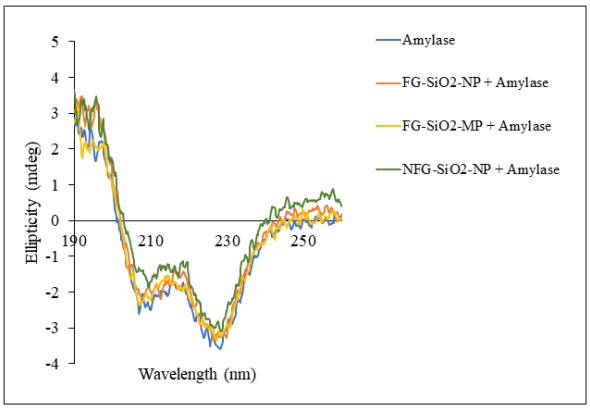

(B)

	Helix (%)	**Strand (%)**	**Turns (%)**	**Unordered (%)**
Amylase	4.8	35.6	18.3	41.3
Amy-FG-SiO_2-NP	4.6	36.6	18.8	40.1
Amy-FG-SiO_2-MP	4.6	35.7	18.6	41.3
Amy-NFG-SiO_2-NP	4.2	37.2	19.0	39.7

Figure 4. 4 Alteration of secondary structure of HSA in the presence of SiO_2 particles. **(A)** CD spectra of HSA in the presence and absence of SiO_2 particles. **(B)** Table Summarises the secondary structure features of HSA assessed using CD after interacting with SiO_2 particles. The concentration of HSA and the SiO_2 Particles in the CD study was 0.15 $mg.mL^{-1}$ and 1 $mg.mL^{-1}$, respectively.

4.4.5 Impact of protein interacted SiO_2 particles on HSA activity

The HSA inhibition activities of pure protein and milk interacted SiO_2 were evaluated, and the results are shown in Figure 4.5. Characteristic FTIR peak at 1500–1700 cm^{-1} confirmed the presence of proteins on the surface of BSA and milk interacted particles (Figure SI 4.2). The inhibitory action of SiO_2 particles on HSA decreased significantly when the particles were precoated with BSA before interacting with HSA (Figure 4.5A). Among the tested particles, FG-SiO_2-NP showed the most significant difference when interacted with BSA. While, the pristine FG-SiO_2-NP showed 12% inhibition of HSA activity, it was only 6% when protein interacted FG-SiO_2-NP was used (50% recovery). Contradictory to our expectations, however, milk interacted SiO_2 particles had higher HSA inhibition in comparison to pristine SiO_2 particles (Figure 4.5A). The increase in HSA inhibition was evident in FG-SiO_2-MP, where ~2.5 fold increase in HSA inhibition was observed for milk interacted particles in comparison to the inhibition of HSA by pristine particles.

We suspected that the increase in HSA inhibition shown by milk interacted particles is because of the presence of protease enzyme in the biocorona. Therefore, we measured the protease enzyme activity of milk interacted SiO_2 particles. As shown in Figure 4.5 B, the protease activities on milk interacted SiO_2 particles (2 mg) were shown to be ~ 30 mU for FG-SiO_2-NP and FG-SiO_2-MP. Among the particles, food-grade particles had the highest level of protease activity. Notably, the protease activity on particles interacted milk was higher than that from the same concentration of milk- the enhancement of protease activity- suggestive of protease enrichment on the surface of particles.

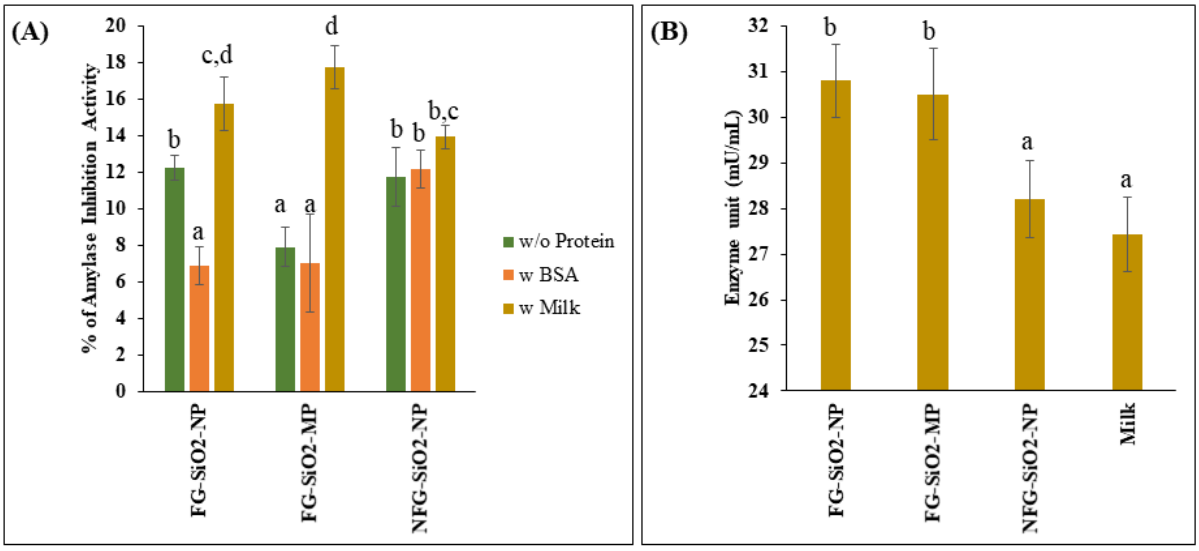

Figure 4. 5 Impact of protein interacted SiO_2 particles on HSA activity. (A) HSA enzyme inhibition activity of pristine SiO_2 particles, BSA interacted SiO_2 particles, and milk interacted SiO_2 particles **(B)** activity of protease on milk interacted SiO_2 particles. Means with different small letters are significantly different (Duncan, $p<0.05$).

4.5 Discussion

HSA constitutes a significant proportion of salivary proteins and plays an important role in the initial digestion of starch, glycogen and other polysaccharides in the mouth. Previous studies from our group had reported the preferential binding of amylase onto dietary nanoparticles [26]. As a sequel to that study, we were interested in assessing the consequences of amylase binding onto particle surface on its structure and function. In addition, we were interested in understanding if the effect could be different when nanoparticles surfaces are modified by food metrics. This study revealed the differential effects of food grade SiO_2 nanoparticles, microparticles, and non-food grade SiO_2 nanoparticles on HSA activity and that surface modification by food matrix could influence its effect on amylase activity.

Among the tested particles, nanoparticles of food grade SiO_2 showed the highest level of HSA inhibition (Figure 4.3A). HSA inhibition was concentration dependent, and we followed the inhibition kinetics of the particles. This analysis showed difference among particles in the type of HSA inhibition where FG-SiO_2-NPs showed a non-competitive type inhibition while micro sized and the non-food grade SiO_2 nanoparticles showed a mixed type inhibition (Figure 4.3B, C, and D). Non-competitive inhibition is a type of mixed inhibition involving enzyme-substrate-inhibitor complex while in a competitive binding, the inhibitor (particle in this case) precludes the binding of substrate. We also noticed that the protein binding affinity of food grade SiO_2 nanoparticles to be relatively higher in comparison to other particles (Table 4.1 and Figure SI 4.3). The K_q (binding affinity) value for food grade SiO_2 nanoparticles was ~ 5 times higher than that of micro particles and non-food grade SiO_2 nanoparticles. The outcomes from enzyme inhibition assay were found to be in line with the binding affinity data where stronger affinity of FG-SiO_2-NPs corresponded with higher inhibition of the HSA. Moreover, the quenching effect of FG-SiO_2-NP was found to be concentration dependant whereas, there was no significant fluorescence quenching with increasing concentration of FG-SiO_2-MP and NFG-

SiO_2-NP (Figure SI 4.3). The fluorescence quenching is also an indicator of the change in the tertiary structure of proteins [27]. Interestingly, as observed by CD spectroscopy there was no drastic change in the secondary structure of HSA when interacted with different grades of SiO_2 particles (Figure 4.4). Taken together, these results suggest that the interaction of particles with HSA has minimal effect on secondary structure but changes their tertiary structure where the effect was higher for FG-SiO_2-NPs. Thus, while we observed a negative impact of food grade SiO_2 particles on the function and binding affinity for HSA, there are studies reporting the potential of using SiO_2 nanoparticles for the immobilization of enzymes. For instance, SiO_2 particles are reported to immobilize amylase for applications in laundry detergents [14] and modified magnetic nanoparticles to increase the thermal stability and enzyme activity of amylase [28]. These reported studies and the current observation prove that different grades of SiO_2 nanoparticles (food grade and non-food grade) showed different levels of HSA inhibition despite their comparable size are suggestive of factors other than particle size involved in determining binding affinity and inhibition of HSA. We argue that the differences in enzyme inhibition and binding affinities could be explained based on the differences in the surface chemistry of these materials and how it responds to features of HSA.

According to Zhuravlev model, the presence of silanol groups and siloxane bridges are the factors determining surface properties of amorphous SiO_2 [29]. The negative surface charge (of pristine SiO_2 particles) and hydrophilic nature of silanol groups (at neutral pH) and hydrophobic nature of siloxane ring structure provide anchoring points for proteins on SiO_2 particles. As observed by FTIR spectra, FG-SiO_2-NPs have higher Si−OH groups on their surfaces in comparison to NFG-SiO_2-NPs and FG-SiO_2-MPs (Figure 4.2). In addition, the higher content of branched and cyclic siloxane groups on the surface of FG-SiO_2-MPs and NFG-SiO_2-NPs differentiated them from FG-SiO_2-NPs in terms of surface chemistry. The outcomes of protein-particle interactions, however, are dictated by how the surface chemistry

of SiO_2 particle interact with unique features of proteins defined by charge, hydrophobicity, and divalent cation binding sites etc. HSA structure consists of three domains (A, B and C); of which the catalytic amino acid residues (Asp197, Glu233 and Asp 300) are located in domain A [30]. In addition, domain A has a chloride ion coordinated by side chains of Arg 195, Asn 298, and Arg 337 and a calcium ion that is coordinated by His201 from domain A and Asn100, Arg158 and Asp167 from domain B [30]. The calcium ion by virtue of its location stabilizes the structural integrity of the A and B domains, orients the His l01 in the substrate-binding cleft and provides an asymmetric environment for substrate binding [31]. The chloride ion is assumed to play a role in stabilizing the structural organization of catalytic sides by diminishing the possibility of non- productive and unfavourable electrostatic interactions that otherwise might exist between basic and acidic residues located in the active-site region [30]. Given the relevance of calcium and chlorine binding motifs in binding on to nanoparticles, it is likely that binding of HSA molecules to SiO_2 particles disrupt the structural integrity of A and B domains and the substrate binding. The relative amounts of silanol groups and siloxane groups on different particles differentiate the extent and type of enzyme inhibition. Thus, while more studies are warranted on the molecular interactions of amylase with SiO_2 nanoparticles, we reason that FG-SiO_2-NP with relatively higher silanol groups disrupt molecular structure of HSA and affirm the binding through hydrophilic interactions leading to non-competitive type of amylase inhibition.

The observation from current studies showed that HSA inhibition requires direct interaction of SiO_2 surface with protein molecule. Therefore, we argued that pristine SiO_2 particles modified by surface adsorbed proteins and other biomolecules, as in the case of those incorporated in food, would not exhibit enzyme inhibition. The hypothesis was tested by surface modification of pristine SiO_2 particles with either pure proteins (BSA) or those suspended and recovered from skimmed milk (as a model food matrix). As expected, the surface modification of SiO_2

particles using BSA decreased the HSA inhibitory potential of particles (Figure 4.5A). The formation of BSA layer (as confirmed with DLS and FTIR) over the surface of SiO_2 particles precludes the direct interaction of HSA with SiO_2 surface chemistry. The potential of albumin as a binding partner of HSA was reported recently [32]. Thus, the protein-protein interaction that does not compromise the function is thought to anchor HSA onto these particles but without major disruption in its function.

Silica particles applied in food are likely to acquire surface coating of biomolecules before its likely interaction with HSA. As such, it is unlikely that the pristine surface of silica particles would interact with HSA. While this could be in most of the cases of SiO_2 used in food, we also tested SiO_2 particles retrieved from milk (pasteurized skimmed milk) for their effect on HSA. Contradictory to the effect of BSA, particles interacted with milk showed a higher HSA inhibition (Figure 4.5A). Based on results from the BSA interacted particles, we ruled out the possibility of the disruption of the structure of HSA. We suspected the presence of protease in the biocorona of SiO_2 particles retrieved from milk. The protease present in these particles could digest HSA which will be observed as decreased HSA activity. This investigations in fact showed the presence of protease activity in milk interacted particles (Figure 4.5B). This observation exemplifies possibilities of undesired outcome arising from unexpected phenomena when nanoparticles interact with a food matrix.

4.6 Conclusion

In conclusion, the current studies delineated differential effects of different grades of SiO_2 particles to bind with HSA and their effect on the structure and function of HSA. Among different grades of SiO_2 tested, FG-SiO_2-NP showed higher binding affinity, potential disruption of tertiary structure and partial loss of enzyme function. This studies showed that direct interaction of SiO_2 nanoparticles with HSA is needed for the alteration in structure and function of HSA and that effect could be shielded by modifying the surface of SiO_2 particles. These studies also showed that the food matrix interacted particles can affect the functionality of HSA differently depending on the type of food matrix. Outcome from this study also signifies the molecular interaction between digestive enzymes and dietary nanoparticles that could cause adverse effects on nutrient assimilation.

4.7 References

1. Frewer, L. J., et al., *Consumer attitudes towards nanotechnologies applied to food production.* Trends in food science and technology. 2014, **40**, 211.
2. McCracken, C., P.K. Dutta, and W.J. Waldman, *Critical assessment of toxicological effects of ingested nanoparticles.* Environmental science: Nano, 2016. **3**(2): p. 256-282.
3. Setyawati, M.I., C.Y. Tay, and D.T. Leong, *Mechanistic investigation of the biological effects of SiO2, TiO2, and ZnO nanoparticles on intestinal cells.* Small, 2015. **11**(28): p. 3458-3468.
4. Powell, J.J., et al., *Origin and fate of dietary nanoparticles and microparticles in the gastrointestinal tract.* Journal of autoimmunity, 2010. **34**(3): p. J226-J233.
5. Bettini, S., et al., *Food-grade TiO(2) impairs intestinal and systemic immune homeostasis, initiates preneoplastic lesions and promotes aberrant crypt development in the rat colon.* Scientific reports, 2017. **7**: p. 40373-40373.
6. Winter, M., et al., *Activation of the inflammasome by amorphous silica and TiO2 nanoparticles in murine dendritic cells.* Nanotoxicology, 2011. **5**(3): p. 326-340.
7. Lamson, G.N., et al., *Anionic nanoparticles enable the oral delivery of proteins by enhancing intestinal permeability.* Nature biochemical engineering, 2019. **4**: p. 84-96.
8. Younes, M., et al., *Re-evaluation of silicon dioxide (E 551) as a food additive.* EFSA journal, 2018. **16**(1).
9. Docter, D., et al., *The nanoparticle biomolecule corona: lessons learned - challenge accepted?* Chemical society reviews, 2015. **44**(17): p. 6094-6121.
10. Ke, P.C., et al., *A Decade of the Protein Corona.* ACS nano, 2017.
11. Jafari, S,. et al., *Mesoporous silica nanoparticles for therapeutic/diagnostic applications.*Biomedicine and pharmacotherapy, 2019. **109**: p.1100-1111.

12. Butterworth, P.J., F.J. Warren, and P.R. Ellis, *Human α-amylase and starch digestion: An interesting marriage.* Starch-stärke, 2011. **63**(7): p. 395-405.

13. Vertegel, A.A., R.W. Siegel, and J.S. Dordick, *Silica Nanoparticle Size Influences the Structure and Enzymatic Activity of Adsorbed Lysozyme.* Langmuir, 2004. **20**(16): p. 6800-6807.

14. Soleimani, M., A. Khani, and K. Najafzadeh, *α-Amylase immobilization on the silica nanoparticles for cleaning performance towards starch soils in laundry detergents*. Journal of molecular catalysis B: enzymatic, 2012. **74**(1): p. 1-5.

15. Phue, W.H., et al., *A comparative analysis of different grades of silica particles and temperature variants of food-grade silica nanoparticles for their physicochemical properties and effect on trypsin.* Journal of agricultural and food chemistry, 2019. **67**(44): p. 12264-12272.

16. George, S., et al., *Differential effect of solar light in increasing the toxicity of silver and titanium dioxide nanoparticles to a fish cell line and zebrafish embryos*, Environmental science and technology. 2014, **48**, 6374.

17. Tenzer, S., et al., *Rapid formation of plasma protein corona critically affects nanoparticle pathophysiology.* Nature nanotechnology, 2013. **8**(10): p. 772-781.

18. Lou, W., et al., *Antioxidant and a-amylase inhibitory activities of tannic acid.* Journal of food science and technology, 2018. **55**(9): p. 3640-3646.

19. Castanho, M.A. and M.J. Prieto, *Fluorescence quenching data interpretation in biological systems: the use of microscopic models for data analysis and interpretation of complex systems.* Biochimica et biophysica acta (BBA)-biomembranes, 1998. **1373**(1): p. 1-16.

20. Saputra, R.E., Y. Astuti, and A. Darmawan, *Hydrophobicity of silica thin films: The deconvolution and interpretation by Fourier-transform infrared spectroscopy*.

Spectrochimica acta part A: molecular and biomolecular spectroscopy, 2018. **199**: p. 12-20.

21. Darmawan, A., et al., *Structural evolution of nickel oxide silica sol-gel for the preparation of interlayer-free membranes.* Journal of non-crystalline solids, 2016. **447**: p. 9-15.
22. Bae, J.-Y., J. Jang, and B.-S. Bae, *Transparent, thermally stable methyl siloxane hybrid materials using sol-gel synthesized vinyl-methyl oligosiloxane resin.* Journal of sol-gel science and technology, 2017. **82**(1): p. 253-260.
23. Cornish-Bowden, A., *A simple graphical method for determining the inhibition constants of mixed, uncompetitive and non-competitive inhibitors.* Biochemical journal, 1974. **137**(1): p. 143-144.
24. Krupyanko, V., *Correction of Dixon plots.* European chemical bulletin, 2015. **4**(1-3): p. 142-153.
25. Holzwarth, G. and P. Doty, *The ultraviolet circular dichroism of polypeptides1*. Journal of the american chemical society, 1965. **87**(2): p. 218-228.
26. Srinivasan, D., et al., *The type of dietary nanoparticles influences salivary protein corona composition.* NanoImpact, 2020: p. 100238.
27. Chen, Y. and M.D. Barkley, *Toward Understanding Tryptophan Fluorescence in Proteins.* Biochemistry, 1998. **37**(28): p. 9976-9982.
28. Rasouli, N., N. Sohrabi, and E. Zamani, *Influence of a novel magnetic recoverable support on kinetic, stability and activity of beta-amylase enzyme.* Physical chemistry research, 2016. **4**(2): p. 271-283.
29. Zhuravlev, L.T., *The surface chemistry of amorphous silica. Zhuravlev model.* Colloids and Surfaces A: Physicochemical and engineering aspects, 2000. **173**(1): p. 1-38.

30. MacGregor, E.A., Š. Janeček, and B. Svensson, *Relationship of sequence and structure to specificity in the α-amylase family of enzymes.* Biochimica et biophysica acta (BBA) - protein structure and molecular enzymology, 2001. **1546**(1): p. 1-20.

31 Ramasubbu, N., et al., *Structure of human salivary alpha-amylase at 1.6 A resolution: implications for its role in the oral cavity.* Acta crystallogr D biol crystallogr, 1996. **52**(Pt 3): p. 435-46.

32 Crosara, K.T.B., et al., *Revealing the Amylase Interactome in Whole Saliva Using Proteomic Approaches.* BioMed research international, 2018. **2018**: p. 6346954-6346954.

4.8 Supplementary information

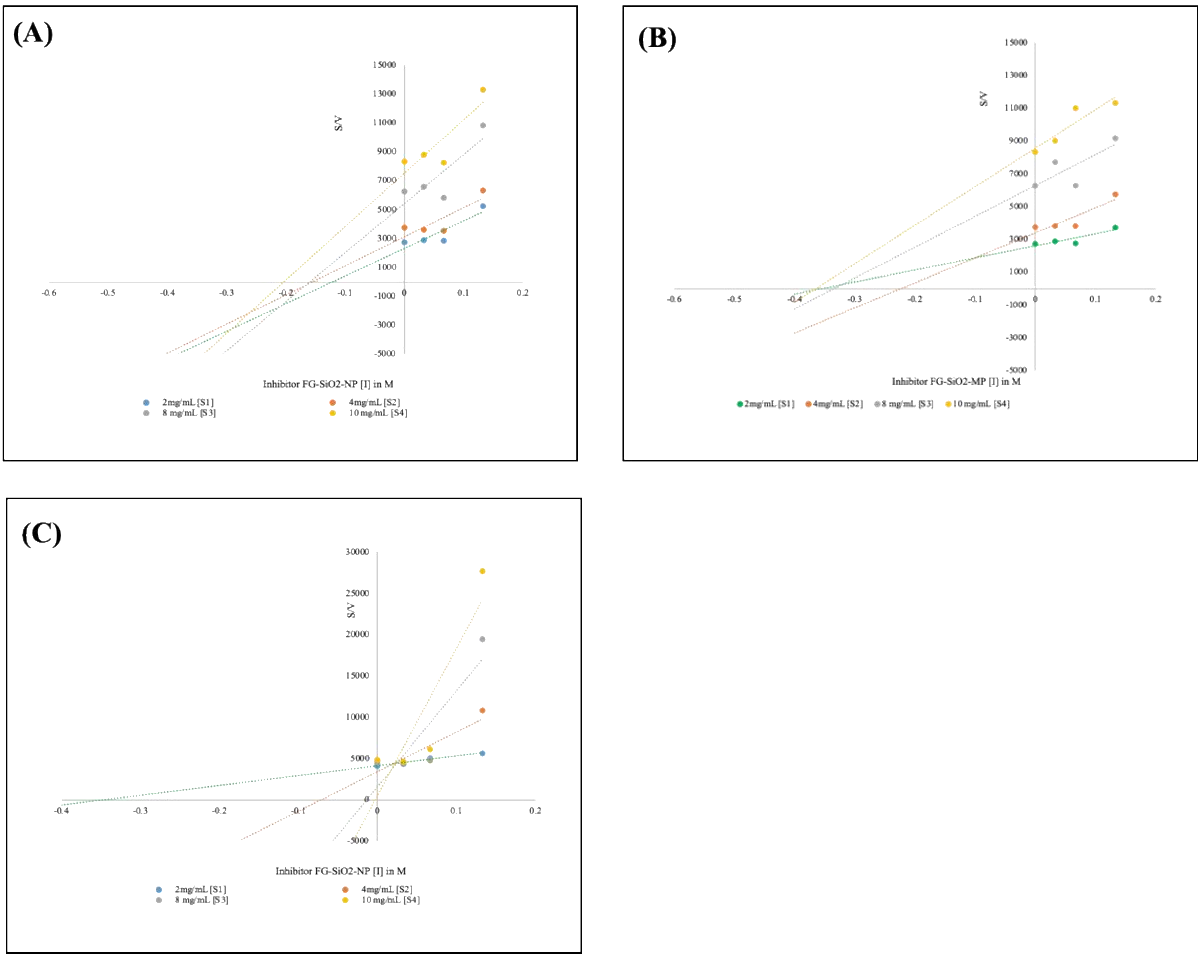

Figure SI 4. 1 Cornish-Bowden coordinates applied to define inhibition mechanism of silica particles on HSA. The data are plotted in the form of S/V against I and each data points are average of 3 determinations.

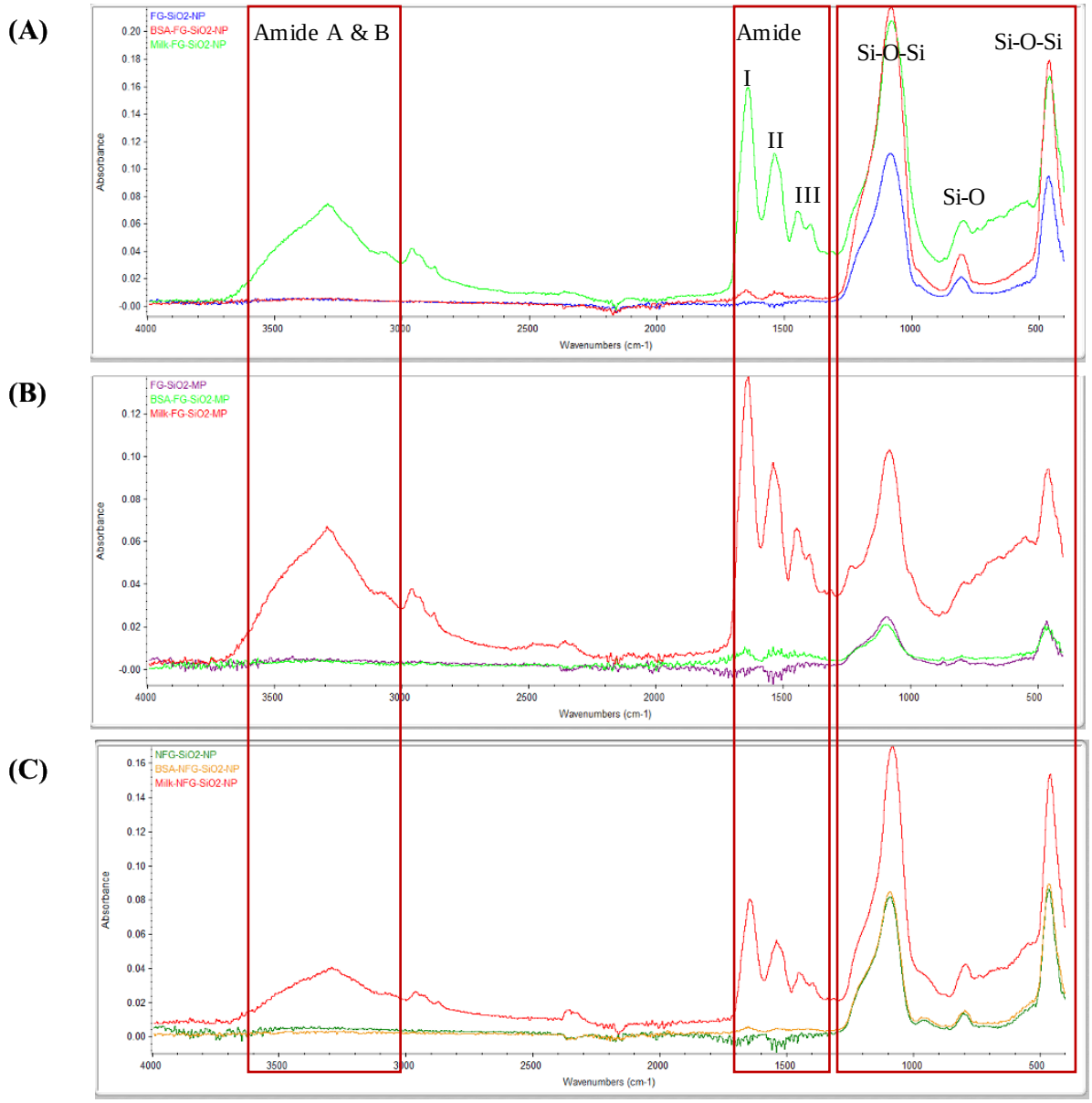

Figure SI 4. 2 FTIR analysis of the formation of protein corona on SiO_2 particles. Protein was interacted with particles in D_2O and the suspended solutions were dropped and dried on the ATR probe before taking the spectra for a wavenumber range of 400-4000 cm^{-1} using ATR-FTIR. The peaks corresponding to proteins and silica are labelled [1, 2] to show the surface coating of particles with proteins.

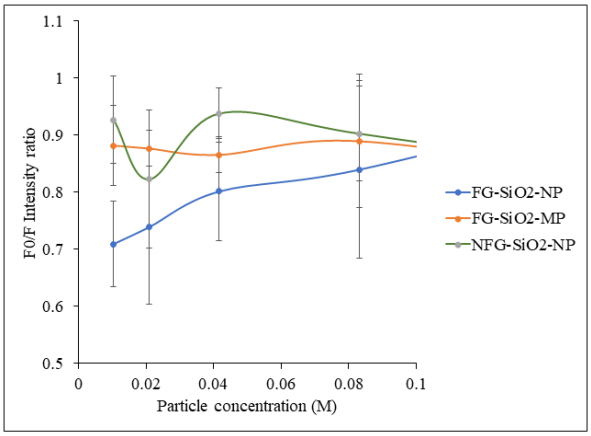

Figure SI 4. 3 Stern-Volmer plots for the fluorescence quenching of HSA, using an excitation wavelength of 280 nm and emission wavelength of 360 nm.

Connecting Text

Studies presented in Chapters 3 and 4 demonstrated the negative impact of pristine and surface-modified SiO_2 NPs on the structure and function of digestive enzymes. These studies demonstrated the impact of DNM interaction on the structure and function of vital proteins. Little is known, however, on factors that determine protein adsorption on to DNMs. Chapter 5 presents studies on understanding the interplay of physicochemical properties of DNMs (silica and titania) and properties of proteins that influence protein adsorption on to DNM surfaces using proteomics and high-resolution advanced imaging techniques. Chapter 5 is published in Nanoscale: Phue, W. H., Bahadi, M., Dynes, J. J., Wang, J., Kuppili, V. S. C., Ismail, A., Hameed, A., George S., (2021).

Chapter 5. Protein-biomolecule interactions play a major role in shaping corona proteome: Studies on milk interacted dietary particles

5.1 Abstract

Despite the significance of surface absorbed proteins in determining the biological identity of nanoparticles (NPs) entering human body, little is known about surface corona and factors that shape their formation on dietary particles used as food additives. In this study, food grade NPs of -silica and -titania and their food additive counterparts (E551 and E171) were interacted with milk proteins or with skim milk and the levels of protein adsorption were quantified. Characteristics of proteins correlating with their level of adsorption to NPs were determined using partial least square regression analysis. Results from individual protein-particle interaction revealed significance of factors such as zetapotential, hydrophobicity and hydrodynamic size of particles, and protein characteristics such as number of beta strand, isoelectric point, number of Ile, Tyr, Ala, Gly, Pro, Asp, and Arg, and phosphorylation sites on their adsorption to particles. Similar regression analysis was performed to identify characteristics of twenty abundant and enriched proteins (identified using LC-MS/MS analysis) for their association with surface corona of milk-interacted particles. Contrary to individual protein-particle interactions, protein characteristics such as helix, turn, protein structure, disulfide bond, number of Cys, Met, Leu, Trp, and Fe binding site were significant for their association with surface corona of milk interacted particles. This difference in factors identified from individual proteins and milk interacted particles suggested possible interactions of proteins with surface adsorbed biomolecules as revealed by scanning transmission X-ray microscopy and other biochemical assays.

Key words: Dietary nanoparticles; Surface-corona; Protein-nanoparticle interaction; Protein-protein interaction; Scanning transmission X-ray microscopy

5.2 Introduction

The use of manufactured inorganic nanoparticles (NPs) as food additives to improve the appearance and shelf-life of food is rising in recent years [1]. NPs added to the food matrix, will adsorb biomolecules on their surface to form surface corona. Proteins are major components of surface corona that determine the biological identity of NPs. Accordingly, studies have shown that protein corona plays a pivotal role in the tissue accumulation of NPs entering human body, cellular uptake, and ultimately potential toxicity [2-4]. As a result, there have been much interest in identifying factors that shape corona proteome of NPs. Most of the studies conducted for understanding the interactions of proteins with particle surfaces were motivated by potential applications of NPs in medicine- specifically as diagnostic and targeted drug delivery platforms. Given the anticipated entry of these NPs into blood, factors underlying interaction of NPs with blood plasma have been explored and been used to explain general principles of protein corona formation [5].

Previous studies with blood plasma and other body fluids interacted particles have shown the significance of physicochemical properties of NPs, nature of suspending media, and protein characteristics in shaping protein-NP interactions [6, 7]. Physicochemical properties of NPs such as, chemical identity [8], size [9], shape, surface charge [10], porosity, crystallinity, functional group [11] and hydrophobicity [12] have shown to play major roles in shaping protein-NP interactions. Prevailing models- based mostly on NPs interacted with plasma proteins- propose the existence of 'hard corona' composed of proteins directly bound to the surface of particles and 'soft corona' which is composed of proteins rapidly exchanging layer of weakly bound proteins [13]. Thus, while much attention has been devoted in understanding factors that shape protein corona on mostly blood plasma interacted particles, similar studies addressing the type and characteristics of proteins adsorbed on NPs incorporated in food and destined to enter human body through oral route is severely lacking. This is despite the

incredibly high levels of particle exposure among general population through dietary uptake [14].

In this work, factors that influence protein adsorption to particle surfaces were investigated using dietary particles and milk proteins. Properties of particles and proteins correlating with level of protein adsorption were determined using multivariate partial least square (PLS) regression analysis. PLS analysis is a regression analysis method which correlates a set of response variables 'y' to a set of predictor variables 'x' [15]. We studied particles interacted with individual milk proteins (α -casein, β -casein, α -lactalbumin, β -lactoglobulin, and BSA), and compared the amount of protein adsorbed (dependent variable) against characteristics of proteins and particles (independent variables) using PLS. Factors identified from one-one interaction studies were compared for predictability of protein abundance on particles retrieved from milk (complex food matrix). We report that factors such as isoelectric point, beta strands and phosphorylation sites identified from individual protein-NP interactions have little relevance in predicting abundance and enrichment of proteins on the surface corona of particles interacted with milk. Instead, factors that facilitate protein-biomolecule interactions seem more relevant in defining the proteome of surface corona on particles suspended in complex mixtures.

5.3 Materials and Methods

5.3.1 Materials

Food grade silica particles (FG-SiO_2-NP) in nano-size (AEROSIL 200F) and food additives silica particles, E551 (SIPERNAT 22) were obtained from Evonik Corporation (NJ, United States). Food grade titania NPs (FG-TiO_2-NP) were purchased from CNMI industrial corporation, China and food additives titania particles (E171) were obtained from Minerals-Water, UK. All particles were used as received. For the individual protein-particle interaction studies, α-casein (cat # C6780), β-casein (cat # C6905), and bovine albumin (cat # A2153), were purchased from Sigma Aldrich (St. Louis, MO, USA). α-Lactalbumin (cat # S0130), β-lactoglobulin (cat # S0131) were obtained from Davisco Foods International Inc. (Eden Prairie, MN, USA). For the multiple proteins-particle interaction studies, Quebon skimmed milk (Agropur Dairy Cooperative, QC, Canada) was purchased from a local grocery store. Unless stated otherwise, all other chemicals were obtained from Sigma Aldrich (St. Louis, MO, USA). Stock buffer of 0.1 M of phosphate buffer (pH 6.5) was prepared using deionized water obtained from a Milli-Q water system (Millipore Sigma, Massachusetts, USA) and were stored at 4°C before making the working concentration prior to each experiment.

5.3.2 Characterization of particles

All particles in their pristine state were characterized for their agglomeration size (and shape), surface charge, and hydrophobicity using transmittance electron microscopy (TEM), dynamic light scattering technique (DLS) and Rose-Bengal assay, respectively. For TEM, 5 µL of particles suspension (100 $\mu g.mL^{-1}$) was dropped onto 200-mesh Cu TEM grids with carbon film and was air-dried at room temperature for an hour. TEM images were acquired at 120 kV accelerating voltage using Tecnai G2 F20 200 kV Cryo-STEM (Field Electron and Ion Company (FEI), Oregon, USA). The hydrodynamic diameter and zeta potential of the particles

were determined using DLS (NanoBrook OMNI Instrument, USA). Particles suspended (50 $\mu g.mL^{-1}$) in PBS buffer (pH 6.5) were filled into pre-rinsed cuvettes and were placed in a DLS instrument. The measurements were carried out at an applied voltage of 100 V. Relative hydrophobicity of the particles was assessed using a dye staining method as reported earlier [16]. Particles suspended in water (5 $mg.mL^{-1}$) were mixed with Rose Bengal (RB) at 2 $\mu g.mL^{-1}$ concentration for 3 h under dark conditions. Subsequently, particles were separated from the supernatant by centrifugation at 20, 000 g for 30 min. RB added to Milli-Q water at the same concentration was used as the baseline control. The absorbance of the supernatant at 542 nm was measured using a UV-vis micro plate reader (Spectra Max M2, Molecular Devices, USA). The partition quotient (PQ) was calculated according to equation 5.1 (Eq. 5.1):

$$PQ = \frac{\text{Amount of RB adsorbed onto particles surface}}{\text{Amount of RB in water}} \qquad \textbf{(Eq. 5.1)}$$

5.3.3 Preparation of protein suspensions

Bovine milk proteins such as α-casein, β-casein, α-lactalbumin, β-lactoglobulin, and bovine albumin were chosen for investigating their adsorption onto the particles. For this, individual protein solutions (50 $\mu g.mL^{-1}$) were prepared in 20 mM phosphate buffer (pH 6.5). Dietary particles (FG-SiO_2-NP, E551, FG-TiO_2-NP and E171) (500 $\mu g.mL^{-1}$) were mixed with 50 $\mu g.mL^{-1}$ protein suspensions. Mixtures of NP and protein were incubated at 37°C for an hour. Controls were prepared by adding the same proportions of deionized water to the protein suspensions.

5.3.4 Quantification of protein adsorption to the particles

The concentrations of bound proteins were measured through a deductive approach. Protein solution containing suspended particle was centrifuged (20,124 g for 15 min) to separate NP/protein assemblies from their unbound components. Subsequently, the level of unbound proteins in the supernatant was measured using Bradford assay. For this, 100 µLs of

supernatant was mixed with 100 µL of Bradford reagent, incubated for 5 min and the absorbance of resulting solution was measured at 595 nm using a plate reader (SpectraMax i3x, Multi-mode Microplate Reader, Molecular Devices, USA). The percentage of bound protein was calculated according to equation 5.2 (Eq. 5.2):

% of bound protein =

$$\frac{(\text{Absorbance of original protein solution} - \text{Absorbance of sample interacted solution})}{\text{Absorbance of original protien solution}} \times 100\%$$

(Eq. 5.2)

Experiments were performed in triplicates and repeated at least three times. The data in this study is expressed as the mean value ± standard deviation (SD). Statistical comparisons were made by one way ANOVA (Duncan) using IBM SPSS statistical analysis software (version 27) and p value ≤ 0.05 was considered significant.

5.3.5 Regression analysis of protein adsorption against protein and particle characteristics

Partial least squares (PLS) (JMP pro 15) analysis was used for identifying characteristics of proteins (x) that correlate with their level of adsorption onto particles (y). For the PLS analysis, the response (% of protein adsorption onto the particles) was transformed using the log function and analysis was performed using SIMPLS algorithms and K-Fold (Number of fold-7) [17]. Variable Importance in Projection (VIP) scores were used to estimate the importance of each variable in the projection used in a PLS model. VIP scores higher than 0.8 were regarded as influential factors in the protein-particle interaction [15].

5.3.6 Proteome of surface corona of particles interacted with milk (model food matrix)

Skimmed milk (with minimal fat content) was used for simulating a food matrix containing multiple proteins [18]. Accordingly, milk sample stored at 4°C was subjected to centrifugation

(20,124 g for 15 min) to remove any debris, and the supernatant was collected for further studies. Dietary particles, 200 µL of 10 mg.mL^{-1}, were added to 800 µL of milk and incubated for 1 hr at 37°C. Particles were then pelleted out by centrifugation (20,124 g rpm) for 15 min in a temperature controlled centrifuge (Sigma 3-30KS, Sigma Zentrifugen, Germany), unbound milk proteins in the supernatant were discarded. To remove the soft corona, the pelleted particles were resuspended in 1 mL of 20 mM sodium phosphate buffer (pH 6.5) and the suspension was centrifuged at 20,124 g for 15 min and the supernatant was discarded. This step was repeated twice to retain hard corona formed on the particles which were used for determining the presence of protein, carbohydrate and lipids as detailed in supplementary information (Figure SI 5.5 & Figure SI 5.6) and protein profiling as detailed below.

5.3.7 One-dimension gel electrophoresis

After the final wash of milk interacted particles, 200 µL of sample buffer containing 62.5 mM Tris-HCl, pH 6.8, 2% SDS, 25% (v/v) glycerol, 0.01% bromophenol blue and 5% β-mercaptoethanol were added to particles pelleted, vortexed and boiled for 5 min. Particles were removed from sample buffer by centrifugation at 20,124 g for 15 min; protein-containing sample solution was collected and transferred into a new Eppendorf tube. Twenty microliters of each samples were loaded to a sample well of a 4-20% SDS-polyacrylamide gel. The proteins were separated in the gel using 100 V for 1.5 hr in running buffer containing 2.5 mM tris, 19.2 mM glycine and 0.01% SDS. The gels were then stained in standard Coomassie blue-methanol-acetic acid solution for 30 min at room temperature (RT). The gels were subsequently washed with destaining solution (40% methanol, 10% acetic acid and 50% water) for 30 min at RT to visualize the protein bands. The gel was further subjected to silver staining to improve clarity [19].

5.3.8 Protein identification by mass spectrometry

LC-MS/MS mass spectrometry analysis using 3000HPLC- orbitrap fusion MS (Thermo Scientific, Canada) was conducted for proteome analysis. After the final wash of milk interacted particles, pelleted particles were resuspended and were incubated in Laemmli buffer for an hour. The suspension was subsequently centrifuged and 40 µL of supernatant solution was loaded onto a single stacking gel band to remove lipids, detergents, and salts. Subsequently, the stacked proteins were reduced with 10 mM DTT, alkylated with iodoacetic acid and then digested with trypsin in accordance with the standard protocol for in-gel digestion [20]. Two microliters of extracted peptides were re-solubilized in 0.1% aqueous formic acid and loaded onto a Thermo Acclaim Pepmap (Thermo, 75 uM ID X 2 cm C18 3 uM beads) precolumn and then onto an Acclaim Pepmap Easyspray (Thermo, 75 uM X 15 cm with 2 uM C18 beads) analytical column for separation using a Dionex Ultimate 3000 uHPLC at 250 nL/min with a gradient of 2-35% organic (0.1% formic acid in acetonitrile) over 2 hr. Peptides were analyzed using a Thermo Orbitrap Fusion mass spectrometer operating at 120,000 resolution (FWHM in MS1, 15,000 FWHM for MS/MS) with HCD sequencing at top speed for all peptides with a charge of 2+ or greater. PROTEOME DISCOVERER version 2.0 was used to extract and deisotoped tandem mass spectra, however charge state deconvolution was not performed. Scaffold (version Scaffold_4.10.0, Proteome Software Inc., Portland, OR) was used to validate MS/MS based peptide and protein identifications. The raw data was converted into *.mgf format (Mascot generic format) for searching using the Mascot 2.6.2 search engine (Matrix Science) against bovine protein sequences (Uniprot 2019). Mascot was searched with a fragment ion mass tolerance of 0.100 Da and a parent ion tolerance of 5.0 ppm. Peptide identifications were accepted if they could be established at greater than 95.0% probability by the Peptide Prophet algorithm [21] with Scaffold delta-mass correction and contained at least 2 identified peptides.

5.3.9 Bioinformatic data analysis

The proteomic data from Scaffold™ was used in bioinformatic tools such as Expasy, Bioinformatics.psb, and heatmapper.ca for the analysis of isoelectric point, venn diagram and cluster analysis respectively [8]. The theoretical isoelectric point for the selected list of proteins was calculated using tools available from Expasy.org (https://web.expasy.org/compute_pi/).

To identify the overlap and the unique protein gene list, we used bioinformatic webtool from Ugent (http://bioinformatics.psb.ugent.be/webtools/Venn/). Fold change value was calculated in Scaffold™ by comparing it with control sample (Milk) and the 'z-score' for all the genes with fold change ≥2 was calculated in heatmapper.ca for data display.

PLS analysis was performed to identify protein factors that correlate with abundant and enriched proteins identified on the surface corona of particles. From the LC-MS/MS data, twenty abundant and enriched proteins of each dietary particles were selected for the regression analysis. The percentage of adsorbed proteins was used as the response and characteristic of dietary particles and proteins were used as predictors.

5.3.10 Prediction of protein network

Protein interaction network (physical and functional) was predicted using the STRING bioinformatics tool (http://string-db.org/). STRING is an open-access software to predict multiple protein interactions along with information about pathway associated, molecular function, gene clustering, and strength of association between two proteins. Protein network was created for entire set of proteins (having at least 2 identified peptides in Scaffold software) bound to respective particles and further refined it to include only those interactions with a confidence score greater than 0.7. The number of nodes and edges, average node degree, and protein-protein interactions (PPI) enrichment values signify the possibility of interaction between proteins. The network was clustered to simplify the complicated dense network and

to obtain a better understanding of the PPI network. The number of clusters was set as 10, based on the rule of thumb $k=(n/2)^{1/2}$, where n is the number of nodes in the cluster [22].

5.3.11 Fourier-transform infrared spectroscopy

Attenuated total reflectance Fourier-transform infrared spectroscopy (ATR-FTIR) was used to identify the milk components attached onto the dietary particles. Dietary particles retracted after interacting with milk (10 $mg.mL^{-1}$) were used for this analysis. Two microliters of sample were dropped on the ATR probe and left 8 min to evaporate water. The FTIR spectra were taken in the range of 400-4000 cm^{-1}, with a resolution of 8 cm^{-1} and 36 scans. Dietary particles without milk treatment were used as controls. Wavenumber corresponding to proteins, lipids and carbohydrates in sample spectra were assigned based on reported values [23].

5.3.12 Scanning transmission X-ray microscopy and Ptychography

Ambient scanning transmission X-ray microscope (STXM) (10ID-1) beamline at the Canadian Light Source (Saskatoon, Canada) was used for imaging and spectroscopic analysis of particles with surface corona [24]. We selected E171 (food grade TiO_2) to image because of its relevance in food application and these particles are relatively bigger in size enabling us to obtain image from isolated or agglomerated particles. For this, milk interacted E171 particles were first washed using distilled water. One microliter of the resulting suspension was deposited onto a silicon nitride (100 nm membrane thickness) window, excess water was removed by wicking off using Kim wipe and the sample was air dried. As a spatial resolution using ptychography is better than conventional STXM absorption imaging, ptychography technique was used for this study. For ptychography data collection, first the photon multiplier tube (PMT) detector was used to find the region of interest and an Andor™ CCD detector (model: DX434-BN, with 1024 x 1024 pixels, pixel size 13 µm) [25] and Andor™ SOLIS software supplied with the CCD detector was used. The CCD detector was cooled to -40 ºC with thermoelectric and water

cooling under a 4 x 10^{-5} Torr vacuum. The O K-edge ptychography dataset, consisting of 61 images from 525 to 560 eV, was obtained from a 2 μm x 2 μm area with a step size of 0.333 μm, scanning points of 6 x 6, and a dwell time of 2300 ms per pixel. The beam spot size on the sample was defocused to 1.665 μm, which ensures that there was 80% overlap of the scanning points. The CCD background signal was measured with the beamline shutter closed. The reference compounds X-ray absorption spectroscopy (XAS) spectra of human serum albumin (protein) (Behringwerke AG), 1,2-dipalmitoyl-sn-glycero-3-phosphocholine (lipid) (Avati polar lipids) and TiO_2 (Sigman-Aldrich) were used from a previous study [26].

5.3.13 Data Analysis

Ptychography reconstruction used the PyPIE code to derive the amplitude and phase images using 200 iterations [27]. An image sequence was created from the ptychography O K-edge images and aligned using Fourier cross-correlation routines. The amplitude images are similar to transmission images collected with the PMT detector but with better resolution. Hence, the amplitude images were subsequently converted to optical density (OD) images using the signal from areas with no sample. The phase images were not analyzed further.

Quantitative maps were derived from the O K-edge ptychography amplitude image sequence using singular value decomposition (SVD) [26] method to fit the spectrum at each pixel to a linear combination of reference spectra of the components (i.e., protein, lipid, polysaccharides and TiO_2) suspected to be present. To gain confidence that proteins, lipids and TiO_2 were indeed present in the system, the reliability of any given component map was checked by deriving a spectrum from "high intensity" pixels by applying a grayscale threshold technique to the component map [26]. In addition to checking whether these derived spectra showed characteristic shape/peaks of proteins, lipids and TiO_2 a linear combination fitting of the

derived spectrum, using the three reference spectra, was performed. All analysis was done with aXis2000, available for free from Dr. Adam Hitchcock's website (http://unicorn.mcmaster.ca/)

5.4 Results

5.4.1 Physicochemical properties of particles studied

In this study, FG-SiO_2-NP, E551, FG-TiO_2-NP, and E171 were characterized prior to their interaction with proteins to assess their size and morphology using TEM as shown in Figure 5.1. TEM analysis of FG-SiO_2 NP showed agglomerates of spherical shaped NPs, and the average diameter of primary particle was around 20 nm (Figure 5.1A). The hydrodynamic size of FG-SiO_2-NP in buffer was ~583.78 nm (Figure 1E). E551 (food grade silica particles) were larger aggregates of size >3000 nm (Figure 1B) which were composed of primary particles of size ~20 nm and hydrodynamic size in buffer was ~3491.92 nm. TEM images of FG-TiO_2-NP and E171 (Figure 5.1C and D) showed pseudo spherical shaped particles. The primary particle size of FG-TiO_2-NP was ~120 nm while that of E171 ranged from 50-300 nm. However, other characterization results such as hydrodynamic size, zetapotential and hydrophobicity of FG-TiO_2-NP and E171 showed insignificant differences between these particles (Figure 5.1E). All the particles tested had a net negative surface charge measured as zeta potential which were -26.25 mV, -19.12 mV, -55.93 mV and -56.65 mV for FG-SiO_2-NP, E551, FG-TiO_2-NP and E171, respectively.

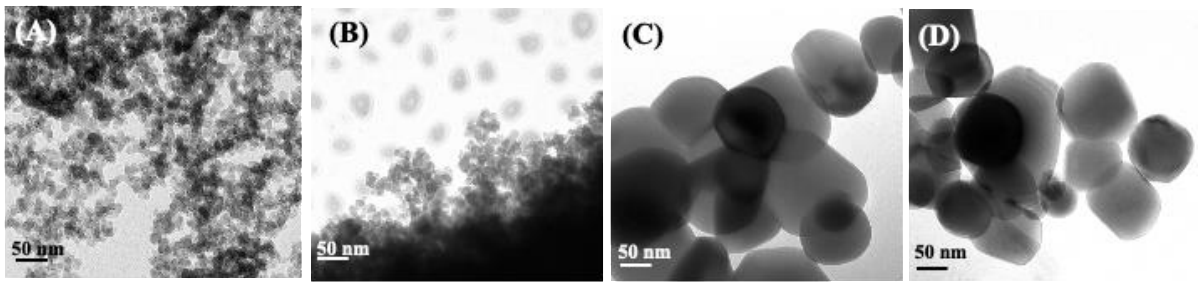

(E)

	Hydrodynamic size [nm ± Std dev]	Zetapotential [mV ± Std dev]	Hydrophobicity [PQ ± Std dev]
FG-SiO_2-NP	583.78^{a} (± 34.46)	-26.25^{b} (± 0.31)	0.019^{a} (± 0.008)
E551	3491.92^{b} (± 2739.73)	-19.12^{c} (± 0.88)	0.011^{a} (± 0.007)
FG-TiO_2-NP	279.83^{a} (±14.02)	-55.93^{a} (±1.71)	0.015^{a} (± 0.012)
E171	252.63^{a} (± 20.25)	-56.65^{a} (± 1.81)	0.015^{a} (±0.01)

Figure 5. 1 Physicochemical properties of particles studied. TEM images of dietary particles were obtained after atmospheric drying of particle suspensions (100 ppm) on 200-mesh Cu TEM grids with carbon film. These images were acquired using Tecnai G2 F20 200 kV Cryo-STEM. **(A)** FG-SiO_2-NP, **(B)** E551, **(C)** FG-TiO_2-NP and **(D)** E171. Tabular data **(E)** summarizes hydrodynamic diameter, zetapotential (obtained using DLS measurement of particle suspensions) and hydrophobicity (measured using Rose Bengal assay) of particles. Average values with different letters in the same column indicate significant differences (Duncan, $P < 0.05$)

5.4.2 Differential adsorption of proteins onto particles

The results of the adsorption of individual proteins on dietary particles tested are given in Figure 5.2A. The percentage of proteins adsorbed varied across particle and protein types. Generally, FG-SiO_2-NPs adsorbed higher amounts of proteins (Figure 5.2A) in comparison with other particles. Relatively, adsorptions of β-casein onto most of the particles were higher in comparison to other proteins. Notably, the relative ranking of proteins adsorbed onto the E551 and FG-SiO_2-NPs were similar. The relative ranking of types of proteins adsorbed differed for SiO_2 and TiO_2 particles although there were similarities within the variants of each types of particles. The presence of proteins on particle surface and their relative abundance when interacted with different proteins individually was further confirmed with SDS-PAGE (Figure SI 5.1).

The % protein bound onto particles were assessed against properties of particles and proteins using PLS to identify factors that correlate with protein adsorption. Physicochemical properties of particles such as hydrodynamic size, zetapotential and hydrophobicity, and characteristics of proteins such as isoelectric point (pI), beta strand, number of amino acids units (Ile, Tyr, Ala, Gly, Pro, Asp, and Arg), influenced protein-SiO_2 particles interaction (Figure 5.2B). Phosphorylation site (S), isoelectric point, number of proline units, N-glycosylation site, number of alanine units and phosphorylation site (Y) were identified to be influencing protein adsorption onto food grade TiO_2 particles (Figure 5.2C).

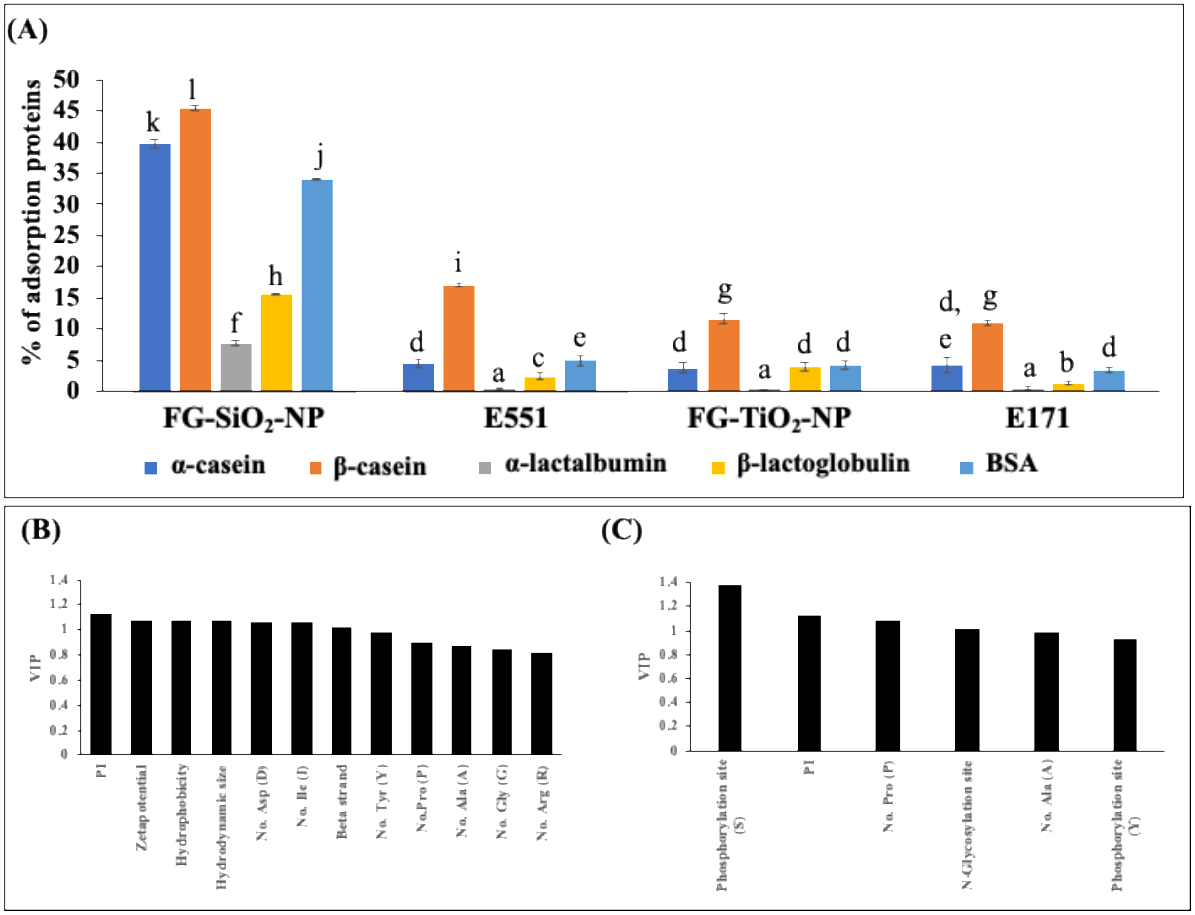

Figure 5. 2 (A) Quantification of protein adsorption on dietary particles. Particles suspended and incubated in protein suspensions were retrieved using centrifugation. The protein concentration of original suspension and that obtained after removal of particles were used for calculating the percentage of proteins adsorbed onto particles. Average values are plotted in the graph and the different letters indicate significant differences (Duncan, $p<0.05$). **The regression analysis using PLS.** Variable importance in projection scores for factors influencing proteins-silica particles interaction **(B)**, and -titania **(C)** were obtained by regression analysis (PLS) for % protein adsorbed on particle surface against their characteristics (n=37).

5.4.3 Composition and proteome profile of the surface corona of milk interacted particles

As detailed in supplementary information, analysis of milk interacted particles using FTIR (Figure SI 5.5) and biochemical assays (Figure SI 5.6) showed the presence of proteins, carbohydrates and lipids in surface corona. Protein bands corresponding to prominent proteins adsorbed onto to the surface of particles are evident in the SDS-PAGE image given in Figure 5.3A. The number of proteins bands and their relative intensities varied depending on the type of particles and size of particles. SDS-PAGE pattern of skim milk proteins contained four major bands and five minor bands. Based on the literature, the major bands were identified as α-casein (e), β-casein (e), β-lactoglobulin (f) and α-lactalbumin (g), and five minor bands were identified as complement C3 (a), lactotransferrin (b), polymeric immunoglobulin receptor (c) and κ-casein (e) (lane 5) [28]. Generally, the amounts of proteins adsorbed on food grade SiO_2 particles were higher in comparison to TiO_2 particles. κ-casein was enriched in the protein corona of SiO_2 particles, which had higher intensity, in comparison to the control (milk), especially in NPs. In comparison to two types of food grade TiO_2 particles, E171 had higher amount of casein adsorbed than that of FG-TiO_2-NP (Figure 5.3A).

Proteome analysis of surface corona on particles generated data for proteins that are abundant on particle surface and those proteins that showed an enrichment in comparison to the milk control. Enrichment of certain types of proteins on particle surface is caused by selective and preferred adsorption of certain types of proteins onto particle surface. Totally 325 milk proteins were identified, in which 171 were identical to the whole milk and the remaining 154 proteins were unique to milk interacted particles suggesting their enrichment. The differences in the composition of the protein corona formed on different particles are evident from the Venn diagram given in Figure 5.3B. A total of 196, 198, 243, and 205 milk proteins were identified in the coronas on FG-SiO_2-NPs, E551, FG-TiO_2-NPs and E171, respectively. It was found that 117 proteins were common to all the particles surface irrespective of the size and chemistry.

The number of unique proteins present in the coronas of FG-SiO_2-NPs, E551, FG-TiO_2-NPs and E171 were 7, 19, 32 and 4, respectively (Figure 5.3B).

Hierarchical cluster analysis showed a difference in the abundance (Figure 5.3C) and enrichment (Figure 5.3D) of proteins present on different particles surface. Differences in protein profiles on different particles are evidenced as distinct clusters. Overall, 117, 122, 170 and 148 proteins found to be significantly enriched on the dietary particles of FG-SiO_2-NP, E551, FG-TiO_2-NP and E171 respectively with fold enrichment of ≥ 2.

Milk proteins were sorted according to their abundance and enrichment and top twenty most abundant and enriched proteins are listed in Table 5.1A and Table 5.1B. Unique proteins on each particle are highlighted in bold and italics. Within the twenty abundant proteins, α-lactalbumin, glycosylation-dependent cell adhesion molecule 1, zinc-α-2-glycoprotein were present only in whole milk sample, while complement factor H, C4b-binding protein alpha chain, fibronectin and fibrinogen beta chain were found exclusively in surface corona of FG-SiO_2-NP. Aniglogenin-1, plasminogen and β-2-microglobulin were unique for protein corona of E551 and heart-type fatty acid binding protein, sodium-dependent phosphate transport protein 2B were only present in corona of E171 sample. Rest of the proteins were present with different relative ranking for their abundance (Table 5.1A). More than 80% of top twenty proteins identified as enriched were conserved among different particles studied although their relative ranking differed (Table 5.1B). Unique proteins on each particle are marked in bold in the list of top twenty enriched proteins provided in Table 5.1B. Generally, metal binding proteins and immune response proteins were prominent in enriched fractions of protein corona of silica particles, while membrane proteins and adaptor proteins were enriched in the protein corona of titania particles.

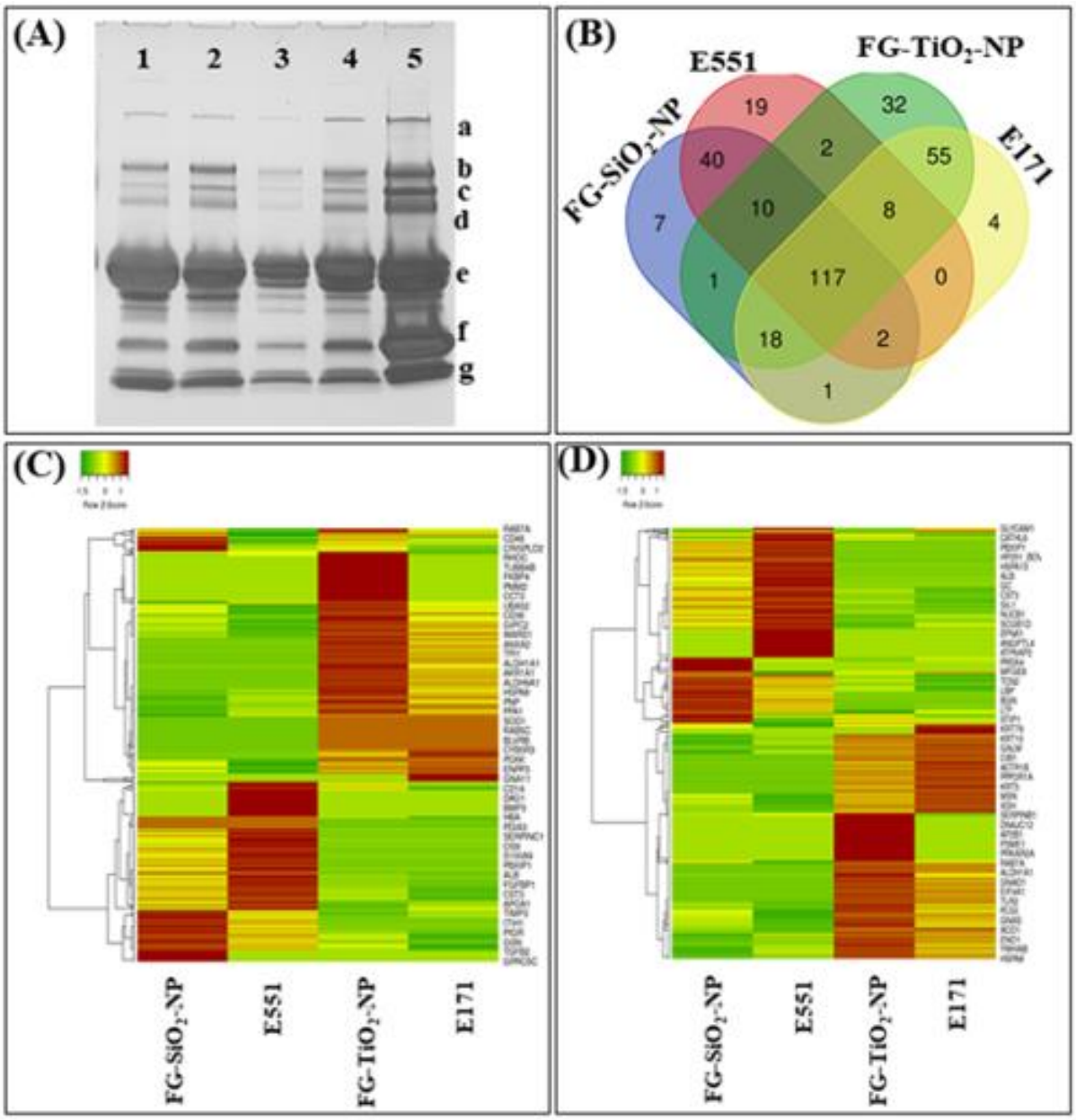

Figure 5. 3 Proteome analysis of milk interacted particles. (A) SDS-PAGE pattern of proteins retrieved from milk interacted particles. Lane (1) milk + FG-SiO_2-NP, (2) milk + E551, (3) milk + FG-TiO_2-NP, (4) milk + E171, and (5) milk

*a=Complement C3, b-Lactotransferrin, c=Polymeric immunoglobulin receptor, d=BSA, e=Casein Fraction (α-casein, β-casein, κ-casein), f=β-Lactoglobulin, g=α-Lactalbumin

(B) Venn diagram shows the number of hard corona proteins identified in tested dietary particles interacted with milk for an hour.

(C) Hierarchical clustering of the abundant milk proteins on each dietary particle compared with bovine milk,

(D) Hierarchical clustering of the enriched milk proteins on each dietary particle compared with bovine milk. Color scheme is based on the z score values of fold change of individual proteins compared with milk.

Table 5. 1 Twenty most abundant (A) and enriched (B) milk proteins identified in the protein corona of each dietary particle's following 1 hr of incubation. Unique proteins identified are highlighted in bold and Italized.

(A)

Milk	**FG-SiO_2-NP**	**E551**	**FG-TiO_2-NP**	**E171**
Beta-lactoglobulin	Lactotransferrin	Lactotransferrin	Alpha-S1-casein	Alpha-S1-casein
Albumin	Kappa-casein	Alpha-S1-casein	Lactotransferrin	Lactotransferrin
Alpha-S1-casein	Polymeric immunoglobulin receptor	Albumin	Kappa-casein	Kappa-casein
Kappa-casein	Alpha-S1-casein	Beta-lactoglobulin	Beta-lactoglobulin	Beta-lactoglobulin
Lactotransferrin	Beta-lactoglobulin	Kappa-casein	Alpha-S2-casein	Alpha-S2-casein
Alpha-lactalbumin	Albumin	Polymeric immunoglobulin receptor	Xanthine dehydrogenase/oxidase	Xanthine dehydrogenase/oxidase

Polymeric immunoglobulin receptor	Complement C3	Alpha-S2-casein	Butyrophilin subfamily 1 member A1	Butyrophilin subfamily 1 member A1
Complement C3	Xanthine dehydrogenase/oxidase	Lactoperoxidase	Beta-casein	Beta-casein
Xanthine dehydrogenase/oxidase	Beta-casein	Complement C3	Complement C3	Complement C3
Alpha-S2-casein	Lactoperoxidase	Serotransferrin	Polymeric immunoglobulin receptor	Polymeric immunoglobulin receptor
Serotransferrin	Alpha-S2-casein	Xanthine dehydrogenase/oxidase	Lactoperoxidase	Lactoperoxidase
Lactadherin	Serotransferrin	Beta-casein	Perilipin-2	Perilipin-2
Butyrophilin subfamily 1 member A1	Lactadherin	Nucleobindin-1	Lactadherin	Lactadherin

Beta-casein	***Complement factor H***	Perilipin-2	Albumin	Albumin
Lactoperoxidase	Butyrophilin subfamily 1 member A1	Lactadherin	Broad substrate specificity ATP-binding cassette transporter ABCG2	Fatty acid synthase
Glycosylation-dependent cell adhesion molecule 1	Perilipin-2	***Angiogenin-1***	Fatty acid synthase	Isocitrate dehydrogenase [NADP] cytoplasmic
Zinc-alpha-2-glycoprotein	Lipoprotein lipase	Butyrophilin subfamily 1 member A1	Isocitrate dehydrogenase [NADP] cytoplasmic	Heat shock cognate 71 protein
Nucleobindin-1	***C4b-binding protein alpha chain***	***Plasminogen***	Heat shock cognate 71 protein	Broad substrate specificity ATP-binding cassette transporter ABCG2
Perilipin-2	***Fibronectin***	***Beta-2-microglobulin***	Serotransferrin	***Fatty acid-binding protein, heart***
Lipoprotein lipase	***Fibrinogen beta chain***	Lipoprotein lipase	Lipoprotein lipase	***Sodium-dependent phosphate transport protein 2B***

(B)

FG-SiO_2-NP	**E551**	**FG-TiO_2-NP**	**E171**
Complement factor H	Complement factor H	Elongation factor 2	Moesin
Cathepsin L1	Cathelicidin-2	Chloride intracellular channel protein 4	Histatherin
Angiogenin-2	Cathepsin L1	Moesin	Elongation factor 2
Cathelicidin-2	Angiogenin-2	Histatherin	Keratin, type I cytoskeletal 10
Moesin	Protein S100-A12	14-3-3 protein epsilon	Chloride intracellular channel protein 4
Tripeptidyl-peptidase 1	Lysosomal alpha-mannosidase	Keratin, type I cytoskeletal 10	UTP--glucose-1-phosphate uridylyltransferase
Lysosomal alpha-mannosidase	Complement component C6	Na(+)/H(+) exchange regulatory cofactor NHE-RF1	***Radixin***

Hemoglobin subunit alpha	***Cathelicidin-3***	Cytoplasmic aconitate hydratase	Heat shock protein HSP 90-alpha
Heat shock 70 kDa protein 1A	Histatherin	14-3-3 protein beta/alpha	Cytoplasmic aconitate hydratase
Complement component C6	Hemoglobin subunit alpha	Heat shock 70 kDa protein 1A	14-3-3 protein epsilon
Heat shock protein HSP 90-alpha	Protein S100-A8	UTP--glucose-1-phosphate uridylyltransferase	Heat shock 70 kDa protein 1A
Coagulation factor XII	***Cathelicidin-6***	Vacuolar protein sorting-associated protein 4B	Tryptophan--tRNA ligase, cytoplasmic
Protein S100-A12	***Hemoglobin subunit beta***	Tryptophan--tRNA ligase, cytoplasmic	Transketolase
Protein disulfide-isomerase A3	***Selenoprotein P***	Unconventional myosin-Ic	Na(+)/H(+) exchange regulatory cofactor NHE-RF1
Histone H2B type 1	Heat shock 70 kDa protein 1A	Transketolase	14-3-3 protein beta/alpha

Histatherin	14-3-3 protein epsilon	***Cytosol aminopeptidase***	Vacuolar protein sorting-associated protein 4B
14-3-3 protein epsilon	Tripeptidyl-peptidase 1	***14-3-3 protein theta***	***Ethylmalonyl-CoA decarboxylase***
Chloride intracellular channel protein 4	Protein disulfide-isomerase A3	Heat shock protein HSP 90-alpha	Unconventional myosin-Ic
Annexin A1	14-3-3 protein beta/alpha	***Rab GDP dissociation inhibitor alpha***	***Glycerol-3-phosphate dehydrogenase [NAD(+)], cytoplasmic***
Protein S100-A8	Transketolase	Annexin A1	***Heat shock protein beta-1***

5.4.4 Factors identified from milk interacted particles were different from those identified from individual protein-particle interactions

PLS analysis was carried out separately for proteins identified as abundant and enriched on particle retrieved from milk. Factors such as N-glycosylation site, helix, turn, and globular shape proteins were identified as prominent factors that correlated with abundant proteins on SiO_2 surface (Figure 5.4A). In TiO_2 particles, factors such as number of aspartic acid, disulphide bonds, number of phosphorylation sites *etc* were identified as influencers of abundant proteins (Figure 5.4B). We noticed a clear distinction between protein characteristics that correlated with abundant and enriched proteins on particle surfaces. In the case of SiO_2 particles, protein characteristics found to influence enrichment were the number of disulphide bonds and number of amino acids such as Tyr, Cys, Trp, Leu (Figure 5.4C) while protein adsorption to TiO_2 particles were influenced by % of helix structure, number of disulphide bonds, and Fe binding sites (Figure 5.4D).

In summary, individual protein-silica particle interaction was influenced by physicochemical properties of the particles and proteins. However, only the characteristics of proteins were found to be correlating with their abundance when particles were interacted with a complex food matrix. Noticeably, properties of proteins identified to positively influence their binding onto particles, as determined from individual protein-particle interactions were not identical to those characteristics identified from milk-NP interactions.

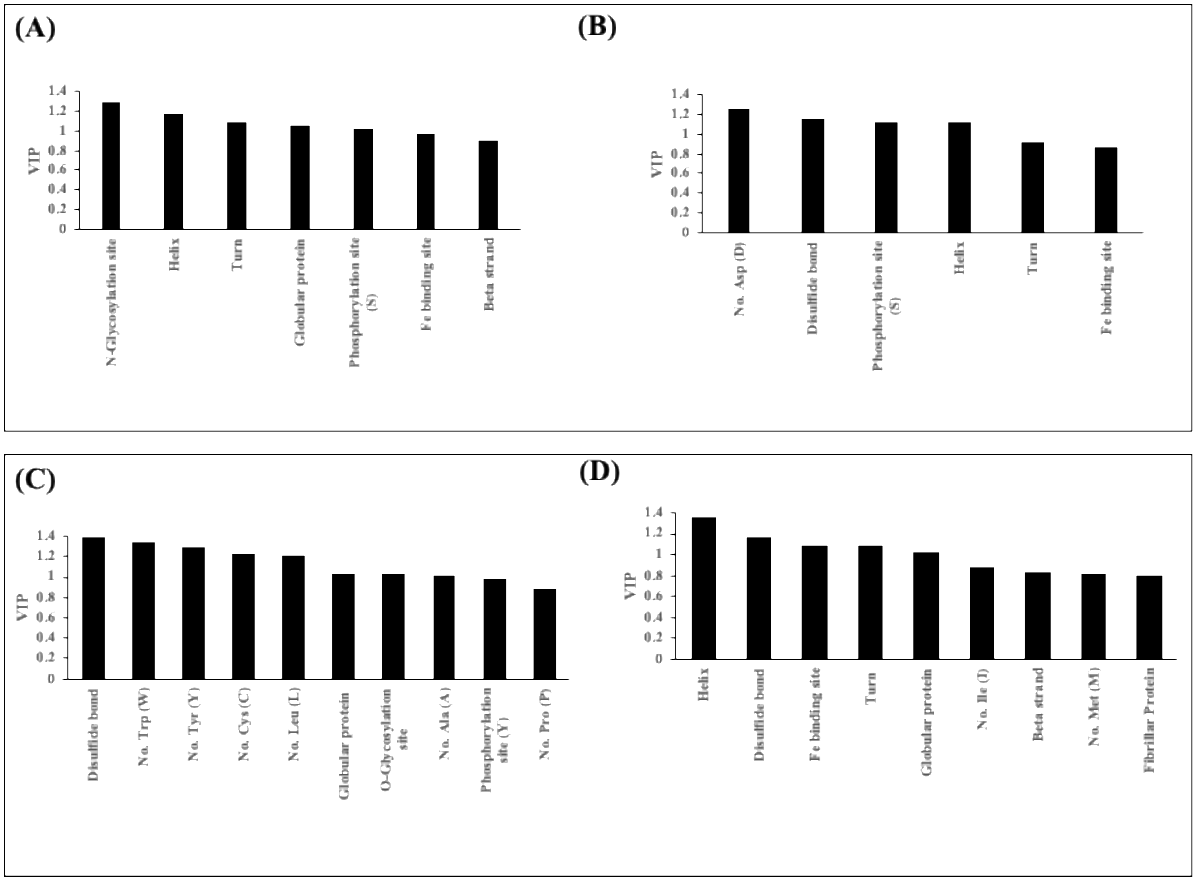

Figure 5. 4 Protein characteristics that correlated with abundance of proteins in silica particles **(A)** and titania particles **(B).** Likewise, protein characteristics that correlated with enrichment of proteins in silica particles **(C)** and titania particles **(D).** Variable importance in projection scores were generated by regression analysis (PLS) of abundance or enrichment of proteins on particle surface against their characteristics (n=39).

5.4.5 Prediction of protein network

Protein-Protein interaction network was generated for each type of NPs using the entire list of proteins ($\geq$ 2 no. of peptides identified in Scaffold software). The width of lines connecting proteins to each other suggest the strength of interactions where in wider the line, stronger the interaction. Figure 5.5 exemplify the protein network developed for proteins identified from FG-SiO_2-NP and those of other particles are given in Figure SI 5.2-5.4. Proteins identified within each cluster had stronger predicted interactions (denoted by solid line) and they interacted weakly with those outside their respective cluster (dotted line).

Cluster 5 identified for FG-SiO_2-NP (Figure 5.5) showed the highest number of proteins with strong predicted interactions. Prominent proteins forming nodes in this cluster included Apolipoprotein (E, A4 and A1), Fibrinogen (G, A and B), alpha-2-HS-glycoprotein *etc*. Cluster 2, was dominated by casein proteins (CSN, CSN1S1, CSN2, CSN3), and Lactalbumin. Similarly, cluster 6 consisted of proteins such as Fibronectin 1, Alpha-actinin-1, Kininogen-1 (KNG1) as prominent proteins forming the nodes. Another prominent cluster 8 consisted of proteins such as Lactoferrin, Ras-related protein Rab-(1B, 7A,8A, 11B,18), Peptidoglycan recognition protein 1, mannosidase alpha class 2B member 1 etc forming nodes. Similar observation could be made in proteins identified from other particles.

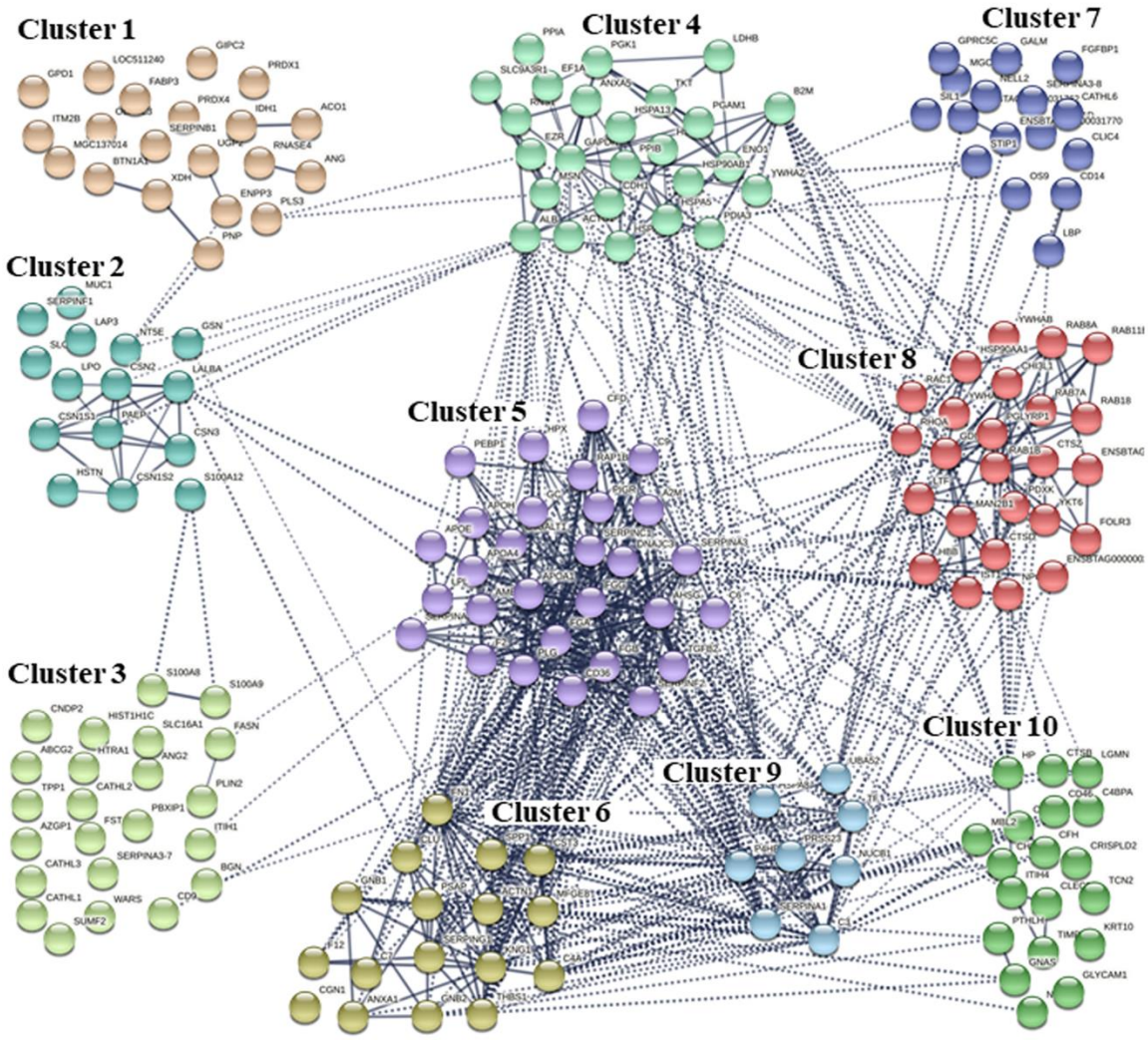

Figure 5. 5 Protein-protein interaction network. Clusters showing protein-protein interactions on FG-SiO_2-NP developed using the STRING software. Proteins are represented as spheres and their interaction denoted through connecting lines- the thickness of which corresponds to strength of protein interaction

5.4.6 Fourier-transform infrared spectroscopy analysis

The representative FTIR spectra of milk interacted dietary particles and control dietary particles are displayed in Figures 5.6F and SI 5.5. The spectra obtained from the milk interacted dietary particles were categorized into three main groups: protein (3290-3068 cm^{-1} and 1650-1540 cm^{-1}); lipid (2980-2800 cm^{-1} and 1466-1392 cm^{-1}) and carbohydrate (3290-3068 cm^{-1} and 1140-1020 cm^{-1}) using reported wavenumbers of biomolecule components [23].

5.4.7 Scanning transmission X-ray microscope (STXM) analysis

The interaction of milk with E171 (TiO_2) particles was investigated using STXM by collecting a ptychographic O K-edge stack of TiO_2 particles exposed to milk. The major biomolecules of milk include proteins, carbohydrates and lipids as shown in the FTIR spectra (Figures 5.6F, and SI 5.5) and biochemical assays (Figure SI 5.6)). Representative O K-edge X-ray absorption spectra of these major biomolecules are shown in Figure 5.6E. The O K-edge X-ray absorption TiO_2 spectrum was similar to that of anatase [29]. Spectral fitting of the O K-edge stack was performed with different combinations of the major biomolecules and TiO_2 spectra. The component maps, including the overlay of the component maps from the protein, lipid and TiO_2 fit are shown in Figure 5.6A-D. The distributions of lipids and saccharides were similar when they were separately included in the spectral fitting with protein and TiO_2. This is attributed to the similarity of their spectra (i.e., features/peak positions) (Figure 5.6E). Thus, differentiating between lipids and saccharides was not readily evident. As such, this analysis showed that biomolecules from milk were associated with the TiO_2 and it appears that there was some separation of the proteins and lipids surrounding the TiO_2 particles and lipid/saccharide layer was more prominent than protein layer. Threshold masking of the component maps and curve fitting of the resulting spectra (Figure SI 5.7 and Table SI 5.1) confirmed that there were areas consisting mainly of protein and lipid/saccharides.

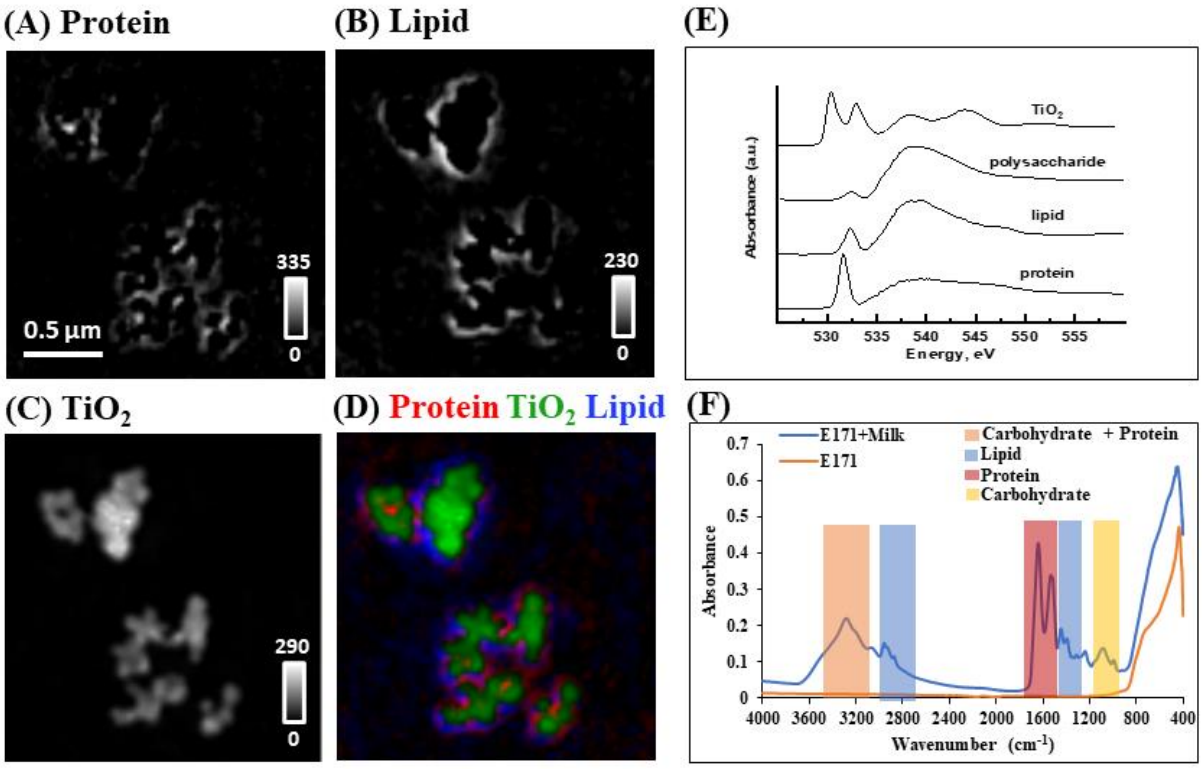

Figure 5. 6 Component maps. (A) protein, **(B)** lipid, **(C)** TiO_2 particle, and **(D)** overlay of rescaled component maps. Red = protein, green = TiO_2, blue = lipid. The gray scale bar indicates material thickness in nm.

(E) Oxygen K-edge X-ray absorption reference spectra of protein (human serum albumin), lipid (1,2-dipalmitoyl-sn-glycero-3-phosphocholine), polysaccharide (xanthan gum) and TiO_2.

(F) FTIR spectra of milk interacted E171 particles. A drop of sample suspension (10 $mg.mL^{-1}$ of particles retrieved from either water or milk) was placed on to the ATR probe, dried for 8 min to remove the water component and the spectra were acquired for a wavenumber range of 4000-400 cm^{-1}. Peaks 2980-2800 cm^{-1} and 1466-1392 cm^{-1} were assigned as lipid, 1650-1540 cm^{-1} were assigned as protein, and 1140-1020 cm^{-1} were assigned as carbohydrate, 3290-3068 cm^{-1} were assigned as protein and carbohydrate, based on reported values [23].

5.5 Discussion

Proteins adsorbed onto the surface of particles have received considerable attention from the scientific community owing to their relevance in determining the biological identity of particles entering human body. Proteins in the surface corona of particles could influence the tissue distribution, cellular uptake and ultimately lead to any adverse biological outcome [2, 3]. Both physicochemical nature of particle as well as properties of proteins are implied in shaping the protein corona formation of particles [7]. However, there are still knowledge gaps on the interplay of these factors when particles encounter a complex system such as food matrix. In this study, the question was answered if the factors identified through studies involving interaction between individual protein and particle can predict the nature of protein corona when particles interact with complex mixtures such as food. The current studies showed that factors involved in protein-protein/biomolecule interactions outweigh those that mediate protein-nanoparticle interactions in defining the protein corona.

The initial attempt was to interact proteins individually with each particle and determine the particle type and proteins showing higher adsorption. As shown in Figure 5.2, it was observed that on an equal mass basis, silica NPs absorb more proteins in comparison to E551 particles and other particles. Protein characteristics such as hydrophobicity, polarity of amino acids, and cysteine have been reported to influence adsorption of proteins onto particle surfaces. Therefore, several characteristics of proteins including their MW, Ip, number of amino acids, cysteine resides, and presence of metal binding sites, secondary structure, *etc* were analysed in this study, for their contribution to particle binding using regression analysis. The current studies showed that factors such as hydrodynamic size, zetapotential, and hydrophobicity of particles and protein characteristics including number of beta strand, number of amino acid, phosphorylation site (S) & (Y), and N-glycosylation site contribute favourably to protein binding. Results from the current study concur with previous findings that α-helix and β-sheet

are likely to interact with hydrophobic NPs by hydrogen bonding [30, 31] and smaller hydrodynamic size of particles increase surface adsorption of proteins [32]. This increased protein binding could be attributed to the nanoscale surface curvature that increases protein affinity [33] and higher surface area with more surface exposed OH groups per volume of SiO_2 NPs [34]. The OH groups on the surface of silica particles are a major binding site for proteins [34, 35]. It is generally accepted that the binding of proteins onto NPs are mediated *via* hydrogen bonding, electrostatic [3], and hydrophobic interactions [36] which are primarily determined by type and abundance of amino acid residues in the primary structure of proteins. Correspondingly, one-one interactions of proteins and particles showed the relevance of amino acids such as Ile, Tyr, Ala, Gly, Pro, Asp, and Arg in favouring protein-NP interactions. Besides, structural rearrangement of proteins during contact with particle surface has also been identified as an important factor influencing the interaction of proteins with NPs [6, 37]. As such, we were interested to see if factors identified from single protein-particle interaction play a vital role in shaping the corona formation of food matrix interacted particles.

Protein profiling using LC-MS/MS showed that some of the low abundant proteins in milk are enriched in the protein corona of the dietary particles. For instance, histatherin protein was enriched in corona of FG-TiO_2-NP, E551 and FG-SiO_2-NP which were respectively 17, 8 and 4-fold higher in comparison to milk. The differences in the level of enrichment on different particles could be attributed to the differences in the surface chemistry of particles as shown previous by studies from the same group [8, 29]. Histatherin is one of the antimicrobial peptides present in milk [38]. Similarly, Cathelicidin and Heat Shock 70 kDa proteins are host response proteins to mastitis infections [39, 40]. Interestingly, this study showed the potential of enriching these proteins with silica particles, opening new possibilities of improving the detection of these proteins as markers of mastitis conditions through milk analysis.

The regression analysis was conducted using the characteristics of the twenty most abundant and enriched proteins to identify factors significant for corona formation. Helix, turn, disulfide bond, glycosylation site, number of amino acid and metal binding sites were found to influence protein-particles interactions. Notably, factors identified through one-one interaction studies were not obviously identified as influencers for corona formation in complex media (milk). This discrepancy has not been reasoned adequately in literature. The significance of protein-protein interaction in shaping the proteome of particle corona is gaining attention. Protein-protein interactions facilitated through binding of motifs with sequences in another polypeptide [41] could act as anchoring points for proteins in surface corona of particles. Domain-specific binding has been identified as the principle force behind functional association of proteins in these networks [41]. Interestingly, protein-protein interaction networks generated using bioinformatic tool STRING, (Figure 5.5 and Figure SI 5.2-5.4), suggested that certain proteins could behave as 'nodes' with possibility of interacting with many other proteins. Examples include protein such as transferrin (cluster 9) and lactoferrin (cluster 8), alpha-lactalbumin and alpha-casein (cluster 2), Apolipoprotein (E, A4 and A1) and Fibrinogen (G, A and B) (cluster 5) *etc*. Incidentally, these proteins are the prominent ones implied in the hard-corona of NPs interacted with blood plasma [7] and are reported to contain multi-interaction domains [41]. Prevailing models suggest the formation of 'hard corona' where the proteins in hard corona interact directly with the particle surface and 'soft corona' consisting of proteins interacting with proteins of hard-corona [42]. After washing, proteins retained onto the particles are generally accepted as 'hard corona'.

Previous studies addressing protein corona on NPs were mostly focused on either protein-particles or protein-protein interactions [43], although influences of other biomolecules (*e.g* lipids and carbohydrates) were suspected. Dietary particles exposed to the food matrix are likely to accumulate lipids and carbohydrate on their surface. Consequently, the network of

biomolecular interactions are likely to be more complex than protein-protein or protein-particle interactions. For example, the phospholipid head groups of lipid could interact with hydrophilic portions of proteins or the surface of the particles [44]. In fact, examination of particle surface using FTIR (Figure 5.6F, and SI 5.5), secondary biochemical assays (Figure SI 5.6) and STXM (Figure 5.6A-D) showed the presence of lipids and carbohydrates apart from proteins in the surface corona of milk interacted particles. Presence of discrete and overlapping regions in protein and lipids maps (Figure 6F) suggest direct binding of individual biomolecules onto NP surface and their mutual interactions.

Based on results from the current studies, we argue that protein characteristics that mediate their interaction with other proteins and other biomolecules are more pronounced than those characteristics mediating direct interaction of proteins with surfaces of particles for the association of proteins in surface corona of particles. Protein characteristics and physicochemical properties of particles may play a crucial role for binding of 'pioneer' proteins onto particle surface. Majority of the proteins associated with surface corona are, however, not bound to particles directly but to these pioneer proteins or biomolecules that bind directly to particle surface. Therefore, we propose that proteins or other biomolecules (such as lipids) with high affinity for the particle surface form the base and provide anchoring points for other proteins to bind. Protein-protein interactions and lipid-protein interactions appear to be strong enough to withstand the removal of peripheral layer of proteins during washing, especially at the interstitial spaces and play a pivotal role in determining the proteome of hard-corona on particles dispersed in complex media. This new knowledge will refine the current understanding of the fundamental principles dominating the complex biomolecular interactions involved in surface corona formation. As such this information will be highly relevant for understanding the transformation of dietary nanoparticles in food, their fate and transport in

human digestive tract and for explaining the alteration in allergenicity of food components in the presence of nanoparticles.

5.6 References

1. Frewer, L.J., et al., *Consumer attitudes towards nanotechnologies applied to food production.* Trends in food science & technology, 2014. **40**(2): p. 211-225.
2. Dobrovolskaia, M.A., M. Shurin, and A.A. Shvedova, *Current understanding of interactions between nanoparticles and the immune system*. Toxicology and applied pharmacology, 2016. **299**: p. 78-89.
3. Marichal, L., et al., *Protein Corona Composition of Silica Nanoparticles in Complex Media: Nanoparticle Size does not Matter.* Nanomaterials, 2020. **10**(2): p. 240.
4. Tenzer, S., et al., *Rapid formation of plasma protein corona critically affects nanoparticle pathophysiology.* Nature nanotechnology, 2013. **8**(10): p. 772-781.
5. Park, S.J., *Protein–nanoparticle interaction: corona formation and conformational changes in proteins on nanoparticles.* International journal of nanomedicine, 2020. **15**: p. 5783.
6. Dhar, S., et al., *Role of Physicochemical Properties of Protein in Modulating the Nanoparticle-Bio interface.* bioRxiv, 2018: p. 484972.
7. Monopoli, M.P., et al., *Physical− chemical aspects of protein corona: relevance to in vitro and in vivo biological impacts of nanoparticles.* Journal of the american chemical society, 2011. **133**(8): p. 2525-2534.
8. Srinivasan, D., et al., *The type of dietary nanoparticles influences salivary protein corona composition.* NanoImpact, 2020: p. 100238.
9. Tenzer, S., et al., *Nanoparticle size is a critical physicochemical determinant of the human blood plasma corona: a comprehensive quantitative proteomic analysis.* ACS nano, 2011. **5**(9): p. 7155-7167.

10. Walkey, C.D., et al., *Nanoparticle size and surface chemistry determine serum protein adsorption and macrophage uptake.* Journal of the american chemical society, 2012. **134**(4): p. 2139-2147.

11. Zhao, Z., et al., *Effect of physicochemical and surface properties on in vivo fate of drug nanocarriers.* Advanced drug delivery reviews, 2019. **143**: p. 3-21.

12. Cedervall, T., et al., *Understanding the nanoparticle–protein corona using methods to quantify exchange rates and affinities of proteins for nanoparticles.* Proceedings of the national academy of sciences, 2007. **104**(7): p. 2050-2055.

13. Milani, S., et al., *Reversible versus irreversible binding of transferrin to polystyrene nanoparticles: soft and hard corona.* ACS nano, 2012. **6**(3): p. 2532-2541.

14. Buzea, C., I.I. Pacheco, and K. Robbie, *Nanomaterials and nanoparticles: sources and toxicity.* Biointerphases, 2007. **2**(4): p. MR17-MR71.

15. Farrés, M., B. Piña, and R. Tauler, *Chemometric evaluation of Saccharomyces cerevisiae metabolic profiles using LC–MS.* Metabolomics, 2015. **11**(1): p. 210-224.

16. Xiao, Y. and M.R. Wiesner, *Characterization of surface hydrophobicity of engineered nanoparticles.* Journal of hazardous materials, 2012. **215**: p. 146-151.

17. De Jong, S., *SIMPLS: an alternative approach to partial least squares regression*. Chemometrics and intelligent laboratory systems, 1993. **18**(3): p. 251-263.

18. Cedervall, T., et al., *Food chain transport of nanoparticles affects behaviour and fat metabolism in fish.* PloS one, 2012. **7**(2): p. e32254.

19. Kavran, J.M. and D.J. Leahy, *Silver staining of SDS-polyacrylamide Gel*, in *Methods in Enzymology*. Elsevier, 2014. p. 169-176.

20. Shevchenko, A., et al., *In-gel digestion for mass spectrometric characterization of proteins and proteomes.* Nature protocols, 2006. **1**(6): p. 2856-2860.

21. Keller, A., et al., *Empirical statistical model to estimate the accuracy of peptide identifications made by MS/MS and database search.* Analytical chemistry, 2002. **74**(20): p. 5383-5392.

22. Jayaraman, A., K. Jamil, and H.A. Khan, *Identifying new targets in leukemogenesis using computational approaches.* Saudi journal of biological sciences, 2015. **22**(5): p. 610-622.

23. Deniz, E., et al., *Differentiation of beef mixtures adulterated with chicken or turkey meat using FTIR spectroscopy.* Journal of food processing and preservation, 2018. **42**(10): p. e13767.

24. Kaznatcheev, K.V., et al., *Soft X-ray spectromicroscopy beamline at the CLS: commissioning results.* Nuclear instruments and methods in physics research section A: accelerators, spectrometers, detectors and associated equipment, 2007. **582**(1): p. 96-99.

25. Wang, C., et al., *Background noise removal in x-ray ptychography.* Applied optics, 2017. **56**(8): p. 2099-2111.

26. Dynes, J.J., et al., *Speciation and quantitative mapping of metal species in microbial biofilms using scanning transmission X-ray microscopy.* Environmental science & technology, 2006. **40**(5): p. 1556-1565.

27. Sun, T., et al., *Soft X-ray Ptychography Chemical Imaging of Degradation in a Composite Surface-Reconstructed Li-Rich Cathode.* ACS nano, 2020. **15**(1): p. 1475-1485.

28. Costa, F.F., et al., *Microfluidic chip electrophoresis investigation of major milk proteins: study of buffer effects and quantitative approaching.* Analytical methods, 2014. **6**(6): p. 1666-1673.

29. Henderson, G., X. Liu, and M. Fleet, *Titanium coordination in silicate glasses investigated using OK-edge X-ray absorption spectroscopy.* Mineralogical magazine, 2003. **67**(4): p. 597-607.

30. Shemetov, A.A., I. Nabiev, and A. Sukhanova, *Molecular interaction of proteins and peptides with nanoparticles.* ACS nano, 2012. **6**(6): p. 4585-4602.

31. Anand, G., et al., *Conformational transitions of adsorbed proteins on surfaces of varying polarity.* Langmuir, 2010. **26**(13): p. 10803-10811.

32. Tanaka, T., et al., *Protein adsorption characteristics of nanoparticle-assembled hollow microspheres of hydroxyapatite and their composites with PLLA microporous membranes.* Heliyon, 2019. **5**(4): p. e01490.

33. Xia, X.-R., N.A. Monteiro-Riviere, and J.E. Riviere, *An index for characterization of nanomaterials in biological systems.* Nature nanotechnology, 2010. **5**(9): p. 671-675.

34. Mathé, C., et al., *Structural determinants for protein adsorption/non-adsorption to silica surface.* PloS one, 2013. **8**(11): p. e81346.

35. Phue, W.H., et al., *A comparative analysis of different grades of silica particles and temperature variants of food-grade silica nanoparticles for their physicochemical properties and effect on trypsin.* Journal of agricultural and food chemistry, 2019. **67**(44): p. 12264-12272.

36. Taha, M. and M.-J. Lee, *Influence of the alanine side-chain methyl group on the peptide-gold nanoparticles interactions.* Journal of molecular liquids, 2020. **302**: p. 112528.

37. Marichal, L., et al., *From Protein Corona to Colloidal Self-Assembly: The Importance of Protein Size in Protein–Nanoparticle Interactions.* Langmuir, 2020. **36**(28): p. 8218-8230.

38. Rattray, K., M. Lay, and A. Molenaar, *Detection of Histatherin: a Potential Antimicrobial Peptide.*

39. Boehmer, J.L., *Proteomic analyses of host and pathogen responses during bovine mastitis.* Journal of mammary gland biology and neoplasia, 2011. **16**(4): p. 323-338.

40. Abdelmegid, S., et al., *Identification of host defense-related proteins using label-free quantitative proteomic analysis of milk whey from cows with Staphylococcus aureus subclinical mastitis.* International journal of molecular sciences, 2018. **19**(1): p. 78.

41. Vasti, C., et al., *Relevance of protein–protein interactions on the biological identity of nanoparticles.* Colloids and surfaces B: biointerfaces, 2018. **166**: p. 330-338.

42. Ke, P.C., et al., *A decade of the protein corona.* ACS nano, 2017. **11**(12): p. 11773-11776.

43. Auría-Soro, C., et al., *Interactions of nanoparticles and biosystems: microenvironment of nanoparticles and biomolecules in nanomedicine.* Nanomaterials, 2019. **9**(10): p. 1365.

44. Le, Q.-C., et al., *Interactions between phospholipids and titanium dioxide particles*. Colloids and surfaces B: biointerfaces, 2014. **123**: p. 150-157.

5.7 Supporting information

5.7.1 Protein preparation for one-dimension gel electrophoresis

Bovine milk protein (α-casein, β-casein, α-lactalbumin, β-lactoglobulin, bovine albumin) were selected for this experiment. One milligram per millilitre of each proteins were dissolved in PBS (pH 6.5). Two hundred microliter of each protein solution (1 $mg.mL^{-1}$) were mixed with 100 µL of dietary particles (10 $mg.mL^{-1}$) and the resulting solutions were incubated at 37°C for an hour. Controls were prepared by adding the same proportions of deionized water to the proteins mixture. After one hour incubation, the solution was centrifuged at 14,000 rpm for 15 min and the supernatant was discarded. This step was repeated twice to retain only hard corona formed on the particles.

5.7.2 One-dimension gel electrophoresis

After the final wash of milk interacted particles, 200 µL of sample buffer containing 62.5 mM Tris-HCl, pH 6.8, 2% SDS, 25% (v/v) glycerol, 0.01% bromophenol blue and 5% β-mercaptoethanol were added to one set of particles pelleted, vortexed and boiled for 5 mins. Particles were removed from sample buffer by centrifugation at 14,000 rpm for 15 min; protein-containing sample solution was collected and transferred into a fresh tube. Twenty-five microliters of each protein-nanoparticles samples and 10 uL of each individual protein (as a control) were loaded to a sample well of a 4-20% SDS-polyacrylamide gel. The proteins were separated in the gel using 90 V for 1.5 hr in running buffer containing 2.5 mM tris, 19.2 mM glycine and 0.01% SDS. The gels were then stained in standard Coomassie blue-methanol-acetic acid solution for 30 mins at RT. The gels were subsequently washed with destaining solution (40% methanol, 10% acetic acid and 50% water) for 30 min at RT to visualize the protein bands. The gel was then stained in silver staining by following the reference method [1].

As shown in Figure SI 5.1, the intensity of casein protein band were increased in silica particles adsorbed protein mixture sample. This data confirms the pattern of quantitative determination of protein adsorption onto particles given in Figure 5.2A.

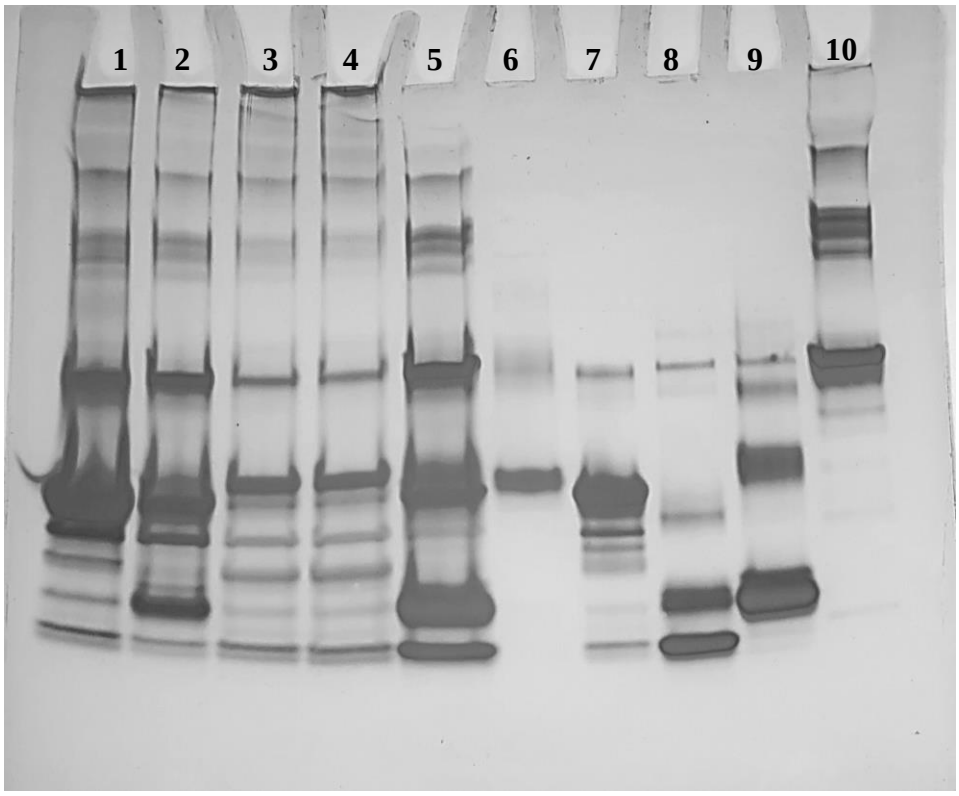

Figure SI 5. 1 SDS-PAGE gels of milk individual mixed proteins adsorbed on dietary particles. Lane (1) mixed proteins + FG-SiO2-NP, (2) mixed proteins + E551, (3) mixed proteins + FG-TiO2-NP, (4) mixed proteins + E171, (5) mixed proteins, (6) α-casein, (7) β-casein, (8) α-lactalbumin, (9) β-lactoglobulin, and (10) bovine serum albumin (BSA)

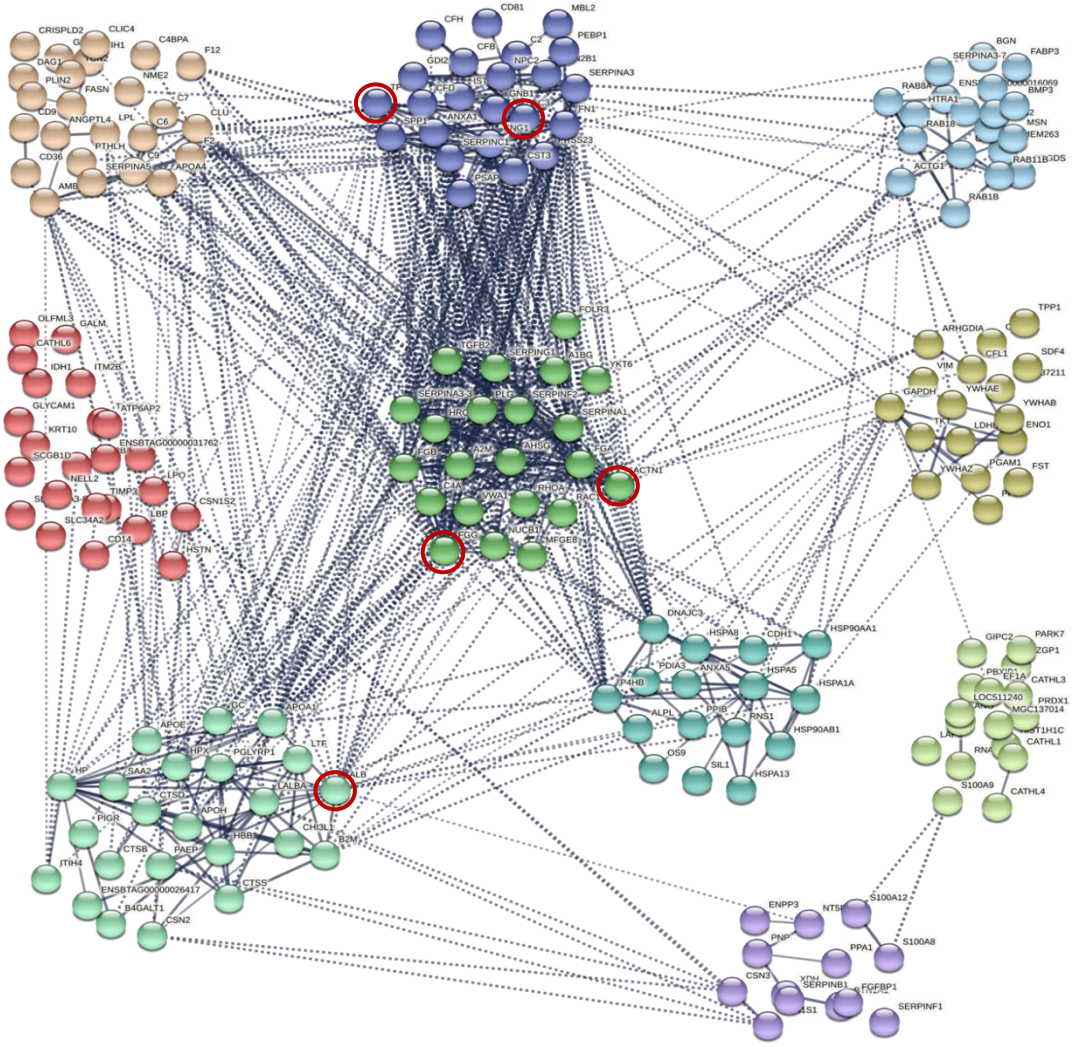

Figure SI 5. 2 Protein-protein interaction network clustering with entire list of proteins (≥ 2 no. of peptides identified in Scaffold software) on E551 identified by LC-MS/MS proteomics were developed using the STRING software. Proteins are represented as nodes and their interaction denoted through connecting lines- the thickness of which corresponds to strength of protein interaction

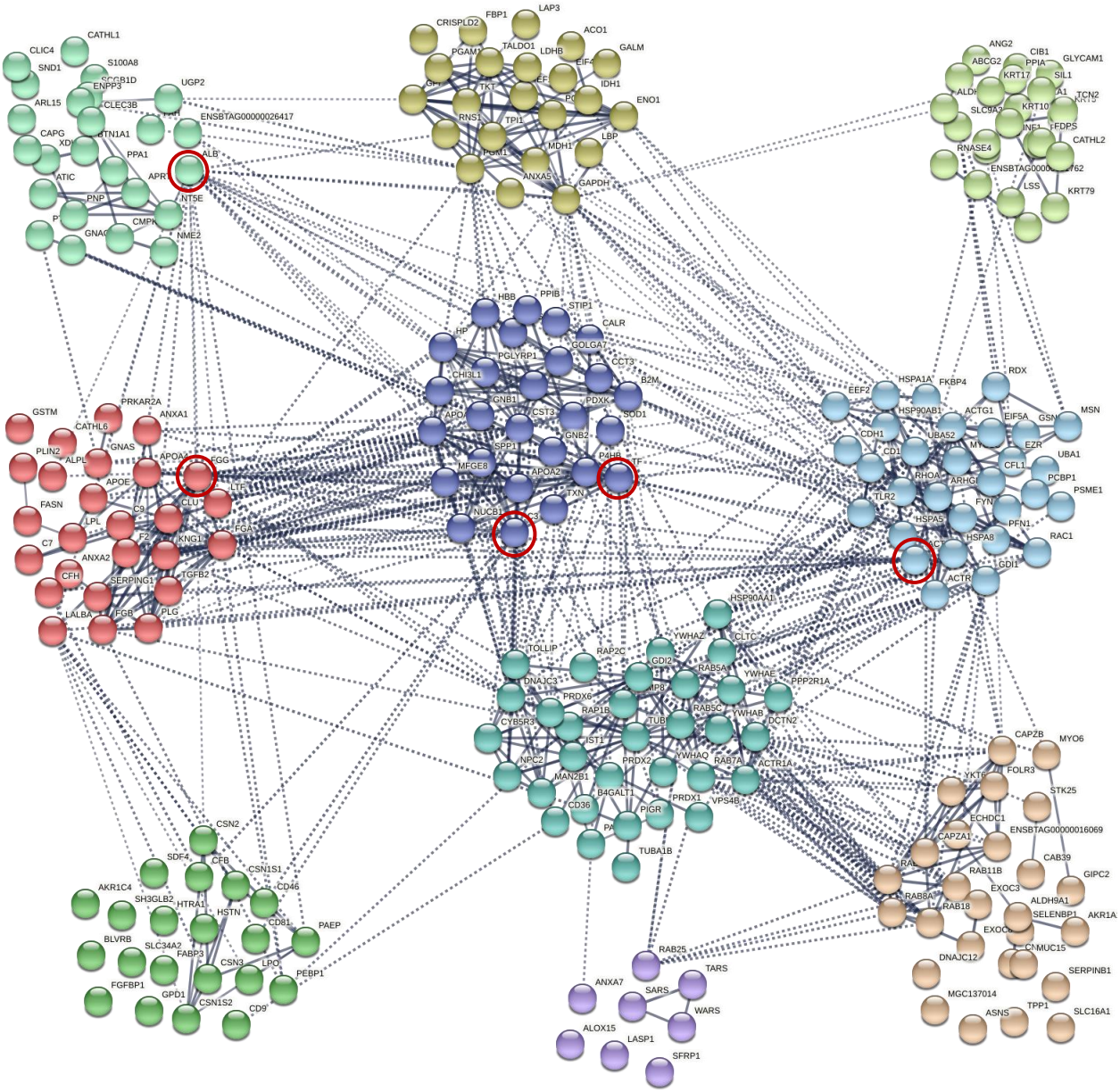

Figure SI 5. 3 Protein-protein interaction network clustering with entire list of proteins ($\geq$ 2 no. of peptides identified in Scaffold software) on FG-TiO_2-NP identified by LC-MS/MS proteomics were developed using the STRING software. Proteins are represented as nodes and their interaction denoted through connecting lines- the thickness of which corresponds to strength of protein interaction

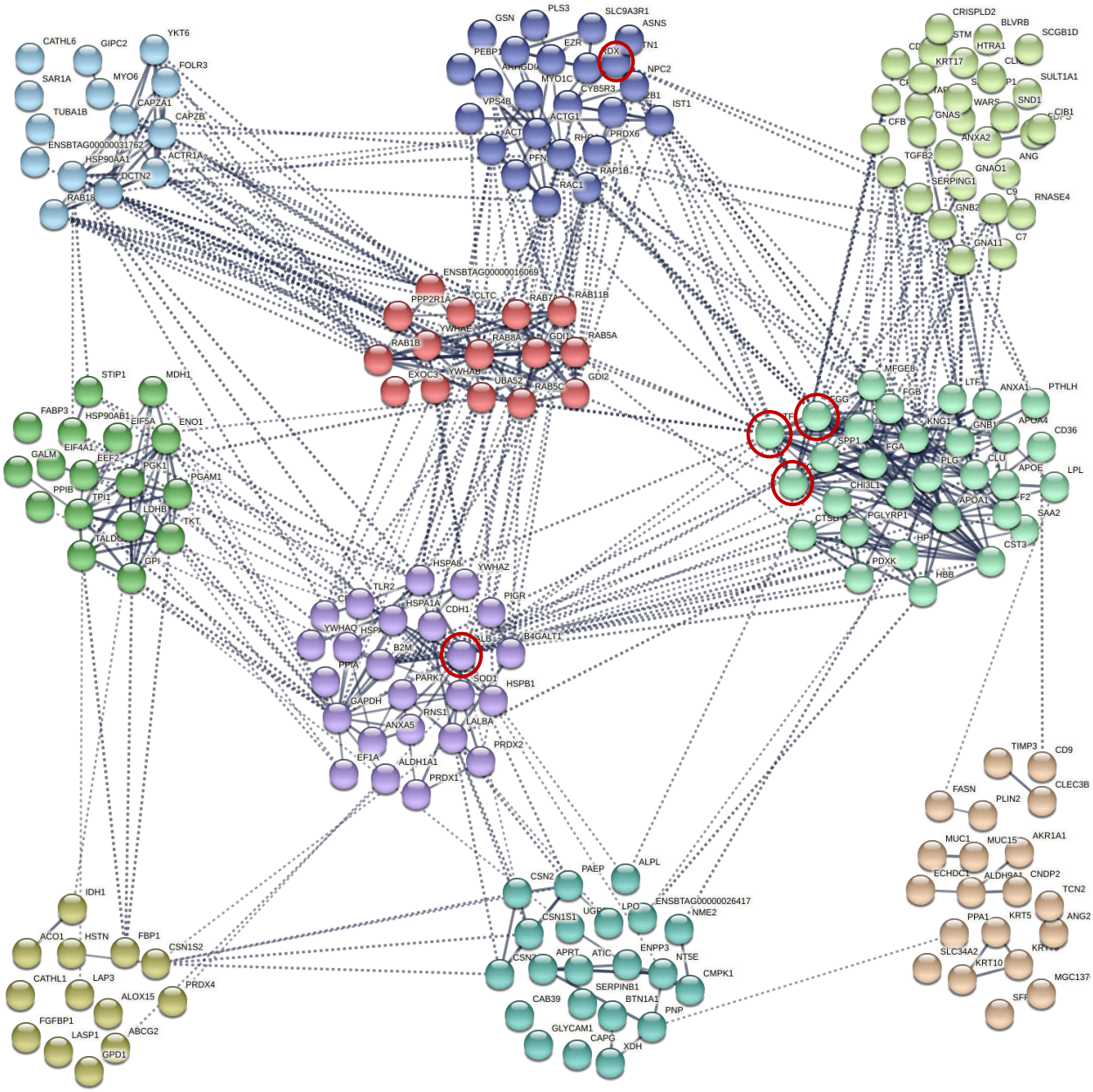

Figure SI 5. 4 Protein-protein interaction network clustering with entire list of proteins (≥ 2 no. of peptides identified in Scaffold software) on E171 identified by LC-MS/MS proteomics were developed using the STRING software. Proteins are represented as nodes and their interaction denoted through connecting lines- the thickness of which corresponds to strength of protein interaction

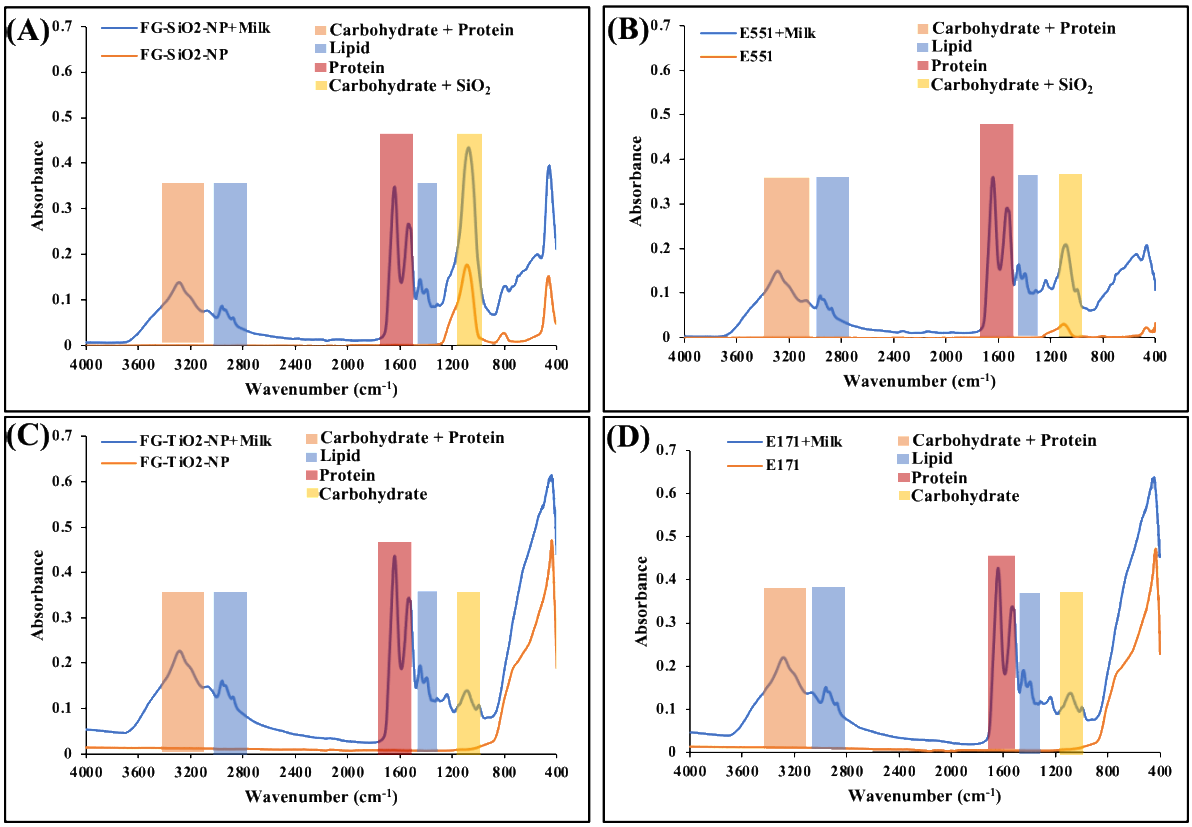

Figure SI 5. 5 FTIR spectra of milk interacted dietary particles. Food grade particles of SiO_2 and TiO_2 were interacted with skim milk for 1 hr, washed and suspended in water (10 $mg.mL^{-1}$), a drop of sample suspension was placed on to ATR probe, dried for 8 mins to remove water component and the spectra were taken for a wavenumber range of 4000-400 cm^{-1} using ATR-FTIR (Nicolet Summit FTIR Spectrometer, MA, USA). **(A)** Milk interacted FG-SiO_2-NP in comparison with pristine FG-SiO_2-NP, **(B)** milk interacted E551 in comparison with pristine E551, **(C)** milk interacted FG-TiO_2-NP in comparison with pristine FG-TiO_2-NP, **(D)** milk interacted E171 in comparison with pristine E171.

Peak assignments were based on published peer reviewed articles [2]. IR method have been used to determine the compositions of milk since 1964 [3]. In fact, determination of major components of milk (fat, lactose and protein) using IR is now an official method [4]. The minor contributions of proteins to absorbance at 3000-2800 cm^{-1} is negligible to obscure signal from lipid. Based on verified FTIR studies,[2] absorbance of IR in region between 1650-1540 cm^{-1}

was assigned as protein peak, 1140-1020 cm^{-1} as carbohydrate, 2980-2800 cm^{-1} and 1466-1392 cm^{-1} as lipid and region between 3290-3068 cm^{-1} was assigned as protein and carbohydrate.

SI 5.7 Determination of presence of proteins, carbohydrates and lipids on milk interacted particles

SI 5.7.1 Determination of proteins adsorbed onto particles interacted with milk

Milk interacted particles were prepared as detailed in the main manuscript. Particles were washed and suspended in water (1 $mg.mL^{-1}$) and 15 µL of the particle suspension was retrieved and mixed with 15 µL of protein eluting buffer containing 2% SDS in 20 mM sodium phosphate buffer [5]. The suspension was incubated for 1 hr at room temperature for elution of proteins from the surface of particles. The samples were centrifuged for 15 min at 20,124 g to separate the particles from the solution. Ten microliters of resulting supernatant were mixed with 100 µL of Pierce 660 containing 50 mM ionic detergent compatible reagent (IDCR) [5]. After 5 min of incubation at room temperature, the absorbance was measured at 660 nm using micro plate reader (SpectraMax i3x, Multi-mode Microplate Reader, Molecular Devices, USA). The percentage of protein adsorbed onto particles was calculated based on the absorbance value determined for skim milk (not interacted with particles) using the same protocol, and the absorbance value determined for protein eluted from particle surface.

5.7.2 Determination of total carbohydrates adsorbed onto particles interacted with milk

Total carbohydrate present on particles interacted with milk was determined using phenol-sulfuric acid method [6]. For this, milk interacted particles were washed and suspended in water (1 $mg.mL^{-1}$) and 50 µL of particle suspensions were added to wells in a 96 well plate. Subsequently, 150 µL of concentrated H_2SO_4 and 30 µL of 5% phenol in distilled water were added. The plate was incubated in 5 min at 90°C, followed by cooling to room temperature. The absorbance was measured at 490 nm. The percentage of carbohydrate adsorbed onto

particles was calculated based on absorbance value determined in skim milk (not interacted with particles) using the same protocol, and the absorbance value in the particle suspension.

5.7.3 Determination of total lipids adsorbed onto particles interacted with milk

Total lipids present on particles interacted with milk was determined using Sudan black B staining, according to protocol reported but with modification [7]. Sudan-black B staining solution was prepared by adding 500 mg of Sudan-black B, 20 mL of acetone, 15 mL of acetic acid and 85 mL of water. The dye solution was stirred for 30 mins at room temperature and undissolved dye was removed by centrifugation at 20,124 g for 15 min. Five hundred microliters of milk interacted particle suspensions (1 $mg.mL^{-1}$) were mixed with 500 µL of dye solution and incubated for 30 min at RT. Subsequently, the samples were centrifuged at 20,124 g for 15 mins to collect the stained total lipid and washed with water for 3 times. The dye on particles was redissolved in 200 µL of acetone and the suspension was centrifuged at 20,124 g for 15 min to remove particles from the solution. Ten microliters of supernatant were mixed with 190 µL of water and the absorbance was measured at 600 nm. The percentage of lipids adsorbed onto particles was calculated based on absorbance value determined in skim milk (not interacted with particles) using the same protocol, and the absorbance value of dye eluted from particles.

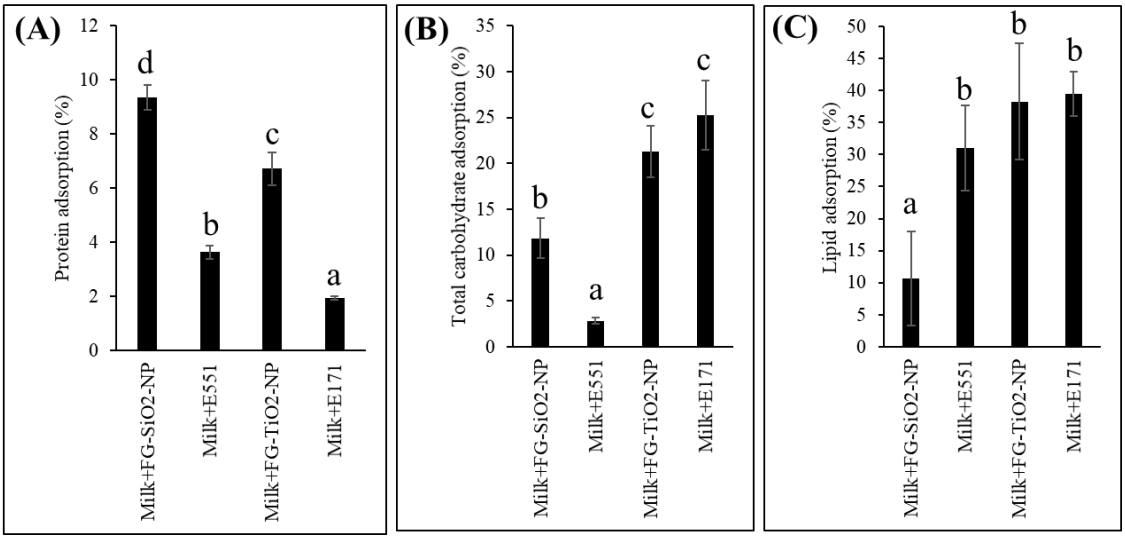

Figure SI 5. 6 Quantification of the presence of proteins, carbohydrates and lipids in the surface corona of dietary particles. (A) The presence of proteins adsorbed onto milk interacted particles were confirmed through Pierce 660 as detailed. **(B)** the presence of carbohydrate in the surface corona was confirmed by Phenol-sulphuric acid method, **(C)** the percentage of lipids in the surface corona was confirmed by Sudan-black B staining method. Average values are plotted in the graph and the different letters indicate significant differences (Duncan, $p<0.05$).

This studies confirmed the presence of proteins, carbohydrates and lipids (which may contain triglycerides, fatty acids, phospholipids, sterols, lipo-proteins, fat soluble vitamins, etc). There was difference among particles for the relative amount of proteins, carbohydrates and lipids in surface corona. Generally, the presence of carbohydrates and lipids were higher in particles of TiO_2 in comparison to SiO_2 and for proteins vice versa. Total fat present in skim milk is in the range of 0.04-0.3% and it is composed of triacylglycerols, diacylglycerols, monoacylglycerols, free fatty acids, phospholipids and sterols and the ratio of phospholipids to total fat is relatively higher in skim milk.[8] The presence of fat soluble vitamins (Vitamin A and Vitamin D) may also contribute to the total lipids determined using Sudan Black B staining.

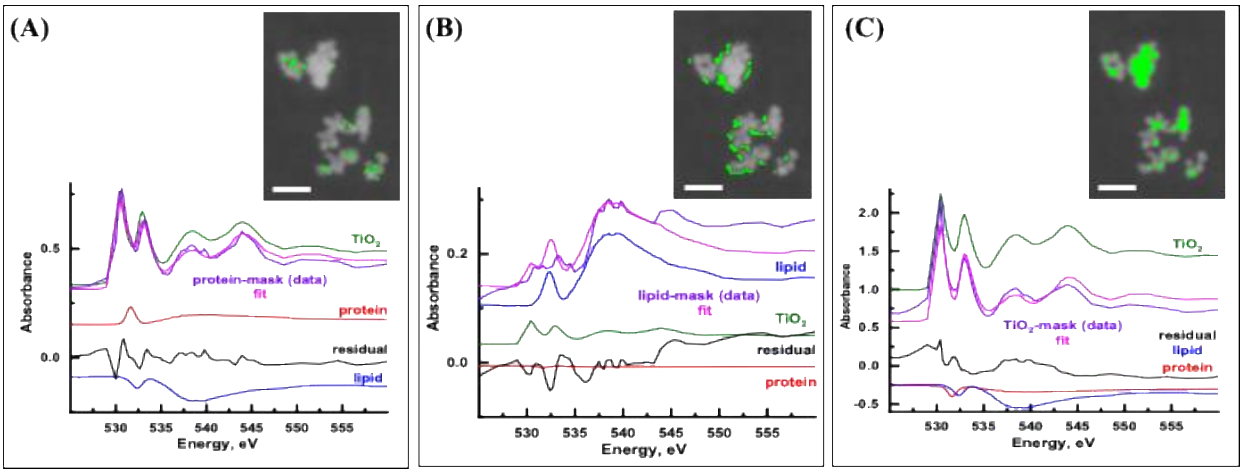

Figure SI 5. 7 Linear combination fitting of the derived spectra using the reference spectra from Figure 5.6. (A). (A) Protein derived, **(B)** lipid derived, and **(C)** TiO_2 derived spectra. The derived spectra were determined by threshold masking of the pixels with high intensity from their respective component map. The insert shows the location of the pixels (green) on the average image of the O K-edge stack.

Table SI 5. 1 Amount of protein, lipid and TiO_2 in the spectra derived by threshold masking of the pixels with high intensity from their respective component map as determined by linear combination fitting using the reference spectra from Figure 5.6.

Component	Thickness (nm) of components from the derived spectra		
	Protein	Lipid	TiO_2
Protein[a]	158	-6.50	-274
Lipid[b]	-119	143	-331
TiO_2	58.3	5.90	171
Chi-squared	0.051	0.042	0.74

a - albumin, b - 1,2-dipalmitoyl-sn-glycero-3-phosphocholine

5.8 SI References

1. Kavran, J.M. and D.J. Leahy, *Silver staining of SDS-polyacrylamide Gel*, in *Methods in Enzymology*. Elsevier, 2014. p. 169-176.
2. Deniz, E., et al., *Differentiation of beef mixtures adulterated with chicken or turkey meat using FTIR spectroscopy.* Journal of food processing and preservation, 2018. **42**(10): p. e13767.
3. Goulden, J.D.S., *Analysis of milk by infra-red absorption.* Journal of dairy research, 1964. **31**(3): p. 273-284.
4. Ismail, F.R.V.D.V.J.S.G.E.A.A., *Assessment of Fourier Transform Infrared Analysis of Milk.* Journal of AOAC international, 1992. **75**(5): p. 780-785.
5. Srinivasan, D., et al., *The type of dietary nanoparticles influences salivary protein corona composition.* NanoImpact, 2020. **19**: p. 100238.
6. Masuko, T., et al., *Carbohydrate analysis by a phenol-sulfuric acid method in microplate format.* Anal Biochem, 2005. **339**(1): p. 69-72.
7. Clark, G., *Staining Procedures Used by the Biological Stain Commission.* 4th Edition, Williams & Wilkins, Baltimore, London, 1981: p. 393-394.
8. MacGibbon, A.K.H., *Composition and Structure of Bovine Milk Lipids*. Advanced Dairy Chemistry, Volume 2: Lipids, 2020. p. 1-32.

Connecting Text

Studies presented in Chapters 3 and 4 showed that the structure and function of proteins change when they get adsorbed onto the surfaces of DNMs. Proteome analysis of the surface corona of milk interacted DNMs, as presented in Chapter 5, showed preferential adsorbtion of milk proteins implied in milk allergy. Guaging from these studies, it was evident that DNM interaction with milk could (1) magnify the concentration of milk allergens on particle surfaces, (2) would alter the structure of adsorbed proteins. Therefore, it was necessary to address the alteration in antigenicity (antibody affinity) and allergenicity (measured as mast cell degranulation) of milk allergens interacted with DNMs. Therefore, chapter 6 examined the alteration in milk proteins' antigenicity and allergenicity when interacting with DNMs of SiO_2 and TiO_2. Chapter 6 is published in Food and Chemical Toxicology, Phue, W. H., Xu. K., George S., (2022).

Chapter 6. Inorganic food additive nanomaterials alter the allergenicity of milk proteins

6.1 Abstract

While inorganic nanomaterials are copiously incorporated in food products, their impact on the allergenicity of food proteins is largely unknown. This study analysed the effect of widely used food additive nanomaterials (silica and titania) on the antigenicity and allergenicity of milk proteins (β-lactoglobulin and casein) and skimmed milk. Changes in the antigenicity of milk proteins in the presence of dietary nanomaterials were identified using an indirect-ELISA assay, while the change in allergenicity was studied using mast cell (LAD2) sensitized using allergic human sera. Results showed an enhancement in the allergenicity of milk proteins/skimmed milk interacted with particles (both silica and titania). Similarly, mast cell degranulation (a proxy for allergenicity) was higher when exposed to particle interacted skim milk where nanomaterials of titania showed the highest effect, and this tendency was retained even after subjecting to simulated gut digestion. Particles induced alterations in the structure of milk proteins, as evidenced by current studies, are reasoned to expose epitopes that increase allergenicity of milk proteins.

Keywords: Milk allergy; Inorganic food additive materials; Allergenicity; E551; E171

6.2 Introduction

Food allergy is defined as 'an adverse health effect arising from a specific immune response that occurs reproducibly on exposure to a given food' [1]. The increasing occurrence of life-threatening episodes and lack of effective treatment options make food allergies a growing public health concern worldwide. Bovine milk is a major source of animal proteins for human nutrition. Unfortunately, however, milk allergy is one of the most common food allergies in young children, affecting 2-3% of the general population [2]. Research has shown that most of the sensitive children overcome food allergies by the age of 3; however, the reaction still can develop or appear in adulthood [3, 4]. The adverse outcome from milk allergy span from cutaneous reactions, respiratory episodes, gastrointestinal (GI) distress to life threatening anaphylactic shock [2, 5, 6].

There are around 20 proteins reported to induce IgE-mediated allergy in cow milk, and 10 of them are reported in the official Allergen Nomenclature Database from the World Health Organization and International Union of Immunological Societies (WHO/IUIS) [7]. The conformation of a protein is a crucial factor determining its allergenicity. Studies have shown that extremes of pH and temperature conditions encountered during food processing could alter conformational and linear epitopes in allergenic proteins whereby changing their antigenicity and allergenicity [7-9]. For instance, Maleki *et al* reported that the allergenicity of peanut increased 90-fold higher after roasting which they related with protein modifications caused by the Maillard reaction [10]. Allergenicity to proteins could increase, decrease or remain unchanged in response to food processing conditions given the possibilities of destruction of epitope sequences, formation of new epitopes, increased accessibility of epitopes facilitated by change in structural conformational of proteins depending on the type and extent of food processing conditions [2].

Inorganic food additive materials such as silicon dioxide (E551) and titanium dioxide (E171) have been used by food industries as anticaking agents and white pigment, respectively [11]. As reported earlier, 33% of E551 (food-grade SiO_2) and 36% of E171 (food-grade TiO_2) exist in nanometric size range (<100 nm in diameter) [12, 13]. Recent studies from the same group have shown that proteins of relevance to milk allergy could be enriched when particles are dispersed in milk [14] and the interaction

of proteins with dietary particles could alter the structure and function of proteins [14, 15]. However, the consequence of particle-milk protein interaction on antigenicity and allergenicity of milk proteins have not been addressed. Since interactions of particles with proteins altered protein structures, it was reasonable to hypothesize that interactions of dietary particles with prominent food proteins could alter its antigenic and allergic properties. This hypothesis was tested by studying the alterations of the IgG binding (using ELISA) and allergenicity (using mast cell degranulation assay) of milk and individual milk proteins (β-lactoglobulin and casein) in the presence of food-grade particles of silica and titania.

6.3 Materials and methods

6.3.1 Materials

Food-grade silicon dioxide particles (FG-SiO_2-NP) in nano-size (AEROSIL 200F) and food additive silicon dioxide particles, E551 (SIPERNAT 22) were obtained from Evonik Corporation (NJ, United States). Food grade titanium dioxide nanoparticles (FG-TiO_2-NP, cat # A020-II) were purchased from CNMI industrial corporation, China, and food additive titanium dioxide particles (E171, cat # 13463-67-7) were obtained from Minerals-Water, UK. All particles were used as received. Casein (cat # 5890) was purchased from Sigma Aldrich (St. Louis, MO, USA), and β-lactoglobulin (cat # S0131) was obtained from Davisco Foods International Inc. (Eden Prairie, MN, USA). Quebon skimmed milk (Agropur Dairy Cooperative, QC, Canada) was purchased from a local grocery store. For enzyme-linked immunosorbent assay (ELISA), primary antibody for casein (Anti-casein rabbit antibody- cat # ab166596), primary antibody for β-lactoglobulin (Anti-LGB rabbit antibody- cat # ab112893) and secondary anti-rabbit antibody (cat # 6721) were purchased from Abcam (Cambridge, UK). Unless stated otherwise, all other chemicals were obtained from Sigma Aldrich (St. Louis, MO, USA). Stock buffer of 0.1 M of phosphate buffer (pH 6.5) was prepared using deionized water obtained from a Milli-Q water system (Millipore Sigma, Massachusetts, USA) and was stored at 4°C before making the working concentration (20 mM) prior to each experiment.

6.3.2 Characterization of pristine dietary particles and milk interacted dietary particles

Silica and titania particles obtained initially in powder form were dispersed in distilled Milli-Q water (deionized water) at 10 $mg.mL^{-1}$ concentration (stock solution) for further studies. Skimmed milk with minimal fat content was used as a model food matrix for studying the transformation of milk allergenicity in the presence of dietary particles. Skimmed milk stored at 4˚C was centrifuged (17,000 g for 10 min) to remove any debris, and the supernatant was collected for further use. Aliquots (100 µL) of dietary particles were added to 900 µL of milk (final concentration 10 $mg.mL^{-1}$) and incubated for 1 h at 37°C. Control particle samples were prepared by adding the same proportions of 20 mM sodium phosphate buffer (pH 6.5) (no proteins) to the particle solution. Particles were then pelleted out

by centrifugation (20,000 g) for 15 min in a temperature-controlled centrifuge (Sigma 3-30KS, Sigma Zentrifugen, Germany) at 4°C, unbound milk proteins in the supernatant were discarded. Particle pellets were resuspended in 1 mL of 20 mM sodium phosphate buffer (pH 6.5) and the resulting suspension was centrifuged at 20,000 g for 15 min, and the supernatant was discarded to avoid loosely bound proteins forming the 'soft corona' on particle surface [14]. This step was repeated twice to retain hard corona formed on the particles. Particles thus obtained were used freshly for further studies.

Pristine and milk interacted particles suspended in 1 mL of 20 mM sodium phosphate buffer (pH 6.5) to achieve 1 $mg.mL^{-1}$ concentration were characterized for their size (and shape), and surface charge using transmittance electron microscopy (TEM), and dynamic light scattering technique (DLS), respectively. For TEM, 5 µL of particles suspension (100 $\mu g.mL^{-1}$) was dropped onto 200-mesh Cu TEM grids with carbon film and was air-dried at room temperature for an hour. TEM images were acquired at 120 kV accelerating voltage using Tecnai G2 F20 200 kV Cryo-STEM (Field Electron and Ion Company (FEI), Oregon, USA). The hydrodynamic diameter and zeta potential of the particles were determined using DLS (Nanobook OMNI Instrument, USA). For this, working concentrations of particles were prepared at 50 $\mu g.mL^{-1}$ in PBS buffer (pH 6.5). The scattering angle was kept at 90° with a holder temperature of 25°C, and monodispersion medium viscosity of 0.89 mPa s. The measurements were run at an applied voltage of 100 V.

6.3.3 Quantification of protein adsorption on dietary particles

After the final wash of milk interacted particles, 100 µL of 20 mM sodium phosphate buffer was added to achieve a particles' concentration of 10 $mg.mL^{-1}$. To quantify the protein in the hard corona, strongly adsorbed protein layer that is retained after washing of milk interacted dietary particles [16], 25 µL of washed particle suspensions were mixed with 25 µL of protein eluting buffer (containing 2% sodium dodecyl-sulfate (SDS) in 20 mM sodium phosphate buffer) and was incubated for 1 h at room temperature [17]. Particles were separated from the solution by centrifugation at 20,000 g for 15 min, and the protein eluted to the supernatant was used for protein quantification as detailed elsewhere [17]. For this, 10 µL of supernatant were mixed with 100 µL of Pierce 660 (Thermo Fischer Scientific, MA, U.S.A) containing 50 mM ionic detergent compatible reagent (IDCR) (Thermo Fischer Scientific, MA,

U.S.A). The resulting mix was incubated for 5 min at room temperature before measuring the absorbance at 660 nm using a microplate reader (SpectraMax i3x, Multi-mode Microplate Reader, Molecular Devices, USA). Protein concentration was calculated using a standard curve obtained using bovine serum albumin.

SDS-PAGE of eluted proteins from milk interacted particles was conducted to determine prominent proteins associated with surface corona. Twenty microliters of the milk interacted particles samples were mixed with sample buffer containing 62.5 mM Tris-HCl, pH 6.8, 2% SDS, 25% (v/v) glycerol, 0.01% bromophenol blue. Subsequently, 5% β-mercaptoethanol was added to one set of particles pelleted, vortexed, and boiled for 5 min. Particles were removed from sample buffer by centrifugation at 20,000 g for 15 min; protein-containing sample solution was collected and transferred into a fresh tube. Fifteen microliters of each sample were loaded to a sample well of a gradient (4-20%) SDS-polyacrylamide gel. Proteins were separated in the gel using 100 V for 1.5 h in a running buffer containing 2.5 mM tris, 19.2 mM glycine and 0.01% SDS. The gel was then stained in standard Coomassie blue-methanol-acetic acid solution for 30 min at room temperature. These gels were subsequently washed with de-staining solution (40% methanol, 10% acetic acid and 50% water) for 30 min at RT to visualize the protein bands.

6.3.4 Analysis of alteration in protein secondary structure by attenuated total reflection Fourier-transform infrared (ATR-FTIR) spectroscopy

The ATR-FTIR spectra of β-lactoglobulin and casein before and after interacting with dietary particles were used to assess changes in the secondary structure of proteins upon binding with the dietary particles. For this, equal volumes of the proteins (10 mg.mL^{-1}) and dietary particles (10 mg.mL^{-1}) were mixed in a clean glass tube and were incubated at 37°C for 1 h. Pure protein samples were prepared by adding the same proportions of DI water to the protein solution. Two microliters of sample were dropped on the ATR probe and left to dry for 15 min. FTIR spectra were collected in the wavelength range of 4000-400 cm^{-1} at a resolution of 4 cm^{-1} and 128 scans in Nicolet Summit ATR-FTIR spectrometer (ThermoFisher Scientific, MA, USA). Each spectrum was corrected for background

noise. FTIR peaks corresponding to particles were subtracted from the spectrum of the protein-particle complex. Fourier self-deconvolution was used to resolve overlapping bands in the FTIR spectrum in the range of amide I 1700-1600 cm^{-1} [18] by OMNIC software.

6.3.5 Quantitative analysis of free thiol group by Ellman's assay

Intra and inter molecular disulphide bonds are determinants of protein structure and formation of conformational IgE epitopes [19]. Therefore, we determined the disruption of disulfide bonds when proteins were interacted with dietary particles as detailed previously [20]. Briefly, 200 µL of 1 $mg.mL^{-1}$ proteins (pure or particle interacted) and 50 µL of 2 mM 5,5'-dithio-bis-2-nitrobenzoic acid (DTNB) were added to 100 µL of tris buffer (1M) in an Eppendorf tube. The solution was topped up to 1 mL with DI water. The absorbance of the resulting solution was measured using SpectraMax i3x multi-mode microplate reader at 412 nm. Different concentrations of acetylcysteine were used for preparing the standard curve, and protein denatured by 6 M guanidinium chloride was used as a positive control.

6.3.6 Assessing changes in the quaternary structure of proteins in presence of dietary particles

The changes in the quaternary structure of proteins interacted with particles were determined using changes in the intrinsic fluorescence of tryptophan, tyrosine, and phenylalanine. The emission intensity of protein suspension (0.1 mM in 20 mM phosphate buffer- pH 6.5) was compared with those containing various concentration of dietary particles (0 mM-100 mM). The quenching studies were repeated at different temperatures 20°C, 25°C, 30°C and 35°C to identify the type of interaction between particles and proteins. The binding affinity of each particle to proteins was calculated using the Stern-Volmer equation 6.1 (Eq. 6.1),

$$F_0/F = 1 + K_{sv}.[Q] = 1 + K_q\, r^0\, [Q] \qquad \text{(Eq. 6.1)}$$

Where F_0 and F represent the steady-state fluorescence intensities in the absence and presence of silica particles, respectively, K_q is the biomolecular quenching constant, and r^0 is the fluorescence lifetime in

the absence of particles. The value of r^0 is a constant: 1.28 ns for β-lactoglobulin [21] and 0.982 ns for casein [22]. K_{sv} is the Stern-Volmer quenching constant, and [Q] is the concentration of the particles.

6.3.7. Protein identification of *in vitro* digested milk samples by one-dimension gel electrophoresis

Milk in the presence of different dietary particles was passed through the *in vitro* digestion system. The simulated *in vitro* digestion was conducted, and digestion fluid (SSF, SGF and SIF) were prepared as reported earlier [23]. Briefly, 100 µL of the dietary particles (SiO_2 and TiO_2) (10 $mg.mL^{-1}$) were mixed with 900 100 µL of milk and dilute with simulated salivary fluid (SSF) in a 1:1 (v/v) ratio at pH 7 (oral phase). The solutions were kept in this oral phase for 2 min at 37°C in continuous orbital shaking condition. Subsequently, the oral phase solution was mixed with simulated gastric fluid (SGF), that contained gastric enzymes, pepsin and gastric lipase in a 1:1 ratio (v/v) at pH3 (gastric phase). The gastric phase solutions were incubated at 37°C for 2 h under agitation following which the resulting gastric chyme was mixed with simulated intestinal fluid (SIF) which contained bile salts and pancreatin, in a 1:1 (v/v) ratio at pH7. The resulting suspension was incubated at 37°C for another 2 hrs under agitation. The enzyme (amylase, pepsin, gastric lipase and pancreatin present in the resulting solution) activities were terminated by boiling the suspension for 10 min. The resulting solutions were used for antigenicity and allergenicity testing (as detailed below). Parallelly, particles-protein complex present in this mix were separated by centrifugation at 20,000 g for 15 mins. Particle pallet thus obtained was suspended in 50 µL of PBS buffer (pH 6.5) and was mixed with 100 µL of SDS sample buffer containing 62.5 mM Tris-HCl, pH 6.8, 2% SDS, 25% (v/v) glycerol, 0.01% bromophenol blue and 5% β-mercaptoethanol to elute proteins adsorbed onto particles. The suspension was vortexed, boiled for 5 min and centrifuged (20,000 g for 15 min) to remove particles . The resulting solution containing denatured protein -was transferred to a fresh Eppendorf tube. Twenty microliters of each sample were loaded to each sample well of a 4-20% SDS-polyacrylamide gel for electrophoresis as detailed earlier.

6.3.8. Testing for alteration in the antigenicity of milk proteins interacted with particles

Nine hundred microliters of skimmed milk and milk proteins (1 mg.mL^{-1} of β-lactoglobulin and casein) were mixed with 100 µL of dietary particles (10 mg.mL^{-1}). The control sample was prepared by adding the same proportions of 20 mM sodium phosphate buffer (pH 6.5) (without particle) to the protein solution.

Change in the antigenicity of milk proteins when interacted with dietary particles were analysed using ELISA assay. ELISA plate was prepared by coating 100 µL milk proteins or milk proteins interacted with particles (50 ng.mL^{-1}) onto the wells of microliter plate (Nunc Maxisorp 96-well ELISA plate) in coating buffer (0.1 M Na_2HPO_4 (pH 9.5) in DI water) overnight at 4°C. The uncoated samples were discarded, and free binding sites of the wells were blocked with blocking buffer containing 2% BSA in 1X TBS (50 mM Tris-HCl and 150 mM NaCl in deionized (DI) water) for 1 h at 37°C. These wells were then incubated with primary antibody (pAb) at 1:5000 dilution for β-lactoglobulin pAb and 1:2000 for casein pAb in blocking buffer for 1 h at room temperature (RT). The wells were washed to remove unbinding antibodies with washing buffer (IX TBS added with 0.05% Tween-20) for four times and the plate was further incubated for 1 h at RT with secondary antibody at a 1:10000 dilution in blocking buffer. Substrate solution (5 mM of tetramethylbenzidine-TMB) was added after a final washing step (4X) with washing buffer and incubated for 5 mins at RT for the enzymatic color development. The reaction was stopped by adding 100 µL of 2 M sulphuric acid. The absorbance was measured at 450 nm using the microplate reader, and IgG binding sites were calculated using a standard curve of control β-lactoglobulin and casein proteins.

6.3.9. Human mast cell degranulation assay to assess allergenicity of milk in presence and absence of dietary particles

Human Laboratory of Allergic Diseases 2 (LAD2) mast cells (kindly supplied by Dr. A. S. Kirshenbaum, National Institutes of Health, Bethesda, MD, USA) were cultured in StemPro-34 serum-free medium (Gibco #10640) with STEM PRO-34 nutrient supplement (Gibco #10641-025), 1% (v/v) penicillin-streptomycin, 1 % (v/v) L-glutamin-200 mM, 0.2% (v/v) primocin-50 mg, and 100 ng.mL^{-1} rhSCF at 37°C and 5% CO_2. Hemi-depletions were performed weekly as instructed by the supplier. The

release of β-hexosaminidase was detected according to a reported method [24]. Briefly, LAD2 cells (1 x 10^5 cells/well) were seeded on a 96-well plate in a complete cell culture medium for overnight and then cells were sensitized by diluted sera (1:50, v/v in complete cell culture medium) obtained from milk allergy patients (supplied by PlasmaLab International, Everett, WA, USA.). Specific IgE levels for f2 allergen of patient's sera were 20.886 kU/L, 19.267 kU/L, 55.582 kU/L, 74.7 kU/L, and 41.9 kU/L, respectively. After incubating for 24 h, 80 µL of cell supernatant were carefully removed by multichannel pipette. Allergic activation was induced by incubating with 100 µL of milk in the presence of dietary particles (milk protein concentration-100 ng.mL^{-1}) for 3 h in Tyrode's buffer (135 mM NaCl, 5 mM KCl, 1.8 mM $CaCl_2$, 1 mM $MgCl_2$, 5.6 mM glucose, and 20 mM HEPES at pH-7.4). Positive controls were prepared by adding 100 µL of 0.1% triton X-100 in Tyrode's buffer to the sensitized cells. The supernatant from the LAD2 cells incubated with particles interacted proteins/milk (50 µL) was incubated with 50 µL of *p*-nitrophenyl-*N*-acetyl*B* -D-glucosamide (substrate for β-hexosaminidase) dissolved in 0.1 M citrate buffer (pH 4.5) for 90 min at 37°C. The enzyme reaction was terminated by adding 100 µL 0.1 M glycine-carbonate buffer (1 M glycine and 1 M sodium carbonate, pH-10). The absorbance of the hydrolyzed substrate was measured using SpectraMax i3x multi-mode microplate reader at 405 nm. The cell degranulation results are expressed as the percentage of β-hexosaminidase released relative to the positive control (triton X-100) sample. These experiments were repeated with milk samples subjected to *in vitro* digestion in the absence and presence of dietary particles.

6.3.10. Statistical analysis

Experiments were performed in triplicates and replicated at least three times. The data collected in this study are expressed as the mean value ± standard deviation (SD). Statistical comparisons were made by Duncan (one-way ANOVA) and paired t-test, and p-value ≤ 0.05 was considered a significant difference.

6.4 Results

6.4.1 Characterization of the particles

The physicochemical properties of pristine dietary particles and protein interacted particles were evaluated by TEM and DLS, and the results are shown in Figure 6.1 and SI 6.1. TEM was carried out to verify the presence of surface corona milk interacted particles and to determine the particles' size, shape, and agglomeration status. The presence of a semi-transparent layer, characterized by a lower electron density, suggestive of surface corona formation on particles was evident on particles interacted with milk (red arrow in Figure 6.1B). FG-SiO_2-NP was constituted by spherically shaped particles of ~20 nm diameter and showed agglomeration (Figure 6.1B), while E551 showed aggregation (interconnected particles) (Figure 6.1D). The overall hydrodynamic size of FG-SiO_2-NP and E551 were 539.62 (pdi 0.29) nm and 35635.85 (0.53) nm, respectively (tabular data, Figure 6.1J). Pristine titania nanoparticles (Figure 6.1F) and E171 (Figure 6.1H) were pseudo-spherical in shape and their primary sizes were ~120 nm and 50-300 nm, respectively. The hydrodynamic size of FG-TiO_2-NP and E171 were 448.59 nm (pdi 0.19) and 335.98 nm (0.24), respectively (tabular data, Figure 6.1J). Milk interacted silica and titania particles showed surface corona on the outer surface of the aggregated or agglomerated particles and in the interstitial spaces between the particles (see arrow in Figure 6.1C, E, G and I). The thickness of corona layers ranged from 200-700 µm (tabular data, Figure 6.1J). Except for FG-SiO_2-NPs, the hydrodynamic sizes of particles generally reduced after interacting with milk or milk proteins. Zeta potential measured using DLS for all tested particles showed a net negative surface charge, and generally, the surface charge of all tested particles increased after acquiring surface corona.

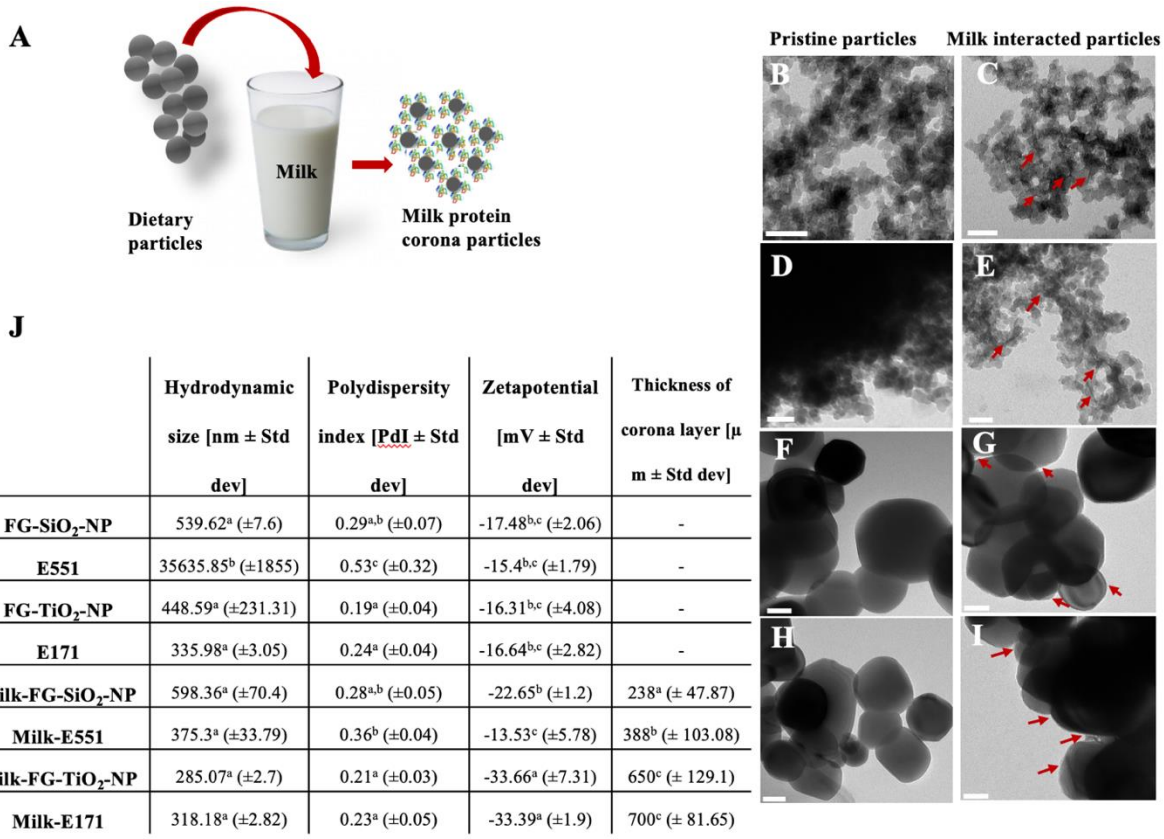

J

	Hydrodynamic size [nm ± Std dev]	Polydispersity index [PdI ± Std dev]	Zetapotential [mV ± Std dev]	Thickness of corona layer [µm ± Std dev]
FG-SiO_2-NP	539.62^{a} (±7.6)	0.29^{a,b} (±0.07)	-17.48^{b,c} (±2.06)	-
E551	35635.85^{b} (±1855)	0.53^{c} (±0.32)	-15.4^{b,c} (±1.79)	-
FG-TiO_2-NP	448.59^{a} (±231.31)	0.19^{a} (±0.04)	-16.31^{b,c} (±4.08)	-
E171	335.98^{a} (±3.05)	0.24^{a} (±0.04)	-16.64^{b,c} (±2.82)	-
Milk-FG-SiO_2-NP	598.36^{a} (±70.4)	0.28^{a,b} (±0.05)	-22.65^{b} (±1.2)	238^{a} (± 47.87)
Milk-E551	375.3^{a} (±33.79)	0.36^{b} (±0.04)	-13.53^{c} (±5.78)	388^{b} (± 103.08)
Milk-FG-TiO_2-NP	285.07^{a} (±2.7)	0.21^{a} (±0.03)	-33.66^{a} (±7.31)	650^{c} (± 129.1)
Milk-E171	318.18^{a} (±2.82)	0.23^{a} (±0.05)	-33.39^{a} (±1.9)	700^{c} (± 81.65)

Figure 6. 1 Characterization of pristine and milk interacted dietary particles by TEM and DLS. The images were obtained by dropping 5 µL of particles suspension (100 µg.mL^{-1}) onto 200-mesh Cu TEM grids with carbon film and using TEM (Tecnai G2 F20 200 kV Cryp-STEM). Scale bar: 50 nm. **(A)** Schematic of the protein corona formation, **(B)** FG-SiO_2-NP, **(C)** Milk-FG-SiO_2-NP, **(D)** E551, **(E)** Milk-E551, **(F)** FG-TiO_2-NP, **(G)** Milk-FG-TiO_2-NP, **(H)** E171, **(I)** Milk-E171, and **(J)** hydrodynamic diameter, polydispersity index and, surface charge of dietary particles in the presence and absence of milk in PBS are determined using DLS, and thickness of corona layer onto the dietary particles. Means with different small letters in the same column are significantly different to each other (Duncan, $P < 0.05$)

6.4.2 Quantification of protein corona formation

Proteins adsorbed onto the particles were quantified with colorimetric assay and SDS-PAGE, and the results are shown in Figure 6.2A, and B. FG-SiO_2-NP had the highest amount of proteins adsorbed on its surface followed by E551, FG-TiO_2-NP and E171. Total protein estimation from particle surface concurred with the gel electrophoresis results where protein bands from FG-SiO_2-NP were darker and thicker (Figure 6.2B). Predominant milk proteins recovered from the hard-corona formed on particles (both titania and silica), as revealed in SDS-PAGE, were bands corresponding to β-lactoglobulin and casein (Figure 6.2B, lane 6). Based on this observation, we chose these proteins for antigenicity and allergenicity studies.

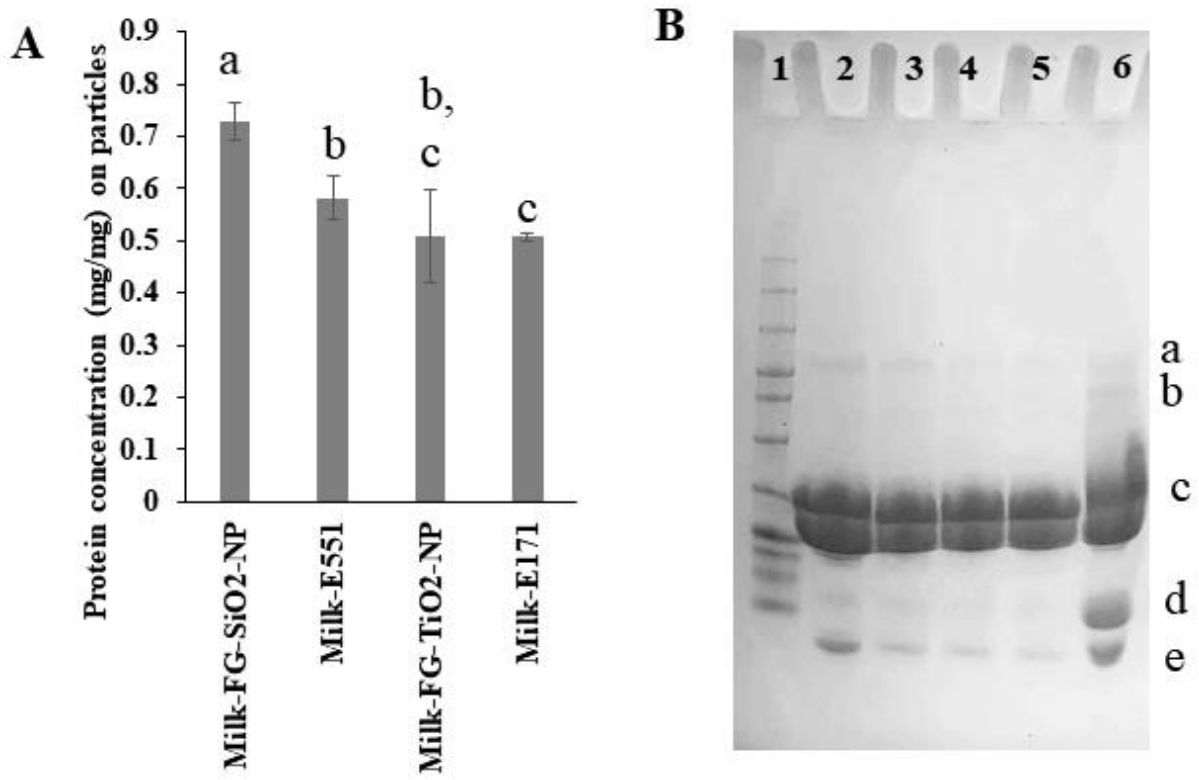

Figure 6. 2 Quantification of protein adsorption on dietary particles. (A) Particles suspended and incubated in protein suspensions were retrieved using centrifugation. The protein corona concentration was quantified by Pierce 660 containing 50 mM ionic detergent compatible reagent (IDCR). Average values are plotted in the graph with different small letters indicate significant differences (Duncan, $p < 0.05$). **(B)** SDS-PAGE pattern of proteins retrieved from milk interacted particles. Lane (1) Marker, (2) milk-FG-SiO_2-NP, (3) milk-E551, (4) milk-FG-TiO_2-NP, (5) milk-E171, and (6) milk.

* a=Polymeric immunoglobulin receptor, b=BSA, c=Casein Fraction (α-casein, β-casein, κ-casein), d=β-Lactoglobulin, e=α-Lactalbumin.

6.4.3 Antigenicity of milk proteins increased when interacted with dietary particles

Figure 6.3A shows the workflow schematic for identifying the antigenicity of protein after interacting with dietary particles. Changes in antigenicity of β-lactoglobulin and casein in the presence of dietary particles are evident from Figure 6.3B, C, Figure SI 6.2A and B. Generally, antigenicity of β-lactoglobulin increased in the presence of dietary particles in comparison of non-interacted protein (Figure 6.3B). The antigenicity towards β-lactoglobulin increased in milk samples interacted with FG-SiO_2-NP and E171 while it remained unchanged for E551 and decreased in the case of FG-TiO_2-NP (Figure SI 6.2A). The effect of particles on the antigenicity of casein in the presence of dietary particles is shown in Figure 6.3C. Casein antigenicity increased in the presence of all tested dietary particles, and it was highest in the presence of FG-SiO_2-NP (Figure 6.3C). In addition, the casein antigenicity was not significantly different from milk sample containing FG-TiO_2-NP (Figure SI 6.2B).

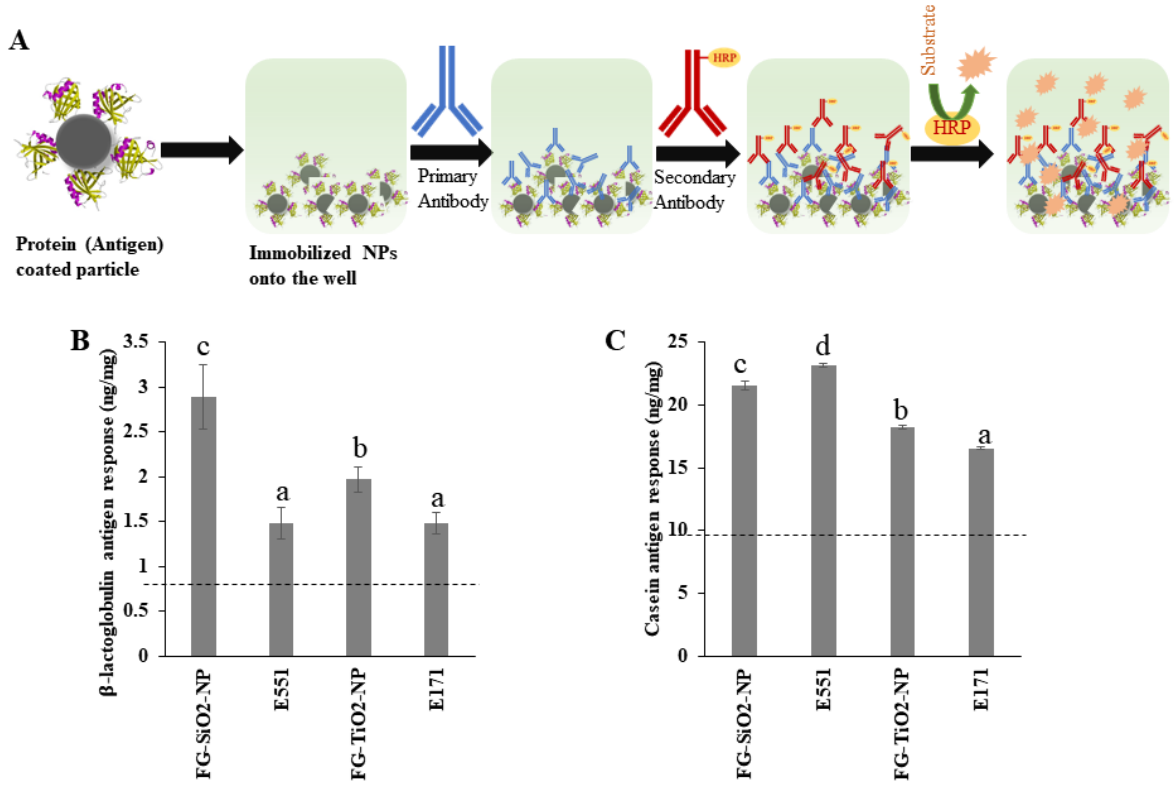

Figure 6. 3 Quantification of the antigen response in the presence of inorganic dietary particles by indirect enzyme-linked immunosorbent assay (ELISA). (A) Schematics of the indirect-ELISA for quantifying antigenicity of the proteins. ELISA plates were coated with antigen (50 ng.mL^{-1}) **(B)** the rabbit anti-b-lactoglobulin in 1:5000 dilution was added to the plate, **(C)** the rabbit anti-casein in 1:2000 dilution was added to the plate, followed by adding the HRP linked anti-rabbit antibody (1:10000) and HRP substrate 3,3',5,5'-Tetramethylbenzidine (TMB). The colorimetric signal was measured at 450 nm by micro plate reader. Average values are plotted in the graph with different small letters indicate significant differences (Duncan, $p < 0.05$).

*The dotted line represents the antigenicity of control protein.

6.4.4 Structural transformation of proteins after interacting with dietary particles

The ATR-FTIR spectra of the proteins in the presence and absence of the particles are presented in Figure 6.4A and B. The amide I region of the infrared spectra of proteins is sensitive to their secondary structure [25]. E551 interacted β-lactoglobulin showed the highest level of secondary structure disruption followed by FG-SiO_2-NP, E171 and FG-TiO_2-NP when compared with pure β-lactoglobulin sample (Figure 6.4A). Notably, the α-helix structure of FG-TiO_2-NP interacted β-lactoglobulin increased compared to the control. The secondary structure of E551 interacted casein also showed changes- the severity of which followed E551> FG-SiO_2-NP> FG-TiO_2-NP> E171> pure casein protein (Figure 6.4B).

6.4.5 Quantitative analysis of free thiol group in the presence of dietary particles

Free thiol content was estimated using Ellman's assay to study the effect of unfolding of protein in the presence of dietary particles. As shown in Figure 6.4 C and D, the presence of FG-TiO_2-NP and E171 in both proteins (β-lactoglobulin and casein) resulted in significantly higher free thiol content compared to control proteins, while FG-SiO_2-NP and E551 had similar free thiol concentrations as the native protein.

6.4.6 Binding affinity of β-lactoglobulin and casein to dietary particles

The fluorescence intensity measured at 25, 30, 35 and 40°C suggested changes in the stability of tertiary structure of proteins (β-lactoglobulin and casein) when interacted with dietary particles (Figure 6.4E). The type of fluorescence quenching of when proteins bind to particles was distinguished using Stern-Volmer diagrams. The Stern-Volmer plots were not entirely linear when the quencher concentration was higher (> 15 mM), especially in the case of titania particles. This is due to the inner filter effect or concentration quenching [26]. However, as determined from the linear response in lower particle concentrations, titania particles induced dynamic quenching. Generally, the bimolecular quenching rate (K_q) of β-lactoglobulin and casein were higher when they were interacted with titania particles compared to silica particles (Figure 6.4E). For instance, the K_q values for β-lactoglobulin and casein

when interacted with silica particles (FG-SiO_2-NP and E551) in comparison with titania particles (FG-TiO_2-NP and E171) were ~ 6 and 60 times lower, respectively. In comparison to FG-SiO_2-NP and E551, the quenching constant and quenching rate were higher in β-lactoglobulin adsorbed onto E551 while higher in casein adsorbed onto FG-SiO_2-NP. The quenching constant and quenching rates were higher in FG-TiO_2-NP compared to FG-TiO_2-NP and E171 (Figure 6.4E).

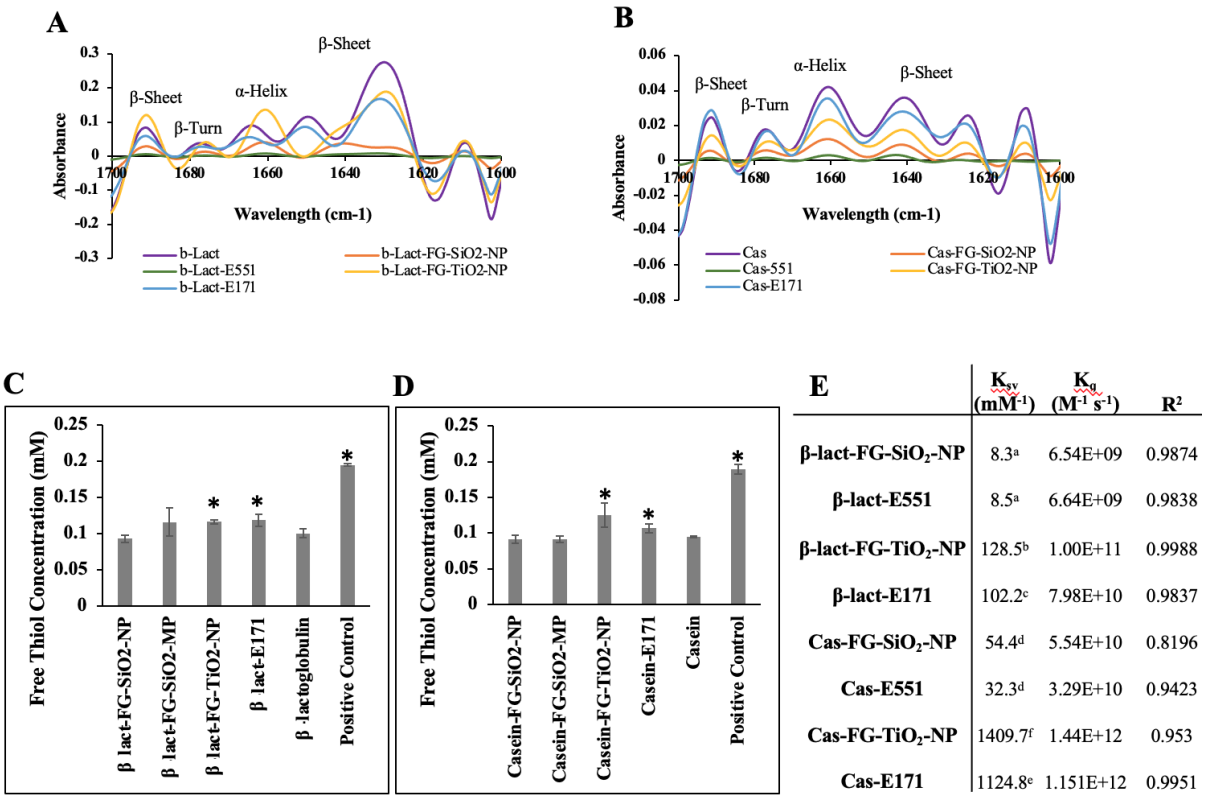

E

	K_{sv} (mM^{-1})	K_q ($M^{-1}\ s^{-1}$)	R^2
β-lact-FG-SiO_2-NP	8.3[a]	6.54E+09	0.9874
β-lact-E551	8.5[a]	6.64E+09	0.9838
β-lact-FG-TiO_2-NP	128.5[b]	1.00E+11	0.9988
β-lact-E171	102.2[c]	7.98E+10	0.9837
Cas-FG-SiO_2-NP	54.4[d]	5.54E+10	0.8196
Cas-E551	32.3[d]	3.29E+10	0.9423
Cas-FG-TiO_2-NP	1409.7[f]	1.44E+12	0.953
Cas-E171	1124.8[e]	1.151E+12	0.9951

Figure 6. 4 Characterization of protein conformational changing by FTIR and fluorescence quenching. (A) FTIR analysis of the secondary structure of b-lactoglobulin in the presence of inorganic dietary particles. **(B)** FTIR analysis of the secondary structure of casein in the presence of inorganic dietary particles. Samples (protein+particle) suspended in water were dropped and dried on the ATR probe before taking the spectra for a wavenumber range of 4000-400 cm-1 using ATR-FTIR. The spectra were generated by Fourier self-deconvolution of wavenumber of amide I band between 1700-1600 cm^{-1}. **(C)** Free thiol content of b-lactoglobulin in the presence of dietary particles. **(D)** Free thiol content of casein in the presence of dietary particles. * Indicate statistical significance in comparison to control protein, $p \leq 0.05$, N=3. **(E)** Table summarizes binding affinity of b-lactoglobulin and casein: Stern-Volmer constant (K_{sv}) and bimolecular quenching rate parameter (K_q) of b-lactoglobulin in the presence of inorganic dietary particles calculated from Stern-Volmer plot. Means with different small letters in the same column are significantly different to each other (Duncan, $P < 0.05$)

6.4.7 Quantitative analysis of mast cell degranulation

Food antigens bind to specific IgE on the surface of mast cells, trigger degranulation leading to allergy symptoms. As shown in Figure 6.5, dietary particles interacted with milk samples caused a significant increase in LAD2 degranulation, indicated by the release of β-hexosaminidase. The presence of food additive titanium dioxide (E171) showed the highest level of LAD2 degranulation, followed by FG-TiO_2-NPs. In order to understand the protein stability during gastric digestion in the presence of dietary particles, the allergenicity of milk in the presence of dietary particles was tested after passing through the simulated gut digestion system. Contrary to the expectations, the β-hexosaminidase release was still higher for milk samples subjected to *in vitro* digestion in the presence of FG-TiO_2-NP and E171 particles. Notably, however, the degranulation was slightly decreased in the presence of FG-SiO_2-NP and E551 particles.

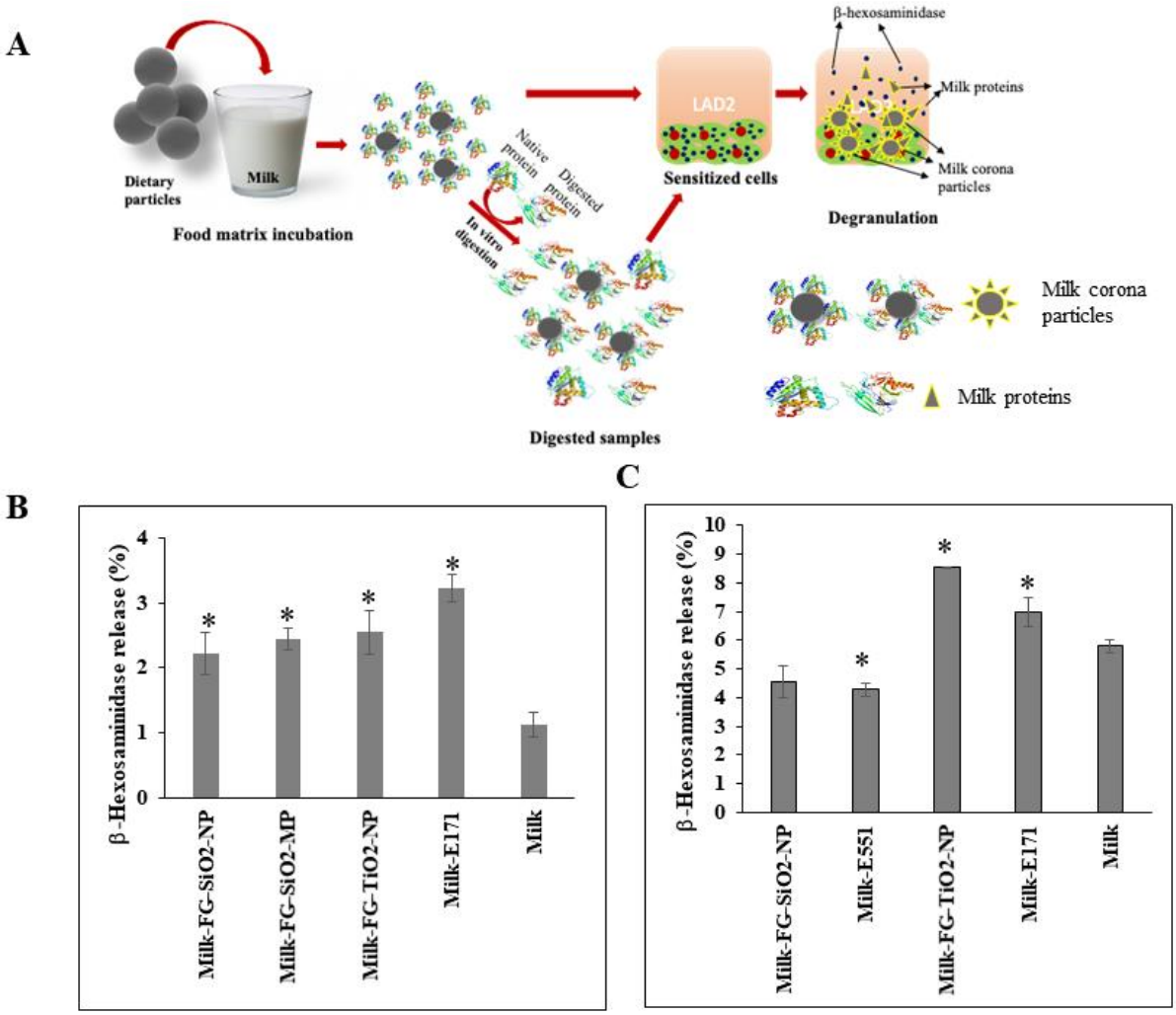

Figure 6. 5 Allergenicity of milk in the presence of dietary particles on mast cells. (A) Schematics of the degranulation assay to evaluate milk allergenicity in the presence of dietary particles and *in vitro* digested samples. **(B)** The release of b-hexosaminidase was measured by LAD2 degranulation assay after triggering with milk. Milk in the presence of dietary particles was diluted by Tyrode's buffer (100 ng.mL^{-1}) and exposed to the sensitized LAD2 cell to trigger the cell degranulation. **(C)** The release of b-hexosaminidase was measured by LAD2 degranulation assay after exposing to *in vitro* digested milk in the presence and absence of dietary particles.

* Indicate statistical significance in comparison to control protein, $p \leq 0.05$, N=3.

6.5 Discussion

E551 and E171 are common inorganic food additives materials used in food products, including dairy products. Milk is one of the "big eight" food allergens where casein and β-lactoglobulin are identified as major food allergens in milk [24]. Understanding the consequence of particle interaction on allergenicity of milk is pivotal for understanding the relevance of food additive nanoparticles in shaping health and disease outcomes of food components. The current studies demonstrated that dietary nanoparticles alter the structure and increase the allergenicity of milk proteins- an observation that has far-reaching implications given the rising incidences of food allergy.

TEM examination of particles interacted with milk showed the presence of surface corona as a translucent layer of thickness that varied from 200-700 µm (Figure 6.1J). As shown in the previous studies, the surface corona of milk interacted particles is constituted by protein, lipids and carbohydrates as major classes of biomolecules [14]. Generally, OH groups present on particle surfaces has high surface energy and mediate agglomeration of particles in the absence of matrix molecules. When suspended in complex media such as milk, these OH groups interact with functional groups on biomolecules through hydrogen bonding to mediate their binding onto surfaces [27, 28]. These biomolecule-particle interactions facilitate the retention of biomolecules on the surface and provide a net negative surface charge (Figure 6.1, tabular data). The electrostatic and steric hindrance (from adsorbed biomolecules) keeps particles separated when suspended in complex media [29], which could explain the reduced hydrodynamic size of milk interacted particles (Figure 6.1, tabular data). As observed under TEM, the primary size of E551 is similar to FG-SiO_2-NP. However, E551 is more agglomerated and had less interstitial space in comparison to FG-SiO_2-NP. Aggregation of primary particles that leads to reduced interstitial space (that provide anchoring points for biomolecules) could be the reason for the lower level of surface adsorbed proteins in E551 in comparison to FG-SiO_2-NPs (Figure 6.2). However, both silica particles (E551 and FG-SiO_2-NPs) were much smaller than titania particles (E171 and FG-TiO_2-NPs). Evidently, the lesser surface area to volume ratio could explain the lower amount of surface corona proteins in titania particles compared to silica particles (Figure 6.2).

Previous studies from the same group showed that the adsorption of proteins onto the surface of particles could disrupt the structural conformation of the protein [15, 30]. Particle mediated alteration in the tertiary and secondary structures was found to reduce the activity of enzymes relevant to human nutrition [14, 15, 30]. Therefore, it was rational to hypothesize that particle-protein interactions could alter allergenicity to proteins implied in prevalent food allergy. Generally, the IgG-binding activity of β-lactoglobulin and casein increased after interacting with particles suggesting that binding proteins to particle surface-enhanced antibody accessibility to epitopes (Figure 6.3B and C). FG-SiO_2-NPs showed higher antigenicity than E551 (food grade silica particles), which could be explained by the higher level of protein adsorption by FG-SiO_2-NPs, as discussed above. However, the antigenicity of β-lactoglobulin and casein in the milk sample presented of E551 and FG-TiO2-NP did not have the same impact as pure proteins. Presence of other biomolecules such as lipids, carbohydrates, and metabolites in the surface corona of milk interacted particles might have also influenced the antigenicity of β-lactoglobulin, and casein adsorbed on particles interacted with milk.

Alterations in protein conformation during unfolding can affect the IgE reactivity and influence the allergenicity of the proteins [31]. Therefore, we analyzed the changes in proteins' secondary and tertiary structures through FTIR, fluorescence quenching, and free thiol content. Fluorescence quenching suggestive of changes in tertiary structure was more evident when proteins were interacted with titania particles in comparison to silica particles. Similarly, the availabilities of free thiol groups in β-lactoglobulin and casein were also relatively higher when these proteins were interacted with titania. Interestingly, however, the secondary structures of proteins were not affected noticeably by interacting with titania as much as with silica particles. These data suggest that interactions of proteins with titania particles induce changes in tertiary or quaternary structure but silica-induced changes at secondary structure of proteins. Notably, however, the increase in antigenicity of proteins was higher when interacted with silica particles than with titania particles. This discrepancy might be due to the lower amount of proteins adsorbed onto titania particles in comparison to silica particles (on an equal mass basis of particles used) which might offset any enhancement in the antigenicity of proteins adsorbed on titania particles.

Mast cell degranulation assay is primarily used as a proxy to measure the ability of an antigen to trigger the release of inflammatory mediators such as histamine and β-hexosaminidase when primed mast cell encounter antigen [32]. Although histamine is the major mediator for allergenic responses, it is less desirable for *in vitro* investigations as its half-life in the extracellular fluid is short (1 min) [33]. For this reason, the release of β-hexosaminidase is widely used to perform the cell degranulation assay, which constitutes late-phase activation and a longer half-life (8-24 hours). The mast cell stimulated by human milk allergy patient sera activates the FceRI signalling (the high-affinity IgE receptor) and triggers the cell degranulation and allergic mediators by antigen [34]. This results showed that the level of β-hexosaminidase release increased in the presence of dietary particles (Figure 6.5B). As observed for antigenicity, the increase in allergenicity could also be ascribed to the increasing availability of linear epitope as a result of conformational changes induced by protein-particle interactions. While these studies showed the implications of dietary nanoparticles in exacerbating the adverse allergic response towards milk proteins, we also questioned the relevance of this observation when subjected to digestive enzymes. As such, the immunogenic potential of protein is very much dependent on its stability when exposed to digestive environment [32]. Therefore, we examined the allergenicity of particle-interacted proteins that were subjected to *in vitro* digestion system simulating protein digestion in human gastro-intestinal system [32]. Notably, the allergenicity of titania interacted milk increased compared to milk alone after subjecting to *in vitro* digestion. As evident from protein binding affinity studies, titania particles strongly interact with milk proteins, and that strong interaction is envisaged as the reason for increased stability of the proteins during the digestion steps. In addition, the digestive enzymes adsorbed on the particles, and incomplete digestion of milk protein in the presence of dietary particles, as evident from SDS-PAGE (Figure SI 6.3) could have triggered stronger allergen response in sensitized cells when exposed to *in vitro* digested mix of particles and milk.

This studies demonstrated that particle mediated alterations in protein structure could enhance allergenicity of milk proteins. Although, many studies have addressed the influence of different food processing conditions on the food allergies, the role of nanoparticles present in widely used food additives in shaping immunogenic potential of food proteins has been overlooked. Apart from inducing

alterations in protein structure, interaction of allergenic proteins could also enhance the bioavailability of allergenic epitopes. The increased bioavailability result from the resistance of proteins adsorbed onto particles to complete digestion and possible particle enabled trespass of intact allergen surface adsorbed proteins across epithelial layer (as revealed by recent studies from the same group). Thus, while these studies suggest the role of dietary particle in enhancing allergenicity of food proteins, more studies using animal models are warranted for gaining deeper understanding on how dietary nanoparticles could alter the biology of food allergy. Nonetheless, this findings have far-reaching implications for managing severity of food allergy and in making dietary choices given the rising incidences of food allergies globally and their association with consumption of highly processed food often containing inorganic nanoparticles of silica and titania.

6.6 References

1. Boyce, J.A., et al., *Guidelines for the diagnosis and management of food allergy in the United States: summary of the NIAID-sponsored expert panel report.* Journal of the american academy of dermatology, 2011. **64**(1): p. 175-192.

2. Castillo, D.S. and A. Cassola, *Novel sensitive monoclonal antibody based competitive enzyme-linked immunosorbent assay for the detection of raw and processed bovine beta-casein.* PloS one, 2017. **12**(7): p. e0182447.

3. Pelto, L., et al., *Milk hypersensitivity in young adults.* European journal of clinical nutrition, 1999. **53**(8): p. 620-624.

4. Bengtsson, U., et al., *Double blind, placebo controlled food reactions do not correlate to IgE allergy in the diagnosis of staple food related gastrointestinal symptoms.* Gut, 1996. **39**(1): p. 130-135.

5. Fiocchi, A., et al., *Diagnosis and rationale for action against cow's milk allergy (DRACMA): a summary report.* Journal of allergy and clinical immunology, 2010. **126**(6): p. 1119-1128. e12.

6. Turnbull, J., H. Adams, and D. Gorard, *The diagnosis and management of food allergy and food intolerances.* Alimentary pharmacology & therapeutics, 2015. **41**(1): p. 3-25.

7. Madsen, J.L., et al., *The impact of structural integrity and route of administration on the antibody specificity against three cow's milk allergens-a study in Brown Norway rats.* Clinical and translational allergy, 2014. **4**(1): p. 1-11.

8. Mine, Y. and J.W. Zhang, *Comparative studies on antigenicity and allergenicity of native and denatured egg white proteins.* Journal of agricultural and food chemistry, 2002. **50**(9): p. 2679-2683.

9. Burks, A.W., et al., *Allergenicity of peanut and soybean extracts altered by chemical or thermal denaturation in patients with atopic dermatitis and positive food challenges*. Journal of allergy and clinical immunology, 1992. **90**(6): p. 889-897.

10. Maleki, S.J., et al., *The effects of roasting on the allergenic properties of peanut proteins.* Journal of allergy and clinical immunology, 2000. **106**(4): p. 763-768.

11. Athinarayanan, J., et al., *Identification of nanoscale ingredients in commercial food products and their induction of mitochondrially mediated cytotoxic effects on human mesenchymal stem cells*. Journal of food science, 2015. **80**(2): p. N459-N464.

12. Dekkers, S., et al., *Presence and risks of nanosilica in food products.* Nanotoxicology, 2011. **5**(3): p. 393-405.

13. Weir, A., et al., *Titanium dioxide nanoparticles in food and personal care products.* Environmental science & technology, 2012. **46**(4): p. 2242-2250.

14. Phue, W.H., et al., *Protein-biomolecule interactions play a major role in shaping corona proteome: Studies on milk interacted dietary particles.* Nanoscale, 2021.

15. Phue, W.H., et al., *Food grade silica nanoparticles cause non-competitive type inhibition of human salivary α-amylase because of surface interaction.* Nano select, 2020.

16. Milani, S., et al., *Reversible versus irreversible binding of transferrin to polystyrene nanoparticles: soft and hard corona*. ACS nano, 2012. **6**(3): p. 2532-2541.

17. Srinivasan, D., et al., *The type of dietary nanoparticles influences salivary protein corona composition*. NanoImpact, 2020: p. 100238.

18. Yang, H., et al., *Obtaining information about protein secondary structures in aqueous solution using Fourier transform IR spectroscopy.* Nature protocols, 2015. **10**(3): p. 382-396.

19. Pekar, J., D. Ret, and E. Untersmayr, *Stability of allergens.* Molecular immunology, 2018. **100**: p. 14-20.

20. Riener, C.K., G. Kada, and H.J. Gruber, *Quick measurement of protein sulfhydryls with Ellman's reagent and with 4, 4'-dithiodipyridine.* Analytical and bioanalytical chemistry, 2002. **373**(4): p. 266-276.

21. Gorji, E.G., et al., *Characterization of resveratrol–milk protein interaction.* Journal of food engineering, 2015. **167**: p. 217-225.

22. Panja, S., D.K. Khatua, and M. Halder, *Investigations on the effect of fatty acid additives on casein micelles: role of ethylenic unsaturation on the interaction and structural diversity.* ACS omega, 2018. **3**(1): p. 821-830.

23. Brodkorb, A., et al., *INFOGEST static in vitro simulation of gastrointestinal food digestion.* Nature protocols, 2019. **14**(4): p. 991-1014.

24. Wang, C., et al., *Effect of ultrasound treatment on allergenicity reduction of milk casein via colloid formation.* Journal of agricultural and food chemistry, 2020. **68**(16): p. 4678-4686.

25. Dousseau, F. and M. Pezolet, *Determination of the secondary structure content of proteins in aqueous solutions from their amide I and amide II infrared bands. Comparison between classical and partial least-squares methods.* Biochemistry, 1990. **29**(37): p. 8771-8779.

26. Koka, V.D., *A Study of the Effects of Titanium Dioxide Nanoparticles on the Fluorescent Intensity of Fluorescent Compounds in the Presence of Known Quenchers.* East Tennessee State University, theses and dissertations. 2011.

27. Barhoum, A., et al., *Roles of in situ surface modification in controlling the growth and crystallization of CaCO 3 nanoparticles, and their dispersion in polymeric materials.* Journal of materials science, 2015. **50**(24): p. 7908-7918.

28. Kongsinlark, A., G.L. Rempel, and P. Prasassarakich, *Synthesis of monodispersed polyisoprene–silica nanoparticles via differential microemulsion polymerization and mechanical properties of polyisoprene nanocomposite.* Chemical engineering journal, 2012. **193**: p. 215-226.

29. Chanteau, B., J. Fresnais, and J.-F. Berret, *Electrosteric enhanced stability of functional sub-10 nm cerium and iron oxide particles in cell culture medium*. Langmuir, 2009. **25**(16): p. 9064-9070.

30. Phue, W.H., et al., *A comparative analysis of different grades of silica particles and temperature variants of food-grade silica nanoparticles for their physicochemical properties and effect on trypsin*. Journal of agricultural and food chemistry, 2019. **67**(44): p. 12264-12272.

31. Besler, M., H. Steinhart, and A. Paschke, *Stability of food allergens and allergenicity of processed foods*. Journal of chromatography B: biomedical sciences and applications, 2001. **756**(1-2): p. 207-228.

32. Thomas, K., et al., *Evaluating the effect of food processing on the potential human allergenicity of novel proteins: international workshop report*. Food and chemical toxicology, 2007. **45**(7): p. 1116-1122.

33. Huang, L., et al., *A rapid and sensitive assay based on particle analysis for cell degranulation detection in basophils and mast cells.* Pharmacological research, 2016. **111**: p. 374-383.

34. Hussain, S., J.A. Vanoirbeek, and P.H. Hoet, *Interactions of nanomaterials with the immune system*. Wiley Interdisciplinary Reviews: Nanomedicine and nanobiotechnology, 2012. **4**(2): p. 169-183.

6.7 Supporting information

6.7.1 Hydrodynamic size of dietary particles

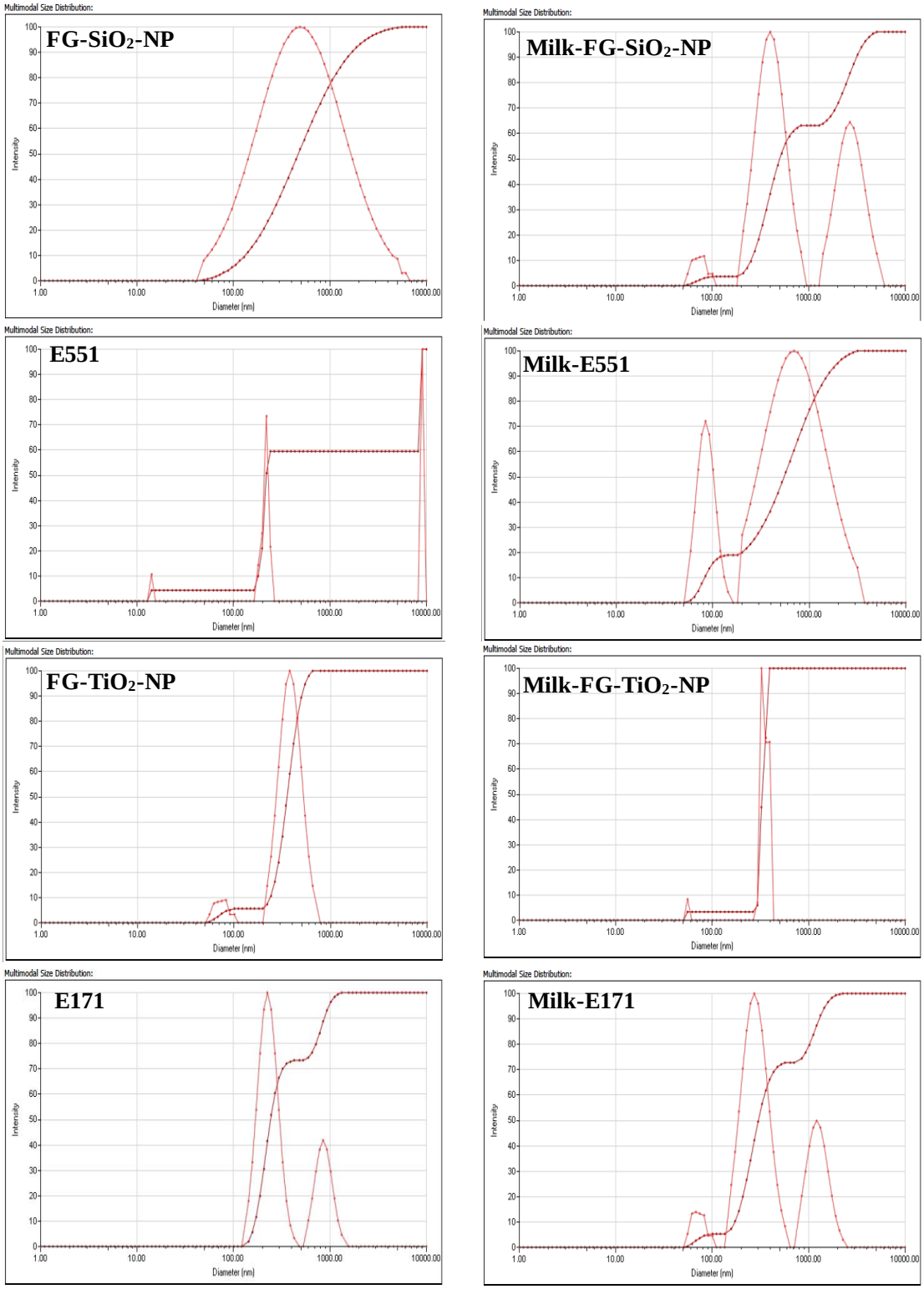

Figure SI 6. 1 Dynamic light scattering (DLS) curves of the pristine dietary particles and milk corona dietary particles

6.7.2 Quantification of the antigen response

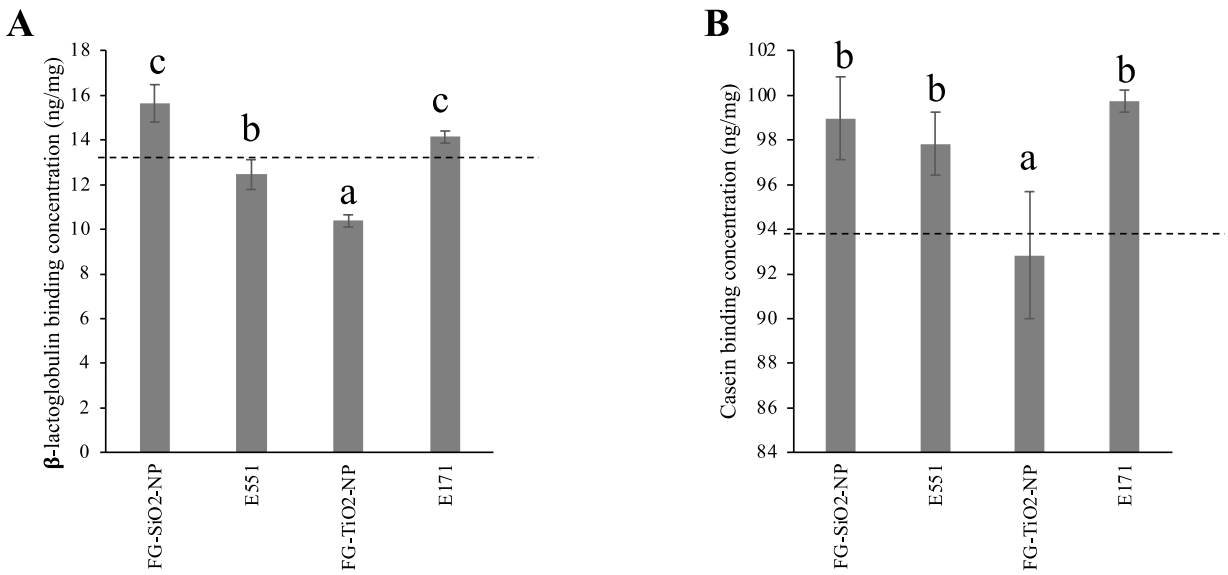

Figure SI 6. 2 Quantification of the antigen response of milk samples in the presence of inorganic dietary particles by indirect enzyme-linked immunosorbent assay (ELISA). (A) the rabbit anti-b-lactoglobulin in 1:5000 dilution was added to the plate, **(B)** the rabbit anti-casein in 1:2000 dilution was added to the plate, followed by adding the HRP linked anti-rabbit antibody (1:10000) and HRP substrate 3,3',5,5'-Tetramethylbenzidine (TMB). The colorimetric signal was measured at 450 nm by micro plate reader. Average values are plotted in the graph with different small letters indicate significant differences (Duncan, $p < 0.05$). *The dotted line represents the antigenicity of milk in the absence of dietary particles.

6.7.3 Identification of protein digestion pattern after subjecting milk to in vitro digestion in the presence and absence of dietary particles by one dimension gel electrophoresis

After the samples were passed through the in vitro digestion system and stopped the enzyme activities, the samples were centrifuged at 20,000 g for 15 mins to separate particles from the solution. The pallet was suspended in 50 mL of PBS buffer (pH 6.5). 50 mL of pallet and supernatant samples were mixed with 100 uL of sample buffer containing 62.5 mM Tris-HCl, pH 6.8, 2% SDS, 25% (v/v) glycerol, 0.01% bromophenol blue and 5% β-mercaptoethanol.

The mixture was vortexed and boiled for 5 min, and debris and particles were removed from the sample buffer by centrifugation at 20,000 g for 15 min. A protein-containing sample solution was collected and transferred into a new Eppendorf tube. Twenty microliters of each sample were loaded to each sample well of a 4-20% SDS-polyacrylamide gel. The proteins were separated in the gel using 100 V for 1.5 hr in running buffer containing 2.5 mM tris, 19.2 mM glycine and 0.01% SDS. The gels were then stained in standard Coomassie blue-methanol-acetic acid solution for 30 min at RT. The gels were subsequently washed with destaining solution (40% methanol, 10% acetic acid and 50% water) for 30 min at RT to visualize the protein bands. The gel was further subjected to silver staining to improve clarity (Kavran and Leahy 2014).

Bands corresponding to prominent proteins adsorbed onto the surface of particles after in vitro digestion are evident in the SDS-PAGE image given in SI 1 A and B. The relative intensities varied depending on the type and size of particles. The digested proteins (supernatant and pallet) in the presence and absence of dietary particles were compared with the undigested milk sample. Most of the proteins got digested, and the intensity of digested protein bands was less in supernatant samples after removing dietary particles from the samples. The intensity of pallet samples was higher in the presence of dietary particles. The bands in the lower molecular weight (~10 kd) were the mixture of digested milk proteins and enzymes. All these proteins play a role in triggering the allergic reaction of sensitized LAD2 cells.

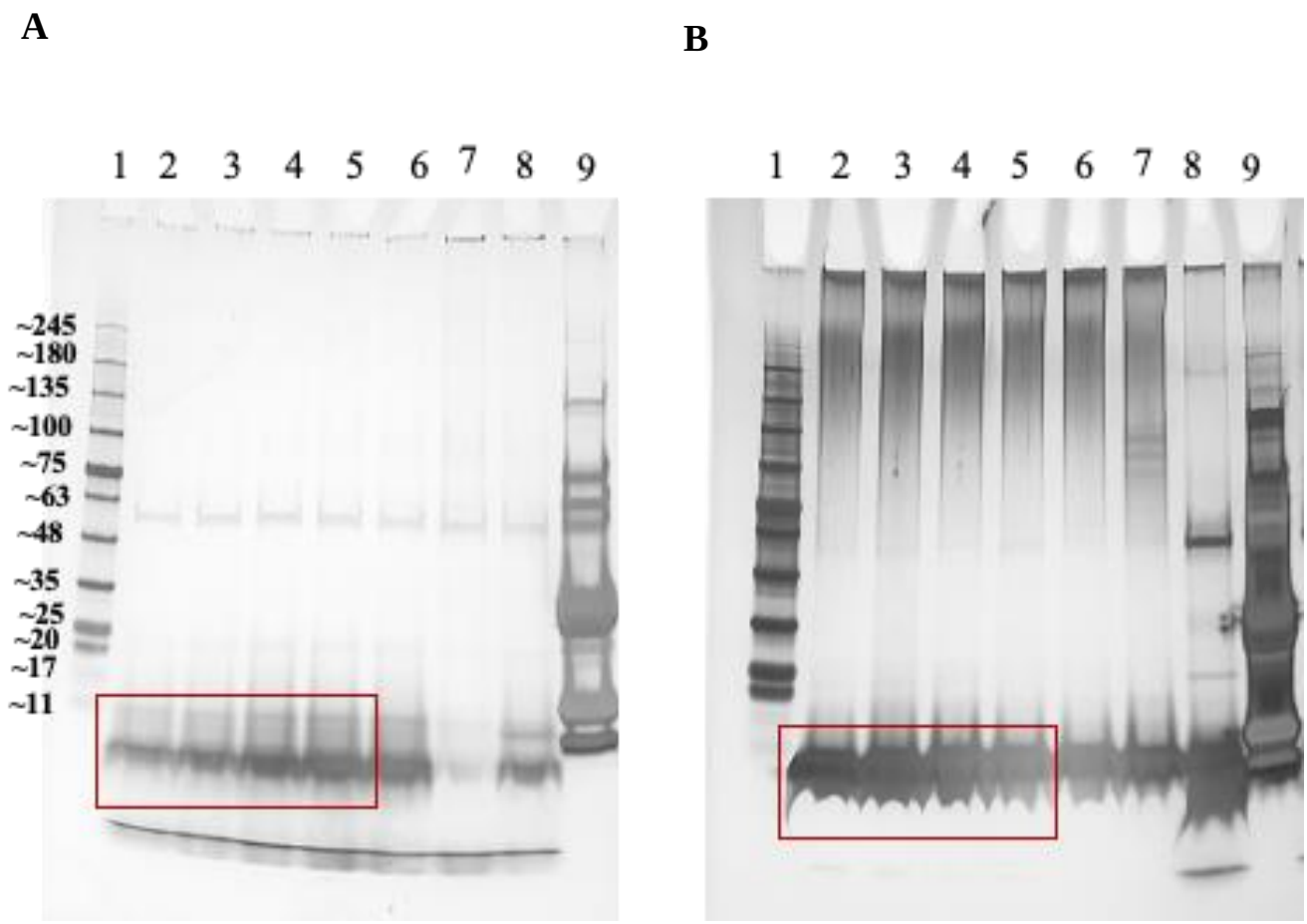

Figure SI 6. 3 SDS-PAGE of in vitro digested milk in the presence and absence of dietary particles. (A) Supernatant and **(B)** Pellet. Lane (1) Marker, (2) FG-SiO2-NP+Milk, (3) E551+Milk, (4) FG-TiO2-NP+Milk, (5) E171+Milk, (6) Milk, (7) Gastric Juice, (8) Milk (not centrifuge), and (9) Milk (not digested).

Chapter 7. General Conclusions

7.1 Conclusions

The increasing interest in utilizing DNMs for improving food quality, safety, or nutritional value is attributable to their unique physicochemical properties. However, the behaviour of nanoparticles is peculiar within the human body compared to larger particles or bulk materials. This research provides new perspectives on the potential health hazardous effect of DNMs used as food additives. Specifically, this thesis enhances the understanding of the transformation of DNM and their interactions with proteins of relevance to human nutrition and food allergy.

Initially, the variations were tested in the surface chemistry of different grades of silica particles (food grade vs non-food grade, nano vs micron) and the processing induced alterations on the surface chemistry of food grade nano silica. At elevated temperatures, the surface chemistry transformation of silica particles affected the binding affinity of protein-particles as exemplified with the digestive enzyme trypsin. The food-grade silica nanoparticles showed higher affinity, which can lead to a loss of secondary structure of the trypsin, thus resulting in partial loss of trypsin activity. The reduced protein hydrolysis resulting from the alteration in structure of trypsin suggests the potential negative effect of DNMs in diet on nutrient absorption.

When the DNMs are added to food or enter the human body, their surface become adsorbed with biomolecules, especially proteins. That protein corona covers the surface chemistry of the particles, thus altering their biological identity. The second study revealed the consequences of surface modification of silica nanoparticles by pure protein and food matrix. When the pristine particles interacted with human salivary amylase (HSA) directly, that altered the enzyme structure and caused inhibition activity of HSA. However, when the surface chemistry of particles was shielded by a single protein bovine serum albumin (BSA), the enzyme inhibition activities decreased due to indirect interaction with particles and enzymes. Paradoxically, the amylase inhibition activities increased in food matrix (milk) coated particles due to the

presence of protease enzyme from the milk sample and its digested HSA. These studies highlight when the food matrix interacts with the DNMs, HSA functions differed depending on the type of coated proteins. This finding signified the molecular interaction between digestive enzymes and DNMs that could lead to adverse effects on nutrient intake from food.

The third chapter of the thesis evaluated critical factors that determine the protein corona formation onto the dietary particles. During the protein corona formation, characteristics of proteins such as β-strand, isoelectric point, number of amino acid residues and characteristics of DNMs; zeta-potential, hydrophobicity, and hydrodynamic size correlated with their level of adsorption onto DNMs. However, when dispersed in a complex matrix that contains other biomolecules such as lipids, and sugars the interaction of proteins with other biomolecules were more important in determining their retention on particle surface.

After interacting with DNMs, the structural conformation of proteins was transformed, and that could alter the antigenicity and allergenicity of food proteins. As detailed in Chapter 6, particle-mediated alterations in protein structure could affect the allergenicity of milk proteins. In addition to inducing alterations of the protein structure, the interaction of allergenic proteins could also enhance the availability of allergenic epitopes. In addition, proteins adsorbed on particle surface resist their digestion which could also lead to an increased bioavailability of intact proteins. Nonetheless, this findings have far-reaching implications for managing the severity of food allergy and making dietary choices given the rising incidences of food allergies globally and their association with consumption of highly processed food often containing inorganic DNMs of silica and titania.

In short, these studies revealed that the surface chemistry of food additives silica nanoparticles was altered when exposed to different food handling temperatures. The structural conformation of proteins will change when interacted with pristine nanoparticles, thereby affecting the functional, nutritional and allergic properties of the proteins.

7.2 Scientific contributions

The work presented in this thesis contributes to several research novelties as follow:

- Studies showed that DNMs used in food do change in response to food handling temperature and this could make it different from pristine particles during their interaction with biological targets such as digestive enzymes.
- For the first time, protein-biomolecule interactions were discovered to play a major role in shaping the type and amount of proteins found on the hard-corona of particles dispersed in a food matrix.
- The transformation of an immune characteristic of food components in the presence of DNMs was also revealed.

7.3 Recommendations for future research

Findings from studies mentioned above open many windows for further exploration. Given below are the immediate priorities for future research:

- Transformation of DNMs in human gastro-intestinal system should be studied using in vitro and in vivo models to gain more insight into the fate of ingested DNMs
- The immune response to DNMs used in food, in their pristine as well as incorporated in food matrix state should be studied. Suggest studying the implication of DNMS on gut immune system as implied in the inflammatory diseases and food allergy.
- The role of DNMs in shaping food allergy warrants further investigation using *in vivo* models.

General Reference List

Note: Following the Guidelines for Manuscript Style Thesis Preparation, each manuscript chapter (Chapters 3-6) contains its own reference list. Hence, the following reference list corresponds to the remaining chapters of the thesis (Chapters 1 and 2).

1. Scheu, M., et al., *Mapping nanotechnology patents: The EPO approach.* World patent information, 2006. **28**(3): p. 204-211.
2. Taylor, M.R., *Assuring the safety of nanomaterials in food packaging: the regulatory process and key issues.* 2008.
3. Rashidi, L. and K. Khosravi-Darani, *The applications of nanotechnology in food industry.* Critical reviews in food science and nutrition, 2011. **51**(8): p. 723-730.
4. Ameta, S.K., et al., *Use of Nanomaterials in Food Science*, in *Biogenic Nano-Particles and their Use in Agro-ecosystems*. Springer, 2020. p. 457-488.
5. Chang, P.-S., H. Umakoshi, and H. Kim, *Nanotechnology for food engineering: Biomembrane and nanocarriers*. Hindawi, 2019,
6. Gatoo, M.A., et al., *Physicochemical properties of nanomaterials: implication in associated toxic manifestations.* BioMed research international, 2014. **2014**.
7. Lynch, I. and K.A. Dawson, *Protein-nanoparticle interactions.* Nano today, 2008. **3**(1-2): p. 40-47.
8. Mahmoudi, M., et al., *Cell "vision": complementary factor of protein corona in nanotoxicology.* Nanoscale, 2012. **4**(17): p. 5461-5468.
9. Phue, W.H., et al., *A comparative analysis of different grades of silica particles and temperature variants of food-grade silica nanoparticles for their physicochemical properties and effect on trypsin.* Journal of agricultural and food chemistry, 2019. **67**(44): p. 12264-12272.

10. Barisik, M., et al., *Size dependent surface charge properties of silica nanoparticles*. The journal of physical chemistry C, 2014. **118**(4): p. 1836-1842.
11. George, S., *Nanomaterial properties: implications for safe medical applications of nanotechnology*, in *Nanotechnology in Endodontics*. Springer, 2015. p. 45-69.
12. Whitesides, G.M., *Nanoscience, nanotechnology, and chemistry.* Small, 2005. **1**(2): p. 172-179.
13. Rasmussen, K., et al., *Regulatory status of nanotechnologies in food in the EU*, in *Nanomaterials for Food Applications*. Elsevier, 2019. p. 381-410.
14. Huang, Q., *Nanotechnology in the food, beverage and nutraceutical industries*. Elsevier, 2012.
15. Reiners, R., *Definition and standardization of nanomaterials.* Safety aspects of engineered nanomaterials. Pan stanford publishing Pte. Ltd, Singapore, 2013: p. 1-27.
16. Calzolai, L., D. Gilliland, and F. Rossi, *Measuring nanoparticles size distribution in food and consumer products: a review*. Food additives and contaminants: Part A, 2012. **29**(8): p. 1183-1193.
17. Henshaw, D.L. and M.J. O'Carroll, *Scientific committee on emerging and newly identified health risks (SCENIHR).* Brussels: european commission, 2009.
18. Plan, S., *The national nanotechnology initiative.* 2007.
19. Ahmed, S., et al., *A review on plants extract mediated synthesis of silver nanoparticles for antimicrobial applications: a green expertise.* Journal of advanced research, 2016. **7**(1): p. 17-28.
20. Hosek, J., *Nanotechnology technology technical standarization review*. Nanocon, 2012. **10**: p23-25.
21. Hannink, R.H. and A.J. Hill, *Nanostructure control of materials*. Woodhead publishing, 2006.

22. Brock, S.L., *Nanostructures and Nanomaterials: Synthesis, Properties and Applications.* ACS, 2004.

23. Casey, P., *Nanoparticle technologies and applications*, in *Nanostructure control of materials*. Elsevier, 2006. p. 1-31.

24. Schaefer, H.-E., *Nanoscience: the science of the small in physics, engineering, chemistry, biology and medicine*. Springer Science & Business Media, 2010.

25. Meng, Q., et al., *Electrical and optical properties of nano aluminum film/particle structure.* Journal of wuhan university of technology-mater. Sci. Ed., 2017. **32**(5): p. 989-993.

26. Chhatre, A., et al., *Color and surface plasmon effects in nanoparticle systems: Case of silver nanoparticles prepared by microemulsion route.* Colloids and surfaces A: physicochemical and engineering aspects, 2012. **404**: p. 83-92.

27. Haruta, M., *Size-and support-dependency in the catalysis of gold.* Catalysis today, 1997. **36**(1): p. 153-166.

28. Gerberich, W., et al., *Superhard silicon nanospheres.* Journal of the mechanics and physics of solids, 2003. **51**(6): p. 979-992.

29. Liu, C., et al., *Chemical control of superparamagnetic properties of magnesium and cobalt spinel ferrite nanoparticles through atomic level magnetic couplings.* Journal of the american chemical society, 2000. **122**(26): p. 6263-6267.

30. Yaktine, A. and L. Pray, *Nanotechnology in food products: workshop summary*. National academies press, 2009.

31. Gallocchio, F., S. Belluco, and A. Ricci, *Nanotechnology and food: brief overview of the current scenario.* Procedia food science, 2015. **5**: p. 85-88.

32. Frewer, L.J., et al., *Consumer attitudes towards nanotechnologies applied to food production.* Trends in food science & technology, 2014. **40**(2): p. 211-225.

33. Organization, W.H., *FAO/WHO Expert Meeting on the Application of Nanotechnologies in the Food and Agriculture Sectors: Potential Food Safety Implications: Meeting Report*. World Health Organization, 2010.

34. Cockburn, A., et al., *Approaches to the safety assessment of engineered nanomaterials (ENM) in food.* Food and chemical toxicology, 2012. **50**(6): p. 2224-2242.

35. Weiss, J., et al., *Solid lipid nanoparticles as delivery systems for bioactive food components.* Food biophysics, 2008. **3**(2): p. 146-154.

36. Espitia, P.J.P., et al., *Zinc oxide nanoparticles: synthesis, antimicrobial activity and food packaging applications.* Food and bioprocess technology, 2012. **5**(5): p. 1447-1464.

37. Peters, R., et al., *Inventory of Nanotechnology applications in the agricultural, feed and food sector.* EFSA supporting publications, 2014. **11**(7): p. 621E.

38. Cao, Y., et al., *Consideration of interaction between nanoparticles and food components for the safety assessment of nanoparticles following oral exposure: A review*. Environmental toxicology and pharmacology, 2016. **46**: p. 206-210.

39. Organization, W.H., *Evaluation of certain food additives and contaminants. Eightieth report of the Joint FAO/WHO Expert Committee on Food Additives.* World Health Organization technical report series, 2016 (995): p. 1.

40. Winkler, H.C., M. Suter, and H. Naegeli, *Critical review of the safety assessment of nano-structured silica additives in food.* Journal of nanobiotechnology, 2016. **14**(1): p. 1-9.

41. Heroult, J., et al., *The potential of asymmetric flow field-flow fractionation hyphenated to multiple detectors for the quantification and size estimation of silica nanoparticles in a food matrix.* Analytical and bioanalytical chemistry, 2014. **406**(16): p. 3919-3927.

42. Bi, F., et al., *Development of antioxidant and antimicrobial packaging films based on chitosan, D-α-tocopheryl polyethylene glycol 1000 succinate and silicon dioxide nanoparticles.* Food packaging and shelf life, 2020. **24**: p. 100503.

43. Additives, E.P.o.F., et al., *Re-evaluation of silicon dioxide (E 551) as a food additive*. EFSA journal, 2018. **16**(1): p. e05088.

44. Additives, E.P.o.F., et al., *Re-evaluation of sodium aluminium silicate (E 554) and potassium aluminium silicate (E 555) as food additives.* EFSA journal, 2020. **18**(6): p. e06152.

45. Yokel, R.A., *Aluminum in food–the nature and contribution of food additives.* Food additive, Intech, 2012: p. 203-228.

46. Ali, S.S., et al., *Nanobiotechnological advancements in agriculture and food industry: Applications, nanotoxicity, and future perspectives.* Science of the total environment, 2021: p. 148359.

47. Peters, R.J., et al., *Characterization of titanium dioxide nanoparticles in food products: analytical methods to define nanoparticles.* Journal of agricultural and food chemistry, 2014. **62**(27): p. 6285-6293.

48. Additives, E.P.o.F. and N.S.a.t. Food, *Re-evaluation of titanium dioxide (E 171) as a food additive.* EFSA journal, 2016. **14**(9): p. e04545.

49. de Oliveira Mallia, J., et al., *Nanoparticle food applications and their toxicity: current trends and needs in risk assessment strategiesNanoparticles and Food Toxicity.* Journal of food protection, 2021.

50. EFSA Panel on Food Contact Materials, E., Flavourings and P. Aids, *Safety assessment of the substance zinc oxide, nanoparticles, for use in food contact materials.* EFSA journal, 2016. **14**(3): p. 4408.

51. Kumar, S., et al., *Biodegradable hybrid nanocomposite of chitosan/gelatin and green synthesized zinc oxide nanoparticles for food packaging.* Foods, 2020. **9**(9): p. 1143.

52. Carbone, M., et al., *Silver nanoparticles in polymeric matrices for fresh food packaging.* Journal of king saud university-science, 2016. **28**(4): p. 273-279.

53. Videira-Quintela, D., O. Martin, and G. Montalvo, *Recent advances in polymer-metallic composites for food packaging applications.* Trends in food science & technology, 2021.

54. Additives, E.P.o. and P.o.S.u.i.A. Feed, *Safety and efficacy of iron oxide black, red and yellow for all animal species.* EFSA journal, 2016. **14**(6): p. e04482.

55. Voss, L., et al., *The presence of iron oxide nanoparticles in the food pigment E172.* Food chemistry, 2020. **327**: p. 127000.

56. Additives, E.P.o.F. and N.S.a.t. Food, *Scientific Opinion on the re-evaluation of gold (E 175) as a food additive.* EFSA journal, 2016. **14**(1): p. 4362.

57. Hauser, E.A., *The colloid science of silica and silicones.* Clays and clay minerals, 1955. **4**(1): p. 45-53.

58. Berzelius, J.J., *Jöns Jacob Berzelius.* 1934.

59. Greenwood, N.N. and A. Earnshaw, *Chemistry of the Elements*. Elsevier, 2012.

60. Bergna, H.E. and W.O. Roberts, *Colloidal silica: fundamentals and applications*. CRC press, 2005.

61. Eckert, H., *Structural characterization of noncrystalline solids and glasses using solid state NMR.* Progress in nuclear magnetic resonance spectroscopy, 1992. **24**(3): p. 159-293.

62. Roggers, R., et al., *The practicality of mesoporous silica nanoparticles as drug delivery devices and progress toward this goal.* Aaps pharmscitech, 2014. **15**(5): p. 1163-1171.

63. Organization, W.H., *Principles for the safety assessment of food additives and contaminants in food.* 2001.

64. EFSA Panel on Food Contact Material, E., Flavourings and P. Aids, *Statement on the safety assessment of the substance silicon dioxide, silanated, FCM Substance No 87 for use in food contact materials.* EFSA journal, 2014. **12**(6): p. 3712.

65. Unger, K., *Chapter 1 General chemistry of silica.* Journal of chromatography library, 1979. **16**: p. 1-14.

66. Vansant, E.F., P. Van Der Voort, and K.C. Vrancken, *Characterization and chemical modification of the silica surface*. Elsevier, 1995.

67. Wisconsin, D., *Report to the Natural Resources Board: Silica Study.* Madison, WI, 2011.

68. Peng, L., et al., *Investigation of the states of water and OH groups on the surface of silica.* Colloids and surfaces A: physicochemical and engineering aspects, 2009. **334**(1-3): p. 112-115.

69. Zhang, H., et al., *Processing pathway dependence of amorphous silica nanoparticle toxicity: colloidal vs pyrolytic.* Journal of the american chemical society, 2012. **134**(38): p. 15790-15804.

70. Peri, J. and A. Hensley Jr, *The surface structure of silica gel.* The journal of physical chemistry, 1968. **72**(8): p. 2926-2933.

71. Zhuravlev, L., *The surface chemistry of amorphous silica. Zhuravlev model.* Colloids and surfaces A: physicochemical and engineering aspects, 2000. **173**(1-3): p. 1-38.

72. Ranjan, R., *Surface modification of silica nanoparticles*. University of Akron, 2008.

73. Barthel, H., L. Rösch, and J. Weis, *Fumed silica-production, properties, and applications.* Organosilicon chemistry set: from molecules to materials, 2005: p. 761-778.

74. Sha, B., et al., *Potential application of titanium dioxide nanoparticles in the prevention of osteosarcoma and chondrosarcoma recurrence.* Journal of nanoscience and nanotechnology, 2013. **13**(2): p. 1208-1211.

75. Hussein, F. and M. Shaheed, *Preparation and applications of titanium dioxide and zinc oxide nanoparticles.* Journal of environmental analytical chemistry, 2015. **2**(109): p. 2380-2391.1000.

76. Weir, A., et al., *Titanium dioxide nanoparticles in food and personal care products.* Environmental science & technology, 2012. **46**(4): p. 2242-2250.

77. Linsebigler, A.L., G. Lu, and J.T. Yates Jr, *Photocatalysis on TiO2 surfaces: principles, mechanisms, and selected results.* Chemical reviews, 1995. **95**(3): p. 735-758.

78. Diebold, U., *The surface science of titanium dioxide.* Surface science reports, 2003. **48**(5-8): p. 53-229.

79. Roy, A., *Artists' pigments. A handbook of their history and characteristics, 2.* Washington, DC: national gallery of art, 1993.

80. Riederer, J., et al., *Artists' pigments: a handbook of their history and characteristics V. 3*. Washington archetype publications, London, 1997.

81. Proquin, H., et al., *Titanium dioxide food additive (E171) induces ROS formation and genotoxicity: contribution of micro and nano-sized fractions.* Mutagenesis, 2017. **32**(1): p. 139-149.

82. Cancer, I.A.f.R.o., *Carbon black, titanium dioxide, and talc*. Vol. 93. IARC press, International agency for research on cancer, 2010.

83. Bourikas, K., C. Kordulis, and A. Lycourghiotis, *Titanium dioxide (anatase and rutile): surface chemistry, liquid–solid interface chemistry, and scientific synthesis of supported catalysts.* Chemical reviews, 2014. **114**(19): p. 9754-9823.

84. Degabriel, T., *Study of the interaction between proteins and TiO2 NPs: nature of the interfacial processes*. Paris 6, 2015.

85. Hwu, Y., et al., *X-ray absorption of nanocrystal TiO2*. Nanostructured materials, 1997. **9**(1-8): p. 355-358.

86. Authority, E.F.S., *Calcium silicate and silicon dioxide/silicic acid gel added for nutritional purposes to food supplements.* EFSA journal, 2009. **7**(6): p. 1132.

87. Secretariat, E., *Food additives and nanotechnologies.*

88. Dekkers, S., et al., *Presence and risks of nanosilica in food products.* Nanotoxicology, 2011. **5**(3): p. 393-405.

89. Mojsiewicz-Pieńkowska, K. and J. Łukasiak, *Analytical fractionation of silicon compounds in foodstuffs.* Food control, 2003. **14**(3): p. 153-162.

90. Dekkers, S., et al., *Knowledge gaps in risk assessment of nanosilica in food: evaluation of the dissolution and toxicity of different forms of silica.* Nanotoxicology, 2013. **7**(4): p. 367-377.

91. Peters, R., et al., *Presence of nano-sized silica during in vitro digestion of foods containing silica as a food additive.* ACS nano, 2012. **6**(3): p. 2441-2451.

92. Fröhlich, E.E. and E. Fröhlich, *Cytotoxicity of nanoparticles contained in food on intestinal cells and the gut microbiota.* International journal of molecular sciences, 2016. **17**(4): p. 509.

93. French, R.A., et al., *Influence of ionic strength, pH, and cation valence on aggregation kinetics of titanium dioxide nanoparticles.* Environmental science & technology, 2009. **43**(5): p. 1354-1359.

94. Scotter, M.J., *Methods for the determination of European Union-permitted added natural colours in foods: a review*. Food additives and contaminants, 2011. **28**(5): p. 527-596.

95. Hoshino, Y., H. Lee, and Y. Miura, *Interaction between synthetic particles and biomacromolecules: fundamental study of nonspecific interaction and design of nanoparticles that recognize target molecules.* Polymer journal, 2014. **46**(9): p. 537-545.

96. Bharti, B., J. Meissner, and G.H. Findenegg, *Aggregation of silica nanoparticles directed by adsorption of lysozyme.* Langmuir, 2011. **27**(16): p. 9823-9833.

97. Yadav, I., V. Aswal, and J. Kohlbrecher. *Interaction of lysozyme protein with different sized silica nanoparticles and their resultant structures*. AIP Conference Proceedings. AIP Publishing LLC, 2016.

98. Fei, L. and S. Perrett, *Effect of nanoparticles on protein folding and fibrillogenesis*. International journal of molecular sciences, 2009. **10**(2): p. 646-655.

99. Satzer, P., et al., *Protein adsorption onto nanoparticles induces conformational changes: Particle size dependency, kinetics, and mechanisms.* Engineering in life sciences, 2016. **16**(3): p. 238-246.

100. Mahmoudi, M., et al., *Irreversible changes in protein conformation due to interaction with superparamagnetic iron oxide nanoparticles.* Nanoscale, 2011. **3**(3): p. 1127-1138.

101. Momeni, L., et al., *Interaction of TiO2 nanoparticle with trypsin analyzed by kinetic and spectroscopic methods.* Monatshefte für chemie-chemical monthly, 2017. **148**(2): p. 199-207.

102. Strobel, C., et al., *Effects of the physicochemical properties of titanium dioxide nanoparticles, commonly used as sun protection agents, on microvascular endothelial cells.* Journal of nanoparticle research, 2014. **16**(1): p. 1-16.

103. Pederzoli, F., et al., *Protein corona and nanoparticles: how can we investigate on?* Wiley Interdisciplinary Reviews: Nanomedicine and nanobiotechnology, 2017. **9**(6): p. e1467.

104. Rahman, M., et al., *Nanoparticle and protein corona*, in *Protein-nanoparticle interactions*. Springer, 2013. p. 21-44.

105. Cheng, X., et al., *Protein corona influences cellular uptake of gold nanoparticles by phagocytic and nonphagocytic cells in a size-dependent manner.* ACS applied materials & interfaces, 2015. **7**(37): p. 20568-20575.

106. Van Der Zande, M., et al., *Sub-chronic toxicity study in rats orally exposed to nanostructured silica.* Particle and fibre toxicology, 2014. **11**(1): p. 1-19.

107. Nishimori, H., et al., *Histological analysis of 70-nm silica particles-induced chronic toxicity in mice.* European journal of pharmaceutics and biopharmaceutics, 2009. **72**(3): p. 626-629.

108. Fent, K., et al., *Assessment of uptake and toxicity of fluorescent silica nanoparticles in zebrafish (Danio rerio) early life stages.* Aquatic toxicology, 2010. **100**(2): p. 218-228.

109. van Kesteren, P.C., et al., *Novel insights into the risk assessment of the nanomaterial synthetic amorphous silica, additive E551, in food.* Nanotoxicology, 2015. **9**(4): p. 442-452.

110. Bantz, C., et al., *The surface properties of nanoparticles determine the agglomeration state and the size of the particles under physiological conditions.* Beilstein journal of nanotechnology, 2014. **5**(1): p. 1774-1786.

111. Teubl, B.J., et al., *The buccal mucosa as a route for TiO2 nanoparticle uptake.* Nanotoxicology, 2015. **9**(2): p. 253-261.

112. Pedata, P., et al., *In vitro intestinal epithelium responses to titanium dioxide nanoparticles.* Food research international, 2019. **119**: p. 634-642.

113. Déciga-Alcaraz, A., et al., *Irreversible disruption of the cytoskeleton as induced by non-cytotoxic exposure to titanium dioxide nanoparticles in lung epithelial cells.* Chemico-biological interactions, 2020. **323**: p. 109063.

114. Tassinari, R., et al., *Oral, short-term exposure to titanium dioxide nanoparticles in Sprague-Dawley rat: focus on reproductive and endocrine systems and spleen.* Nanotoxicology, 2014. **8**(6): p. 654-662.

115. Gui, S., et al., *RETRACTED ARTICLE: Intragastric exposure to titanium dioxide nanoparticles induced nephrotoxicity in mice, assessed by physiological and gene expression modifications.* Particle and fibre toxicology, 2013. **10**(1): p. 1-16.

116. Bouwmeester, H., et al., *Review of health safety aspects of nanotechnologies in food production.* Regulatory toxicology and pharmacology, 2009. **53**(1): p. 52-62.

117. Otsuki, T., M. Di Gioacchino, and C. Petrarca, *Allergy and Immunotoxicology in Occupational Health-The Next Step*. Springer, 2020.

118. Alsaleh, N.B. and J.M. Brown, *Engineered nanomaterials and type I allergic hypersensitivity reactions.* Frontiers in immunology, 2020. **11**: p. 222.

119. Boraschi, D. and A. Duschl, *Nanoparticles and the immune system: safety and effects*. Academic press, 2013.

120. Alenius, H. and K. Savolainen, *Allergy and Immunity Induced by Nanomaterials*, in *Interaction of Nanomaterials with the Immune System*. Springer, 2020. p. 149-165.

121. Weinberg, E.G., *The WAO white book on allergy 2011-2012*. Current allergy and clinical immunology, 2011. **24**(3): p. 156-157.

122. Hamann, C.R., et al., *The cost of nickel allergy: a global investigation of coin composition and nickel and cobalt release.* Contact dermatitis, 2013. **68**(1): p. 15-22.

123. Park, E.-J., et al., *Repeated-dose toxicity and inflammatory responses in mice by oral administration of silver nanoparticles.* Environmental toxicology and pharmacology, 2010. **30**(2): p. 162-168.

124. Larsen, S.T., et al., *Nano titanium dioxide particles promote allergic sensitization and lung inflammation in mice.* Basic and clinical pharmacology and toxicology, 2010. **106**(2): p. 114-117.

125. Yazdi, A.S., et al., *Nanoparticles activate the NLR pyrin domain containing 3 (Nlrp3) inflammasome and cause pulmonary inflammation through release of IL-1α and IL-1β.* Proceedings of the national academy of sciences, 2010. **107**(45): p. 19449-19454.